Lipidomic analysis of adipose-derived extracellular vesicles reveals their potential as lipid mediators of obesity-associated metabolic complications

Alexia Blandin[1,2], Grégory Hilairet[2], Maharajah Ponnaiah[3], Simon Ducheix[1], Isabelle Dugail[4], Bertrand Cariou[1], Marie Lhomme[3] and Soazig Le Lay[1,2*]

[1]Université de Nantes, CHU Nantes, CNRS, INSERM, l'institut du thorax, F-44000 Nantes, France.

[2]Université d'Angers, SFR ICAT, France

[3]ICANalytics, Institute of Cardiometabolism and Nutrition, Assistance Publique-Hôpitaux de Paris, Pitié-Salpêtrière Hospital, Paris, France

[4]UMRS 1269 INSERM/Sorbonne University, Nutriomics, UMRS 1269, F-75013, Paris, France

[*]**Correspondence to** soazig.lelay@inserm.fr

Keywords : extracellular vesicles, lipids, obesity, adipocyte

Abbreviation :

AdEV, adipose extracellular vesicles; AT, adipose tissue; EV, extracellular vesicles; HOMA-IR, homeostasic model assessment of insulin-resistance; IR, insulin-resistance; lEV, large extracellular vesicles; sEV, small extracellular vesicles; T2D, type 2 diabetes; VAT, visceral adipose tissue.

Manuscript description:

5 Figures, 4 Supplemental Figures, 5 Supplemental Tables

Abstract

Adipose extracellular vesicles (AdEV) transport lipids that could participate to the development of obesity-related metabolic dysfunctions. This study aimed to define mice AdEV lipid signature in either healthy or obesity context by a targeted LC-MS/MS approach.

Distinct clustering of AdEV and visceral adipose tissue (VAT) lipidomes by principal component analysis reveals specific lipid composition of AdEV compared to source VAT. Comprehensive analysis identifies enrichment of ceramides and phosphatidylglycerols in AdEV compared to VAT in lean conditions. Lipid subspecies commonly enriched in AdEV highlight specific AdEV-lipid sorting. Obesity impacts AdEV lipidome, driving triacylglycerols and sphingomyelins enrichment in obese versus lean conditions. Obese mice AdEV also display elevated phosphatidylglycerols and acid arachidonic subspecies contents highlighting novel biomarkers and/or mediators of metabolic dysfunctions.

Our study identifies specific lipid-fingerprints for plasma, VAT and AdEV that are informative of the metabolic status and underline the signaling capacity of lipids transported by AdEV in obesity-associated complications.

150 words

Introduction

Epidemic obesity, with nearly 40 % of the world's adult population being overweight or obese, is the greatest threat to global health, by increasing risk of type 2 diabetes (T2D), cardiovascular and liver diseases. Multiple factors (environmental, genetic and biological) interact to cause obesity. Adipose tissue (AT) hypertrophy and consecutive metabolic dysfunction specifically lead to systemic lipid overflow, lipotoxic fat depots in peripheral organs and low-grade inflammation via dysregulated production of adipokines, which, altogether, participate in the settings of metabolic complications. Recent evidences indicate that a significant part of the AT secretome is in the form of AT-derived extracellular vesicles (AdEV), that may contribute to the development of obesity-related metabolic complications (1, 2).

Others and we previously demonstrated significant increase of plasma EV concentrations in patients with obesity, with a strong positive association with HOMA-IR indicating insulin-resistance (IR) and subsequent T2D risk (3, 4). AdEV are viewed as critical mediators of metabolic alterations since the injection of AdEV derived from obese AT into healthy mice triggers IR (5, 6). Efforts to understand how AdEV promote metabolic dysfunction have focused on their protein or miRNA composition and subsequent transfer to recipient cells (5-7). However, little attention was paid to their potential as lipid species carriers even if some lipids, like ceramides or diacylglycerols (DAG), are recognized as potent mediators of IR development in skeletal muscle or liver (8, 9).

High-resolution lipidomic analysis applied on EV from different cell sources identified up to 2,000 different lipid species (10, 11), which provided a basis for structural properties which likely participate in EV stability in biofluids (12). A recent study also pointed out that adipocytes can release neutral lipid-filled EV, via a lipase-independent pathway distinct from that used in canonical lipid mobilization by lipolytic release of free fatty acids (13). Others highlight the participation of AdEV in the transport of free fatty acids fueling melanoma aggressiveness with energetic substrates (14). In line, studies focusing on non-adipose derived EV demonstrated that palmitate-induced EVwere enriched in ceramides, supporting the idea that EV contribute to sphingolipid efflux pathway (15, 16). Moreover, EV can transfer ceramides to macrophages or muscle cells thereby inducing IR in recipient cells (17, 18). Previous lipidomic studies on cultured 3T3-L1 adipocyte-derived EV identified a predominance of phospholipids,

sphingolipids and traces of glycerolipids, reflecting the composition of adipocyte plasma membrane (19, 20). We could also appreciate subtle differences in EV lipid fingerprint depending on EV subtype, namely large EV (lEV) shed from the plasma membrane and small EV (sEV) which originate from the endosomal system (10, 11, 21). Our previous work highlighted a specific cholesterol enrichment in 3T3-L1 adipocyte sEV in agreement with the role of this sterol in EV biogenesis, whereas adipocyte lEV presented high amounts of externalized phosphatidylserine (PS) in line with the pro-coagulant potential of this EV subclass (19).

Considering the role assigned to AdEV as lipid transporters and as mediators of obesity-related metabolic complications, we aimed to compare AdEV lipid content, with respect to secreting AT and circulating lipids, in the lean and pathophysiological context of obesity. To this purpose, we performed a targeted lipidomic analysis to compare the lipidome of sEV and lEV with source visceral AT (VAT) and with plasma in lean and obese (*ob/ob*) mice. We present here comprehensive lipid maps revealing specific adipose EV lipid sorting when compared to secreting VAT. We demonstrated that AdEV lipidome is more dependent on VAT pathophysiological state rather than on EV subtype and we identified some specific AdEV lipid classes or species closely related to the obese state. Particularly, enrichment in some EV lipid subspecies may constitute novel candidates/mediators in metabolic dysfunctions associated with obesity.

Methods

Animal experimentation

Adult mice heterozygous (*Ob*/+) for the leptin spontaneous mutation Lep^{ob} were initially obtained from Charles River (JAX^{TM} mice strain) and interbred to obtain a colony. Regular backcross with commercial $Lep^{ob/+}$ is performed to avoid any background drift. At 3-month of age, *ob/ob* animals were identified on the basis of their increased body weight that associates with hyperglycemia, hyperinsulinemia and significant increase of liver and AT mass at the expense of muscle mass (Table S1).

Three-month old lean or obese mice were used to collect VAT explants for EV isolation. We retained only male mice since sex-specific lipid signature has been described in *ob/ob* mice (22). All mice had *ad libitum* access to food and water and were housed in the same open mouse facility on a day/night cycle. Animals were killed in a non-fasted state.

Animal care and study protocols were approved by the French Ministry of Education and Research and the ethics committee N°6 in animal experimentation and were in accordance with the EU Directive 2010/63/EU for animal experiments.

Plasma collection

Mice peripheral blood was collected on EDTA-coated tubes following intracardiac puncture. Platelet-rich plasma was separated from whole blood by a 5 min centrifugation at 1,500 x*g*, and recentrifuged for 5 min at 1,900 *xg* to obtain platelet-free plasma (PFP).

VAT-derived EV isolation

Mice VAT were minced into small pieces (50-150 mm^3) and were placed into Clinicell® 25 cassettes (Mabio, France) filled with 10mL ECBM/Hepes 10mM/BSA FFAfree 0,1% pH 7.4 as previously described (23). Serum-free conditioned medium (CM)after 48h culture was collected, filtered on 100µm cell strainers and use for EV isolationsimilarly to our previous characterization of adipocyte-derived EV reported on EV Track knowledgebase (24) (http://evtrack.org/, ID: EV210202). The absence of serum prevented AdEV preparations from contamination by external bovine source of EV. lEV were recovered from cell-cleared supernatants (1,500 x*g* for 20 min) by centrifugation 1 hour at 13,000 x*g*, followed by two washing steps in NaCl and

resuspended in sterile NaCl. sEV were further isolated from lEV-depleted supernatants following a 100,000 x*g* ultracentrifugation step for 1 hour at 4°C (rotor MLA-50, Beckman Coulter Optima MAX-XP Ultracentrifuge) and two washes in NaCl before resuspension in NaCl.

Nanoparticle Tracking Analysis

EV samples were diluted in sterile NaCl before nanoparticle tracking analysis (NTA). NTA was undertaken using the NanoSight NS300 (Malvern Instruments,Malvern, UK) equipped with a 405 nm laser. Ninety-second videos were recorded in five replicates per sample with optimized set parameters (the detection threshold was set to 5 for both EV subtypes). Temperature was automatically monitored and ranged from 20°C to 21°C. Videos were analyzed when a sufficient number of valid trajectories was measured. Data capture and further analysis were performed using the NTA software version 3.1. EV concentrations are expressed as number of particles secreted by adipocytes, the number of adipocytes present in the secreting VAT being estimated by indirect calculation as we previously described (19).

Western Blotting

VAT explants were resuspended in lysis buffer [50 mM Tris pH 7.4, 0.27 M sucrose, 1 mM Na-orthovanadate pH 10, 1 mM ethylenediaminetetraacetic acid (EDTA), 1 mM ethylene glycol-bis(β-aminoethyl ether)-N,N,N',N'-tetraacetic acid (EGTA), 10mMNa β-glycerophosphate, 50mM NaF, 5 mM Na pyrophosphate, 1% (w/v) Triton X-100, 0.1% (v/v) 2-mercaptoethanol and cOmplete™ Protease Inhibitor Cocktail (Roche Diagnostics). Whole cell lysates were centrifuged at 13 000 x*g* for 10min at 4°C to get rid of insoluble material. Isolated AdEV following differential centrifugation were resuspended in NaCl. AdEV and VAT protein content was estimated by DC-protein assay (BioRad) by using BSA as standard. Protein lysates were stored at -20°C until use.

8µg of protein lysates were diluted in Laemli Buffer 4X (Biorad) in reducing conditions, heated at 95°C for 10 min and migrated on a 4–15% Mini-Protean TGX gel (Biorad) and transferred on to nitrocellulose membranes using Trans Blot Turbo apparatus (Biorad). Membranes were blocked for 90 min at room temperature using TBS blocking buffer (LI-COR Biosciences) and incubated with primary antibodies diluted in the same blocking buffer. Antibodies used for Western-blot were previously detailed (19). IRDye

secondary antibodies (LI-COR Biosciences) were used for protein detection and digital fluorescence was visualized by an Odyssey CLX system (LI-COR Biosciences). Immunoblot quantification was performed following analysis of protein signal by Image Studio® software.

Transmission Electron Microscopy (TEM)

lEV and sEV were fixed for 16 h at 4°C with 2.5% glutaraldehyde (LFG Distribution, Lyon, France) in 0.1 M Sorensen buffer pH 7.4 then deposited on formwar-coated copper grids and negatively stained with phosphotungstic acid 1% (w/v) for 30 seconds. Grids were rinsed with milliQ water, let to air dry and observed with a Jeol JEM 1400 microscope (Jeol, France) operated at 120 KeV.

Lipidomic analyses

All lipidomics analyses were performed on the ICANalytics platform (IHU ICAN, Paris, France). EV lipidomics data originated from 2 independent batches (n=10 lean and n=8 obese), whereas tissue and plasma lipidomics data originated from one batch only (n=4-5 obese, n=4-5 lean). In order to adjust for batch effect in EV, data were combined using a relative difference method with Multi Experiment Viewer (MeV) software version 4.9 (https://sourceforge.net/projects/mev-tm4/) (25). Delta was calculated between the comparison group, and the subsequent relative values were processed for the statistical analysis.

Tissue homogenization. VAT were weighted and supplemented with isopropanol to a final concentration of 80mg/mL. Tissues were homogenized using ceramic beads and the “soft” program of the Precellys Evolution instrument (Bertin Instruments, France).

Lipid extraction. Lipids were extracted from 10µl platelet-free plasma, 50µl EV or 4mg VAT lysate using a modified Bligh and Dyer method. Samples were supplemented with deuterated or odd chain internal standards (CE(18:1d7), cholesterol d7, cer(d18 :1/24 :0d7), LPC(17:1), LPE(18:1d7), PA(15:0/18:1d7), PC(16:0/16:0d9), PC(15:0/18:1d7), PE(15:0/18:1d7), PG(15:0/18:1d7), PI(17:0/20:4), PS(16:0/18:1d31), SM(d18:1/16:0d31), TAG(17:0/17:1/17:0 d5), DG(15:0/18:1d7) from Avanti Polar Lipids) serving for quantification of the endogenous lipid species. Lipids were extracted with 1.2mL methanol/CHCl3 (2:1 v/v) in the presence of the antioxidant BHT and 310µl HCl 0.005N. Phase separation was triggered by addition of 400µl $CHCl_3$ and 400µl

water, followed by a centrifugation 3,600 *xg* for 10min at 4°C. The organic phase was harvested, was dried and then resuspended in 40µl of LC/MS solvent (Chloroform/acetonitrile/Isopropanol (80:19:1 v/v/v)). A control plasma was extracted in parallel and injected every 10 samples to correct for signal drift.

LC-MS/MS analysis of phospholipids and sphingolipids. Lipids were quantified by LC-ESI/MS/MS using a prominence UFLC and a QTrap 4000 mass spectrometer. Sample (4µl) was injected to a kinetex HILIC 2.6µm 2.1x150mm column. Mobile phases consisted of water and acetonitrile containing 30mM ammonium acetate and 0.2% acetic acid. Lipid species were detected using scheduled multiple reaction monitoring (sMRM) in the positive-ion mode reflecting the headgroup fragmentation of each lipid class.

LC-MS/MS analysis of neutral lipids (CE, FC, DAG and TAG). Sample (4µl) was injected to an Ascentis C18 2.7µm 2.1x150mm column. Mobile phases consisted of A (acetonitrile/water(60:40)) and B (isopropanol/acetonitrile (90:10)) in the presence of ammonium formate and formic acid. Lipid species were detected using sMRM in the positive-ion mode reflecting the neutral loss of (RCOO + NH3) for DAG and TAG, the product ion scan of m/z 369 (cholesterol – H_2O) for CE and FC.

Structural elucidation. Structural determination of major PL (PC, PE, PI) chains presented in Table S2 was performed by LC–MS/MS using reversed-phase separation on a Symmetry shield RP8 50 mm × 2.1 mm, 3.5 µm column (Waters Corporation, Milford, MA, USA) as previously described (26) and negative ionization using precursor ion scans of FA chains.

Data processing. An in-house developed R script was used to correct for isotopic contribution on MRM signals from HILIC injections. Features with over 80% missing values were discarded, missing values of the remaining features were imputed using the KNN approach on the MetaboAnalyst open source software. Lipid features whose variability exceeded 30% in the quality controls were removed.

Lipid amounts were expressed as mole percent of total lipids, except for the plasma lipid data that were given in nmol/µl of plasma to allow full comparison with previous reports (27, 28). Such relative quantification presents the advantage to overcome any uncertainties relative to the measurement of protein concentrations from different sample type and exclude any bias relative to the impact of adipocyte hypertrophia on protein content.

Lipid nomenclature. Lipids are abbreviated as follow: Neutral lipids (NL) – cholesteryl

ester (CE), diacylglyceride (DAG), triacylglyceride (TAG); free cholesterol (FC); sphingolipids (SL) – ceramide (Cer), dihydroceramide (DHC), sphingomyelin (SM); Phospholipids (PL) – phosphatitic acid (PA), phosphatidylcholine (PC), phosphatidylethanolamine (PE), phosphatidylglycerol (PG), phosphatidylinositol (PI), phosphatidylserine (PS) and the lyso (L) species (LPC and LPE). Plasmalogenlinkages are denoted by p- (ex : PEp).

The side-chain structures are denoted as “carbon chain length:number of double bonds” and are provided for each chain where they could be determined, or as a total number of all carbons and double bonds where individual chains could not be determined.

***Statistical analysis**.*

Comparison of sample types (plasma, EV subtypes and VAT) and sample groups (lean or obese) were run using paired Wilcoxon, Mann-Whitney-test. Pairing was either sample driven (lEV and sEV from the same mice) or batch driven (lean and obese samples from the same collection date). In order to overcome the batch effects between two studies, we used a Relative difference (RD) calculation strategy, where we calculated the RD between the subject groups within a batch by transforming them into an expression value using MeV software version 4.9 (https://sourceforge.net/projects/mev-tm4/) (25). The outcome of the analysis produces a transformed RD data with log2-fold change values that corresponds to the differences between the given subjects, notified as ‘vs’ (for versus) in the legends.

Hierarchical clustering tree (HCL heatmap) were produced from clustered normalized mean-center data using complete linkage over the features using Pearson correlation distance matrix. Features were considered significant when the p-value was below 0.05 after Benjamini-Hochberg correction controlled for false discovery rate (FDR) (29).

Results

Lipidomic analysis of *obese* mice plasma reflects common lipid alterations associated with obesity

In order to perform comparative lipidomic analysis between the obese and lean state independent of changes in dietary lipid sources, we investigated the leptin-deficient (*ob*/*ob*) mouse which develops obesity on standard chow diet due to spontaneous hyperphagia, but does not require feeding on a high fat diet. We used a complex lipid profiling method based on LC-ESI$^+$-MS/MS analysis that combine HILIC LC separation mode with scheduled multiple reaction monitoring (sMRM) to assess plasma levels of different lipid classes, including phospholipids, sphingolipids and sterols, which have been shown to act as biomarkers or active contributors of obesity-associated metabolic complications (30, 31). Prominent increases in PC, LPC, PI, SM, Cer as well as cholesterol esters and free cholesterol were observed in *ob/ob* mice (Figure 1A-C). These alterations also impacted specifically some other lipid subspecies providing a lipid fingerprint of *ob/ob* mice plasma (Table S3). Our results are in agreement with previous lipidomic analysis performed on *ob/ob* mice plasma that highlighted specific increase in sphingolipids (especially Cer and SM), cholesterol esters and PC subspecies as a hallmark of obesity (27, 28).

Fatty acid distribution on the most abundant phospholipids classes (PC, PE, PI) was elucidated using negative ion mode LC-MS/MS. Fatty acid distribution of minor phospholipids (PS, PG, PA) was extrapolated from these data and from the literature (32) (see Methods and Table S2). This revealed an increase in total lipids containing 18 carbon atoms including stearic acid (C18:0) and oleic acid (C18:1), at the expense of palmitoleic acid (C16:1) (Figure 1D). Besides, a significant increase in arachidonic acid (20:4), mainly retrieved in plasma under its omega 6 form (32), and in docosahexaenoic acid (22:6), the final product of omega-3 fatty acid elongation and desaturation, was also observed likely reflecting higher uptake of essential fatty acids through diet by hyperphagic *ob/ob* mice (31). By this mean, we noticed that plasma lipids from *ob/ob* mice are overall enriched in saturated fatty acids (SFA) and polyunsaturated fatty acids (PUFA) compared to lean controls (Figure 1E).

Altogether, plasma lipid profiling of *ob/ob* mice confirmed circulating lipid biomarkers of obesity. Significantly altered lipid moieties in obese mice plasma recapitulated global

obesity-related changes in human plasma lipidome (30, 33-35), reinforcing the relevance of using the *ob/ob* mice as a preclinical model of obesity.

Obesity impacts adipose tissue lipidome, paralleling plasma lipid alterations

We next investigated the lipid content of VAT collected from 3-month lean and genetically obese mice, that will be further use to produce VAT-derived EV. We provided a comprehensive profiling of the VAT lipidome including phospholipids, sphingolipids, neutral lipids (TAG, DAG) and cholesterol (FC and CE). A total of 354 lipid species were scanned, among which 265 passed the quality control and were subsequently quantified. Based on calibration with internal standards, data were normalized either to total lipid quantified (including neutral lipids) or to total membranous lipids (SL plus PL) and expressed as mol% to investigate the relative changes of AT lipid composition between lean and obese mice.

As expected, the vast majority of lipids in VAT samples were TAG – the lipid form of AT energy stores - reaching 90% of all identified lipids regardless of metabolic condition (Figure 2A). DAG, which is associated with TAG turnover, represented only minor neutral lipid stores (<8%), whereas only traces of CE were detected (0.01%). Besides neutral lipids, other lipids accounted for only 3% of total lipids and mainly included phospholipids and free cholesterol (FC), as well as sphingolipids in smaller proportions. Among phospholipids, PC and PE were the most abundant classes thereby providing the majority of membrane lipids within adipose cell. To explore how obesity context affected the sphingophospholipidome of VAT, we assessed the relative differences of lipid species between lean and obese VAT (Figure 2B). By this mean, we observed significant enrichment of obese VAT in total PG and PI, reflecting respectively higher content of the predominant PG(34:1) and PI(38:4) lipid species in VAT (Figure S1). Conversely, total LPE and PE plasmalogens (PEp) were significantly decreased in *ob/ob* VAT (Figure 2B).

Structural elucidation of membranous lipids on VAT samples revealed a significant increase in C18:0 acyl chains containing lipids, at the expense of C18:2 containing lipids, and a trend to an elevation of polyunsaturated lipids (number of total double bounds>4) (Figure 2C). These lipid enrichments parallel lipid disturbances observed in *ob/ob* mice plasma (see Figure 1D-E), in agreement with the primary lipid storage function of VAT.

Overall, we demonstrated distinct lipidomic profile between lean and obese VAT mirroring the changes in plasma lipidome.

AdEV subtypes secretion is enhanced with obesity

In order to isolate AdEV subtypes from secreted VAT explants collected from lean and obese mice, we implemented a culture system using Clinicell® cassettes, allowing optimal gaz/air exchanges ensuring the full viability of VAT explants (23) (Figure 3A). EV isolation was done from 48h-serum free VAT explant conditioned media using differential (ultra)centrifugation (respectively 13 000 x*g* for lEV and 100 000 x*g* for sEV). TEM imaging on VAT-derived AdEV confirmed the successful isolation of large vesicles surrounded by a kind of matrix layer, by comparison to smaller electron-dense vesicles homogenous in size (Figure 3B). Larger size for lean lEV compared to lean sEV was quantified by NTA measurements, whereas size of AdEV subtypes isolated from obese VAT are very dispersed rendering size differences between obese sEV and obese lEV unsignificant (Figure 3C). Obese lEV concentrations were moreover significantly higher than lean lEV (Figure 3D). A trend towards higher concentrations of obese sEV by comparison to lean sEV was also observed, in agreement with the highly concentrated AdEV productions previously described from high-fat diet mice (5, 14). Biochemical analysis of AdEV subpopulations demonstrated specific enrichment of tetraspanins (CD9, CD63) in sEV by comparison to lEV or secreting VAT (Figure 3E). Conversely, flottilin-2 or Grp94, that we previously identified as specific markers of 3T3-L1 adipocyte-derived lEV (19), were specifically enriched VAT-derived lEV (Figure 3E). No perilipin-1 signal was retrieved in any AdEV preparations suggesting absence of lipid droplet containing vesicles (Figure 3E).

Enrichment of various lipid species in AdEV compared to source VAT illustrates specific EV lipid sorting

Qualitative comparisons between AdEV and VAT lipidomic datasets by principal component analysis (PCA) showed that AdEV segregated from source VAT along the first principal component (PC1) which explained nearly 70% of the variance (Figure 4A). AdEV or VAT separated along PC2 according to the metabolic context (Figure 4A). This highlighted active specific sorting of lipids by VAT-derived EV secretion. Of note, sEV and lEV overlapped in the lean or in the obese context illustrating that AdEV

lipid composition was mainly driven by the metabolic context rather than by AdEV subcellular origin.

Global lipid composition changes between AdEV and VAT mainly related to VAT enrichment in glycerolipids (TAG and DAG) whereas phospholipids and cholesterol were abundantly retrieved in AdEV subtypes, in agreement with their membranous origin (Figure 4B). Thus, data were subsequently expressed as mole % of total PL and SL to focus on membrane lipids. This revealed a significant enrichment in Cer, DHC and PG lipid classes for both sEV and lEV versus lean VAT (Figure 4C-F). Conversely, PI and PE were significantly depleted from lean lEV, with a similar trend observed for lean sEV, by comparison to lean VAT phospholipidome (Figure 4C-D). Similar depletions were observed for obese sEV and lEV compared to source obese VAT (Figure 4E-F). Noticeably, AdEV enrichment in SM by comparison to source VAT was observed in obese samples (Figure 4E-F).

We next investigated specific lipid species either significantly enriched (Figure 4G and Table S4) or depleted (Figure 4F and Table S5) in AdEV subtypes by comparison to source VAT. Sixteen lipid species were found commonly enriched in AdEV, independently of AdEV subtype or metabolic context, which included 11 Cer and 4 PC subspecies as well as PG(36:4) (Figure 4G). By contrast, 17 lipid species commonly depleted in AdEV compared to VAT were identified that included 8 PE subspecies, 8 PC subspecies and PS(40:6) (Figure 4H).

Altogether, compared to source VAT, overall AdEV lipid composition pointed to Cer, DHC and PG enrichment and selective SM accumulation in obesity. Lipid species commonly enriched in AdEV, independently of the pathophysiological state, moreover revealed the selective lipid sorting of Cer subspecies, including DHC, and PG(36:4) as well as some specific PC lipid subspecies. Overall, these lipids represent tracers of AdEV lipid transport and relevant candidates for lipid-associated AdEV mediated signaling in target cells.

Lipid fingerprints differentiate VAT-derived EV subtypes

We next studied how AdEV lipidome is influenced by EV subtype. Comparison of the relative distribution of all lipid classes screened between lEV and sEV highlighted a striking enrichment of TAG in large vesicles by comparison to smaller ones (Figure 5A-B), but no significant changes were observed in CE or DAG content of lEV and sEV (Figure 5B). Alternatively, sEV displayed a specific FC enrichment compared to lEV,

whatever the metabolic status considered (Figure 5C). Among phospholipids, we demonstrated enrichment of lEV in total PC and total LPC, two major structural membrane lipids, as well as in total DHC (Figure 5D-E). At individual species resolution, lean lEV were specifically enriched in short LPC and 34:1 lipid subspecies (PC, PE, PG and SM) and depleted in long polyunsaturated phospholipids over almost all classes (Figure S2).

Obesity impacted similarly lEV and sEV by favoring total PI and PC and by increasing the amount of AdEV-associated major PG(34:1) (Figure S3-S4), partly mirroring obesity-associated lipid changes previously observed in VAT (Figure 2B). Significant total SM and/or SM subspecies enrichment was moreover observed for all AdEV subtypes isolated from obese VAT by comparison to AdEV derived from lean animals, whereas Cer-associated AdEV were by contrast decreased in obesity context (Figure S3 and S4C-D). These similar lipid profiles changes in AdEV subtypes are in agreement with the lack of size differences observed between lEV and sEV when isolated from obese VAT (Figure 3C). These data therefore illustrated that AdEV lipidome is strongly influenced by source VAT, and that isolation of EV subtypes based on vesicle size, for lipidomic studies, is irrelevant in the context of obesity.

Finally, lipid structural elucidation allowed us to pinpoint common altered AdEV lipid species alterations with obesity. We therefore highlighted enrichment of AdEV subtypes isolated from obese VAT in arachidonic acid (20:4)-containing species including 36:4 (PI and PE), 38:4 (PI, PC, PE, PEp) and 38:5 (PI and PE) species (Figure S3 and S4E-F**).** We moreover demonstrated significant enrichment of 18:1-containing species as for LPC(18:1), PG(34:1), PC(34:1) and PC(36:1) in AdEV subtypes derived from obese VAT, at the expense of short and saturated palmitic-containing species as for 32:0 and 34:0 phospholipids (Figures S3 and S4). This translated into a trend for decreased total saturated fatty acid (SFA) in obese lEV and sEV, favoring obese VAT-derived AdEV PUFA enrichment (Figure 5F). Finally, among PE plasmalogens, that are known to display antioxidant properties, we found five species commonly depleted in obese lEV and sEV (PE(16:0p/18:2) PE(18:0p/18:1) PE(18:0p/18:2) PE(18:0p/20:4) PE(18:0p/20:5)) (Figure S3), reflecting significant PEp decrease in source obese VAT (Figure 2B) which may favor adipose oxidative stress.

Discussion

This study aimed to define lipid fingerprints of AdEV subtypes isolated from lean and genetically obese (*ob/ob*) mice in order to determine the signaling capacity of AdEV-transported lipid species in obesity-related complications. We provide here comprehensive lipid maps revealing specific adipose EV lipid sorting when compared to secreting VAT. We demonstrated that the EV lipidome is highly influenced by the pathophysiological state of VAT and identified some specific AdEV lipid classes and species closely related to obesity status. Notably, we suggest that AdEV lipid subspecies enrichment may contribute to the development of metabolic dysfunctions associated with obesity.

Our comparative analysis between source VAT and secreted AdEV revealed distinct lipidomic profiles between both sample types. As expected, AdEV are preferentially composed of membranous lipids in line with their biogenesis. According to PCA, AdEV lipid composition appeared to be much more influenced by the metabolic status (lean or obese) rather than the EV subtype (lEV or sEV). Thus, although major differences in protein contents were reported among EV subtypes, we highlight here an overall stability of the lipid composition of large versus small EV. Moreover, EV subtype distinction based on EV size (large or small) appeared of minor relevance in the obese context. Nonetheless, separation of lEV from sEV from lean VAT allowed us to pinpoint specific lipid features of each EV subtype that might be of particular relevance, especially cholesterol enrichment in sEV, a feature that we already highlighted in sEV isolated from 3T3-L1 adipocytes (19). TAG were found enriched in large EV preparations. These apolar lipids are likely to be localized within the core of the vesicles as reported in a recent study identifying adipocyte-derived EV as neutral lipid-filled vesicles (13). However, it is noteworthy that TAG-enrichment of large vesicles is limited enough to allow particle sedimentation by centrifugation. The absence of perilipin-1 (a specific marker of adipose lipid droplets) argues against EV-based extrusion of lipid droplet organelles, and would rather suggest a TAG-lEV loading which may be interconnected to lysosome-mediated lipid droplet degradation.

Besides these specific EV subtype lipid traits, some EV-lipid enrichments are common to both EV subtypes. We therefore revealed specific sphingolipid (SM, Cer, DHC), LPC and PG AdEV enrichment. Increased relative proportion of cholesterol, Cer and SM

have already been measured in different types of EV, and would be related to the involvement of these lipids in EV biogenesis (10, 36, 37). This type of lipid enrichment may contribute to increase the rigidity of sEV (38), provide higher sEV membrane order degree (39) and increase sEV resistance to non-ionic detergents (40) as it is the case for lipid raft membrane microdomains. Such lipid composition certainly confers an advantage for the stability of these EV in biological fluids and/or their binding or uptake by recipient cells (41).

Conversely, we observed relative decrease of PE and PI in AdEV compared to source VAT, particularly in obese lEV. Such depletion has been previously observed in EV isolated from different cell sources, and was partially compensated by PS sEV enrichment (10). However, it remains unclear how this can impact EV structure since PE and PI are in minority compared to PC EV proportions, whose EV content is moreover enhanced with obesity.

Obesity-associated circulating lipid alterations translated at the level of organs, particularly AT or liver. AT lipidome of diet-induced obese mice is featured by a significant increase in longer and more unsaturated TAG and PL species and characterized by accumulation of lipids made of acyl chains containing 18 carbons (42). Similarly, lipidomic analysis performed on AT from twin pairs discordant for obesity showed that membrane lipids containing longer and more unsaturated fatty acids were more abundant in the obese by comparison to the lean individuals (34). We indeed observed elevated PUFA and C:18 fatty acid increase in plasma, VAT and AdEV suggesting overall lipid equilibrium between plasma, VAT and VAT-derived AdEV.

Besides these overall lipid alterations, numerous studies have pinpointed sphingomyelin metabolites as signaling molecules of pathological biological events related to metabolic dysfunction and identified significant correlations between circulating Cer and DHC as biomarkers of the development of T2D in obese patients (43, 44). In accordance with this hypothesis, we also found elevated plasma Cer levels in obese animals. However, a surprising finding from our study was the relative decrease in ceramides in AdEV derived from obese mice, despite AdEV Cer enrichment with regard to source VAT. Nonetheless, our data are in line with the previously reported increased ceramidases activities and the associated decreased ceramide levels in VAT from *ob/ob* mice (27). Whereas adipose ceramides have been

shown to be critical for driving AT remodeling and controlling whole-body energy expenditure and nutrient metabolism (45), our results suggest that the source of elevated circulating ceramides in obesity is likely to be of hepatic origin. Further studies are warranted to establish whether the defect of sphingolipid metabolism in AT observed in *ob/ob* mice is also present in humans.

The study identified AdEV lipid mediators as potential signaling molecules to explain the pathophysiological responses mediated by AdEV isolated from obese VAT (5, 6). As previously demonstrated for proteins and genetic material, AdEV displayed specific lipid fingerprints indicative of oriented EV lipid sorting. We highlighted some specific lipid enrichment of particular relevance in obese VAT-derived AdEV, which can relay metabolic alterations. Particularly, we demonstrated enrichment of AdEV subtypes isolated from obese VAT in arachidonic acid (20:4)-containing species, which are known to mediate inflammatory signaling notably through the production of prostaglandins, thromboxanes, leukotrienes and lipoxins. Their production is mainly mediated through the action of PLA2, which allows the release of different PUFA from membrane PL.

Therefore, these signaling lipids may be either carried from the parental cells or directly generated within EV, since exosomal activable PLA2 have been detected in exosomes from the mast cell line RBL-2H3 (46). PLA2 from the extracellular milieu may also act on phospholipid EV, as previously described for secreted PLA2-IIA present in inflammatory fluids which acted in concert with EV-associated platelet-type 12-lipoxygenase to generate autonomously 12(S)-hydroxyeicosatetranoic acid within EV (47). EV-associated PLA2 may also contribute to raise EV-LPC content which may serve as a substrate for autotaxin-bound EV therefore contributing to raise the bioactive lipid lysophosphatidic acid (LPA) (48). Knowing the lipogenic, anti-lipolytic and inflammatory role of PLA2-downstream mediators in obesity (49), our data confirm the potential interest of considering EV eicosanoid content to be informative of the metabolic status (i.e. healthy vs obese) (12).

PG subspecies were also found enriched in AdEV from obese mice, reflecting PG lipid class relative accumulation in obese VAT. PG are specific mitochondrial phospholipids, precursors of cardiolipins. Previous studies revealed that PG serum concentration in obese patients was the lipid class (among other blood phospholipids) that was

predominantly and positively associated with body mass index and with AT inflammation (50). Importantly, serum PG levels sharply declined after metabolic improvement following weight loss either induced by nutritional intervention or bariatric surgery in patients with obesity (51). PG are poorly investigated in most of lipidomics studies, but cardiolipins have been shown to be markedly enriched in sEV from different cell sources (10). Whereas PG can act as lipid mediators notably favoring adipose lipid storage (50), PG enrichment might also be related to the presence of mitochondria within EV, recently defined as mitovesicles (52). A recent study evidenced intercellular mitochondria transfer between adipocytes and macrophages in VAT as a mechanism of immunometabolic crosstalk that regulates metabolic homeostasis and which is impaired in obesity (53) . Whether PG AdEV content reflects this mitochondrial extrusion will be need further investigations.

Finally, we found a significant depletion of PE plasmalogens (PEp) in AdEV isolated from *ob/ob* animals as well as in obese VAT. Although these vinyl ether-bound lipids are widespread in all tissues and can represent up to 18% of the total phospholipid mass in humans, their physiological function remains poorly understood (54). PEp have been previously found enriched in EV from platelets (55) and constitute more than half of nematode EV lipid content increasing EV membrane rigidity (56). Interestingly, external addition of an ether lipid precursor to human prostate cancer PC-3 cells to increase cellular ether lipids was found to be associated with changes inthe release and composition of exosomes (57). Plasmalogens have been shown to be involved in membrane trafficking and cell signaling, and display some cellular antioxidants properties (54). Atomistic molecular dynamics simulations demonstrated that PEp contribute to form more compressed, thicker and rigid lipid bilayers (58). Future studies are needed to investigate how EV-associated PEp influence their biophysical and biological properties.

To summarize, we identified specific lipid fingerprints for plasma, VAT and AdEV that are informative of the metabolic status and revealed the potential signaling capacity of lipid species transported by AdEV in obesity-related metabolic complications. These findings open some interesting clinical perspective to develop new biomarkers and or drug targets in the obesity context.

Conflict of Interest statement

There are no conflicts of interest to declare.

Data availability statement

Data are available on request.

Acknowledgments

SLL' financial supports are Société Francophone du Diabète, la fondation d'entreprise Genavie, INSERM. AB is granted by a PhD allocation from INSERM/Région Pays de la Loire. We thank the SCIAM facility, especially F.Manero, for technical assistance for electron microscopy imaging.

Author contributions

Methodology, AB, GH, MP, ID, ML, SLL ; Experimentation and analysis, AB, GH, MP, SD, ML, SLL ; writing-original draft preparation, AB, MP, ML, SLL ; review and edition of the manuscript, AB, GH, MP, SD, ID, BC, ML and SLL; conceptualization, AB, SLL; supervision, project administration and funding acquisition, SLL.

All authors have read and agreed to the published version of the manuscript.

Bibliography

1. Hartwig S, De Filippo E, Goddeke S, Knebel B, Kotzka J, Al-Hasani H, et al. Exosomal proteins constitute an essential part of the human adipose tissue secretome. Biochim Biophys Acta Proteins Proteom. 2019;1867(12):140172.
2. Rome S, Blandin A, Le Lay S. Adipocyte-Derived Extracellular Vesicles: State of the Art. Int J Mol Sci. 2021;22(4).
3. Amosse J, Durcin M, Malloci M, Vergori L, Fleury A, Gagnadoux F, et al. Phenotyping of circulating extracellular vesicles (EVs) in obesity identifies large EVs as functional conveyors of Macrophage Migration Inhibitory Factor. Mol Metab. 2018;18:134-42.
4. Freeman DW, Noren Hooten N, Eitan E, Green J, Mode NA, Bodogai M, et al. Altered Extracellular Vesicle Concentration, Cargo and Function in Diabetes Mellitus. Diabetes. 2018.
5. Deng ZB, Poliakov A, Hardy RW, Clements R, Liu C, Liu Y, et al. Adipose tissue exosome-like vesicles mediate activation of macrophage-induced insulin resistance. Diabetes. 2009;58(11):2498-505.
6. Ying W, Riopel M, Bandyopadhyay G, Dong Y, Birmingham A, Seo JB, et al. Adipose Tissue Macrophage-Derived Exosomal miRNAs Can Modulate In Vivo and In Vitro Insulin Sensitivity. Cell. 2017;171(2):372-84 e12.
7. Thomou T, Mori MA, Dreyfuss JM, Konishi M, Sakaguchi M, Wolfrum C, et al. Adipose-derived circulating miRNAs regulate gene expression in other tissues. Nature. 2017;542(7642):450-5.
8. Petersen MC, Shulman GI. Roles of Diacylglycerols and Ceramides in Hepatic Insulin Resistance. Trends Pharmacol Sci. 2017;38(7):649-65.
9. Kitessa SM, Abeywardena MY. Lipid-Induced Insulin Resistance in Skeletal Muscle: The Chase for the Culprit Goes from Total Intramuscular Fat to Lipid Intermediates, and Finally to Species of Lipid Intermediates. Nutrients. 2016;8(8).
10. Haraszti RA, Didiot MC, Sapp E, Leszyk J, Shaffer SA, Rockwell HE, et al. High-resolution proteomic and lipidomic analysis of exosomes and microvesicles from different cell sources. Journal of extracellular vesicles. 2016;5:32570.
11. Skotland T, Sandvig K, Llorente A. Lipids in exosomes: Current knowledge and the way forward. Prog Lipid Res. 2017;66:30-41.
12. Record M, Silvente-Poirot S, Poirot M, Wakelam MJO. Extracellular vesicles: lipids as key components of their biogenesis and functions. J Lipid Res. 2018;59(8):1316-24.
13. Flaherty SE, 3rd, Grijalva A, Xu X, Ables E, Nomani A, Ferrante AW, Jr. A lipase-independent pathway of lipid release and immune modulation by adipocytes. Science. 2019;363(6430):989-93.
14. Clement E, Lazar I, Attane C, Carrie L, Dauvillier S, Ducoux-Petit M, et al. Adipocyte extracellular vesicles carry enzymes and fatty acids that stimulate mitochondrial metabolism and remodeling in tumor cells. EMBO J. 2020;39(3):e102525.
15. Fukushima M, Dasgupta D, Mauer AS, Kakazu E, Nakao K, Malhi H. StAR-related lipid transfer domain 11 (STARD11)-mediated ceramide transport mediates extracellular vesicle biogenesis. J Biol Chem. 2018;293(39):15277-89.
16. Obata Y, Kita S, Koyama Y, Fukuda S, Takeda H, Takahashi M, et al. Adiponectin/T-cadherin system enhances exosome biogenesis and decreases cellular ceramides by exosomal release. JCI Insight. 2018;3(8).

17. Aswad H, Forterre A, Wiklander OP, Vial G, Danty-Berger E, Jalabert A, et al. Exosomes participate in the alteration of muscle homeostasis during lipid-induced insulin resistance in mice. Diabetologia. 2014;57(10):2155-64.
18. Hirsova P, Ibrahim SH, Krishnan A, Verma VK, Bronk SF, Werneburg NW, et al. Lipid-Induced Signaling Causes Release of Inflammatory Extracellular Vesicles From Hepatocytes. Gastroenterology. 2016;150(4):956-67.
19. Durcin M, Fleury A, Taillebois E, Hilairet G, Krupova Z, Henry C, et al. Characterisation of adipocyte-derived extracellular vesicle subtypes identifies distinct protein and lipid signatures for large and small extracellular vesicles. Journal of extracellular vesicles. 2017;6(1):1305677.
20. Connolly KD, Guschina IA, Yeung V, Clayton A, Draman MS, Von Ruhland C, et al. Characterisation of adipocyte-derived extracellular vesicles released pre- and post-adipogenesis. Journal of extracellular vesicles. 2015;4:29159.
21. Bestard-Escalas J, Maimo-Barcelo A, Lopez DH, Reigada R, Guardiola-Serrano F, Ramos-Vivas J, et al. Common and Differential Traits of the Membrane Lipidome of Colon Cancer Cell Lines and their Secreted Vesicles: Impact on Studies Using Cell Lines. Cancers (Basel). 2020;12(5).
22. Gonzalez-Granillo M, Helguero LA, Alves E, Archer A, Savva C, Pedrelli M, et al. Sex-specific lipid molecular signatures in obesity-associated metabolic dysfunctions revealed by lipidomic characterization in ob/ob mouse. Biol Sex Differ. 2019;10(1):11.
23. Decaunes P, Bouloumié A, Ryden M, Galitzky J. Ex vivo Analysis of Lipolysis in Human Subcutaneous Adipose Tissue Explants. Bio-protocol. 2018;8(3):e2711.
24. Consortium E-T, Van Deun J, Mestdagh P, Agostinis P, Akay O, Anand S, et al. EV-TRACK: transparent reporting and centralizing knowledge in extracellular vesicle research. Nat Methods. 2017;14(3):228-32.
25. Saeed AI, Sharov V, White J, Li J, Liang W, Bhagabati N, et al. TM4: a free, open-source system for microarray data management and analysis. Biotechniques. 2003;34(2):374-8.
26. Camont L, Lhomme M, Rached F, Le Goff W, Negre-Salvayre A, Salvayre R, et al. Small, dense high-density lipoprotein-3 particles are enriched in negatively charged phospholipids: relevance to cellular cholesterol efflux, antioxidative, antithrombotic, anti-inflammatory, and antiapoptotic functionalities. Arterioscler Thromb Vasc Biol. 2013;33(12):2715-23.
27. Samad F, Hester KD, Yang G, Hannun YA, Bielawski J. Altered adipose and plasma sphingolipid metabolism in obesity: a potential mechanism for cardiovascular and metabolic risk. Diabetes. 2006;55(9):2579-87.
28. Giesbertz P, Padberg I, Rein D, Ecker J, Hofle AS, Spanier B, et al. Metabolite profiling in plasma and tissues of ob/ob and db/db mice identifies novel markers of obesity and type 2 diabetes. Diabetologia. 2015;58(9):2133-43.
29. Benjamini Y, Hochberg Y. Controlling the False Discovery Rate: A Practical and Powerful Approach to Multiple Testing. Journal of the Royal Statistical Society Series B (Methodological). 1995;57(1):289-300.
30. Yin X, Willinger CM, Keefe J, Liu J, Fernandez-Ortiz A, Ibanez B, et al. Lipidomic profiling identifies signatures of metabolic risk. EBioMedicine. 2020;51:102520.
31. Sigruener A, Kleber ME, Heimerl S, Liebisch G, Schmitz G, Maerz W. Glycerophospholipid and sphingolipid species and mortality: the Ludwigshafen Risk and Cardiovascular Health (LURIC) study. PLoS One. 2014;9(1):e85724.
32. Quehenberger O, Armando AM, Brown AH, Milne SB, Myers DS, Merrill AH, et al. Lipidomics reveals a remarkable diversity of lipids in human plasma. J Lipid Res. 2010;51(11):3299-305.

33. Piko P, Pal L, Szucs S, Kosa Z, Sandor J, Adany R. Obesity-Related Changes in Human Plasma Lipidome Determined by the Lipidyzer Platform. Biomolecules. 2021;11(2).
34. Pietilainen KH, Rog T, Seppanen-Laakso T, Virtue S, Gopalacharyulu P, Tang J, et al. Association of lipidome remodeling in the adipocyte membrane with acquired obesity in humans. PLoS Biol. 2011;9(6):e1000623.
35. Rauschert S, Uhl O, Koletzko B, Kirchberg F, Mori TA, Huang RC, et al. Lipidomics Reveals Associations of Phospholipids With Obesity and InsulinResistance in Young Adults. J Clin Endocrinol Metab. 2016;101(3):871-9.
36. Trajkovic K, Hsu C, Chiantia S, Rajendran L, Wenzel D, Wieland F, et al. Ceramide triggers budding of exosome vesicles into multivesicular endosomes. Science. 2008;319(5867):1244-7.
37. Skotland T, Hessvik NP, Sandvig K, Llorente A. Exosomal lipid composition and the role of ether lipids and phosphoinositides in exosome biology. J Lipid Res. 2019;60(1):9-18.
38. Laulagnier K, Motta C, Hamdi S, Roy S, Fauvelle F, Pageaux JF, et al. Mast cell- and dendritic cell-derived exosomes display a specific lipid composition and an unusual membrane organization. Biochem J. 2004;380(Pt 1):161-71.
39. Osteikoetxea X, Balogh A, Szabo-Taylor K, Nemeth A, Szabo TG, Paloczi K, et al. Improved characterization of EV preparations based on protein to lipid ratio and lipid properties. PLoS One. 2015;10(3):e0121184.
40. Osteikoetxea X, Sodar B, Nemeth A, Szabo-Taylor K, Paloczi K, Vukman KV, et al. Differential detergent sensitivity of extracellular vesicle subpopulations. Org Biomol Chem. 2015;13(38):9775-82.
41. Skotland T, Sagini K, Sandvig K, Llorente A. An emerging focus on lipids in extracellular vesicles. Advanced drug delivery reviews. 2020;159:308-21.
42. Grzybek M, Palladini A, Alexaki VI, Surma MA, Simons K, Chavakis T, et al. Comprehensive and quantitative analysis of white and brown adipose tissue by shotgun lipidomics. Mol Metab. 2019;22:12-20.
43. Chew WS, Torta F, Ji S, Choi H, Begum H, Sim X, et al. Large-scale lipidomics identifies associations between plasma sphingolipids and T2DM incidence. JCI Insight. 2019;5.
44. Wigger L, Cruciani-Guglielmacci C, Nicolas A, Denom J, Fernandez N, Fumeron F, et al. Plasma Dihydroceramides Are Diabetes Susceptibility Biomarker Candidates in Mice and Humans. Cell reports. 2017;18(9):2269-79.
45. Chaurasia B, Kaddai VA, Lancaster GI, Henstridge DC, Sriram S, Galam DL, et al. Adipocyte Ceramides Regulate Subcutaneous Adipose Browning, Inflammation, and Metabolism. Cell Metab. 2016;24(6):820-34.
46. Subra C, Grand D, Laulagnier K, Stella A, Lambeau G, Paillasse M, et al. Exosomes account for vesicle-mediated transcellular transport of activatable phospholipases and prostaglandins. J Lipid Res. 2010;51(8):2105-20.
47. Duchez AC, Boudreau LH, Naika GS, Bollinger J, Belleannee C, Cloutier N, et al. Platelet microparticles are internalized in neutrophils via the concerted activity of 12-lipoxygenase and secreted phospholipase A2-IIA. Proc Natl Acad Sci U S A. 2015;112(27):E3564-73.
48. Jethwa SA, Leah EJ, Zhang Q, Bright NA, Oxley D, Bootman MD, et al. Exosomes bind to autotaxin and act as a physiological delivery mechanism to stimulate LPA receptor signalling in cells. J Cell Sci. 2016;129(20):3948-57.
49. Abbott MJ, Tang T, Sul HS. The Role of Phospholipase A(2)-derived Mediators in Obesity. Drug Discov Today Dis Mech. 2010;7(3-4):e213-e8.

50. Kayser BD, Lhomme M, Prifti E, Da Cunha C, Marquet F, Chain F, et al. Phosphatidylglycerols are induced by gut dysbiosis and inflammation, and favorably modulate adipose tissue remodeling in obesity. FASEB J. 2019;33(4):4741-54.
51. Kayser BD, Lhomme M, Dao MC, Ichou F, Bouillot JL, Prifti E, et al. Serum lipidomics reveals early differential effects of gastric bypass compared with banding on phospholipids and sphingolipids independent of differences in weight loss. Int J Obes (Lond). 2017;41(6):917-25.
52. D'Acunzo P, Perez-Gonzalez R, Kim Y, Hargash T, Miller C, Alldred MJ, et al. Mitovesicles are a novel population of extracellular vesicles of mitochondrial origin altered in Down syndrome. Sci Adv. 2021;7(7).
53. Brestoff JR, Wilen CB, Moley JR, Li Y, Zou W, Malvin NP, et al. Intercellular Mitochondria Transfer to Macrophages Regulates White Adipose Tissue Homeostasis and Is Impaired in Obesity. Cell Metab. 2021;33(2):270-82 e8.
54. Wallner S, Schmitz G. Plasmalogens the neglected regulatory and scavenging lipid species. Chem Phys Lipids. 2011;164(6):573-89.
55. Pienimaeki-Roemer A, Ruebsaamen K, Boettcher A, Orso E, Scherer M, Liebisch G, et al. Stored platelets alter glycerophospholipid and sphingolipid species, which are differentially transferred to newly released extracellular vesicles. Transfusion. 2013;53(3):612-26.
56. Simbari F, McCaskill J, Coakley G, Millar M, Maizels RM, Fabrias G, et al. Plasmalogen enrichment in exosomes secreted by a nematode parasite versus those derived from its mouse host: implications for exosome stability and biology. Journal of extracellular vesicles. 2016;5:30741.
57. Phuyal S, Skotland T, Hessvik NP, Simolin H, Overbye A, Brech A, et al. The ether lipid precursor hexadecylglycerol stimulates the release and changes the composition of exosomes derived from PC-3 cells. J Biol Chem. 2015;290(7):4225-37.
58. Rog T, Koivuniemi A. The biophysical properties of ethanolamine plasmalogens revealed by atomistic molecular dynamics simulations. Biochim Biophys Acta. 2016;1858(1):97-103.

Figure legends

Figure 1 : Plasma lipidome in lean and obese mice

A-C. Absolute lipid composition of circulating lipid species expressed in nmol/µl plasma. Major lipid families are distinguished : phospholipids (**A**), sphingolipids (**B**) and sterols and glycerolipids (**C**). Minor and major lipids are presented on different graphs for the different families. Void bars are lean conditions, filled bars are obese conditions.

D. Fatty acid composition of plasma phospholipids based on structural elucidation of phospholipids as presented in Table S2. Lipids were regrouped according to the number of carbon atoms present in their acyl chains. Note that the 'y axis' is discontinuous.

E. Unsaturation profiles of plasma phospholipids. Phospholipids were classified as saturated (SFA), monounsaturated (MUFA) and polyunsaturated (PUFA) lipids based on structural elucidation as presented in Table S2. Lipids were regrouped according to the number of double bonds present in their acyl chains. SFA are fully saturated lipids on both chains, MUFA has at least one or 2 monounsaturated chain and no polyunsaturated chain and PUFA have at least one polyunsaturated chain out of the 2.

Results are presented as the mean ± SEM calculated from four independent samples for each metabolic state. Asterisks indicate a significant difference between lean and obese (p-value<0,05*, p<0,01**,p<0,005***, p<0,001****, non-parametric two-way ANOVA test corrected for multiple comparisons by Sidak's test).

Figure 2 : VAT lipidome in lean and obese mice

A. Pie diagram showing the relative lipid classes composition of lean and obese VAT. Besides neutral lipids, other lipids correspond to sphingolipids and phospholipids which are detailed in a sub-pie diagram. Data presented correspond to the mean amount (in mol %) respectively in lean VAT (left pie charts) and obese VAT (right pie charts) from five independent samples for each metabolic state.

B. Relative membrane lipid classes composition of VAT membrane lipids between the obese and lean state. The panel bar plots represent the difference between the mean of obese and lean in the VAT calculated from four independent samples for each

metabolic state. Asterisks indicate the lipid species that differ significantly between the two metabolic states (see methods for statistical analysis, p-value<0,05).

C-D. Total acyl chain length **(C)** and unsaturation profile **(D)** elucidated for sphingolipids and phospholipids of VAT from lean and obese mice. Lipids were grouped according to the number of carbon atoms (**C**) and the number of double bonds (**D**) present in their acyl chains. Complete acid chain length profiles are presented in Table S3 based on structural elucidation performed according to Table S2.

Results are presented as the mean ± SEM calculated from four independent samples for each metabolic state. Asterisks indicate a significant difference between lean and obese (p-value<0,05*, p<0,01**,p<0,005***, p<0,001****, non-parametric two-way ANOVA test corrected for multiple comparisons by Sidak's test).

Figure 3 : AdEV isolation and characterization

A. Schematic representation of VAT-derived EV isolation leading to AdEV subtype isolation, namely lEV and sEV

B. Transmission electron microscopy images of lEV (upper panel) and sEV (lower panel) pellets. Scale bar : 100nm.

C-D. Nanoparticle tracking analysis (NTA) of lEV and sEV populations isolated from VAT-derived conditioned media. lEV (13,000 × g pellet) and sEV (100,000 × g pellet) were collected from VAT conditioned media and resuspended in NaCl. EV mode size **(C)** and EV concentrations (expressed as EV numbers secreted by adipocyte cell) **(D)** were analyzed. No impact of obesity on EV size was observed **(C)**. Abundant EV secretion per adipocyte was observed for lEV and sEV, which is moreover significantly increased by obesity **(D)**. In total, 8 to 10 independent lEV and sEV preparations per metabolic state were analyzed by NTA. Results are presented as mean ± SEM (p-value<0,05*, p<0,01**, Wilcoxon matched pairs rank test for **C**, non-parametric two-way ANOVA test corrected for multiple comparisons by Sidak's test for **D**).

E. Western blot analysis of different EV markers in sEV and lEV preparations. Eight micrograms of VAT explant, lEV or sEV samples were migrated on a SDS-PAGE gel and analyzed by immunoblotting for the tetraspanins CD63, CD9, flotillin-2, Grp94 and perilipin-1. One representative blot for each protein is presented.

Figure 4: AdEV relative lipid composition compared to VAT

A. Principal Component Analysis (PCA) of VAT and EV lipidomes in lean and obese metabolic state. PC1 segregated EV from VAT whereas PC2 segregated samples according to lean or obese metabolic state. sEV and lEV co-segregated in the lean or obese state highlighting the metabolic state as an important driver of EV lipid content.
B. Relative lipid class composition of VAT and VAT-derived EV in the lean and obesity context. Bar plots represent the relative differences (in mol%) between AdEV versus VAT for the respective lipid class analyzed. Significant enrichment of AdEV was observed for sterols, phospholipids and sphingolipids whereas AdEV were significantly depleted in glycerolipids (see methods for statistical analysis, p-value<0,05 for all lipid class analyzed, no asterisks indicated in the panel for better lisibility).
C-F. Relative membranous lipid class composition of sEV and lEV by comparison to source VAT. Relative differences (in mol%) between AdEV and VAT for the respective lipid class analyzed were calculated in the lean (**C-D**) and obesity context (**E-F**), by distinguishing sEV (**C ; E**) from lEV (**D ; F**).
All results in **(B-F)** are presented as the mean ± SEM, calculated from four independent samples for each EV subtype and related source VAT for each metabolic state (see methods for statistical analysis, p-value<0,05*, p<0,01**,p<0,005***).
G-H. Venn diagrams depicting the lipid features that share commonness and uniqueness in their expression in lean sEV, lean lEV, obese sEV and obese lEV against the VAT. Lipid features that are enriched (**G**) or depleted (**H**) are presented. Detailed list of lipid species enriched or depleted in the different subsets are provided in Table S4 and Table S5, respectively.

Figure 5 : AdEV subtypes relative lipid composition in the lean and obese context

A. Pie diagram showing the relative lipid classes composition of AdEV subtypes isolated from lean VAT. A striking TAG enrichment is observed for lean lEV, at the expense of free cholesterol (FC), phosphatidylcholine (PC) and ceramides (Cer) by contrast enriched in lean sEV. Data presented correspond to the mean amount (in mol %) respectively in lean lEV (upper pie chart) and lean sEV (lower pie chart) from five independent samples for each AdEV subtypes.
B. Relative neutral lipid composition of AdEV subtypes isolated from lean and obese VAT conditioned media. Specific enrichment of total TAG (expressed in mol% of total lipids quantified) is observed in lEV compared to sEV, whatever the metabolic state

considered. Data are presented as mean ± SEM, ****p < 0.001 (non-parametric two-way ANOVA test corrected for multiple comparisons by Tukey's test).

C. Relative free cholesterol (FC) composition of AdEV subtypes isolated from lean and obese VAT conditioned media. Small EV displayed specific FC enrichment (expressed as mol% of membranous lipids) in the lean and obese states compared to lEV. Data are presented as mean ± SEM, **p < 0.01 (non-parametric two-way ANOVA test corrected for multiple comparisons by Tukey's test).

D. Relative membranous lipid class composition of AdEV subtypes. Relative differences (in mol%) between lean lEV versus lean sEV for the respective lipid class analyzed were calculated. Asterisks indicate the species that differ significantly between lEV and sEV (see methods for statistical analysis, p-value<0,05*, p<0,01**).

E. Heatmaps of AdEV subtypes lipid fingerprints in the lean context. Lipid subspecies that significantly (p <0.05) differentiated the lean sEV and the lean lEV are plotted in a hierarchical clustering tree (HCL). In red are lipid species that are enriched, and in green are those that are depleted. Major lipid species for each lipid class are underlined in grey.

F. Unsaturation profiles of AdEV phospholipids. Phospholipids were classified as saturated (SFA), monounsaturated (MUFA) and polyunsaturated (PUFA) lipids based on structural elucidation as presented in Table S2. Data are presented as mean ± SEM from 10 lean or 8 obese independent samples, *p < 0.05 (non-parametric two- way ANOVA test corrected for multiple comparisons by Sidak's test).

Supplemental Figure legends

Figure S1 : Detailed phospholipid subpecies in VAT significantly impacted by obesity

Total LPE, PI, PG and PEp are the phospholipid classes significantly impacted by the obese metabolic state in VAT (see Figure 2B). For each of these phospholipid class, significant changes in lipid subspecies are presented as the relative difference between obese and lean VAT (in mol%) (left panel). Date are presented as the mean ± SEM calculated from four independent samples for each metabolic state. Asterisks indicate a significant difference between lean and obese (p-value<0,05*, p<0,01**,p<0,005***, p<0,001****, see methods for statistical analysis).

Relative abundance of each lipid subspecies detected within each phospholipid class is presented as sidebar color-coded scale (LPE, purple ; PI, black ; blue, PG ; Pep, grey). Relative proportions of each phospholipid subspecies for a given phospholipid class is visually represented by color-gradient, the darkest represent the most abundant subspecies quantified whereas the clearest correspond the less represented ones. Phospholipid subspecies distribution is presented in absolute lipid quantified relative to VAT protein (pmole lipid/mg protein).

Figure S2: Differential expression of lipids between AdEV subtypes isolated from lean VAT

Fold change plots of individual lipids in the order of growing chain length in each lipid subclass differentiating lean lEV and lean sEV. Significant lipid species are colored, while non-significant are in grey. Significant threshold: p <0.05.

Figure S3 : Heatmaps of AdEV subtypes lipid fingerprints in the lean and obese context

Lipid subspecies that significantly (p <0.05) differentiated the lean and obese metabolic state are plotted in a hierarchical clustering tree (HCL). In red are lipid species that are enriched, and in green are those that are depleted. HCL tree of lEV and sEV are shown in Fig S3A and S3B respectively.

Figure S4 : Differential expression of lipids retrieved in AdEV subtypes in the lean and obese context

Fold change plots of individual lipids retrieved in AdEV subtypes, in the order of growing chain length in each lipid subclass, differentiating lean and obese metabolic state. Significant lipid species are colored, while non-significant are in grey. Significant threshold: p <0.05.

Supplemental Table legends

Table 1 : Phenotypic characteristics of obese mice and lean control mice

3 month-old male mice (n= 5-10 for each genotype) were weighed as well as respective organ weight at sacrifice (VAT, SAT, Liver and quadriceps muscles). Bloodglucose concentrations and plasma insulin concentrations were measured on the same animals after a 6h fast. Data are presented as mean ± sem, *p<0.05, ***p<0.001, ****p<0.001 following student.t tests.

VAT, Visceral Adipose Tissue ; SAT, Subcutaneous Adipose Tissue

Table S2 : Structural elucidation

Table S3 : Plasma lipid fingerprint of lean and obese mice

Significant lipid changes are expressed as log2 fold change of lipid concentrations in obese mice compared with the respective control mice.

The side-chain structures are denoted as “carbon chain length:number of double bonds” and are provided for each chain where they could be determined, or as a total number of all carbons and double bonds where individual chains could not be determined.

Table S4 : Detailed lipid species significantly enriched in AdEV compared to source VAT corresponding to Venn Diagram presented in Figure 4G

Table S5 : Detailed lipid species significantly depleted in AdEV compared to source VAT corresponding to Venn Diagram presented in Figure 4H

KEY RESOURCES TABLE

REAGENT or RESOURCE	SOURCE	IDENTIFIER
Antibodies		
CD9	BD Biosciences	Cat #553758
CD63	MBL international	Cat #D263-3
Flotillin-2	BD Biosciences	Cat #9101S
Grp94/Endoplasmin	Enzo life Sciences	Cat #ADI-SPA-850
Perilipin-1	Progen	Cat #GP29
IRDye® 800CW and 680RD secondary antibody (anti-mouse and anti-rabbit)	LI-COR Biosciences	Cat #926-32211, #926-32210, #926-68071, #926-68070
Chemicals, peptides, and recombinant proteins		
All internal lipid standards for quantitative lipidomics	Avanti® Polar Lipids	https://avantilipids.com/divisions/lipidomics/lipid-maps-ms-standards
DMEM 4.5g/L Glucose	Gibco part of Thermofisher Scintific	Cat #41966-029
4X Laemmli Sample Buffer	Bio-Rad	Cat #161-0747
Odyssey blocking buffer (TBS)	LI-COR Biosciences	Cat #927-50010
Deposited data		
Lipidomic datasets of AdEV and tissue analyzed	This paper	Supplemental Tables
Experimental models: Organisms/strains		
B6.Cg-Lepob/J	Charles River (JAX™ mice strain)	Stock number #000632
Software and algorithms		
Multi Experiment Viewer (MeV) software version 4.9		https://sourceforge.net/projects/mev-tm4/
MetaboAnalyst open source software		
GraphPad Prism	GraphPad Software, Inc	https://www.graphpad.com/
Image Studio software	LI-COR Biosciences	https://www.licor.com/bio/products/software/image_studio/
Image J	Downloaded from https://imagej.nih.gov/ij/	https://imagej.nih.gov/ij/

Nanosight NTA software (version 3.1)	Malvern Panalytical	https://www.malvernpanalytical.com/en/support/product-support/software/NanoSight-NTA-software-update-v3-10-l2

Figure 1

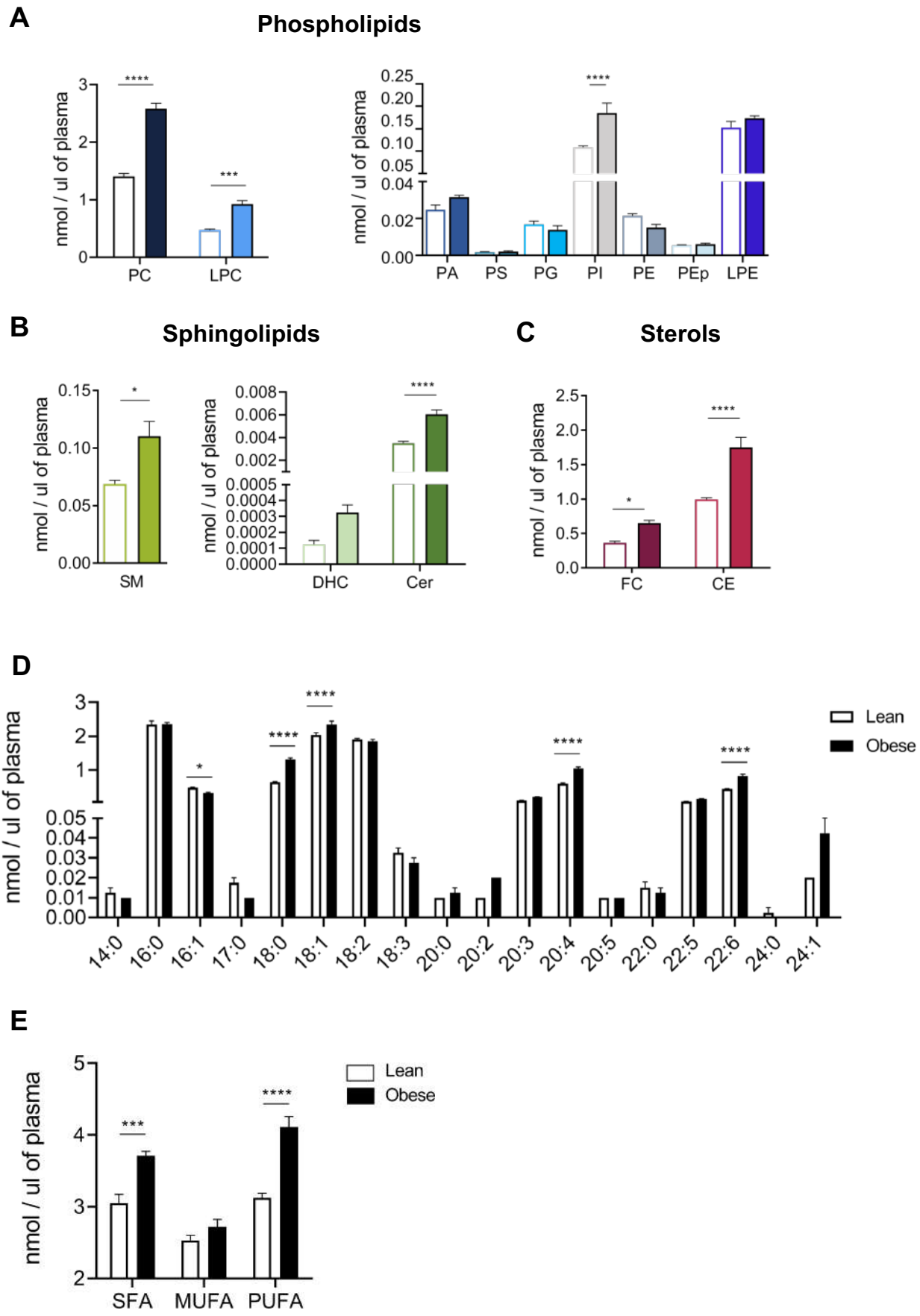
A
Phospholipids
nmol / ul of plasma
PC
LPC
PA
PS
PG
PI
PE
PEp
LPE
B
Sphingolipids
SM
DHC
Cer
C
Sterols
FC
CE
D
Lean
Obese
14:0
16:0
16:1
17:0
18:0
18:1
18:2
18:3
20:0
20:2
20:3
20:4
20:5
22:0
22:5
22:6
24:0
24:1
E
SFA
MUFA
PUFA

Figure 2

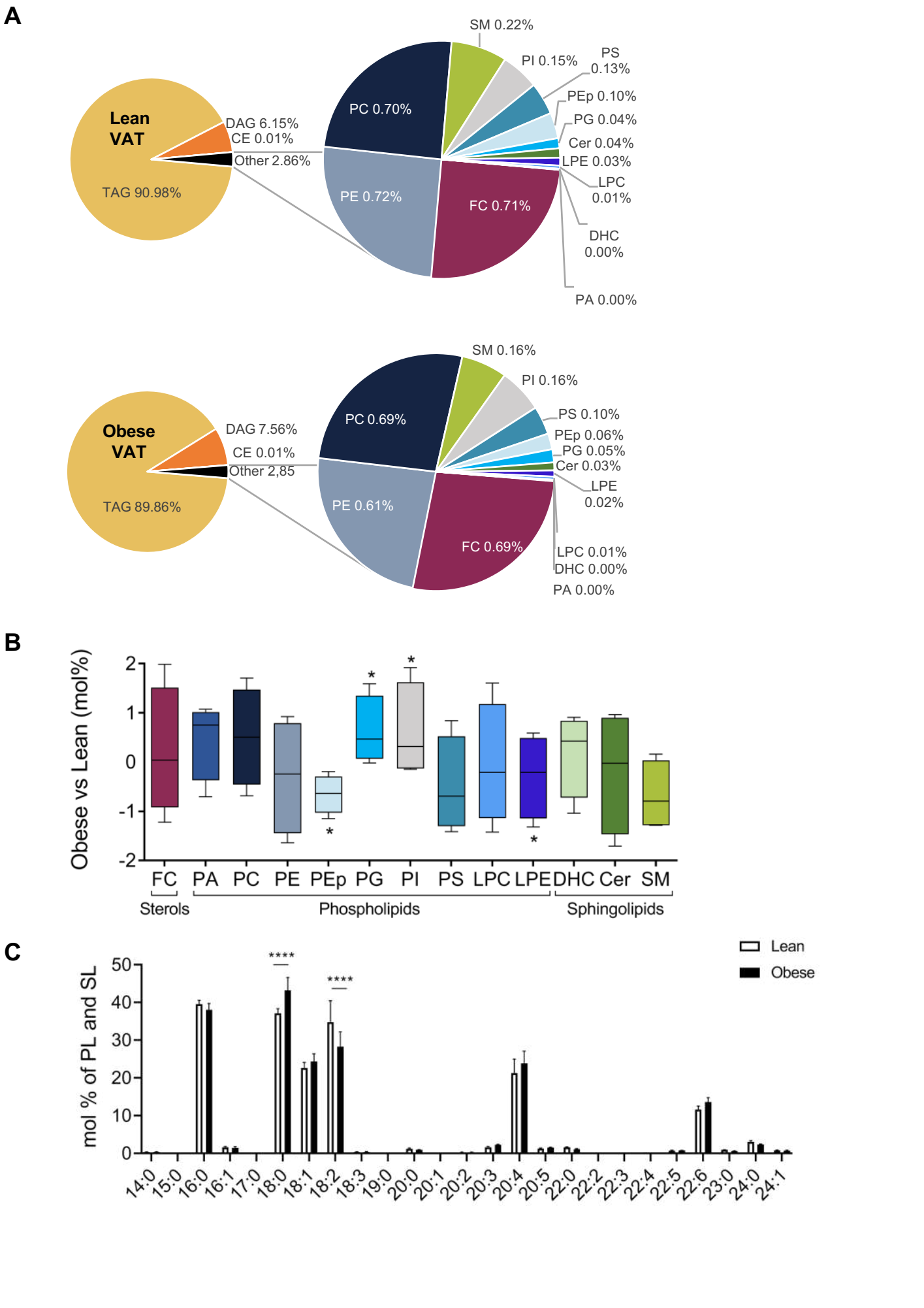
A
Lean VAT
TAG 90.98%
DAG 6.15%
CE 0.01%
Other 2.86%
PC 0.70%
PE 0.72%
FC 0.71%
SM 0.22%
PI 0.15%
PS 0.13%
PEp 0.10%
PG 0.04%
Cer 0.04%
LPE 0.03%
LPC 0.01%
DHC 0.00%
PA 0.00%
Obese VAT
TAG 89.86%
DAG 7.56%
CE 0.01%
Other 2,85
PC 0.69%
PE 0.61%
FC 0.69%
SM 0.16%
PI 0.16%
PS 0.10%
PEp 0.06%
PG 0.05%
Cer 0.03%
LPE 0.02%
LPC 0.01%
DHC 0.00%
PA 0.00%
B
Obese vs Lean (mol%)
FC PA PC PE PEp PG PI PS LPC LPE DHC Cer SM
Sterols
Phospholipids
Sphingolipids
C
mol % of PL and SL
Lean
Obese
****
14:0 15:0 16:0 16:1 17:0 18:0 18:1 18:2 18:3 19:0 20:0 20:1 20:2 20:3 20:4 20:5 22:0 22:2 22:3 22:4 22:5 22:6 23:0 24:0 24:1

Figure 3

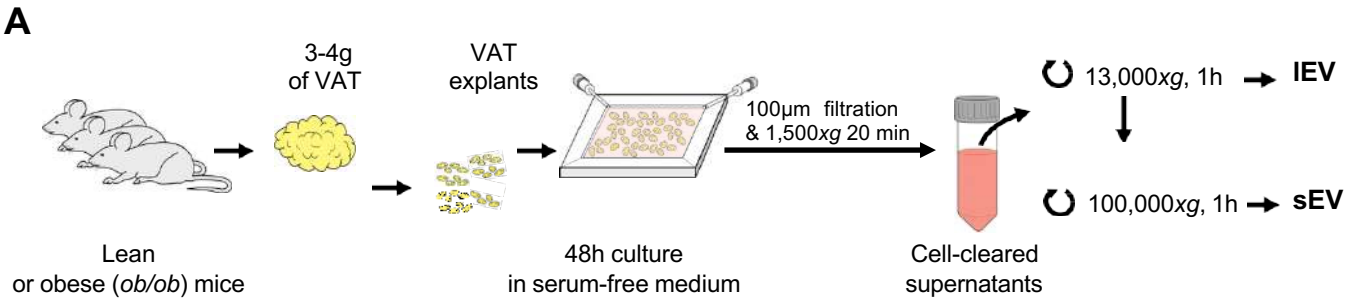
A
3-4g
of VAT
VAT
explants
100µm filtration
& 1,500xg 20 min
13,000xg, 1h
lEV
100,000xg, 1h
sEV
Lean
or obese (ob/ob) mice
48h culture
in serum-free medium
Cell-cleared
supernatants

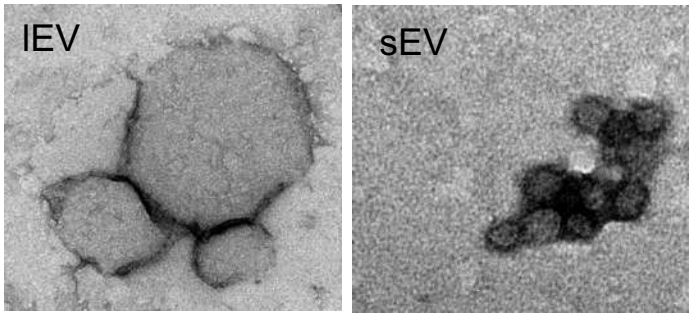
B
lEV
sEV

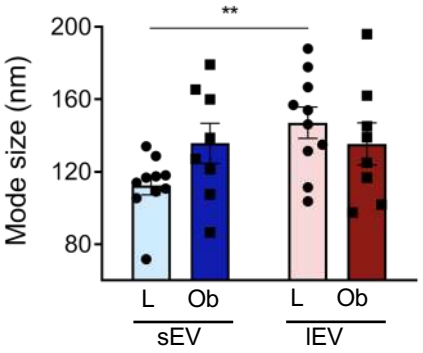
C
Mode size (nm)
200
160
120
80
**
L
Ob
L
Ob
sEV
lEV

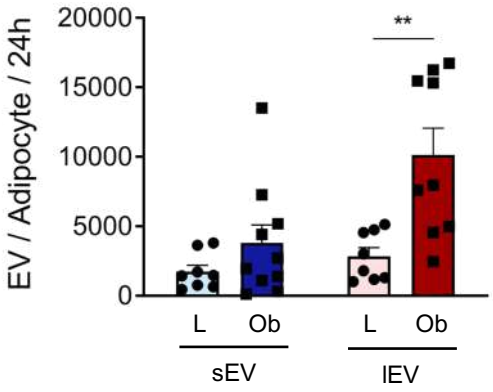
D
EV / Adipocyte / 24h
20000
15000
10000
5000
0
**
L
Ob
L
Ob
sEV
lEV

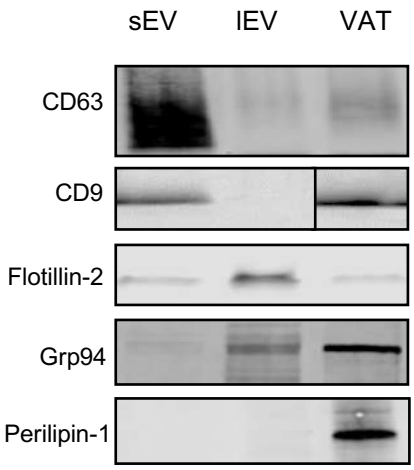
E
sEV
lEV
VAT
CD63
CD9
Flotillin-2
Grp94
Perilipin-1

Figure 4

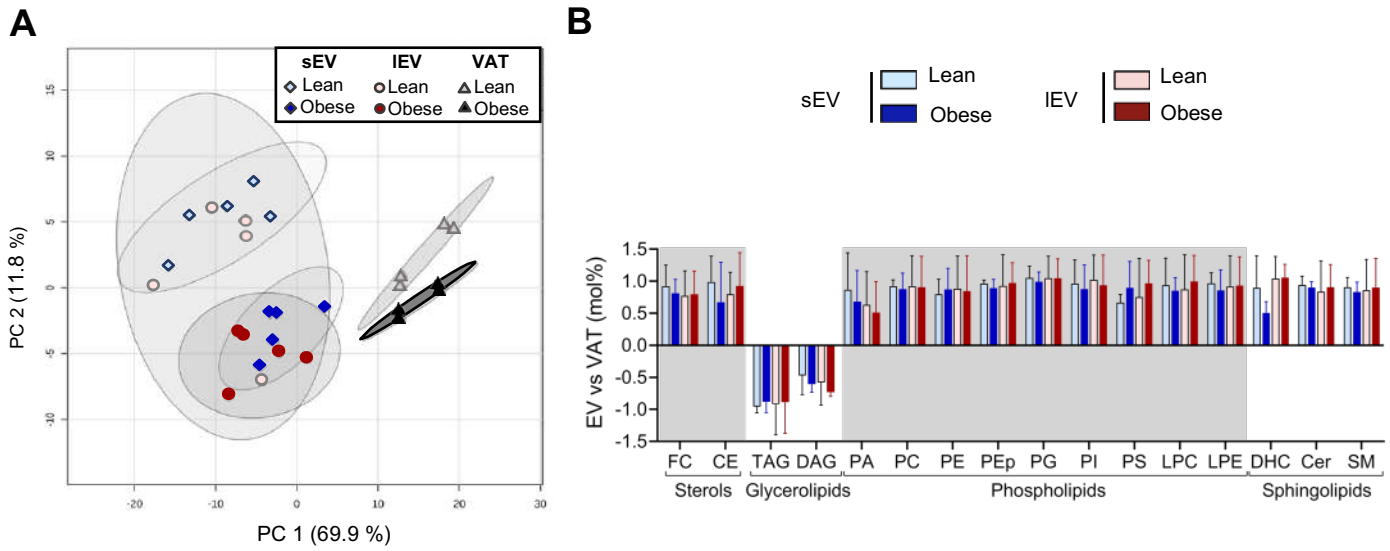

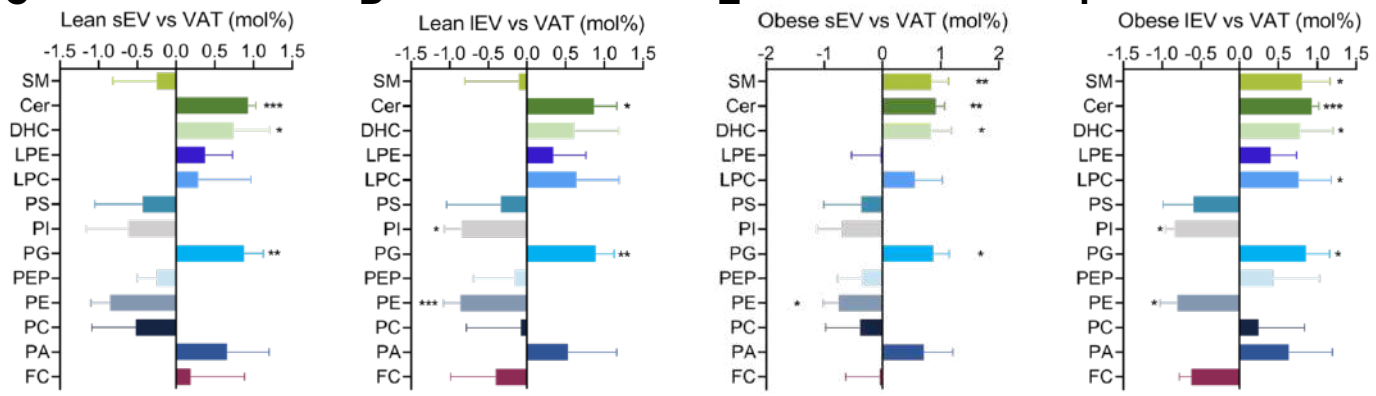

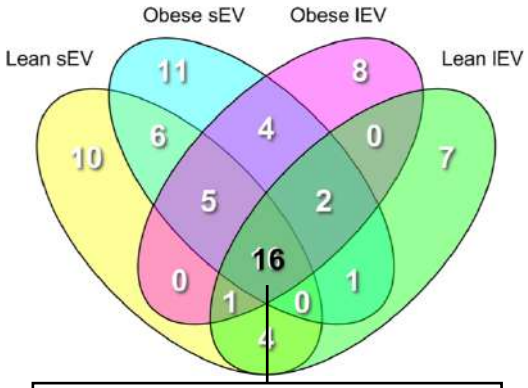

Lipids species commonly enriched in AdEV compared to VAT

Cer(d18:0/16:0)
Cer(d18:0/18:0)
Cer(d18:0/22:0)
Cer(d18:1/14:0)
Cer(d18:1/16:0)
Cer(d18:1/18:0)
Cer(d18:1/25:0)
Cer(d18:1/26:0)
Cer(d18:1/26:1)
Cer(d18:2/16:0)
Cer(d18:2/18:0)

PC(28:0)
PC(30:0)
PC(32:0)
PC(34:1)

PG(36:4)

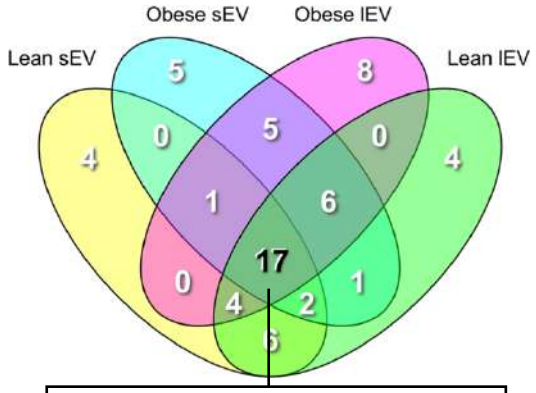

Lipids species commonly depleted in AdEV compared to VAT

PC(36:3)
PC(36:4)
PC(36:5)
PC(38:3)
PC(38:5)
PC(38:6)
PC(40:5)
PC(40:6)

PE(36:3)
PE(36:4)
PE(36:5)
PE(38:4)
PE(38:5)
PE(38:6)
PE(40:6)
PE(40:7)

PS(40:6)

Figure 5

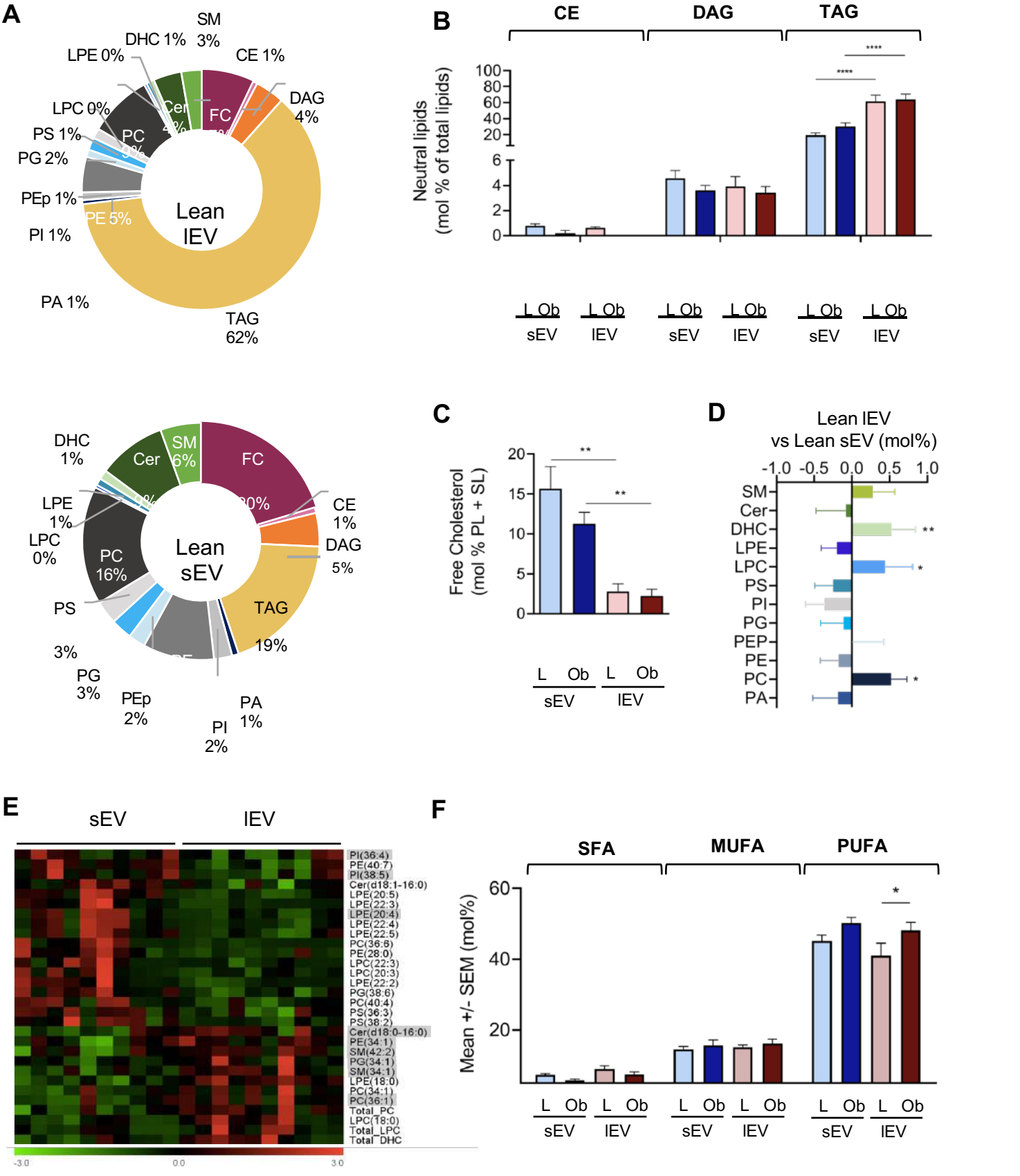
A
SM 3%
DHC 1%
LPE 0%
CE 1%
DAG 4%
LPC 0%
PS 1%
PG 2%
PEp 1%
PE 5%
PI 1%
PA 1%
TAG 62%
Lean IEV
DHC 1%
SM 6%
Cer
FC
CE 1%
LPE 1%
LPC 0%
PC 16%
DAG 5%
PS 3%
TAG 19%
PG 3%
PEp 2%
PA 1%
PI 2%
Lean sEV
B
CE
DAG
TAG
Neutral lipids (mol % of total lipids)
L Ob L Ob L Ob L Ob L Ob L Ob
sEV IEV sEV IEV sEV IEV
C
Free Cholesterol (mol % PL + SL)
L Ob L Ob
sEV IEV
D
Lean IEV vs Lean sEV (mol%)
SM
Cer
DHC
LPE
LPC
PS
PI
PG
PEP
PE
PC
PA
E
sEV
IEV
PI(36:4)
PE(40:7)
PI(38:5)
Cer(d18:1-16:0)
LPE(20:5)
LPE(22:3)
LPE(20:4)
LPE(22:4)
LPE(22:5)
PC(36:6)
PE(28:0)
LPC(22:3)
LPC(20:3)
LPE(22:2)
PG(38:6)
PC(40:4)
PS(36:3)
PS(38:2)
Cer(d18:0-16:0)
PE(34:1)
SM(42:2)
PG(34:1)
SM(34:1)
LPE(18:0)
PC(34:1)
PC(36:1)
Total_PC
LPC(18:0)
Total_LPC
Total_DHC
-3.0
0.0
3.0
F
SFA
MUFA
PUFA
Mean +/- SEM (mol%)
L Ob L Ob L Ob L Ob L Ob L Ob
sEV IEV sEV IEV sEV IEV

Figure S1

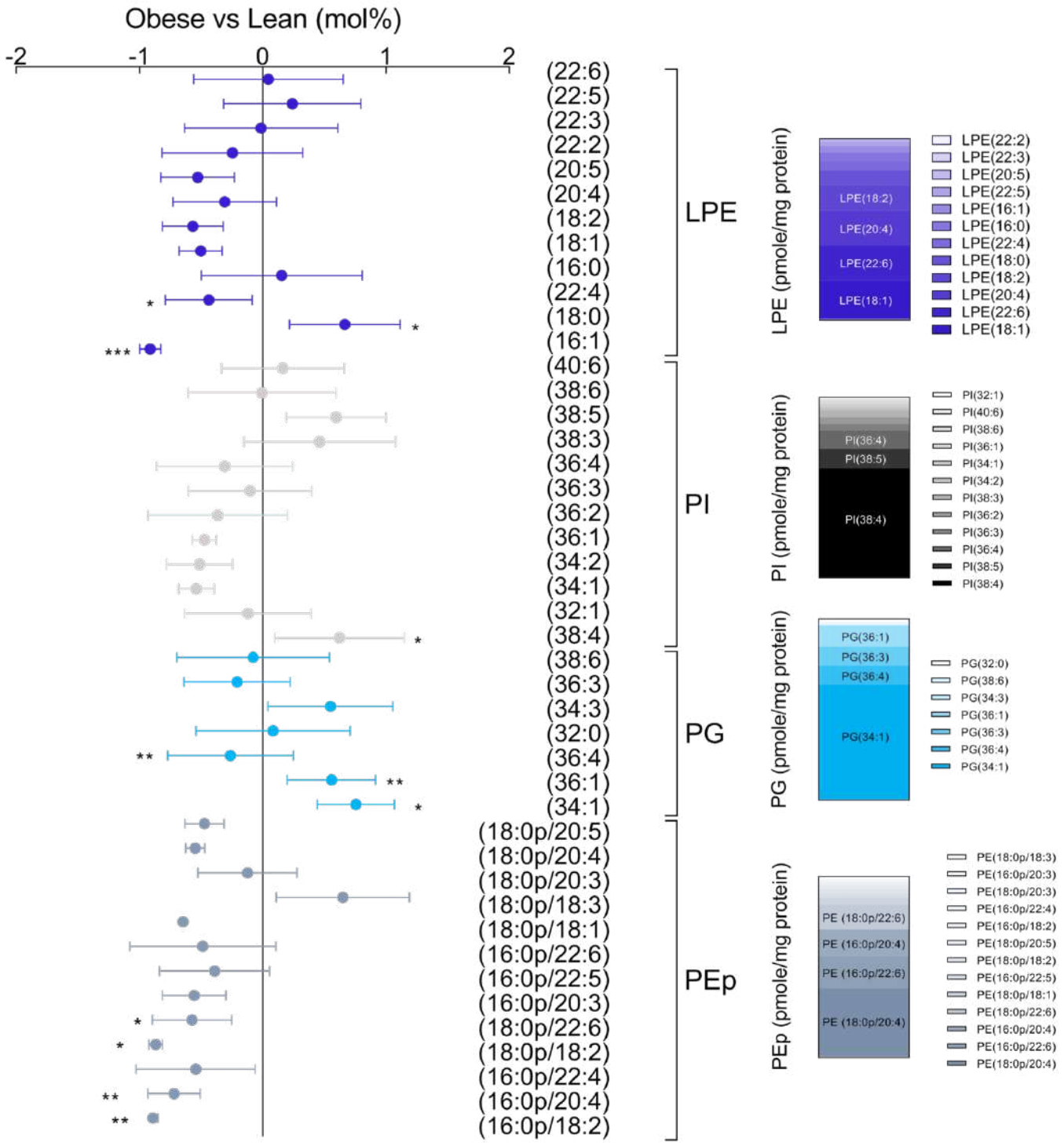
Obese vs Lean (mol%)
-2
-1
0
1
2
(22:6)
(22:5)
(22:3)
(22:2)
(20:5)
(20:4)
(18:2)
(18:1)
(16:0)
(22:4)
(18:0)
(16:1)
(40:6)
(38:6)
(38:5)
(38:3)
(36:4)
(36:3)
(36:2)
(36:1)
(34:2)
(34:1)
(32:1)
(38:4)
(38:6)
(36:3)
(34:3)
(32:0)
(36:4)
(36:1)
(34:1)
(18:0p/20:5)
(18:0p/20:4)
(18:0p/20:3)
(18:0p/18:3)
(18:0p/18:1)
(16:0p/22:6)
(16:0p/22:5)
(16:0p/20:3)
(18:0p/22:6)
(18:0p/18:2)
(16:0p/22:4)
(16:0p/20:4)
(16:0p/18:2)
LPE
PI
PG
PEp
LPE (pmole/mg protein)
LPE(18:2)
LPE(20:4)
LPE(22:6)
LPE(18:1)
LPE(22:2)
LPE(22:3)
LPE(20:5)
LPE(22:5)
LPE(16:1)
LPE(16:0)
LPE(22:4)
LPE(18:0)
LPE(18:2)
LPE(20:4)
LPE(22:6)
LPE(18:1)
PI (pmole/mg protein)
PI(36:4)
PI(38:5)
PI(38:4)
PI(32:1)
PI(40:6)
PI(38:6)
PI(36:1)
PI(34:1)
PI(34:2)
PI(38:3)
PI(36:2)
PI(36:3)
PI(36:4)
PI(38:5)
PI(38:4)
PG (pmole/mg protein)
PG(36:1)
PG(36:3)
PG(36:4)
PG(34:1)
PG(32:0)
PG(38:6)
PG(34:3)
PG(36:1)
PG(36:3)
PG(36:4)
PG(34:1)
PEp (pmole/mg protein)
PE (18:0p/22:6)
PE (16:0p/20:4)
PE (16:0p/22:6)
PE (18:0p/20:4)
PE(18:0p/18:3)
PE(16:0p/20:3)
PE(18:0p/20:3)
PE(16:0p/22:4)
PE(16:0p/18:2)
PE(18:0p/20:5)
PE(18:0p/18:2)
PE(16:0p/22:5)
PE(18:0p/18:1)
PE(18:0p/22:6)
PE(16:0p/20:4)
PE(16:0p/22:6)
PE(18:0p/20:4)

Figure S2

A

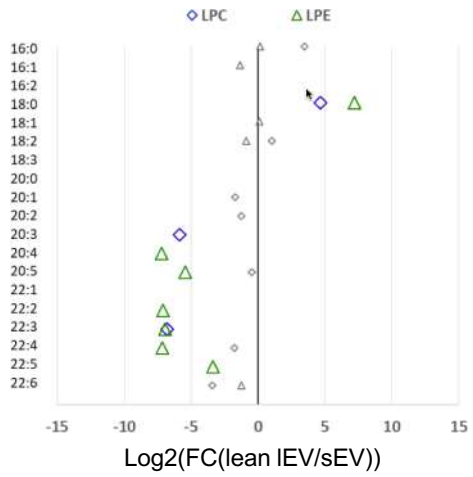
LPC
LPE
16:0
16:1
16:2
18:0
18:1
18:2
18:3
20:0
20:1
20:2
20:3
20:4
20:5
22:1
22:2
22:3
22:4
22:5
22:6
-15
-10
-5
0
5
10
15
Log2(FC(lean lEV/sEV))

B

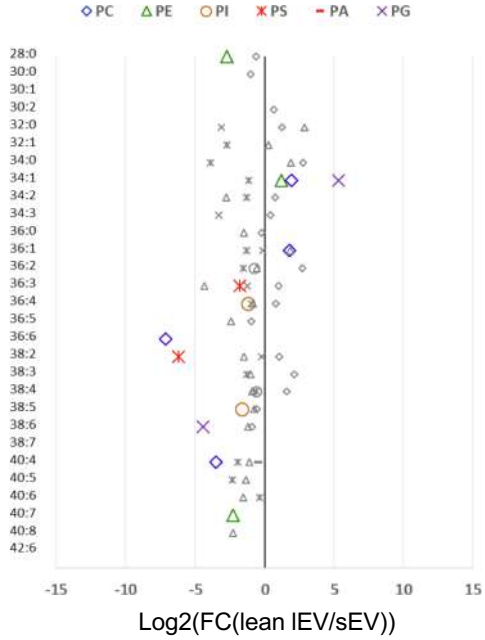
PC
PE
PI
PS
PA
PG
28:0
30:0
30:1
30:2
32:0
32:1
34:0
34:1
34:2
34:3
36:0
36:1
36:2
36:3
36:4
36:5
36:6
38:2
38:3
38:4
38:5
38:6
38:7
40:4
40:5
40:6
40:7
40:8
42:6
-15
-10
-5
0
5
10
15
Log2(FC(lean lEV/sEV))

Figure S3

A lEV

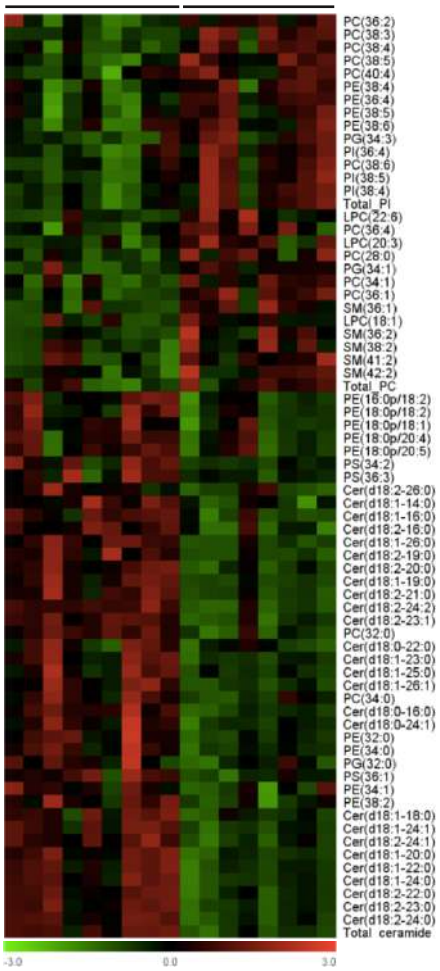

B sEV

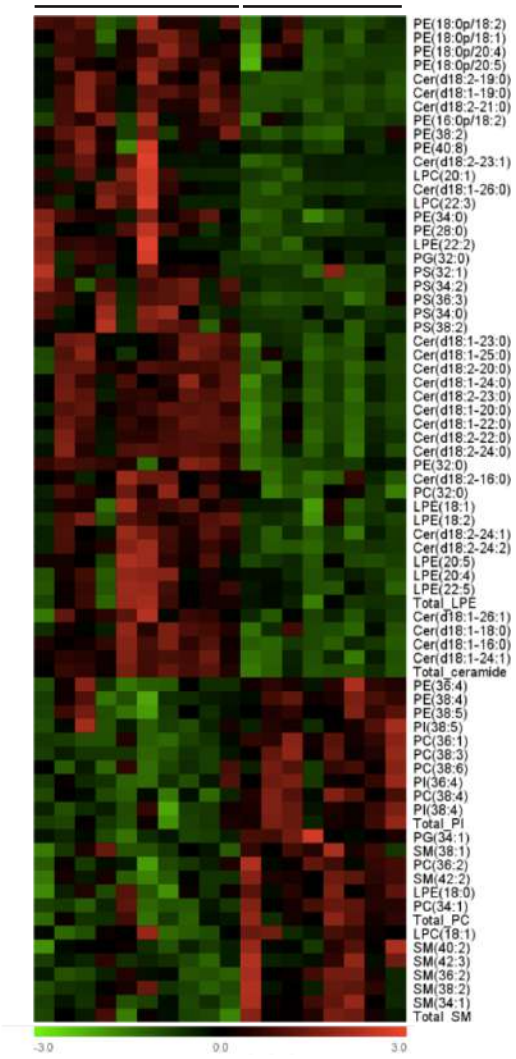

Figure S4

A Obese lEV *vs* lean lEV

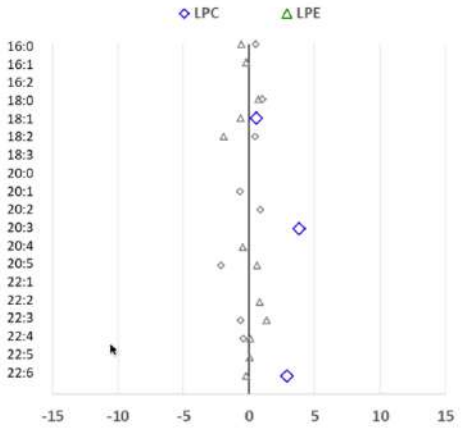

Log2(FC(obese lEV/lean lEV))

B Obese sEV *vs* lean sEV

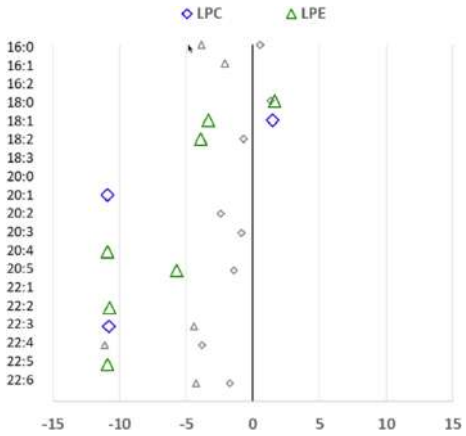

Log2(FC(obese sEV/lean sEV))

C Obese lEV *vs* lean lEV

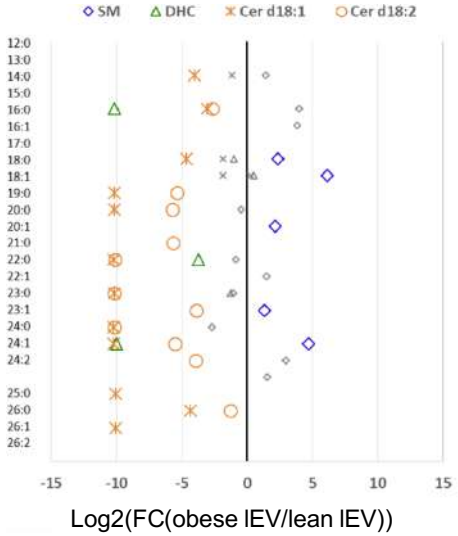

Log2(FC(obese lEV/lean lEV))

D Obese sEV *vs* lean sEV

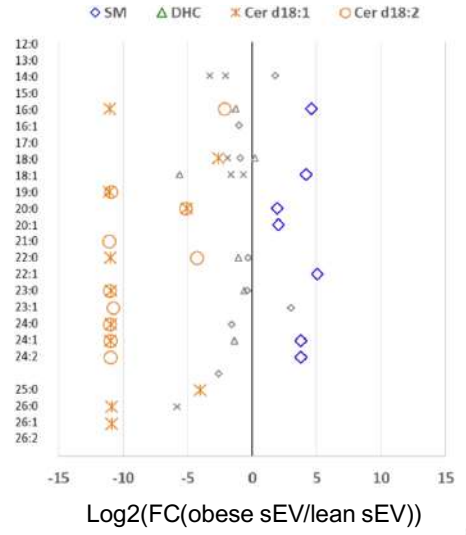

Log2(FC(obese sEV/lean sEV))

E Obese lEV *vs* lean lEV

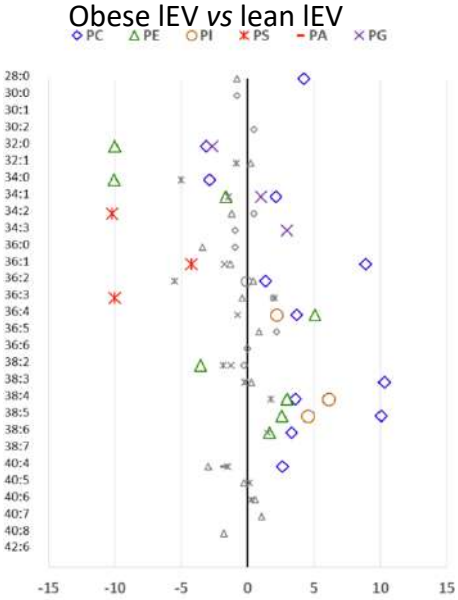

Log2(FC(obese lEV/lean lEV))

F Obese sEV *vs* lean sEV

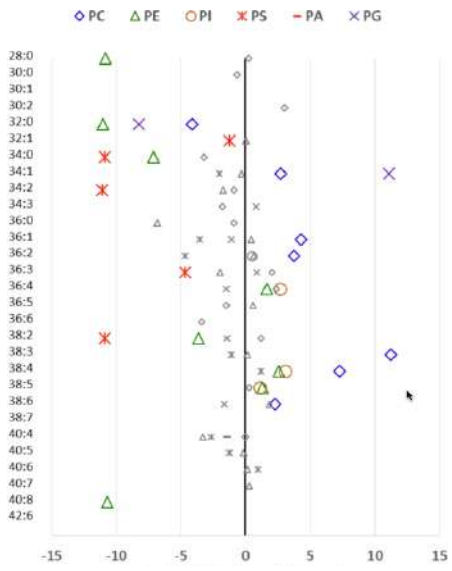

Log2(FC(obese sEV/lean sEV))

Table S1 : Phenotypic characteristics of obese and lean mice

	Lean	Obese (*ob/ob*)
Total weight (g)	27.2 ± 2.1	47.1 ± 6.8****
SAT weight (g)	0.41 ± 0.13	4.91 ± 1.68****
VAT weight (g)	0.80 ± 0.19	3.74 ± 0.98***
Muscle weight (g)	0.44 ± 0.007	0.27 ± 0.02***
Liver weight (g)	1.23 ± 0.15	3.67 ± 0.8****
Glycemia (mg/dL)	135 ± 7	202 ± 23*
Insulinemia	0.82 ± 0.28	3.54 ± 0.60****

Table S2 : Structural elucidation

EV, VAT						
Lipid class	**Lipid subclass**	**Lipid species**	**MS experiment for strcutural elucidation**	**sEV**	**lEV**	**VAT**
	LysoPC	LPC(16:0) LPC(16:1) LPC(16:2) LPC(18:0) LPC(18:1) LPC(18:2) LPC(18:3) LPC(20:0) LPC(20:1) LPC(20:2) LPC(20:3) LPC(20:4) LPC(20:5) LPC(22:3) LPC(22:4) LPC(22:5) LPC(22:6)	[M+H]+ PIS 184m/z			
	LysoPE	LPE(16:0) LPE(16:1) LPE(18:0) LPE(18:1) LPE(18:2) LPE(18:3) LPE(20:3) LPE(20:4) LPE(20:5) LPE(22:1) LPE(22:2) LPE(22:3) LPE(22:4)	[M+H]+ NL 141			

Plasma				
Lipid class	**Lipid subclass**	**Lipid species**	**MS experiment for strcutural elucidation**	**elucidated lipid in plasma**
	LysoPC	LPC(16:0) LPC(16:1) LPC(18:0) LPC(18:1) LPC(18:2) LPC(18:3) LPC(20:3) LPC(20:4) LPC(20:5) LPC(22:5) LPC(22:6)	[M+H]+ PIS 184m/z	
	LysoPE	LPE(16:0) LPE(16:1) LPE(18:0) LPE(18:1) LPE(18:2) LPE(18:3) LPE(20:3) LPE(20:4) LPE(20:5) LPE(22:1) LPE(22:4) LPE(22:5) LPE(22:6)	[M+H]+ NL 141	
	Phosphatidic acid	PA(34:2) PA(36:1) PA(36:2) PA(36:4)	Extrapolated structural elucidation	16:0_18:2 18:0_18:1 18:0_18:2 16:0_20:4
		PC(28:0) PC(30:0)		14:0_14:0 14:0_16:0

	LPE(22:5)				
	LPE(22:6)				
Phosphatidic acid	PA(32:0)	Extrapolated structural elucidation	16:0_16:0	16:0_16:1	16:0_16:2
	PA(36:3)		18:1_18:2	18:1_18:3	18:1_18:4
	PA(36:4)		16:0_20:4	16:0_20:5	16:0_20:6
	PA(38:4)		18:0_20:4	18:0_20:5	18:0_20:6
	PA(38:5)		16:0_22:5	16:0_22:6	16:0_22:7
	PA(40:4)		20:0_20:4	20:0_20:5	20:0_20:6
	PA(40:7)		18:1_22:6	18:1_22:7	18:1_22:8
Phosphatidylcholine	PC(28:0)	Extrapolated structural elucidation	14:0_14:0	14:0_14:1	14:0_14:2
	PC(30:0)	[M-H]- PIS FA chain	14:0_16:0	14:0_16:0	14:0_16:0
	PC(30:1)	Extrapolated structural elucidation	14:0_16:1	14:0_16:2	14:0_16:3
	PC(30:2)		14:1_16:2	14:1_16:3	14:1_16:4
	PC(32:0)	[M-H]- PIS FA chain	16:0_16:0	16:0_16:0	16:0_16:0
	PC(32:1)	Extrapolated structural elucidation	16:0_16:1	16:0_16:2	16:0_16:3
	PC(34:0)		16:0_18:0	16:0_18:0	16:0_18:0
	PC(34:1)		16:0_18:1	16:0_18:1	16:0_18:1
	PC(34:2)	[M-H]- PIS FA chain	18:2_16:0	18:2_16:0	18:2_16:0
	PC(34:3)		18:2_16:1	18:2_16:1	18:2_16:1
	PC(36:0)		18:0_18:0	18:0_18:0	18:0_18:0
	PC(36:1)		18:1_18:0	18:1_18:0	18:1_18:0
	PC(36:2)		18:2_18:0	18:2_18:0	18:2_18:0
	PC(36:3)		18:2_18:1	18:2_18:1	18:2_18:1
	PC(36:4)		20:4_16:0	20:4_16:0	20:4_16:0
	PC(36:5)		20:5_16:0	20:4_16:1	20:5_16:0
	PC(36:6)	Extrapolated structural elucidation	14:0_22:6	14:0_22:7	14:0_22:8
	PC(38:2)		18:0_20:2	18:0_20:3	18:0_20:4
	PC(38:3)	[M-H]- PIS FA chain	20:3_18:0	20:3_18:0	20:3_18:0
	PC(38:4)		20:4_18:0	20:4_18:0	20:4_18:0
	PC(38:5)		20:4_18:1	20:4_18:1	20:4_18:1
	PC(38:6)		22:6_16:0	22:6_16:0	22:6_16:0

Glycerophospholipids	PC(30:1)	Extrapolated structural elucidation	14:0_16:1
	PC(30:2)		14:1_16:2
	PC(32:0)		16:0_16:0
	PC(32:1)		16:0_16:1
	PC(34:1)		16:0_18:1
	PC(34:2)		16:0_18:2
	PC(34:3)		16:1_18:2
	PC(36:0)		18:0_18:0
	PC(36:1)		18:0_18:1
	PC(36:2)		18:0_18:2
	PC(36:3)		18:1_18:2
	PC(36:4)		16:0_20:4
	PC(36:5)		16:1_20:4
	PC(36:6)		14:0_22:6
	PC(38:2)		18:0_20:2
	PC(38:3)		18:0_20:3
	PC(38:4)		18:0_20:4
	PC(38:5)		16:0_22:5
	PC(38:6)		16:0_22:6
	PC(40:4)		20:0_20:4
	PC(40:5)		18:0_22:5
	PC(40:6)		18:0_22:6
	PC(40:7)		18:1_22:6
	PC(40:8)		18:2_22:6
	PE(28:0)		14:0_14:0
	PE(30:0)		14:0_16:0
	PE(30:1)		14:0_16:1
	PE(32:1)		16:0_16:1
	PE(34:1)		16:0_18:1
	PE(34:2)		16:0_18:2
	PE(36:0)		18:0_18:0

Glycerophospholipids		PC(40:4)	Extrapolated structural elucidation	20:0_20:4	20:0_20:5	20:0_20:6
		PC(40:5)		22:5_18:0	20:4_20:1	22:5_18:0
		PC(40:6)	[M-H]- PIS FA chain	22:6_18:0	22:6_18:0	22:6_18:0
		PC(40:7)		22:6_18:1	22:6_18:1	22:6_18:1
		PC(40:8)		20:4_20:4	20:4_20:4	22:6_18:2
	Plasmalogen PE	PE(16:0p/18:1)	[M+H]+ PIS(RCO+PE)			
		PE(16:0p/18:2)				
		PE(16:0p/20:1)				
		PE(16:0p/20:2)				
		PE(16:0p/20:3)				
		PE(16:0p/20:4)				
		PE(16:0p/22:4)				
		PE(16:0p/22:5)				
		PE(16:0p/22:6)				
		PE(18:0p/18:1)				
		PE(18:0p/18:2)				
		PE(18:0p/18:3)				
		PE(18:0p/18:4)				
		PE(18:0p/20:3)				
		PE(18:0p/20:4)				
		PE(18:0p/20:5)				
		PE(18:0p/22:6)				
		PE(18:0p/24:5)				
		PE(18:0p/24:6)				
	amine	PE(28:0)	Extrapolated structural elucidation	14:0_14:0	14:0_14:1	14:0_14:2
		PE(32:0)		16:0_16:0	16:0_16:0	16:0_16:0
		PE(32:1)		16:0_16:1	16:0_16:1	16:0_16:1
		PE(34:0)		16:0_18:0	16:0_18:1	16:0_18:2
		PE(34:1)	[M-H]- PIS FA chain	16:0_18:1	16:0_18:1	16:0_18:1
		PE(34:2)		18:2_16:0	18:2_16:0	18:2_16:0
		PE(36:0)	Extrapolated structural elucidation	18:0_18:0	18:0_18:1	18:0_18:2
		PE(36:1)		18:1_18:0	18:1_18:0	18:1_18:0
		PE(36:2)	[M-H]- PIS FA chain	18:2_18:0	18:2_18:0	18:2_18:0
		PE(36:3)		18:2_18:1	18:2_18:1	18:2_18:1

	Phosphatidylethanolamine	PE(36:1)	Extrapolated structural elucidation	18:0_18:1
		PE(36:2)		18:0_18:2
		PE(36:3)		18:1_18:2
		PE(36:4)		16:0_20:4
		PE(36:5)		16:1_20:4
		PE(38:2)		18:0_20:2
		PE(38:3)		18:0_20:3
		PE(38:4)		18:0_20:4
		PE(38:5)		16:0_22:5
		PE(38:6)		16:0_22:6
		PE(40:4)		20:0_20:4
		PE(40:6)		18:0_22:6
		PE(40:7)		18:1_22:6
		PE(40:8)		18:2_22:6
	plasmalogen PE	PE(16:0p/18:2)	[M+H]+ PIS(RCO+PE)	
		PE(16:0p/20:1)		
		PE(16:0p/20:2)		
		PE(16:0p/20:3)		
		PE(16:0p/20:4)		
		PE(16:0p/22:4)		
		PE(16:0p/22:5)		
		PE(16:0p/22:6)		
		PE(18:0p/18:1)		
		PE(18:0p/18:2)		
		PE(18:0p/18:3)		
		PE(18:0p/20:3)		
		PE(18:0p/20:4)		
		PE(18:0p/20:5)		
		PE(18:0p/22:6)		
	Phosphatidylglycerol	PG(34:1)	Extrapolated structural elucidation	16:0_18:1
		PG(36:1)		18:0_18:1
		PG(36:2)		18:0_18:2
		PI(32:0)		16:0_16:0
		PI(32:1)		16:0_16:1

Phosphatidylethanol	PE(36:4)	Extrapolated structural elucidation	20:4_16:0	20:4_16:0	20:4_16:0
	PE(36:5)		18:3_18:2	18:3_18:2	18:3_18:2
	PE(38:2)		18:0_20:2	18:0_20:3	18:0_20:4
	PE(38:3)	[M-H]- PIS FA chain	20:3_18:0	20:3_18:0	20:3_18:0
	PE(38:4)	Extrapolated structural elucidation	18:0_20:4	18:0_20:5	18:0_20:6
	PE(38:5)	[M-H]- PIS FA chain	20:4_18:1	20:4_18:1	20:4_18:1
	PE(38:6)		22:6_16:0	22:6_16:0	22:6_16:0
	PE(40:4)	Extrapolated structural elucidation	20:0_20:4	20:0_20:5	20:0_20:6
	PE(40:5)		18:0_22:5	18:0_22:5	18:0_22:5
	PE(40:6)		18:0_22:6	18:0_22:6	18:0_22:6
	PE(40:7)		18:1_22:6	18:1_22:7	18:1_22:8
	PE(40:8)		18:2_22:6	18:2_22:7	18:2_22:8
Phosphatidylglycerol	PG(32:0)	Extrapolated structural elucidation	16:0_16:0	16:0_16:1	16:0_16:2
	PG(34:1)		16:0_18:1	16:0_18:2	16:0_18:3
	PG(34:3)		16:1_18:2	16:1_18:3	16:1_18:4
	PG(36:1)		18:0_18:1	18:0_18:2	18:0_18:3
	PG(36:3)		18:1_18:2	18:1_18:3	18:1_18:4
	PG(36:4)		16:0_20:4	16:0_20:5	16:0_20:6
	PG(38:2)		18:0_20:2	18:0_20:2	18:0_20:2
	PG(38:3)		18:0_20:3	18:0_20:3	18:0_20:3
	PG(38:6)		16:0_22:6	16:0_22:7	16:0_22:8
Phosphatidylinositol	PI(32:1)	Extrapolated structural elucidation	16:0_16:1	16:0_16:2	16:0_16:3
	PI(34:1)		16:0_18:1	16:0_18:1	16:0_18:1
	PI(34:2)		16:0_18:2	16:0_18:2	16:0_18:2
	PI(36:1)		18:0_18:1	18:0_18:2	18:0_18:3
	PI(36:2)	[M-H]- PIS FA chain	18:1_18:1	18:1_18:1	18:1_18:1
	PI(36:3)		18:2_18:1	18:2_18:1	18:2_18:1
	PI(36:4)		20:4_16:0	20:4_16:0	20:4_16:0
	PI(38:3)		20:3_18:0	20:3_18:0	20:3_18:0
	PI(38:4)		20:4_18:0	20:4_18:0	20:4_18:0
	PI(38:5)		20:5_18:0	20:5_18:0	20:5_18:0
	PI(38:6)		22:6_16:0	22:6_16:0	22:6_16:0

Phosphatidylinositol	PI(34:1)	Extrapolated structural elucidation	16:0_18:1
	PI(36:1)		18:0_18:1
	PI(36:2)		18:0_18:2
	PI(36:3)		18:1_18:2
	PI(36:4)		16:0_20:4
	PI(38:3)		18:0_20:3
	PI(38:4)		18:0_20:4
	PI(38:5)		16:0_22:5
	PI(38:6)		16:0_22:6
	PI(40:4)		20:0_20:4
	PI(40:5)		18:0_22:5
	PI(40:6)		18:0_22:6
	PI(40:7)		18:1_22:6
Phosphatidylserine	PS(36:1)	Extrapolated structural elucidation	18:0_18:1
	PS(38:4)		18:0_20:4
	PS(40:5)		18:0_22:5
	PS(40:6)		18:0_22:6
Dihydroceramides	Cer(d18:0-16:0)	[M+H]+ PIS 266m/z	
	Cer(d18:0-18:0)		
	Cer(d18:0-18:1)		
	Cer(d18:0-19:0)		
	Cer(d18:0-20:0)		
	Cer(d18:0-24:0)		
	Cer(d18:0-24:1)		
	Cer(d18:0-25:0)		
	Cer(d18:0-26:0)		
	Cer(d18:0-26:1)		
	Cer(d18:0-26:2)		
	Cer(d18:1-14:0)		
	Cer(d18:1-16:0)		
	Cer(d18:1-18:0)		
	Cer(d18:1-18:1)		

		PI(40:6)	Extrapolated structural elucidation	18:0_22:6	18:0_22:7	18:0_22:8
	Phosphatidylserine	PS(32:0)	Extrapolated structural elucidation	16:0_16:0	16:0_16:0	16:0_16:0
		PS(32:1)		16:0_16:1	16:0_16:1	16:0_16:1
		PS(34:0)		16:0_18:0	16:0_18:0	16:0_18:0
		PS(34:1)		16:0_18:1	16:0_18:1	16:0_18:1
		PS(34:2)		16:0_18:2	16:0_18:2	16:0_18:2
		PS(36:1)		18:0_18:1	18:0_18:1	18:0_18:1
		PS(36:2)		18:0_18:2	18:0_18:2	18:0_18:2
		PS(36:3)		18:1_18:2	18:1_18:3	18:1_18:4
		PS(36:5)		16:1_20:4	16:1_20:5	16:1_20:6
		PS(38:2)		18:0_20:2	18:0_20:2	18:0_20:2
		PS(38:3)		18:0_20:3	18:0_20:3	18:0_20:3
		PS(38:4)		18:0_20:4	18:0_20:4	18:0_20:4
		PS(40:4)		20:0_20:4	20:0_20:5	20:0_20:6
		PS(40:5)		18:0_22:5	18:0_22:5	18:0_22:5
		PS(40:6)		18:0_22:6	18:0_22:6	18:0_22:6
	Dihydroceramides (DHC)	Cer(d18:0/13:0)	[M+H]+ PIS 266m/z			
		Cer(d18:0/14:0)				
		Cer(d18:0/15:0)				
		Cer(d18:0/16:0)				
		Cer(d18:0/17:0)				
		Cer(d18:0/18:0)				
		Cer(d18:0/18:1)				
		Cer(d18:0/19:0)				
		Cer(d18:0/20:0)				
		Cer(d18:0/22:0)				
		Cer(d18:0/23:0)				
		Cer(d18:0/24:0)				
		Cer(d18:0/24:1)				
		Cer(d18:0/25:0)				
		Cer(d18:0/26:0)				
		Cer(d18:0/26:1)				
		Cer(d18:0/26:2)				
		Cer(d18:1/12:0)				
		Cer(d18:1/13:0)				
		Cer(d18:1/14:0)				

sphingolipids	Ceramides	Cer(d18:1-19:0)	[M+H]+ PIS 264m/z	
		Cer(d18:1-20:0)		
		Cer(d18:1-22:0)		
		Cer(d18:1-23:0)		
		Cer(d18:1-24:0)		
		Cer(d18:1-24:1)		
		Cer(d18:1-25:0)		
		Cer(d18:1-26:0)		
		Cer(d18:1-26:1)		
	Sphingadienine ceramides	Cer(d18:2-14:0)	[M+H]+ PIS 262m/z	
		Cer(d18:2-16:0)		
		Cer(d18:2-18:0)		
		Cer(d18:2-18:1)		
		Cer(d18:2-19:0)		
		Cer(d18:2-20:0)		
		Cer(d18:2-21:0)		
		Cer(d18:2-22:0)		
		Cer(d18:2-23:0)		
		Cer(d18:2-23:1)		
		Cer(d18:2-24:0)		
		Cer(d18:2-24:1)		
		Cer(d18:2-24:2)		
		Cer(d18:2-26:0)		
		Cer(d18:2-26:1)		
	Sphingomyelin	SM(30:1)	Extrapolated structural elucidation	14:0
		SM(32:1)		16:0
		SM(34:1)		16:0
		SM(34:2)		16:1
		SM(36:1)		18:0
		SM(36:2)		18:0
		SM(38:1)		20:0
		SM(38:2)		20:0
		SM(40:1)		22:0
		SM(40:2)		22:0
		SM(41:1)		23:0
		SM(41:2)		23:0

sphingolipids	Ceramides	Cer(d18:1/15:0)	[M+H]+ PIS 264m/z			
		Cer(d18:1/16:0)				
		Cer(d18:1/18:0)				
		Cer(d18:1/18:1)				
		Cer(d18:1/19:0)				
		Cer(d18:1/20:0)				
		Cer(d18:1/22:0)				
		Cer(d18:1/23:0)				
		Cer(d18:1/24:0)				
		Cer(d18:1/24:1)				
		Cer(d18:1/25:0)				
		Cer(d18:1/26:0)				
		Cer(d18:1/26:1)				
	Sphingadienine ceramides	Cer(d18:2/13:0)	[M+H]+ PIS 262m/z			
		Cer(d18:2/14:0)				
		Cer(d18:2/15:0)				
		Cer(d18:2/16:0)				
		Cer(d18:2/18:0)				
		Cer(d18:2/18:1)				
		Cer(d18:2/19:0)				
		Cer(d18:2/20:0)				
		Cer(d18:2/20:1)				
		Cer(d18:2/21:0)				
		Cer(d18:2/22:0)				
		Cer(d18:2/23:0)				
		Cer(d18:2/23:1)				
		Cer(d18:2/24:0)				
		Cer(d18:2/24:1)				
		Cer(d18:2/24:2)				
		Cer(d18:2/26:0)				
		Cer(d18:2/26:1)				
	elin	SM(30:1)		C14:0	C14:1	C14:2
		SM(32:1)		C16:0	C16:0	C16:0
		SM(34:1)		C16:0	C16:0	C16:0
		SM(34:2)		C16:1	C16:1	C16:1
		SM(36:1)		C18:0	C18:0	C18:0
		SM(36:2)		C18:0	C18:0	C18:0
		SM(38:1)		C20:0	C20:0	C20:0
		SM(42:1)		24:0		
		SM(42:2)		24:1		
		SM(42:3)		24:1		
		SM(42:4)		24:2		
	Cholesteryl esters	CE(16:0)	[M+NH4]+ PIS 369m/z	16:0		
		CE(16:1)		16:1		
		CE(18:0)		18:0		
		CE(18:1)		18:1		
		CE(18:2)		18:2		
		CE(18:3)		18:3		
		CE(20:3)		20:3		
		CE(20:4)		20:4		
		CE(22:5)		22:5		
		CE(22:6)		22:6		
	Diacylglycerols	DG(14:0_16:0)	[M+NH4]+ NL(RCOO+NH3)	14:0		
		DG(14:0_16:1)		14:0		
		DG(16:0_16:0)		16:0		
		DG(14:0_18:1)		14:0		
		DG(14:0_18:2)		14:0		
		DG(16:0_18:0)		16:0		
		DG(16:0_18:1)		16:0		
		DG(16:0_18:2)		16:0		
		DG(16:1_18:1)		16:1		
		DG(16:1_18:2)		16:1		
		DG(16:0_18:3)		16:0		
		DG(16:1_18:3)		16:1		
		DG(18:0_18:0)		18:0		
		DG(18:0_18:1)		18:0		
		DG(18:0_18:2)		18:0		
		DG(18:1_18:1)		18:1		
		DG(16:0_20:3)		16:0		
		DG(16:0_20:4)		16:0		
		DG(18:1_18:3)		18:1		
		DG(18:2_18:2)		18:2		
		DG(16:1_20:4)		16:1		
		DG(18:2_18:3)		18:2		
		DG(16:0_20:5)		16:0		
		DG(18:1_20:3)		18:1		

	Sphingomy	SM(38:2)	Extrapolated structural elucidation	C20:0	C20:0	C20:0			DG(16:0_22:5)		16:0
		SM(40:1)		C22:0	C22:0	C22:0			DG(18:1_20:4)		18:1
		SM(40:2)		C22:0	C22:0	C22:0			DG(16:0_22:6)		16:0
		SM(41:1)		C23:0	C23:0	C23:0			DG(18:2_20:4)		18:2
		SM(41:2)		C23:0	C23:0	C23:0			DG(18:1_22:6)		18:1
		SM(42:1)		C24:0	C24:0	C24:0		Triacylglycerols	TG(48:0-16:0/32:0		TG(16:0_16:0_16:0)
		SM(42:2)		C24:1	C24:1	C24:1			TG(48:1-16:1/32:0		TG(16:0_16:0_16:1)
		SM(42:3)		C24:1	C24:1	C24:1			TG(48:1-18:1/30:0		TG(14:0_16:0_18:1)
		SM(42:4)		C24:2	C24:2	C24:2			TG(48:2-14:1/34:1		TG(14:1_16:0_18:1)
	Cholesteryl esters	CE(16:0)	[M+NH4]+ PIS 369m/z						TG(48:2-16:0/32:2		TG(16:0_16:1_16:1)
		CE(16:1)							TG(48:2-18:1/30:1		TG(14:0_16:1_18:1)
		CE(18:0)							TG(48:2-18:2/30:0		TG(14:0_16:0_18:2)
		CE(18:1)							TG(48:3-14:0/34:3		TG(14:0_16:1_18:2)
		CE(18:2)							TG(48:3-16:1/32:2		TG(16:1_16:1_16:1)
		CE(18:3)							TG(49:1-14:0/35:1		TG(14:0_17:0_18:1)
		CE(20:3)							TG(49:1-15:0/34:1		TG(15:0_16:0_18:1)
		CE(20:4)							TG(49:1-17:0/32:1		TG(16:0_16:1_17:0)
		CE(22:5)							TG(50:0-18:0/32:0		TG(16:0_16:0_18:0)
		CE(22:6)							TG(50:1-14:0/36:1		TG(14:0_18:0_18:1)
	acylglycerols	DG(14:0_16:0)	[M+NH4]+ NL(RCOO+NH3)						TG(50:1-18:1/32:0		TG(16:0_16:0_18:1)
		DG(14:0_16:1)							TG(50:2-18:0/32:2		TG(16:1_16:1_18:0)
		DG(14:0_18:1)							TG(50:2-18:1/32:1		TG(16:0_16:1_18:1)
		DG(14:0_18:2)							TG(50:2-18:2/32:0		TG(16:0_16:0_18:2)
		DG(16:0_16:0)							TG(50:3-14:1/36:2		TG(14:1_18:1_18:1)
		DG(16:0_18:0)							TG(50:3-18:1/32:2		TG(16:1_16:1_18:1)
		DG(16:0_18:1)							TG(50:3-18:2/32:1		TG(16:1_16:0_18:2)
		DG(16:0_18:2)							TG(50:4-14:0/36:4		TG(14:0_16:0_20:4)
		DG(16:0_18:3)							TG(50:4-18:2/32:2		TG(16:1_16:1_18:2)
		DG(16:0_18:4)							TG(51:1-18:1/33:0		TG(16:0_17:0_18:1)
		DG(16:0_20:3)							TG(51:2-15:0/36:2	[M+NH4]+ NL(RCOO+NH3) + extrapolated 2nd and 3rd chains	TG(15:0_18:1_18:1)
		DG(16:0_20:4)							TG(51:2-16:0/35:2		TG(16:0_17:0_18:2)
		DG(16:0_20:5)							TG(52:1-18:1/34:0		TG(16:0_18:0_18:1)
		DG(16:0_22:5)							TG(52:2-16:0/36:2		TG(16:0_18:1_18:1)
		DG(16:0_22:6)							TG(52:3-16:1/36:2		TG(16:1_18:1_18:1)
		DG(16:1_18:1)							TG(52:3-18:2/34:1		TG(16:0_18:1_18:2)
		DG(16:1_18:2)							TG(52:4-16:0/36:4		TG(16:0_16:0_20:4)
		DG(16:1_18:3)							TG(52:4-16:1/36:3		TG(16:1_16:0_20:3)
		DG(16:1_20:4)							TG(52:4-20:4/32:0		TG(16:0_16:0_20:4)

neutral lipids	Di	DG(18:0_18:0)					TG(52:5-20:4/32:1	TG(16:0_16:1_20:4)
		DG(18:0_18:1)					TG(53:2-17:0/36:2	TG(17:0_18:1_18:1)
		DG(18:0_18:2)					TG(54:1-18:1/36:0	TG(18:0_18:0_18:1)
		DG(18:0_20:3)					TG(54:2-18:0/36:2	TG(18:0_18:1_18:1)
		DG(18:0_20:4)					TG(54:3-18:1/36:2	TG(18:1_18:1_18:1)
		DG(18:0_22:6)					TG(54:4-18:0/36:4	TG(18:0_16:0_20:4)
		DG(18:1_18:1)					TG(54:4-18:2/36:2	TG(18:1_18:1_18:2)
		DG(18:1_18:2)					TG(54:4-20:4/34:0	TG(16:0_18:0_20:4)
		DG(18:1_18:3)					TG(54:5-18:1/36:4	TG(18:1_16:0_20:4)
		DG(18:1_20:2)					TG(54:6-18:2/36:4	TG(18:2_16:0_20:4)
		DG(18:1_20:3)					TG(54:6-18:3/36:3	TG(18:3_16:0_20:3)
		DG(18:1_20:4)					TG(54:6-20:4/34:2	TG(16:0_18:2_20:4)
		DG(18:1_22:6)					TG(54:6-22:6/32:0	TG(16:0_16:0_22:6)
		DG(18:2_18:2)					TG(56:6-20:4/36:2	TG(18:1_18:1_20:4)
		DG(18:2_18:3)					TG(56:6-20:5/36:1	TG(18:0_18:1_20:5)
		DG(18:2_20:4)					TG(56:6-22:5/34:1	TG(16:0_18:1_22:5)
		TG(48:0-16:0_32:0)					TG(56:6-22:6/34:0	TG(16:0_18:0_22:6)
		TG(48:1-16:1_32:0)					TG(56:8-20:4/36:4	TG(16:0_20:4_20:4)
		TG(48:1-18:1_30:0)					TG(58:8-22:6/36:2	TG(18:1_18:1_22:6)
		TG(48:2-14:1_34:1)						
		TG(48:2-16:0_32:2)						
		TG(48:2-18:1_30:1)						
		TG(48:2-18:2_30:0)						
		TG(48:3-14:0_34:3)						
		TG(48:3-16:1_32:2)						
		TG(49:1-14:0_35:1)						
		TG(49:1-15:0_34:1)						
		TG(49:1-17:0_32:1)						
		TG(50:0-18:0_32:0)						
		TG(50:1-14:0_36:1)						
		TG(50:1-18:1_32:0)						
		TG(50:2-18:0_32:2)						
		TG(50:2-18:1_32:1)						
		TG(50:2-18:2_32:0)						
		TG(50:3-14:1_36:2)						
		TG(50:3-18:1_32:2)						
		TG(50:3-18:2_32:1)						
		TG(50:4-14:0_36:4)						

	Triacylglycerols	TG(50:4-18:2_32:2)	[M+NH4]+ NL(RCOO+NH3)	
		TG(51:0-18:0_33:0)		
		TG(51:1-18:1_33:0)		
		TG(51:2-15:0_36:2)		
		TG(51:2-16:0_35:2)		
		TG(51:2-16:1_35:1)		
		TG(52:1-18:1_34:0)		
		TG(52:2-16:0_36:2)		
		TG(52:3-16:1_36:2)		
		TG(52:3-18:2_34:1)		
		TG(52:4-16:0_36:4)		
		TG(52:4-16:1_36:3)		
		TG(52:4-20:4_32:0)		
		TG(52:5-20:4_32:1)		
		TG(53:2-17:0_36:2)		
		TG(54:1-18:1_36:0)		
		TG(54:2-18:0_36:2)		
		TG(54:2-20:2_34:0)		
		TG(54:3-18:1_36:2)		
		TG(54:3-20:3_34:0)		
		TG(54:4-18:0_36:4)		
		TG(54:4-18:2_36:2)		
		TG(54:4-20:4_34:0)		
		TG(54:5-18:1_36:4)		
		TG(54:5-20:4_34:1)		
		TG(54:5-22:5_32:0)		
		TG(54:6-18:2_36:4)		
		TG(54:6-18:3_36:3)		
		TG(54:6-20:4_34:2)		
		TG(54:6-22:6_32:0)		
		TG(56:6-20:4_36:2)		
		TG(56:6-20:5_36:1)		
		TG(56:6-22:5_34:1)		
		TG(56:6-22:6_34:0)		
		TG(56:8-20:4_36:4)		
		TG(58:8-22:6_36:2)		

Table S3 : Plasma lipid fingerprints of lean and obese mice

		obese *vs* lean	
		Log2FC	*p* value
Neutral Lipids			
Cholesterol esters	CE(16:1)	0.92818	0.0036
	CE(18:1)	1.106	0.0245
	CE(18:3)	0.27607	0.0088
	CE(20:3)	1.6667	0.0071
	CE(20:4)	1.4249	0.0088
	CE(22:5)	1.6288	0.0058
	CE(22:6)	1.1984	0.0054
Diacylglycerols	DG(16:0_18:2)	-1.7555	0.0118
	DG(16:1_18:1)	-1.2459	0.0163
	DG(16:1_18:2)	-3.2715	0.0012
	DG(18:2_18:2)	-2.5228	0.0049
	DG(18:1_20:3)	1.2761	0.0142
	DG(16:0_22:6)	-1.0062	0.0492
	DG(18:2_20:4)	-2.5898	0.0116
	DG(18:1_22:6)	-1.8364	0.0121
Triacylglycerols	TG(48:0-16:0_32:0)	-1.1351	0.0488
	TG(48:1-16:1_32:0)	-1.4872	0.0362
	TG(48:2-14:1_34:1)	-1.1552	0.0379
	TG(48:2-16:0_32:2)	-2.2711	0.0033
	TG(48:2-18:1_30:1)	-1.4775	0.0154
	TG(48:2-18:2_30:0)	-2.9261	0.0030
	TG(48:3-14:0_34:3)	-3.5451	0.0045
	TG(48:3-16:1_32:2)	-2.4038	0.0043
	TG(49:1-14:0_35:1)	-1.1129	0.0040
	TG(49:1-15:0_34:1)	-1.7034	0.0140
	TG(50:2-18:0_32:2)	-2.1336	0.0025
	TG(50:2-18:1_32:1)	-1.1721	0.0143
	TG(50:2-18:2_32:0)	-2.6086	0.0040
	TG(50:3-18:1_32:2)	-1.8793	0.0132
	TG(50:3-18:2_32:1)	-3.599	0.0006
	TG(50:4-14:0_36:4)	-3.5617	0.0015
	TG(50:4-18:2_32:2)	-3.522	0.0016
	TG(51:1-18:1_33:0)	-1.4596	0.0056
	TG(51:2-15:0_36:2)	-1.9691	0.0183
	TG(51:2-16:0_35:2)	-1.8693	0.0049
	TG(52:3-18:2_34:1)	-2.7666	0.0009
	TG(52:4-16:0_36:4)	-3.4432	0.0008
	TG(52:4-16:1_36:3)	-2.9304	0.0057
	TG(52:4-20:4_32:0)	-0.99352	0.0347
	TG(52:5-20:4_32:1)	-2.0387	0.0064
	TG(54:1-18:1_36:0)	-2.2306	0.0344
	TG(54:4-18:0_36:4)	-2.6158	0.0043
	TG(54:4-18:2_36:2)	-2.2552	0.0042
	TG(54:5-18:1_36:4)	-2.839	0.0020
	TG(54:6-18:2_36:4)	-2.8723	0.0065
	TG(54:6-18:3_36:3)	-3.0976	0.0024
	TG(54:6-20:4_34:2)	-1.9806	0.0038
	TG(54:6-22:6_32:0)	-2.2953	0.0478
	TG(56:6-20:5_36:1)	-1.9816	0.0018
	TG(56:6-22:5_34:1)	-1.4341	0.0105
	TG(56:8-20:4_36:4)	-2.1677	0.0021
	TG(58:8-22:6_36:2)	-1.7758	0.0159
Sphingolipids			
Ceramides	Cer(d18:0/18:0)	0.86002	0.0499
	Cer(d18:0/18:1)	0.83728	0.0468
	Cer(d18:0/20:0)	0.94519	0.0342
	Cer(d18:0/24:1)	1.4545	0.0284
	Cer(d18:1/14:0)	2.48	0.0217
	Cer(d18:1/16:0)	1.739	0.0154
	Cer(d18:1/18:0)	4.2423	0.0273
	Cer(d18:1/18:1)	2.0894	0.0198
	Cer(d18:1/19:0)	1.3885	0.0223
	Cer(d18:1/20:0)	2.2942	0.0007
	Cer(d18:1/23:0)	0.45342	0.0434
	Cer(d18:1/24:1)	1.475	0.0060

	Cer(d18:1/26:0)	1.1633	0.0211
	Cer(d18:1/26:1)	1.1369	0.0148
	Cer(d18:2/16:0)	0.96748	0.0121
	Cer(d18:2/18:0)	2.5047	0.0135
	Cer(d18:2/18:1)	1.0745	0.0097
	Cer(d18:2/20:1)	1.1138	0.0224
	Cer(d18:2/24:0)	-0.69124	0.0300
	Cer(d18:2/26:1)	0.75984	0.0003
Sphingomyelins	SM(30:1)	0.73017	0.0485
	SM(32:1)	0.85632	0.0143
	SM(34:1)	0.89942	0.0426
	SM(38:1)	1.1291	0.0296
	SM(42:1)	-1.0103	0.0217
	SM(42:4)	1.0539	0.0424
Phospholipids			
Phosphatidic acids	PA(34:2)	-0.57105	0.0130
	PA(38:4)	0.75981	0.0031
Phosphatidylcholines	PC(34:1)	1.0244	0.0078
	PC(36:1)	1.9891	0.0028
	PC(36:3)	0.89001	0.0171
	PC(38:2)	0.78019	0.0243
	PC(38:3)	1.9731	0.0071
	PC(38:4)	1.5209	0.0156
	PC(38:5)	1.1312	0.0088
	PC(38:6)	0.69253	0.0106
	PC(40:4)	0.99161	0.0198
	PC(40:5)	1.6062	0.0016
	PC(40:6)	1.3364	0.0083
	PC(40:7)	1.1116	0.0098
Phosphatidylethanolamines	PE(32:1)	-1.1644	0.0455
	PE(34:2)	-1.7663	0.0221
	PE(36:2)	-0.44408	0.0409
	PE(36:3)	-1.2293	0.0246
	PE(36:5)	-1.1424	0.0208
	PE(38:2)	-0.65029	0.0479
	PE(38:5)	-0.6575	0.0495
	PE(40:5)	-0.74282	0.0105
	PE(40:7)	-0.7277	0.0405
	PE(40:8)	-0.37791	0.0384
Phosphatidylglycerols	PG(34:2)	-1.2053	0.0096
	PG(38:3)	1.1116	0.0400
Phosphatidylinositols	PI(34:2)	-1.3178	0.0000
	PI(36:1)	0.61879	0.0059
	PI(36:2)	-0.64978	0.0055
	PI(38:2)	2.1895	0.0030
	PI(38:3)	2.0998	0.0031
	PI(38:4)	0.80225	0.0163
	PI(40:4)	1.0617	0.0150
	PI(40:5)	0.66546	0.0223
Phosphatidylserines	PS(38:4)	0.63661	0.0219
	PS(40:4)	0.5581	0.0441
LysoPC	LPC(16:0)	0.63904	0.0181
	LPC(16:1)	0.65309	0.0260
	LPC(18:0)	1.1258	0.0093
	LPC(18:1)	1.5026	0.0111
	LPC(20:0)	-1.4801	0.0157
	LPC(20:1)	0.52554	0.0372
	LPC(20:3)	1.958	0.0068
	LPC(20:4)	1.2664	0.0476
	LPC(20:5)	0.76202	0.0192
	LPC(22:5)	0.8625	0.0033
	LPC(22:6)	0.81978	0.0466
LysoPE	LPE(18:2)	-0.83845	0.0214
	LPE(18:3)	-0.7949	0.0050
	LPE(20:5)	-0.44755	0.0238
	LPE(22:1)	-0.6372	0.0429
PE Plasmalogens	PE(16:0p/20:3)	0.64188	0.0185
	PE(16:0p/20:4)	0.30424	0.0294
	PE(18:0p/18:1)	0.50645	0.0063
	PE(18:0p/20:4)	0.54511	0.0385

Table S4 : Detailed lipid species significantly enriched in AdEV compared to source VAT corresponding to Venn Diagram presented in Figure 4G

Sample type	Lean sEV	Obese sEV	Obese lEV	Lean lEV	Lean lEV + Obese sEV	Lean sEV + Obese sEV	Lean lEV + Lean sEV	Obese lEV + Obese sEV	Lean lEV + Obese lEV + Obese sEV	Lean lEV + Lean sEV + Obese lEV	Lean sEV + Obese lEV + Obese sEV	Lean lEV + Lean sEV + Obese lEV + Obese sEV
Number of lipid species retrieved	**10**	**11**	**8**	**7**	**1**	**6**	**4**	**4**	**2**	**1**	**5**	**16**
Lipid species enriched in AdEV subtypes	Cer(d18:2/22:0) Cer(d18:2/23:0) Cer(d18:2/24:0) Cer(d18:2/24:1) LPE(20:4) LPE(22:4) LPE(22:5) PA(32:0) PE(16:0p/22:4) PS(34:1)	PA(40:4) PC(34:0) PC(36:2) PE(32:0) PG(36:1) PG(38:2) SM(36:1) SM(36:2) SM(38:1) SM(40:1) SM(42:2)	Cer(d18:0/23:0) LPC(18:0) LPC(18:1) LPC(20:2) LPC(22:3) LPE(22:3) PE(18:0p/18:3) SM(42:3)	Cer(d18:2/14:0) Cer(d18:2/18:1) LPE(18:0) PC(30:1) PG(32:0) PS(32:0) PS(36:5)	Cer(d18:2/26:0)	Cer(d18:1/23:0) Cer(d18:1/24:0) Cer(d18:1/24:1) Cer(d18:2/20:0) Cer(d18:2/21:0) PG(38:3)	Cer(d18:1/18:1) Cer(d18:1/19:0) Cer(d18:2/19:0) Cer(d18:2/24:2)	LPC(20:1) PC(30:2) SM(34:1) SM(38:2)	Cer(d18:2/23:1) PG(34:3)	LPC(22:4)	Cer(d18:0/20:0) Cer(d18:0/24:1) Cer(d18:1/20:0) Cer(d18:1/22:0) PG(36:3)	Cer(d18:0/16:0) Cer(d18:0/18:0) Cer(d18:0/22:0) Cer(d18:1/14:0) Cer(d18:1/16:0) Cer(d18:1/18:0) Cer(d18:1/25:0) Cer(d18:1/26:0) Cer(d18:1/26:1) Cer(d18:2/16:0) Cer(d18:2/18:0) PC(28:0) PC(30:0) PC(32:0) PC(34:1) PG(36:4)

Table S5 : Detailed lipid species significantly depleted in AdEV compared to source VAT corresponding to Venn Diagram presented in Figure 4H

Sample type	Lean sEV	Obese sEV	Obese lEV	Lean lEV	Lean lEV + Obese sEV	Lean sEV + Obese sEV	Lean lEV + Lean sEV	Obese lEV + Obese sEV	Lean lEV + Obese lEV + Obese sEV	Lean lEV + Lean sEV + Obese lEV	Lean sEV + Obese lEV + Obese sEV	Lean lEV + Lean sEV + Obese lEV + Obese sEV
Number of lipid species retrieved	4	5	8	4	1	6	5	6	4	1	2	17
Lipid species depleted in AdEV subtypes	LPC(16:0) PC(34:3) SM(32:1) SM(38:1)	LPC(20:3) LPC(22:6) PE(18:0p/18:2) PE(18:0p/20:5) PI(36:1)	PA(38:5) PC(36:0) PC(36:6) PE(16:0p/22:6) PE(40:5) PI(34:1) PS(36:3) PS(38:2)	PC(38:2) PE(38:2) SM(40:1) SM(42:4)	PI(36:3)	PE(34:1) PE(34:2) SM(38:2) SM(40:2) SM(41:1) SM(41:2)	PC(38:4) PC(40:4) PC(40:8) PE(18:0p/22:6) PE(34:0)	PE(28:0) PE(38:3) PE(40:8) PI(38:3) PI(38:6) PI(40:6)	PE(36:2) PI(36:4) PI(38:4) PI(38:5)	PC(40:7)	PE(32:1) PI(36:2)	PC(36:3) PC(36:4) PC(36:5) PC(38:3) PC(38:5) PC(38:6) PC(40:5) PC(40:6) PE(36:3) PE(36:4) PE(36:5) PE(38:4) PE(38:5) PE(38:6) PE(40:6) PE(40:7) PS(40:6)

Table S3 : Plasma lipid fingerprints of lean and obese mice

		obese *vs* lean	
		Log2FC	*p* value
Neutral Lipids			
Cholesterol esters	CE(16:1)	0.92818	0.0036
	CE(18:1)	1.106	0.0245
	CE(18:3)	0.27607	0.0088
	CE(20:3)	1.6667	0.0071
	CE(20:4)	1.4249	0.0088
	CE(22:5)	1.6288	0.0058
	CE(22:6)	1.1984	0.0054
Diacylglycerols	DG(16:0_18:2)	-1.7555	0.0118
	DG(16:1_18:1)	-1.2459	0.0163
	DG(16:1_18:2)	-3.2715	0.0012
	DG(18:2_18:2)	-2.5228	0.0049
	DG(18:1_20:3)	1.2761	0.0142
	DG(16:0_22:6)	-1.0062	0.0492
	DG(18:2_20:4)	-2.5898	0.0116
	DG(18:1_22:6)	-1.8364	0.0121
Triacylglycerols	TG(48:0-16:0_32:0)	-1.1351	0.0488
	TG(48:1-16:1_32:0)	-1.4872	0.0362
	TG(48:2-14:1_34:1)	-1.1552	0.0379
	TG(48:2-16:0_32:2)	-2.2711	0.0033
	TG(48:2-18:1_30:1)	-1.4775	0.0154
	TG(48:2-18:2_30:0)	-2.9261	0.0030
	TG(48:3-14:0_34:3)	-3.5451	0.0045
	TG(48:3-16:1_32:2)	-2.4038	0.0043
	TG(49:1-14:0_35:1)	-1.1129	0.0040
	TG(49:1-15:0_34:1)	-1.7034	0.0140
	TG(50:2-18:0_32:2)	-2.1336	0.0025
	TG(50:2-18:1_32:1)	-1.1721	0.0143
	TG(50:2-18:2_32:0)	-2.6086	0.0040
	TG(50:3-18:1_32:2)	-1.8793	0.0132
	TG(50:3-18:2_32:1)	-3.599	0.0006
	TG(50:4-14:0_36:4)	-3.5617	0.0015
	TG(50:4-18:2_32:2)	-3.522	0.0016
	TG(51:1-18:1_33:0)	-1.4596	0.0056
	TG(51:2-15:0_36:2)	-1.9691	0.0183
	TG(51:2-16:0_35:2)	-1.8693	0.0049
	TG(52:3-18:2_34:1)	-2.7666	0.0009
	TG(52:4-16:0_36:4)	-3.4432	0.0008
	TG(52:4-16:1_36:3)	-2.9304	0.0057
	TG(52:4-20:4_32:0)	-0.99352	0.0347
	TG(52:5-20:4_32:1)	-2.0387	0.0064
	TG(54:1-18:1_36:0)	-2.2306	0.0344
	TG(54:4-18:0_36:4)	-2.6158	0.0043
	TG(54:4-18:2_36:2)	-2.2552	0.0042
	TG(54:5-18:1_36:4)	-2.839	0.0020
	TG(54:6-18:2_36:4)	-2.8723	0.0065
	TG(54:6-18:3_36:3)	-3.0976	0.0024
	TG(54:6-20:4_34:2)	-1.9806	0.0038
	TG(54:6-22:6_32:0)	-2.2953	0.0478
	TG(56:6-20:5_36:1)	-1.9816	0.0018
	TG(56:6-22:5_34:1)	-1.4341	0.0105
	TG(56:8-20:4_36:4)	-2.1677	0.0021
	TG(58:8-22:6_36:2)	-1.7758	0.0159
Sphingolipids			
Ceramides	Cer(d18:0/18:0)	0.86002	0.0499
	Cer(d18:0/18:1)	0.83728	0.0468
	Cer(d18:0/20:0)	0.94519	0.0342
	Cer(d18:0/24:1)	1.4545	0.0284
	Cer(d18:1/14:0)	2.48	0.0217
	Cer(d18:1/16:0)	1.739	0.0154
	Cer(d18:1/18:0)	4.2423	0.0273
	Cer(d18:1/18:1)	2.0894	0.0198
	Cer(d18:1/19:0)	1.3885	0.0223
	Cer(d18:1/20:0)	2.2942	0.0007
	Cer(d18:1/23:0)	0.45342	0.0434
	Cer(d18:1/24:1)	1.475	0.0060

	Cer(d18:1/26:0)	1.1633	0.0211
	Cer(d18:1/26:1)	1.1369	0.0148
	Cer(d18:2/16:0)	0.96748	0.0121
	Cer(d18:2/18:0)	2.5047	0.0135
	Cer(d18:2/18:1)	1.0745	0.0097
	Cer(d18:2/20:1)	1.1138	0.0224
	Cer(d18:2/24:0)	-0.69124	0.0300
	Cer(d18:2/26:1)	0.75984	0.0003
Sphingomyelins	SM(30:1)	0.73017	0.0485
	SM(32:1)	0.85632	0.0143
	SM(34:1)	0.89942	0.0426
	SM(38:1)	1.1291	0.0296
	SM(42:1)	-1.0103	0.0217
	SM(42:4)	1.0539	0.0424
Phospholipids			
Phosphatidic acids	PA(34:2)	-0.57105	0.0130
	PA(38:4)	0.75981	0.0031
Phosphatidylcholines	PC(34:1)	1.0244	0.0078
	PC(36:1)	1.9891	0.0028
	PC(36:3)	0.89001	0.0171
	PC(38:2)	0.78019	0.0243
	PC(38:3)	1.9731	0.0071
	PC(38:4)	1.5209	0.0156
	PC(38:5)	1.1312	0.0088
	PC(38:6)	0.69253	0.0106
	PC(40:4)	0.99161	0.0198
	PC(40:5)	1.6062	0.0016
	PC(40:6)	1.3364	0.0083
	PC(40:7)	1.1116	0.0098
Phosphatidylethanolamines	PE(32:1)	-1.1644	0.0455
	PE(34:2)	-1.7663	0.0221
	PE(36:2)	-0.44408	0.0409
	PE(36:3)	-1.2293	0.0246
	PE(36:5)	-1.1424	0.0208
	PE(38:2)	-0.65029	0.0479
	PE(38:5)	-0.6575	0.0495
	PE(40:5)	-0.74282	0.0105
	PE(40:7)	-0.7277	0.0405
	PE(40:8)	-0.37791	0.0384
Phosphatidylglycerols	PG(34:2)	-1.2053	0.0096
	PG(38:3)	1.1116	0.0400
Phosphatidylinositols	PI(34:2)	-1.3178	0.0000
	PI(36:1)	0.61879	0.0059
	PI(36:2)	-0.64978	0.0055
	PI(38:2)	2.1895	0.0030
	PI(38:3)	2.0998	0.0031
	PI(38:4)	0.80225	0.0163
	PI(40:4)	1.0617	0.0150
	PI(40:5)	0.66546	0.0223
Phosphatidylserines	PS(38:4)	0.63661	0.0219
	PS(40:4)	0.5581	0.0441
LysoPC	LPC(16:0)	0.63904	0.0181
	LPC(16:1)	0.65309	0.0260
	LPC(18:0)	1.1258	0.0093
	LPC(18:1)	1.5026	0.0111
	LPC(20:0)	-1.4801	0.0157
	LPC(20:1)	0.52554	0.0372
	LPC(20:3)	1.958	0.0068
	LPC(20:4)	1.2664	0.0476
	LPC(20:5)	0.76202	0.0192
	LPC(22:5)	0.8625	0.0033
	LPC(22:6)	0.81978	0.0466
LysoPE	LPE(18:2)	-0.83845	0.0214
	LPE(18:3)	-0.7949	0.0050
	LPE(20:5)	-0.44755	0.0238
	LPE(22:1)	-0.6372	0.0429
PE Plasmalogens	PE(16:0p/20:3)	0.64188	0.0185
	PE(16:0p/20:4)	0.30424	0.0294
	PE(18:0p/18:1)	0.50645	0.0063
	PE(18:0p/20:4)	0.54511	0.0385

Table S4 : Detailed lipid species significantly enriched in AdEV compared to source VAT corresponding to Venn Diagram presented in Figure 4G

Sample type	Lean sEV	Obese sEV	Obese lEV	Lean lEV	Lean lEV + Obese sEV	Lean sEV + Obese sEV	Lean lEV + Lean sEV	Obese lEV + Obese sEV	Lean lEV + Obese lEV + Obese sEV	Lean lEV + Lean sEV + Obese lEV	Lean sEV + Obese lEV + Obese sEV	Lean lEV + Lean sEV + Obese lEV + Obese sEV
Number of lipid species retrieved	**10**	**11**	**8**	**7**	**1**	**6**	**4**	**4**	**2**	**1**	**5**	**16**
Lipid species enriched in AdEV subtypes	Cer(d18:2/22:0) Cer(d18:2/23:0) Cer(d18:2/24:0) Cer(d18:2/24:1) LPE(20:4) LPE(22:4) LPE(22:5) PA(32:0) PE(16:0p/22:4) PS(34:1)	PA(40:4) PC(34:0) PC(36:2) PE(32:0) PG(36:1) PG(38:2) SM(36:1) SM(36:2) SM(38:1) SM(40:1) SM(42:2)	Cer(d18:0/23:0) LPC(18:0) LPC(18:1) LPC(20:2) LPC(22:3) LPE(22:3) PE(18:0p/18:3) SM(42:3)	Cer(d18:2/14:0) Cer(d18:2/18:1) LPE(18:0) PC(30:1) PG(32:0) PS(32:0) PS(36:5)	Cer(d18:2/26:0)	Cer(d18:1/23:0) Cer(d18:1/24:0) Cer(d18:1/24:1) Cer(d18:2/20:0) Cer(d18:2/21:0) PG(38:3)	Cer(d18:1/18:1) Cer(d18:1/19:0) Cer(d18:2/19:0) Cer(d18:2/24:2)	LPC(20:1) PC(30:2) SM(34:1) SM(38:2)	Cer(d18:2/23:1) PG(34:3)	LPC(22:4)	Cer(d18:0/20:0) Cer(d18:0/24:1) Cer(d18:1/20:0) Cer(d18:1/22:0) PG(36:3)	Cer(d18:0/16:0) Cer(d18:0/18:0) Cer(d18:0/22:0) Cer(d18:1/14:0) Cer(d18:1/16:0) Cer(d18:1/18:0) Cer(d18:1/25:0) Cer(d18:1/26:0) Cer(d18:1/26:1) Cer(d18:2/16:0) Cer(d18:2/18:0) PC(28:0) PC(30:0) PC(32:0) PC(34:1) PG(36:4)

Table S5 : Detailed lipid species significantly depleted in AdEV compared to source VAT corresponding to Venn Diagram presented in Figure 4H

Sample type	Lean sEV	Obese sEV	Obese lEV	Lean lEV	Lean lEV + Obese sEV	Lean sEV + Obese sEV	Lean lEV + Lean sEV	Obese lEV + Obese sEV	Lean lEV + Obese lEV + Obese sEV	Lean lEV + Lean sEV + Obese lEV	Lean sEV + Obese lEV + Obese sEV	Lean lEV + Lean sEV + Obese lEV + Obese sEV
Number of lipid species retrieved	**4**	**5**	**8**	**4**	**1**	**6**	**5**	**6**	**4**	**1**	**2**	**17**
Lipid species depleted in AdEV subtypes	LPC(16:0) PC(34:3) SM(32:1) SM(38:1)	LPC(20:3) LPC(22:6) PE(18:0p/18:2) PE(18:0p/20:5) PI(36:1)	PA(38:5) PC(36:0) PC(36:6) PE(16:0p/22:6) PE(40:5) PI(34:1) PS(36:3) PS(38:2)	PC(38:2) PE(38:2) SM(40:1) SM(42:4)	PI(36:3)	PE(34:1) PE(34:2) SM(38:2) SM(40:2) SM(41:1) SM(41:2)	PC(38:4) PC(40:4) PC(40:8) PE(18:0p/22:6) PE(34:0)	PE(28:0) PE(38:3) PE(40:8) PI(38:3) PI(38:6) PI(40:6)	PE(36:2) PI(36:4) PI(38:4) PI(38:5)	PC(40:7)	PE(32:1) PI(36:2)	PC(36:3) PC(36:4) PC(36:5) PC(38:3) PC(38:5) PC(38:6) PC(40:5) PC(40:6) PE(36:3) PE(36:4) PE(36:5) PE(38:4) PE(38:5) PE(38:6) PE(40:6) PE(40:7) PS(40:6)

Extracellular vesicles are stable carriers of adiponectin with insulin-sensitive properties

Alexia Blandin[1,2#], Jérémy Amosse[2,3#], Grégory Hilairet[2], Maëva Durcin[2], Xavier Prieur[1], Luisa Vergori[2], Cédric Dray[4], Jean-Philippe Pradère[4], Joëlle DUPONT[5], Pierre-Henri Ducluzeau[5,6], Séverine Dubois[7], Jérôme Boursier[7,8], Bertrand Cariou[9] and Soazig Le Lay[1,2*]

[#]These authors equally contributed

[1] Université de Nantes, CNRS, INSERM, l'institut du thorax, F-44000 Nantes, France.

[2] Univ Angers, *SFR* ICAT, F-49000 Angers, France

[3] IRSET Laboratory, Inserm, UMR 1085, Rennes, France

[4] Restore UMR1301 Inserm, 5070 CNRS, Université Paul Sabatier, France.

[5] CNRS, IFCE, INRAE, Université de Tours, PRC, F-37380, Nouzilly, France

[6] Service de Médecine Interne, Unité d'Endocrinologie Diabétologie et Nutrition, Centre Hospitalier Universitaire et Faculté de Médecine, Université de Tours, Tours, France

[7] CHU Angers, Angers, France

[8] Univ Angers, CHU Angers, HIFIH, *SFR* ICAT, F-49000 Angers, France

[9] Université de Nantes, CHU Nantes, CNRS, INSERM, l'institut du thorax, F-44000 Nantes, France.

Keywords:
Obesity; extracellular vesicles; adipose tissue; adiponectin; exosomes; adipokines

Abbreviations :

AT, adipose tissue ; BAT, brown adipose tissue ; DPP4, dipeptidyl peptidase-4 ; EV, extracellular vesicles; FGF-1, fibroblast growth factor-1 ; HOMA-IR, Homeostatic Model Assessment of Insulin Resistance ; ICAM-1, intercellular adhesion molecule-1 ; IR, insulin resistance, NAFLD, Non-Alcoholic Fatty Liver Disease ; PAI-1, plasminogen activator inhibitor-1 ; RBP4, retinol binding protein 4 ; VAT, visceral adipose tissue; SAT, subcutaneous adipose tissue; T2D, Type 2 Diabetes; WAT, white adipose tissue.

[*]**Correspondence:** soazig.lelay@inserm.fr

Manuscript description:

4 Figures, 4 Supplemental Figures, 1 Supplemental Table, 1 Key Resources Table

Word count : 25 371 characters including spaces including introduction, results and discussion and figure legends.

Abstract

Adipose tissue (AT) plays a critical role in the metabolic crosstalk between organs, partly mediated by adipokines. Recent studies evidenced AT-derived extracellular vesicles (EV) as important mediators of obesity-associated metabolic dysfunctions. In this context, we performed AT-derived EV adipokine profiling to identify EV-associated factors that could mediate EV metabolic effects.
We evidenced the ability of AT to secrete both large (lEV) and small (sEV) EV subpopulations, a secretion that is enhanced in obese (ob/ob) mice compared to lean animals. Adiponectin was the most enriched adipokine in adipocyte-derived EV, predominantly in sEV, where it is present under its oligomeric active forms. Adiponectin mainly distributes at the EV external surface for both visceral AT-derived EV and plasma EV, as a result of unspecific adsorption of soluble adiponectin, with adiponectin-associated EV content paralleling adiponectinemia. We further demonstrate that EV-associated adiponectin maintains its insulin-sensitizing properties on target cells and that its injection in high fat diet-fed mice prevent the animals from the development of insulin resistance.
Altogether, our results highlight EV as new original carriers of metabolic active forms of adiponectin, that are likely to participate to its beneficial effects.

186 words

Introduction

Extracellular vesicles (EV) are mediators of cell-to-cell communication that participate in the development of various pathologies (Couch et al., 2021). EV identify membrane-derived vesicle subtypes that differ by their size, origin and composition (van Niel et al., 2018). Small EV (sEV) refer to endolysosomal-derived exosomes whereas large EV (lEV) define microvesicles budding directly from the plasma membrane. Both EV subtypes are secreted in the extracellular space and circulate via biofluids, allowing EV to exert paracrine or endocrine effects. EV circulating levels were found to be increased in obese patients in comparison with lean healthy subjects (Amosse et al., 2018; Santamaria-Martos et al., 2020; Stepanian et al., 2013). Moreover, EV plasma levels were correlated with BMI and HOMA-IR suggesting a potential role of EV in the pathogenesis of type 2 diabetes (T2D) (Amosse et al., 2018; Freeman et al., 2018; Li et al., 2016; Santamaria-Martos et al., 2020).
We previously documented the ability of adipocytes to secrete high quantities of lEV and sEV, which display specific protein and lipid signatures (Durcin et al., 2017). Adipocyte-derived EV secretion is induced by lipid and inflammatory signals, two metabolic traits of obesity (Camino et al., 2020; Durcin et al., 2017; Mleczko et al., 2018). Accordingly, sEV secretion by adipose tissue (AT) is enhanced in different preclinical models of obesity (Deng et al., 2009; Lazar et al., 2016). Blood injections of obese AT-derived sEV into lean mice promoted whole body insulin resistance (IR) when compared to injections of lean AT-derived sEV (Deng et al., 2009). The metabolic effects of adipocyte-derived sEV rely on the intercellular transfer of EV cargos including genetic material, proteins, lipids or even organelles. AT-derived sEV serve as carriers of miRNA (Thomou et al., 2017; Ying et al., 2017), adipokines (Kranendonk et al., 2014), proteins (Crewe et al., 2018), neutral lipid carriers (Flaherty et al., 2019) or mitochondria (Crewe et al., 2021), illustrating a versatile and complex mode of communication that participate to the development of obesity-associated metabolic complications.

Recent evidences support that AT-derived EV take an important part of the AT secretome and its metabolic effects, leading us to characterize the adipokine profiling of lean and obese adipocyte-derived EV subtypes. We identified adiponectin as the most enriched adipokine in AT-derived EV, preferentially associated with the sEV subtype, whose content was mainly driven by unspecific adsorption of this hormone to these nanovesicles. EV nonetheless provide stable carriers for adiponectin delivery and maintain its insulin-sensitizing properties *in vitro* and *in vivo*. Our results therefore provide new understandings in adiponectin-related metabolic responses by highlighting EV as delivery platforms of metabolic active forms of adiponectin molecules.

Methods

All key resources used in this study are presented as supplemental material in a Key Resource Table (KRT).

Human studies. Institutional ethics committee approved the study and consent was obtained from each patient. Patients with Metabolic syndrome (MS) were included from the NUMEVOX cohort (NCT00997165) at the Department of Endocrinology and Nutrition of Angers University Hospital according to eligibility criteria previously described (Amosse et al., 2018). Twenty-seven patients with MS (11 females/16 males) and stratified in two groups according to their BMI (in $kg.m^{-2}$): 10 overweight patients (27<BMI<30) and 17 obese patients (BMI>30) and compared to 8 control patients (4 females/4 males, BMI <27). Clinical parameters of the patients included in the study were measured as previously described (Amosse et al., 2018) and are presented in Table S1. Plasma adiponectin levels were also measured in some patients by Elisa (R&DSystems) and was further correlated with plasma adiponectin^{+} EV detected by flow cytometry in the same patients.

Human adipose tissue explants were collected from three fat depots (Mesenteric, Epiploon and subcutaneous) from patients undergoing a bariatric surgery and included in the prospective monocentric METABOSE cohort (Nutrition Department, CHU Tours) following patient written consent and after local ethical committee agreement (CNIL n° 18254562).

Animal experimentation and in vivo EV treatment. Adult mice heterozygous (ob/+) for the leptin spontaneous mutation Lep^{ob} were initially obtained from Charles River (B6.Cg-*Lep* ^{ob}/J, Stock N° 000632, JAX^{TM} mice strain) and interbred to obtain a colony. Regular backcross with commercial Lep$^{ob/+}$ is performed to avoid any background drift. 3 to 5-month-old lean (ob/+ or +/+) or obese (ob/ob) mice were used for plasma collection following intracardiac puncture and adipose tissue dissection.

Mice expressing specifically Zs-Green in adipocytes (AdipoZS1) were obtained following the crossing of RCL-ZsGreen (B6.Cg-Gt(ROSA)26Sor$^{tm6(CAG-ZsGreen1)Hze/J}$, Stock N°007906, JAX^{TM} mice strain) with mice expressing a tamoxifen-inducible cre recombinase, Cre-ERT2, under the control of the adiponectin gene promoter (C57BL/6-Tg(Adipoq-cre/ERT2)1Soff/J, Stock N°025124, JAX^{TM} mice strain).

Adipocyte-specific expression Adiponectin KO (Adpn KO) mice were obtained from the Jackson Laboratory (B6;129-Adipoq^{tm1Chan}/J, Stock N° 008195) and interbred to obtain a colony.

Male C57BL/6 (B6) mice were fed with high-fat diet (HFD) (61% fat calories, 20% protein calories, and 20% carbohydrate calories, #D12492, Safe Diets) or a normal chow diet *ad libitum* directly after weaning (at 4-5 weeks of age) and for 4 weeks. During this HFD, visceral adipose tissue (VAT)-derived EV were adoptively transferred into recipient mice twice a week by intraperitoneal injection (i.p.). Each injection contains 5µg of EV proteins resuspended into 100µl NaCl 0.9%, a quantity that was chosen since it corresponds to the EV protein mean quantity secreted by 500mg of VAT (that

corresponds to the mean VAT weight of a lean mice) over 48hr. In the control groups, 100µl sterile NaCl 0.9% was injected as vehicle.
All mice had ad libitum access to food and water and were housed in the same open mouse facility on a 12/12hr light-dark cycle day/night cycle. Animal care and study protocols were approved by the French Ministry of Education and Research and the ethics committee N°6 in animal experimentation and were in accordance with the EU Directive 2010/63/EU for animal experiments. At sacrifice, mice tissues are collected and used as explants for EV production or fixed in PFA 4% for immunohistochemistry or frozen in liquid nitrogen and stored at -80°C for protein lysates.

Glucose tolerance test (GTT). GTT was performed in the 4th week of sEV injections. Food was removed 6hr before the initiation of the intra-peritoneal GTT) At time 0, a single dose of glucose (2g/kg) was administered by i.p. injection and blood glucose levels were monitored using a glucometer (AccuCheck, Roche) on 2.5µl samples collected from the tail. GTT was also performed on standard diet (SD)-fed mice as a control for normal glucose tolerance response.

AMPK phosphorylation assay. EV-associated adiponectin action on AMPK pathway was investigated by measuring AMPK phosphorylation on Threonine 172 in target tissues. After 6hr fasting, mice were anesthetized and parts of liver and muscle were collected to measure AMPK phosphorylation.

Insulin-stimulated AKT phosphorylation assay. EV-associated adiponectin insulin sensitive effects action was evaluated by measuring insulin-stimulated AKT phosphorylation on Serine 473 in insulin cells/target tissues.
For *in vitro* experiments, palmitate-treated hepatocytes incubated or not with sEV (as described in cell culture section) were treated for 5min with insulin (100nM) prior protein lysate preparations. One representative blot together with the quantification of p-Akt/Akt ratio as fold increase over basal condition (NaCl) are presented.
For *in vivo* experiments, phosphorylation of AKT in response to 0.5U/kg body weight insulin injection in the *vena cava* of 6hr-fasted mice was studied in tissue lysates collected at different time points following insulin stimulation : liver at 3min, skeletal muscle at 7min and VAT at 10min.

Primary adipocytes and adipose tissue explants culture. 3 to 4g of mice AT were used for collagenase adipocyte isolation as previously described (Durcin et al., 2017) or minced into small pieces for VAT, subcutaneous AT (SAT) or brown adipose tissue (BAT) explants. Adipocytes or adipose tissue explants culture were placed into Clinicell® 25 cassette filled with 10mL ECBM/Hepes 10mM/BSA FFA free 0,1% pH 7.4 as previously described (Decaunes et al., 2018). Serum-free conditioned medium (CM) after 48hr culture was collected, filtered on 100µm cell strainer and use for EV isolation.

AT-derived EV isolation. CM was first spun at 1,500x*g* for 20 min to remove cells and cell debris. lEV were recovered from cell-cleared supernatants (1,500x*g* for 20 min) by centrifugation 60min at 13,000*xg*, followed by two washing steps in NaCl and resuspended in sterile NaCl 0.9%. sEV were further isolated from lEV-depleted supernatants following a 100,000x*g* ultracentrifugation step for 1hr at 4°C (rotor MLA-50, Beckman Coulter Optima MAX-XP Ultracentrifuge) and two washes in NaCl. EV protein content was estimated by DC-protein assay kit by using BSA as standard. Purity of isolated EV was checked on density gradients by loading 20-45µg of each EV subtype at the bottom of an iodixanol density gradient as previously described (Kowal et al., 2016) with adaptations to fit the gradient in tubes required for the MLS-50 rotor. Briefly, EV were resuspended in 1.35mL of buffer containing 0.25M sucrose, 10mM Tris pH 8.0, 1mM EDTA (pH 7.4) and mixed 1:1 with 60% (wt/vol) stock solution of iodixanol/Optiprep™. Next, 1.2mL and 1.1mL of 20% and 10% iodixanol solutions were successively layered on top of vesicles and tubes were centrifuged for 2.5hr at 268,000x*g* at 4°C in MLS-50. 10 fractions of 500µl were collected from the top of the tube. Density fractions was assessed with a refractometer (R-5000, Atago). Fractions collected were then diluted with 500µl PBS and ultracentrifuged for 30min at 100,000*xg* in MLA-130 rotor. Concentrated fractions were resuspended in 22.5µl PBS and loaded on Western-blot.

Plasma/Serum EV isolation. Mice and human peripheral blood was collected on EDTA-coated tubes as previously described (Amosse et al., 2018). Platelet-free plasma (PFP) was subjected to two series of centrifugations, each at 21,000x*g* for 45min to pellet lEV. The lEV-depleted PFP was further ultracentrifuged two times at 100,000x*g* for 1hr to isolate sEV. PFP adiponectin concentrations was measured using 2µl PFP and total EV-depleted PFP samples according to adiponectin ELISA kit manufacturer's protocol (R&D systems). Mouse serum was collected on heparinized capillary tubes and EV-free serum was prepared following the ultracentrifugation protocol described for EV-depleted PFP.

Adiponectin clearance. The clearance of native adiponectin was determined by injecting 200µl of wild-type serum or EV-free serum (following serum-EV depletion by a two times 100,000x*g* ultracentrifugation for 1hr), both diluted to a quarter in NaCl, into the tail vein of 8-week-old Adpn KO mice as previously described (Halberg et al., 2009). Blood samples were subsequently collected at the indicated time points in heparinized capillary tubes. The levels of circulating adiponectin at the various time points in the Adpn KO mice were determined by adiponectin measurement using a commercial ELISA kit and following the manufacturer's protocol (R&D systems).

Mouse EV biodistribution. 66µg of AT-derived sEV protein were labeled with 800CW N-hydroxisuccinimide (NHS)-ester IRDye at a 0.03mg dye for 1mg EV total protein in a final volume of 100µl of sterile NaCl0.9% according to the manufacturer's instructions (LICOR Biosciences).

Labeled EV were recentrifuged (100,000x*g* for 1hr) and the EV pellet was resuspended in 100µl sterile NaCl 0.9%. The total volume of labeled EV were injected via i.p. or intravenous (vein tail) injections in lean B6 control mice. Organ fluorescent background was also evaluated respectively following the injection of 100µl of NaCl 0.9% or EV-free NHS-ester labeling supernatant. Mice were sacrified 3hr post-injection, organs were collected immediately then imaged with a Licor Odyssey® infrared imager to evaluate labeled sEV biodistribution. Each organ is demarcated, then fluorescence intensity is measured in the respective organ surface with Image J software and expressed as fluorescence intensity per surface unit.

EV enzymatic assays. 20µg of EV were incubated with 20µg/ml of Proteinase K (PK) in the presence or not of 1% Triton X100 or left untreated, in a final volume of 1 ml for 1hr at 37°C. PMSF (5 mM) was added 5 min at 37°C and PK was inactivated by placing the mix assay at 90°C for 10min. Similarly, EV were either incubated with Trypsin-EDTA 0,25% or left untreated, in a final volume of 200µl for 20min at 37°C. EV-free serum was added to inactivate trypsin. Trypsin-treated EV were further enriched by adiponectin following their incubation with 500µl EV-depleted VAT conditioned medium. Following enzymatic treatment, lEV and sEV were, respectively, repelleted at 13,000x*g* or 100,000x*g* for 1hr and resuspended in 22.5µl PBS and loaded on Western-blot.

Cell culture. HepG2 cells were maintained in high-glucose DMEM with 10% FBS at 37°C and seeded in 6-well plates (200,000 cells/well) for experiments. Before experiments, culture medium was changed to low-glucose DMEM 0.5% BSA for 5hr then 0.3mM palmitate was added during 24hr to induce insulin resistance. Hepatocytes, rendered or not insulin resistant following palmitate exposure, were incubated for 24hr with different sEV concentrations (5, 10 or 20µg/mL) as indicated in Figure 3A. The concentration of 10µg/mL of sEV was classically used as a reference in others Figures as we previously demonstrated sEV-induced cellular effects without inducing any detrimental cellular effects (Fleury et al., 2016) Insulin-response was evaluated by measuring Akt phosphorylation on cell lysates following 100nM insulin stimulation for 5min. Transfection of pre-designed siRNA was performed high-glucose DMEM 10% FBS medium using 25nM siRNA and RNAiMax Lipofectamine according to the manufacturer's instructions (Invitrogen).
Stable fluorescent venus tagged adiponectin (Adpn-Venus) or venus tag (Venus) lentiviral plasmids were respectively transfected in packaging cells to produce lentiviral particles used to further infect HEK293 cells as previously described (Briand et al., 2014). Stable Adpn-Venus or Venus expressing HEK293 were selected and maintained by Zeocin selection (250µg/mL) in high glucose DMEM, 10% FBS medium. Stable Adpn-Venus or Venus cells were then cultured in 15cm cell culture plates in high glucose DMEM, 10% FBS medium, then serum-deprived for 48hr to allow collection of HEK293 supernatants from which Adpn-Venus or Venus sEV were isolated following classical 100,000x*g* ultracentrifugation procedure. For internalization experiments, HepG2 cells were seeded on glass coverslips, incubated with 10µg/mL Adpn-Venus sEV and fixed with PFA 4% and mounted in Mowiol at the different time points presented. After DAPI staining, sEV internalization was visualized by

confocal laser fluorescence (Zeiss LSM 710). Fluorescence quantification was performed using ImageJ software. Quantification of Adpn-sEV Venus internalization is presented as % of cell fluorescence, the 24hr time point being set to 100%.

Western-Blotting. 5-10µg of protein lysates were prepared and migrated on SDS-PAGE for western-blot as previously described (Durcin et al., 2017). Detection of adiponectin multimeric forms was achieved through migration of samples under non-reducing conditions (DTT was excluded from Laemmli buffer) and unheated conditions. IRDye® (LI-COR Biosciences) secondary antibodies were used and digital fluorescence visualized by Odyssey CLX system (LICOR). Immunoblot quantification was performed following analysis of protein signal by Image Studio® software. Antibodies used are listed in KRT Table and one representative blot for each protein is presented (among the mentioned independent experiment performed).

Nanoparticle tracking analysis (NTA). EV concentration and size were determined by NTA analysis (NanoSight NS300 equipped with a 405 nm laser, Malvern Instruments), as previously described (Durcin et al., 2017). EV samples were diluted 100 fold in sterile NaCl 0.9% prior NTA analysis. Video imaging was recorded with optimized set parameters (the detection threshold was set to 7 and 5, respectively, for lEV and sEV). Temperature was automatically monitored and ranged from 20°C to 21°C. Videos were analyzed when a sufficient number of valid trajectories was measured. Data capture and further analysis were performed using the NTA software version 3.1. At least three independent biological samples of each EV subtype were analyzed, and the presented results correspond to the mean of the five videos taken for a given biological sample.

sEV Immunocapture. An alternative immunocapture-based method was also used to confirm adiponectin presence in VAT-derived EV by using the exosome isolation kit pan CD9/CD63/CD81 according to the manufacturer's protocol (Myltenyi Biotec). Briefly, 50µl of exosome isolation microbeads were incubated for 1hr with 2mL pre-cleared VAT explant supernatants prior loading on a equilibrated "µ" column placed in the magnetic field of the quadroMACS™ separator (Myltenyi Biotec). After four washing with isolation buffer, elution of $CD9^+CD63^+CD81^+$ positive sEV was performed by placing the column outside of the magnetic separator and the labeled vesicles were flushed out. Eluted sEV were further used for Western blot analysis.

Protein arrays. Mice adipokine array kits were incubated with 50µg of each EV subtype (lEV or sEV), and processed according to manufacturer's protocol (R&D systems). Protein signals were revealed using ChemiSmart 500 imager (Vilber Lourmat). Signal intensity of spots (two per protein, measured as pixels number) was quantified using Image J Software and expressed as pixels mean of the two spots/µg of protein loaded on membrane. Results presented are the mean of signal intensity (mean pixels per µg of protein) obtained for each protein out of two independent blotting

experiments. Only detectable protein signals out of the 38 adipokines tested are presented (see list in Figure S1C).

Flow cytometry assays. Flow cytometry lEV phenotyping was performed from the analysis of PFP as previously described (Amosse et al., 2018). Five µl PFP fixed with PFA 2% in PBS for 15min at room temperature, then washed by 1.5mL PBS, was used for adiponectin detection. lEV were pelleted (21,000x*g*, 15 min) and permeabilized with 100µl PBS/saponin 0.1% for 5 min at RT, prior incubation with 10µl of FITC-conjugated specific antibody. Irrelevant human immunoglobulin G (IgG) was used as an isotype-matched negative control for each sample and subtracted from the value obtained. Data obtained are expressed as percent of total EV analyzed.

Immunohistology. Five µm adipose tissue cuts were processed for immunohistochemistry. Classical hematoxylin/eosin and Picrosirius red staining were respectively performed to assess AT structural morphology and fibrosis.

Statistical analysis. Data are analyzed using GraphPad Prism Software and presented as dot plots representing independent experiments. Statistical analysis of the results was performed by using adapted statistical tests indicated in the figure legends. The differences were considered significant when *p* value<0.05 and stated as follow: **p*<0.05, ***p*<0.01, ****p*<0.005 and *****p*<0.001.

Results

Obesity increases EV subtypes secretion from fat depots.

EV isolation was performed from cultured VAT conditioned media using differential ultracentrifugation, respectively 13,000x*g* for lEV and 100,000x*g* for sEV. Significant EV mean size differences observed between lEV and sEV were still maintained when EV subtypes were isolated from obese VAT (Figure 1A). In agreement with EV subcellular origin, a specific enrichment of flottilin-2 membranous protein was observed in lEV whereas sEV were enriched in tetraspanins (Alix, CD9, CD63) (Figure 1B). Obese VAT-derived sEV displayed a strong enrichment in CD63 (Figure 1C). Comparison of EV secretion according to fat location revealed the common ability of VAT, SAT and BAT to secrete lEV and sEV, although VAT appeared as the highest producer of EV subtypes over the others fat depots (Figure 1D). Obesity moreover increased adipose EV secretion for VAT (Figure 1E) and SAT (Figure S1 A), whereas similar EV production was measured from lean and obese BAT (Figure S1B). Measurement of EV secretion originating from human fat biopsies from obese patients confirmed the ability of VAT (i.e. epiploon and mesenteric fat depots) to secrete more sEV per gram of fat in comparison to subcutaneous AT (Figure 1F).

Adipocyte-derived EV-adipokine profiling identifies adiponectin as an EV-abundant protein.

Quantifying circulating EV derived from adipocytes implies the identification of adipocyte-specific proteins specifically sorted by EV, among which adipokines represent main candidates. By blotting EV isolated from VAT-isolated adipocytes with adipokine arrays, we revealed similar adipokine pattern for lEV and sEV and identified adiponectin and resistin as the most EV-enriched adipokines. In addition, lower amount of dipeptidyl peptidase-4 (DPP4), fibroblast growth factor-1 (FGF-1), endocan, lipocalin, intercellular adhesion molecule-1 (ICAM-1), retinol binding protein 4 (RBP4) or plasminogen activator inhibitor-1 (PAI-1) were also detected in lean isolated adipocyte-derived lEV and sEV preparations (Figure 1G, Figure S1C). Similar adipokine EV profiles were obtained when arrays were blotted with VAT-derived EV subtypes from lean or obese (ob/ob) mice highligting that adipocyte secretome was mainly driven adipokine EV content (Figure S1D-E).

Since adiponectin appeared as the most abundant and specific adipocyte EV marker, we next focused on adiponectin association to VAT-derived EV subtypes. We demonstrated its specific enrichment within sEV by comparison to lEV in lean conditions (Figure 1H, Figure S1F). Under non-reducing conditions, high and middle molecular weight forms of adiponectin, recognized as metabolically active forms, were particularly enriched in the sEV population (Figure 1I). EV-associated adiponectin levels dropped in obese conditions, reaching undetectable levels in obese VAT-derived EV (Figure 1H-I). When submitted to a density gradient, lEV-associated adiponectin colocalized with lEV markers flotillin-2 and β-actin (Figure S1G), whereas sEV-associated adiponectin floated in fraction 3 enriched in CD9 and CD63 (Figure S1H). Soluble adiponectin (still

present in EV-free VAT conditioned media) and sEV-associated adiponectin were retrieved in different fractions, excluding any contamination of sEV-associated adiponectin by non-vesicular adiponectin (Figure S1I). By using an immunocapture technique allowing the isolation of $CD9^+CD63^+CD81^+$-enriched sEV, we further confirmed adiponectin presence in immunoprecipitated sEV (Figure S1J).

Adiponectin-associated EV mainly distributes on the EV external face.

In order to characterize vesicular adiponectin association, we subjected VAT-derived sEV to a proteinase K (PK) protection assay. The majority of sEV-associated adiponectin signal disappeared following PK treatment illustrating the distribution of adiponectin mainly on EV external surface (Figure 1J-K). We next tested the ability of EV to stick non-vesicular secreted adiponectin by incubating sEV, derived either from obese VAT or HEK cells (which displayed low or no adiponectin protein signal, respectively) with EV-free VAT conditioned media as a source of soluble adiponectin. We observed important adsorption of adiponectin to sEV. This association was totally abolished when sEV were pre-treated with trypsin, highlighting the involvement of EV extracellular proteins in adiponectin binding to EV surface, irrespective of sEV cellular source (Figure 1L). Adiponectin levels adsorbed to obese VAT-derived sEV did not overpass the adiponectin content of lean VAT-derived sEV suggesting a limitation of the number of adiponectin molecules that could stick to sEV, likely inherent to steric hindrance led by sEV size (Figure S1J).

EV constitute stable conveyors of adiponectin in the blood circulation.

We next tracked fluorescent VAT-derived EV isolated from mice expressing the fluorescent protein ZS-Green specifically in adipocytes (Figure S2A-B). Flow cytometry analysis identified around 2% of $ZsGreen^+$ EV in mice plasma (Figure 2A), a percentage which might be underestimated since the laser beam of the flow cytometer does not resolve light scattered by particles smaller than 100 nm, therefore excluding sEV quantification. Total EV depletion from mouse plasma led to a nearly 20% drop in adiponectinemia identifying plasma EV as effective conveyors of adiponectin (Figure 2B). We confirmed the presence of oligomeric adiponectin forms in plasma EV, mostly enriched in the sEV subpopulation, whose content dropped in obese mice following plasma adiponectin levels (Figure S2C). Similarly to VAT-derived EV, plasma EV-associated adiponectin distributed at the external face of lEV and sEV as proven by adiponectin signal disappearance following PK treatment (Figure S2D). We next measured the clearance rate of plasma adiponectin following injection of WT serum (depleted or not of EV) into the tail vein of adiponectin KO mice. We demonstrated a drastic reduction of blood adiponectin stability in the absence of EV suggesting that EV act as stable scaffolds of metabolic active forms of adiponectin in the circulation (Figure 2C).

We finally explored the physiological relevance of adiponectin-EV trafficking in human blood samples collected from healthy, overweight or obese patients (Table S1). As for mice, adiponectin content detected in plasma-derived sEV was drastically reduced in patients with obesity compared to healthy

controls (Figure S2E). Adiponectin also distributed at the external face of human plasma sEV, although we identified a significant intravesicular pool that was degraded after triton X100 sEV membrane permeabilization (Figure S2F). Flow-cytometry analysis of patient platelet-free plasma demonstrated an elevation of plasma lEV concentrations in obese patients (Figure S2G). We previously reported that this elevation of circulating lEV in obese patients was associated with a significant increase of platelet and endothelial cell-derived lEV and a trend towards an increase of lEV pro-coagulant activity of lEV (Amosse et al., 2018). In the absence of saponin membrane permeabilization, we identified a small portion (≈2.5%) of adiponectin$^+$ plasma lEV in control healthy patients that dropped and was close to background in overweight and obese patients (Figure 2D, white bars), therefore paralleling the drop of plasma adiponectin levels during obesity (Table S1). Accordingly, adiponectin$^+$ lEV levels measured in the absence of saponin strongly correlates with plasma adiponectinemia measured in the same patients (Figure 2E). Besides, saponin treatment significantly increased adiponectin-positiveness of lEV in all patient groups revealing a second pool of adiponectin enclosed within the vesicles (Figure 2D, grey bars), that did not associate with plasma adiponectin levels (Figure 2F). Altogether, our results demonstrate that EV definitely convey adiponectin but its unspecific sticking that is closely related to patient adiponectinemia precludes its use for the quantification of adipocyte-derived EV.

Adiponectin-associated sEV mediates insulin sensitizing effects in target cells.

Adiponectin is recognized as an insulin-sensitizing hormone by signaling on target tissues, like the liver and skeletal muscle, mainly via the adiponectin receptors AdipoR1 and R2. Treatment of hepatocytes, rendered insulin-resistant following palmitate exposition, with 5 µg/ml of lean VAT-derived sEV was sufficient to fully restored insulin-induced AKT phosphorylation, suggesting that the high adiponectin content of these sEV mediate these insulin sensitizing effects (Figure 3A). Accordingly, incubation of obese VAT-derived sEV on palmitate-treated HepG2 failed to restore insulin sensitivity whereas enrichment of these obese sEV with adiponectin (following their preincubation with EV-free conditioned media) fully counteracted insulin-resistance (Figure 3B). Adiponectin is likely not the sole molecule which will vary in VAT-secreted EV according to the lean or obese status. We therefore switched to stable HEK293 cell lines expressing either a fluorescent-tagged adiponectin Venus or the Venus tag alone to isolate sEV carrying these respective molecules (Figure S3A-B). Adiponectin-Venus sEV can readily and efficiently target HepG2 cells as demonstrated by their rapid and time-dependent hepatocyte internalization (Figure 3C). Adiponectin-Venus sEV reversed insulin resistance of palmitate-treated hepatocytes by contrast to Venus sEV firmly establishing the crucial role of adiponectin in insulin-sensitizing effects of lean VAT-derived sEV (Figure 3D). Insulin sensitive effects are likely to be mediated through the binding of adiponectin-associated sEV to the two canonical adiponectin receptors, since silencing both AdipoR1 and AdipoR2 are necessary to reduce sEV beneficial effects (Figure 3E and Figure S3C).

Collectively, our results demonstrate that adiponectin-associated EV displays same beneficial metabolic properties as soluble adiponectin, likely through binding to regular adiponectin receptors

and downstream signaling cascades.

EV are biological conveyors of bioactive adiponectin to metabolic tissues

We next question the ability of adiponectin-enriched sEV to mediate insulin-sensitizing effects *in vivo*. We then performed adoptive transfer of lean-VAT through repetitive intraperitoneal (i.p) EV injections in mice fed an HFD over 4 weeks, to mimic physiological VAT-derived EV diffusion. Biodistribution of NHS ester-covalently labeled sEV identified vascularized tissues such as lungs, liver, kidney, pancreas and spleen as sEV main targets, as commonly reported EV biodistribution regardless of the EV administration (Kang et al., 2021), whereas fluorescent sEV were also retrieved in VAT depots (Figure 4A, Figure S4A). Nonetheless, we cannot exclude that such sEV, involving the reaction of NHS-ester amine-reactive group with the primary amines of proteins, impact sEV protein structuration and thereby sEV targeting. We first highlighted the specific ability of lean VAT-derived sEV to significantly improve glucose tolerance of obese mice, in comparison to lean VAT-derived lEV or NaCl (vehicle) injections, arguing favorably for a role of adiponectin specifically enriched in sEV in these beneficial effects (Figure S4B-C). In order to delineate the role of adiponectin-associated sEV in these insulin-sensitive effects, we next compared the effects of adoptive transfer of lean VAT-derived sEV with the ones of VAT-derived sEV from adiponectin KO mice. Adiponectin-deficient sEV failed to prevent the progressive hyperglycemia developed by WT mice over the course of HFD as did lean VAT-derived sEV (Figure 4B). Accordingly, adiponectin KO VAT-derived sEV did not improve glucose tolerance as did control sEV (Figure 4C-D). No differences in mouse total weight nor in metabolic tissue weights were observed (Figure S4C-D) and histological processing of VAT did not evidence any morphological alterations of VAT (Figure S4E-F). Improvement of glucose homeostasis was accompanied by enhanced insulin-stimulated AKT phosphorylation in liver, muscle, VAT of HFD WT recipient mice following control sEV injections but not following adiponectin-deficient sEV or NaCl injections (Figure 4E-G). Canonical adiponectin signaling downstream the AdipoR also includes AMPK activation, which thereby would control negatively lipogenic and fatty oxidation pathways. Accordingly, we revealed a trend towards AMPK activation in the liver and skeletal muscle following control sEV injections but not with adiponectin-deficient sEV (Figure 4H-I).

Discussion

We identified adiponectin as the most enriched adipokine in adipocyte-derived EV, whose content was mainly driven by its unspecific adsorption to these nanovesicles. EV nonetheless provide stable carriers for adiponectin delivery which maintains its insulin-sensitizing properties *in vitro* and *in vivo*.

We confirmed the AT capacity to secrete both lEV and sEV, whose secretion were both enhanced in the obesity context as previously demonstrated for sEV (Deng et al., 2009; Lazar et al., 2016). Whereas obesity did not impact EV subtype size, we revealed a CD63 enrichment in obese VAT-derived sEV, in agreement with previous data reporting higher level of CD63 in HFD mature adipocyte-derived sEV (Pan et al., 2019). This may reflect an unexplained selective enhancement of $CD63^+$-sEV secretion pathway in obese conditions. We moreover highlighted VAT, both in mice and humans, as higher EV providers than subcutaneous AT depots. This higher secretion ability may be linked to adipocyte size, since VAT adipocytes are more hypertrophied than subcutaneous ones. VAT is also known to be more susceptible to metabolic alterations associated with chronic obesity including hypoxia, inflammation or lipotoxic lipids influx, stimuli which have all been described to induce adipocyte EV secretion (Camino et al., 2020; Durcin et al., 2017; Mleczko et al., 2018). A recent study demonstrated distinct protein content between sEV isolated from human obese VAT or SAT, characterized by a particular enrichment of proteins implicated in inflammation or insulin-resistance in sEV from VAT (Camino et al., 2021). Altogether, these data reinforce the idea that adipose VAT-derived sEV could actively participate to visceral obesity-associated cardiometabolic complications.

In this regard, the identification of a specific marker of adipocyte-derived EV to trace and quantify them in the blood would be of particular interest. Among adipokine signature retrieved in VAT-derived EV, adiponectin is the sole hormone to be recognized as specifically secreted by adipocytes. We didn't detect neither leptin nor IL-6 or TNFα in adipocyte-derived EV suggesting that adipokine EV sorting is controlled by specific mechanisms. We also identified traces of RBP4, a protein previously retrieved in obese AT-derived sEV that has been suggested to participate to the induction of macrophage activation-induced insulin resistance (Deng et al., 2009). We confirmed adiponectin association to VAT-derived EV and circulating EV, mainly distributing at the EV outer membrane as also demonstrated by others for serum adiponectin-associated sEV (Garcia-Martin et al., 2022; Phoonsawat et al., 2014). Although in the minority, an intravesicular pool of adiponectin was still detectable following EV external enzymatic treatment. Recent data have evidenced the ability of adiponectin to stimulate, through T-cadherin binding, endothelial sEV production and re-secretion of adiponectin as an exosomal cargo contributing to raise significantly the adiponectin circulating pool (Obata et al., 2018). Such selective adiponectin EV sorting could account for the intravesicular presence of the adipokine. We moreover demonstrated that external adiponectin-associated EV occurs by unspecific sticking. Noticeably, sEV are specifically enriched in extracellular matrix

proteins when compared to lEV subpopulation, a reason which may explain their higher capacity to bind adiponectin (Durcin et al., 2017; Kowal et al., 2016). In agreement with adiponectin adsorption on EV, adiponectin EV content fully parallels adiponectinemia. Since vesicular adiponectin sticking is not restricted to EV of adipocyte origin, we conclude on the lack of reliability and robustness of any quantitative assays that will use this adipokine to identify circulating adipocyte-derived EV.

Previous reports demonstrated that lean AT macrophages-derived sEV transfer into HFD recipient mice improved insulin sensitivity, an ability which was linked to macrophage-derived EV miRNA produced in the lean state (Ying et al., 2021; Ying et al., 2017). Similarly, we demonstrated beneficial effects of lean VAT-derived sEV injections on glucose homeostasis of HFD recipient mice that was dependent on the presence of adiponectin-associated sEV. We observed improved liver, muscle and AT insulin sensitivity. Patrolling macrophages have been evidenced as main target cells of circulating EV based on live tracking EV imaging (Hyenne et al., 2019; Verweij et al., 2019). Moreover, AT macrophages ($CD11b^+/F4/80^+$) macrophages, among other AT SVF cells, uptake important quantities of adipocyte-derived sEV (Crewe et al., 2018). Therefore, we cannot exclude that the internalization of lean VAT-derived sEV by immune cells may contribute to reduce inflammation and improve indirectly the metabolic profile of recipient HFD mice.

Altogether, our results therefore provide new understandings in adiponectin-related metabolic responses by highlighting EV as stable scaffolds of molecular active forms of adiponectin. Our results open new EV-based therapeutic perspectives for adiponectin delivery which might promising for the treatment of diabetes developed by lipodystrophic or obese patients.

Conflict of Interest statement

There are no conflicts of interest to declare.

Competing interests

AB and SLL declare that the research described in this paper is patent pending: European Patent Application EP21306717.6.

Data availability statement

Data are available on request.

Author contributions

Methodology, AB, JA, GH, MV, SLL ; Experimentation and analysis, AB, JA, GH, MD, LV, CD, J-PP,SLL ; patient recruitment, JD, PHD, JB, SD ; writing-original draft preparation, AB, SLL ; review and edition of the manuscript, AB, JA, GH, MD, XP, LV, CD, J-PP, JD, PHD, SD, JB, BC and SLL; conceptualization, AB, JA, SLL; supervision, project administration and funding acquisition, SLL.
All authors have read and agreed to the published version of the manuscript.

SLL is the guarantor of this work and, as such, had full access to all the data in the study and take responsibility for the integrity of the data and the accuracy of the data analysis.

Acknowledgments

We thank Pr Weiping Han (Laboratory of Metabolic Medicine, Singapore Bioimaging Consortium) for providing Venus-adiponectin lentiviral plasmid. We thank Mireille Wertheimer for technical assistance with plasmid purification. We thank Quentin Massicot and Julien Chaigneau for histological cut image analysis. We thank the staff of Centre Hospitalo-Universitaire d'Angers for analysis of clinical data of Numevox cohort. We thank J-C Gimel (INSERM U1066, MINT Team, Angers, France) for providing access to NTA technology. We thank Dr. Nicolas Blanchard (INSERM U1291, Toulouse, France) for giving the Zs-Green1 mouse line. We thank the SCIAM platform, especially Florence Manero, for electron microscopy imaging and technical assistance. We thank the SCAHU platform for mouse housing and technical assistance for animal functional exploration.
This work was supported by a research grant from Genavie, Société Francophone du Diabète (SFD) and INSERM. JA and MD are recipients of a doctoral fellowship from French Ministry of Education and Research. AB is a recipient of a doctoral fellowship co-financed by INSERM/Région Pays de La Loire.

References

Amosse, J., Durcin, M., Malloci, M., Vergori, L., Fleury, A., Gagnadoux, F., Dubois, S., Simard, G., Boursier, J., Hue, O., et al. (2018). Phenotyping of circulating extracellular vesicles (EVs) in obesity identifies large EVs as functional conveyors of Macrophage Migration Inhibitory Factor. Mol Metab *18*, 134-142.

Briand, N., Prado, C., Mabilleau, G., Lasnier, F., Le Liepvre, X., Covington, J.D., Ravussin, E., Le Lay, S., and Dugail, I. (2014). Caveolin-1 expression and cavin stability regulate caveolae dynamics in adipocyte lipid store fluctuation. Diabetes *63*, 4032-4044.

Camino, T., Lago-Baameiro, N., Bravo, S.B., Molares-Vila, A., Sueiro, A., Couto, I., Baltar, J., Casanueva, E.F., and Pardo, M. (2021). Human obese white adipose tissue sheds depot-specific extracellular vesicles and reveals candidate biomarkers for monitoring obesity and its comorbidities. Transl Res.

Camino, T., Lago-Baameiro, N., Bravo, S.B., Sueiro, A., Couto, I., Santos, F., Baltar, J., Casanueva, F.F., and Pardo, M. (2020). Vesicles Shed by Pathological Murine Adipocytes Spread Pathology: Characterization and Functional Role of Insulin Resistant/Hypertrophied Adiposomes. Int J Mol Sci *21*.

Couch, Y., Buzas, E.I., Vizio, D.D., Gho, Y.S., Harrison, P., Hill, A.F., Lotvall, J., Raposo, G., Stahl, P.D., Thery, C., et al. (2021). A brief history of nearly EV-erything - The rise and rise of extracellular vesicles. Journal of extracellular vesicles *10*, e12144.

Crewe, C., Funcke, J.B., Li, S., Joffin, N., Gliniak, C.M., Ghaben, A.L., An, Y.A., Sadek, H.A., Gordillo, R., Akgul, Y., et al. (2021). Extracellular vesicle-based interorgan transport of mitochondria from energetically stressed adipocytes. Cell Metab.

Crewe, C., Joffin, N., Rutkowski, J.M., Kim, M., Zhang, F., Towler, D.A., Gordillo, R., and Scherer, P.E. (2018). An Endothelial-to-Adipocyte Extracellular Vesicle Axis Governed by Metabolic State. Cell *175*, 695-708 e613.

Decaunes, P., Bouloumié, A., Ryden, M., and Galitzky, J. (2018). Ex vivo Analysis of Lipolysis in Human Subcutaneous Adipose Tissue Explants. Bio-protocol *8*, e2711.

Deng, Z.B., Poliakov, A., Hardy, R.W., Clements, R., Liu, C., Liu, Y., Wang, J., Xiang, X., Zhang, S., Zhuang, X., et al. (2009). Adipose tissue exosome-like vesicles mediate activation of macrophage-induced insulin resistance. Diabetes *58*, 2498-2505.

Durcin, M., Fleury, A., Taillebois, E., Hilairet, G., Krupova, Z., Henry, C., Truchet, S., Trotzmuller, M., Kofeler, H., Mabilleau, G., et al. (2017). Characterisation of adipocyte-derived extracellular vesicle subtypes identifies distinct protein and lipid signatures for large and small extracellular vesicles. Journal of extracellular vesicles *6*, 1305677.

Flaherty, S.E., 3rd, Grijalva, A., Xu, X., Ables, E., Nomani, A., and Ferrante, A.W., Jr. (2019). A lipase-independent pathway of lipid release and immune modulation by adipocytes. Science *363*, 989-993.

Fleury, A., Hoch, L., Martinez, M.C., Faure, H., Taddei, M., Petricci, E., Manetti, F., Girard, N., Mann, A., Jacques, C., et al. (2016). Hedgehog associated to microparticles inhibits adipocyte differentiation via a non-canonical pathway. Scientific reports *6*, 23479.

Freeman, D.W., Noren Hooten, N., Eitan, E., Green, J., Mode, N.A., Bodogai, M., Zhang, Y., Lehrmann, E., Zonderman, A.B., Biragyn, A., et al. (2018). Altered Extracellular Vesicle Concentration, Cargo and Function in Diabetes Mellitus. Diabetes.

Garcia-Martin, R., Brandao, B.B., Thomou, T., Altindis, E., and Kahn, C.R. (2022). Tissue differences in the exosomal/small extracellular vesicle proteome and their potential as indicators of altered tissue metabolism. Cell reports *38*, 110277.

Halberg, N., Schraw, T.D., Wang, Z.V., Kim, J.Y., Yi, J., Hamilton, M.P., Luby-Phelps, K., and Scherer, P.E. (2009). Systemic fate of the adipocyte-derived factor adiponectin. Diabetes *58*, 1961-1970.

Hyenne, V., Ghoroghi, S., Collot, M., Bons, J., Follain, G., Harlepp, S., Mary, B., Bauer, J., Mercier, L., Busnelli, I., et al. (2019). Studying the Fate of Tumor Extracellular Vesicles at High Spatiotemporal Resolution Using the Zebrafish Embryo. Dev Cell *48*, 554-572 e557.

Kang, M., Jordan, V., Blenkiron, C., and Chamley, L.W. (2021). Biodistribution of extracellular vesicles following administration into animals: A systematic review. Journal of extracellular vesicles *10*, e12085.

Kowal, J., Arras, G., Colombo, M., Jouve, M., Morath, J.P., Primdal-Bengtson, B., Dingli, F., Loew, D., Tkach, M., and Thery, C. (2016). Proteomic comparison defines novel markers to characterize heterogeneous populations of extracellular vesicle subtypes. Proc Natl Acad Sci U S A *113*, E968-977.

Kranendonk, M.E., Visseren, F.L., van Balkom, B.W., Nolte-'t Hoen, E.N., van Herwaarden, J.A., de Jager, W., Schipper, H.S., Brenkman, A.B., Verhaar, M.C., Wauben, M.H., et al. (2014). Human adipocyte extracellular vesicles in reciprocal signaling between adipocytes and macrophages. Obesity (Silver Spring) *22*, 1296-1308.

Lazar, I., Clement, E., Dauvillier, S., Milhas, D., Ducoux-Petit, M., LeGonidec, S., Moro, C., Soldan, V., Dalle, S., Balor, S., et al. (2016). Adipocyte Exosomes Promote Melanoma Aggressiveness through Fatty Acid Oxidation: A Novel Mechanism Linking Obesity and Cancer. Cancer Res.

Li, S., Wei, J., Zhang, C., Li, X., Meng, W., Mo, X., Zhang, Q., Liu, Q., Ren, K., Du, R., et al. (2016). Cell-Derived Microparticles in Patients with Type 2 Diabetes Mellitus: a Systematic Review and Meta-Analysis. Cell Physiol Biochem *39*, 2439-2450.

Mleczko, J., Ortega, F.J., Falcon-Perez, J.M., Wabitsch, M., Fernandez-Real, J.M., and Mora, S. (2018). Extracellular Vesicles from Hypoxic Adipocytes and Obese Subjects Reduce Insulin-Stimulated Glucose Uptake. Mol Nutr Food Res *62*.

Obata, Y., Kita, S., Koyama, Y., Fukuda, S., Takeda, H., Takahashi, M., Fujishima, Y., Nagao, H., Masuda, S., Tanaka, Y., et al. (2018). Adiponectin/T-cadherin system enhances exosome biogenesis and decreases cellular ceramides by exosomal release. JCI Insight *3*.

Pan, Y., Hui, X., Hoo, R.L.C., Ye, D., Chan, C.Y.C., Feng, T., Wang, Y., Lam, K.S.L., and Xu, A. (2019). Adipocyte-secreted exosomal microRNA-34a inhibits M2 macrophage polarization to promote obesity-induced adipose inflammation. J Clin Invest *129*, 834-849.

Phoonsawat, W., Aoki-Yoshida, A., Tsuruta, T., and Sonoyama, K. (2014). Adiponectin is partially associated with exosomes in mouse serum. Biochem Biophys Res Commun *448*, 261-266.

Santamaria-Martos, F., Benitez, I.D., Latorre, J., Lluch, A., Moreno-Navarrete, J.M., Sabater, M., Ricart, W., Sanchez de la Torre, M., Mora, S., Fernandez-Real, J.M., et al. (2020). Comparative and functional analysis of plasma membrane-derived extracellular vesicles from obese vs. nonobese women. Clin Nutr *39*, 1067-1076.

Stepanian, A., Bourguignat, L., Hennou, S., Coupaye, M., Hajage, D., Salomon, L., Alessi, M.C., Msika, S., and de Prost, D. (2013). Microparticle increase in severe obesity: Not related to metabolic syndrome and unchanged after massive weight loss. Obesity (Silver Spring).

Thomou, T., Mori, M.A., Dreyfuss, J.M., Konishi, M., Sakaguchi, M., Wolfrum, C., Rao, T.N., Winnay, J.N., Garcia-Martin, R., Grinspoon, S.K., et al. (2017). Adipose-derived circulating miRNAs regulate gene expression in other tissues. Nature *542*, 450-455.

van Niel, G., D'Angelo, G., and Raposo, G. (2018). Shedding light on the cell biology of extracellular vesicles. Nat Rev Mol Cell Biol *19*, 213-228.

Verweij, F.J., Revenu, C., Arras, G., Dingli, F., Loew, D., Pegtel, D.M., Follain, G., Allio, G., Goetz, J.G., Zimmermann, P., et al. (2019). Live Tracking of Inter-organ Communication by Endogenous Exosomes In Vivo. Dev Cell *48*, 573-589 e574.

Ying, W., Gao, H., Dos Reis, F.C.G., Bandyopadhyay, G., Ofrecio, J.M., Luo, Z., Ji, Y., Jin, Z., Ly, C., and Olefsky, J.M. (2021). MiR-690, an exosomal-derived miRNA from M2-polarized macrophages, improves insulin sensitivity in obese mice. Cell Metab *33*, 781-790 e785.

Ying, W., Riopel, M., Bandyopadhyay, G., Dong, Y., Birmingham, A., Seo, J.B., Ofrecio, J.M., Wollam, J., Hernandez-Carretero, A., Fu, W., et al. (2017). Adipose Tissue Macrophage-Derived Exosomal miRNAs Can Modulate In Vivo and In Vitro Insulin Sensitivity. Cell *171*, 372-384 e312.

Figure legends

Figure 1: Adiponectin is the most enriched adipokine in VAT-derived EV that distributes on the EV outer surface

A. Lean and obese VAT-derived lEV and sEV mode size comparison.

B-C. EV marker analysis from lean (Ctrl) or ob/ob (Ob) VAT explant-derived EV subpopulations.

D. lEV and sEV secretion from VAT, SAT and BAT explants. EV number secreted per gram of AT per 24h is presented.

E. Increased lEV and sEV secretion from mouse VAT with obesity.

F. EV secretion of human epiploon, mesenteric (mesent.) and subcutaneous (subcut.) AT collected from obese subjects.

G. Quantification of adipokine arrays incubated with isolated adipocyte-derived EV.

H. EV-associated adiponectin content is decreased with obesity. Blot quantification is presented in Figure S1F.

I. Adiponectin forms detected in lean VAT-derived EV. R and NR stand for reducing or non-reducing unheated conditions, respectively. HMW, MMW, LMW stand for high, middle and low-molecular weight. One representative blot out of two independent experiments is shown.

J-K. Proteinase K (PK) protection assay reveals adiponectin-associated sEV surface pool. The transmembrane protein CD9 and internal syntenin-1 are used as positive controls of PK activity and PK/Tx100 combined activities, respectively.

L. EV-adiponectin surface pool adsorption depends on sEV-surface proteins. One representative blot is shown out of *n*=3 for Ob sEV and out of *n*=2 for HEK sEV. Syntenin is presented as a loading control. *ND*, not determined.

Data are presented as mean ± sem, dot-plots representing independent samples. Statistical differences were assessed using one-way ANOVA (A-C, E, J-K), multiple t-tests (D, F, H).

Figure 2: Plasma EV represent stable carriers of adiponectin

A. VAT-derived EV are retrieved in the blood circulation as illustrated by flow cytometry detection of ZsGreen^{+} EV in platelet free-plasma (PFP). Ctrl, control ; AdipoZS1, Cre^{-} AdipoZs1 mice ; AdipoZS1, Cre^{+} AdipoZS1 mice.

B. Adiponectinemia significantly decrease upon plasma EV removal in lean mice.

C. Adiponectin clearance measurement following the injection of serum or EV-depleted serum in adiponectin KO mice. *n*=6 mice injected per group.

D. Analysis of adiponectin-positivity of human plasma lEV by flow-cytometry analysis. Percentage of adiponectin^{+} lEV retrieved in plasma patients before (white bars) and after saponin permeabilization (grey bars) is presented for control (BMI<=27), overweight (27<BMI<30) and obese (BMI>30) patients.

E-F. Linear regression between adiponectinemia and adiponectin^{+} lEV rates measured for patients in the absence (**E**) or presence of saponin (**F**).

Data are presented as mean ± sem, dot-plots representing independent experiments. The connected lines identify the same sample analyzed before/after EV depletion (for B) or saponin treatment (for D). Statistical differences were assessed using Mann-Whitney test (A-B), multiple t-tests (C), Wilcoxon matched-pairs signed rank test (D).

Figure 3: EV-associated adiponectin maintains its insulin-sensitive properties in target cells

A-B. Adiponectin-enriched sEV reverses insulin-resistance in hepatocytes. Ins, Insulin ; Palm, palmitate.

C. Rapid and time-dependent hepatocyte internalization of fluorescent adiponectin-Venus (Adpn-Venus) internalization in hepatocytes.

D. Adiponectin-enrichment of sEV is responsible for their insulin sensitive effects.

E. Silencing of both AdipoR1 and AdipoR2 significantly reduces Adpn-Venus sEV insulin-sensitive effects. Scr, Scramble; R1, AdipoR1; R2, AdipoR2.

Dot-plots represent independent experiments. Data are presented as mean ± sem. Statistical differences were assessed using one-way ANOVA test.

Figure 4: EV-associated adiponectin reverses HFD mice insulin resistance

A. NHS ester-labeled VAT-derived sEV organ biodistribution. Licor-fluorescent tissue imaging is presented in Figure S4A.

B. Adoptive transfer of sEV-associated adiponectin gradually improves HFD-induced mice hyperglycemia.

C-D. Adiponectin-associated sEV specifically improves glucose tolerance of HFD-fed mice. Area under curve (AUC) for GTT are presented in **D**. SD, standard diet.

E-G. Western-blot analysis of AKT phosphorylation levels in liver (**E**), muscle (**F**), VAT (**G**) after insulin injection.

H-I. Western-blot analysis of AMPK phosphorylation levels in liver (**H**) and muscle (**I**) measured in tissue lysates collected from 6hr-fasted animals prior insulin injection.

Dot-plots represent independent animals. Data are presented as mean ± sem. Statistical differences were assessed using two-way ANOVA test (A, B), multiple t-tests (C), one-way ANOVA test (D, E-G).

Supplementary information

Supplemental Figures legends

Figure S1: VAT-derived EV and adiponectin-associated EV characterization

A. Comparison of lEV and sEV secretion from SAT (**A**) and BAT (**B**) from lean and obese mice. EV secretion per total mouse AT is presented. *n*=6-8 for SAT and *n*=5-7 for BAT, mean ± sem, *p<0.05 (1-way ANOVA test).

B. Immunoblots of lean VAT-collagenase isolated adipocytes-derived EV whose quantification is presented in Figure 1G. The list of adipokines displayed on the adipokine array is detailed in the adjacent table. Proteins highlighted in blue correspond to those for which a signal was detected, at least, in one of the EV subtype. Black rectangles correspond to positive controls (reference spots) and red rectangles to negative controls (PBS).

D-E. Quantification of adipokine arrays incubated with lean or obese VAT-derived EV subtypes. 50 µg of each EV subtype was loaded on each protein array and immnunoblots were quantified. Adipokines detected in lean or obese VAT derived lEV (**D**) and lean or obese VAT-derived sEV (**E**) are shown. Results presented are mean of signal intensity obtained for each protein (expressed as mean pixels per µg of protein) of two independent blotting experiments for each membrane. The adipokine profile of VAT-derived EV was similar to the one revealed for lean VAT-collagenase isolated adipocytes-derived EV (**Figure 1G**) identifying adipocytes as major providers of EV-associated adipokines.

F. Quantification of adiponectin signal in lean VAT-derived EV subtypes reveals a particular enrichment of adiponectin in sEV. VAT-derived lEV and sEV (8µg each) were analyzed for the presence of adiponectin in reduced conditions. Each colour represents an independent experiment, with lEV and sEV preparations derived from the same VAT. *n*=6, mean ± sem, *p<0.05, **p<0.01 (1-way ANOVA test).

G-I. Density gradient floatation applied to VAT-derived lEV (**G**) and sEV (**H**), as well as to EV-free VAT explants conditioned media (CM) (**I**). lEV-associated adiponectin is retrieved in fraction 8 (1.175 g/mL) and colocalized with lEV markers flotillin-2 and β-actin, whereas sEV-associated adiponectin is enriched in CD9 and CD63-enriched fraction 3 (1.10 g/mL). Soluble native adiponectin form is retrieved in fractions 6-10, therefore excluding that sEV-associated adiponectin results from contamination by soluble adiponectin oligomers.

J. Isolation of $CD9^+CD63^+CD81^+$-enriched sEV isolated by immunocapture technique demonstrates adiponectin retrieval in sEV.

K. Adiponectin adsorption on obese VAT-derived sEV recapitulates adiponectin EV content of lean VAT-derived sEV. Elisa measurement of adiponectin in sEV isolated from lean VAT (Ctrl), obese VAT prior (Ob) or after incubation with EV-depleted VAT conditioned medium (Adpn-Ob) that leads

to sEV-adiponectin adsorption (as presented in **Figure 1L**). Data are presented as mean ± sem *p<0.05, **p<0.01 (1-way ANOVA test corrected for multiple comparisons by Dunnet's post test).

Figure S2: Circulating lEV concentrations according to their cellular origin.

A. Schematical representation of the animal crossing that has led to the generation of mice expressing specifically Zs-Green in adipocytes (AdipoZS1).

B. ZSGreen fluorescent protein/ZS1 is retrieved in AdipoZS1 VAT-derived lEV and sEV.

C. Adiponectin presence is confirmed in mouse plasma circulating EV. Plasma EV subtypes were isolated from lean and obese mice. 10 µg of each EV subtypes were resolved by SDS-PAGE under reducing conditions (R) or non-reducing unheated conditions (NR). One representative blot for each protein is presented (out of two experiments performed).

D. Proteinase K (PK) protection assay on mice plasma EV subtypes confirms the existence of an adiponectin-associated EV surface pool. The transmembrane protein CD9 and internal MIF cytokine are used as positive controls of PK activity and PK/Tx100 combined activities, respectively. NA, non-acquired. One representative blot for each protein is presented (out of two experiments performed).

E. Western-blot of human plasma sEV confirms decreased amount of adiponectin in sEV isolated from obese patients by comparison to control patients. A representative blot (out of two independent experiments performed) is presented.

F. PK protection assay on human plasma sEV highlights an intravesicular pool as well as an external surface EV pool of adiponectin. The transmembrane protein CD9 is presented as a positive controls of PK activity.

G. Plasma total lEV quantification from Platelet Free Plasma (PFP) samples by flow cytometry. Total plasma lEV are presented as lEV number per µl of plasma sample in plasma from control, overweight and obese patients. Significant increase of total plasma lEV was observed in the obesity context.

Figure S3: Studies using HEK293-derived sEV and measurement of AdipoR silencing efficiency.

A-B. Schematical protocol illustrating production of HEK293-derived sEV (**A**) expressing either a fluorescent-tagged adiponectin Venus or the Venus tag alone (**B**) following stable HEK293 cell lines genesis using lentiviral particles encoding these two fluorescent proteins.

C. Adiponectin receptor silencing efficiency assessed by RT-PCR mRNA expression in HepG2 cells transfected by siRNA against adipoR1, AdipoR2 or AdipoR1 and AdipoR2. % of silencing is presented by comparison to siRNA scramble transfection set to 100%. Individual dot plots correspond to independent individual measurements. Significant differences are indicated as follow : *p<0.05, ***p<0.001 (2-way ANOVA test, comparison vs Scramble condition) for AdipoR1 mRNA expression, $^{\#}$p<0.05, $^{\#\#}$p<0.001 (2-way ANOVA test, comparison vs Scramble condition) for AdipoR2 mRNA expression.

Figure S4: Supplemental information for VAT-derived sEV injections in HFD-fed mice

A- Tissue imaging of tissues collected 3 hrs post i.p injection of 800CW infrared NHS ester-labeled VAT-derived sEV, free NHS-ester dye and NaCl. One representative tissue collection is shown (out of 3 independent mice experimentations performed by condition).

B-C. GTT test performed during the 4th week of adoptive transfer of lean VAT-derived lEV and sEV into HFD-fed mice (performed by i.p. injections 2 times a week during 4 weeks). Standard diet (SD) is presented as control to demonstrate HFD-induced glucose intolerance. Corresponding AUC are presented in panel **C**.

D-E. Repetitive i.p. injections of Ctrl sEV, Adpn-KO sEV or NaCl (vehicle) do not modify mice total weight (**D**) nor metabolic tissue weight (**E**).

E-F. Classical hematoxylin/Eosin or Picro-Sirius staining do not evidence adipose tissue structural alterations or fibrosis, respectively. Adipocyte size was measured on VAT histological cuts (**F**), is unchanged following 4 weeks of repetitive injections of Ctrl sEV, Adpn-KO sEV or NaCl.

Supplemental Table legends

KRT Table: Key Resources Table.

Table S1: Clinical parameters of the patients included in the study

Data are expressed as mean ± SEM and compared using the student t test.

Control vs overweight : *p<0.05, **p<0.01, ***p<0.005, ****p<0.001

Control vs obese : $^{\#}$p<0.05, $^{\#\#}$p<0.01, $^{\#\#\#}$p<0.005, $^{\#\#\#\#}$p<0.001

Overweight vs obese : §p<0.05, §§p<0.01, §§§p<0.005, §§§§p<0.001

F: Female, M: Male

Figure 1.

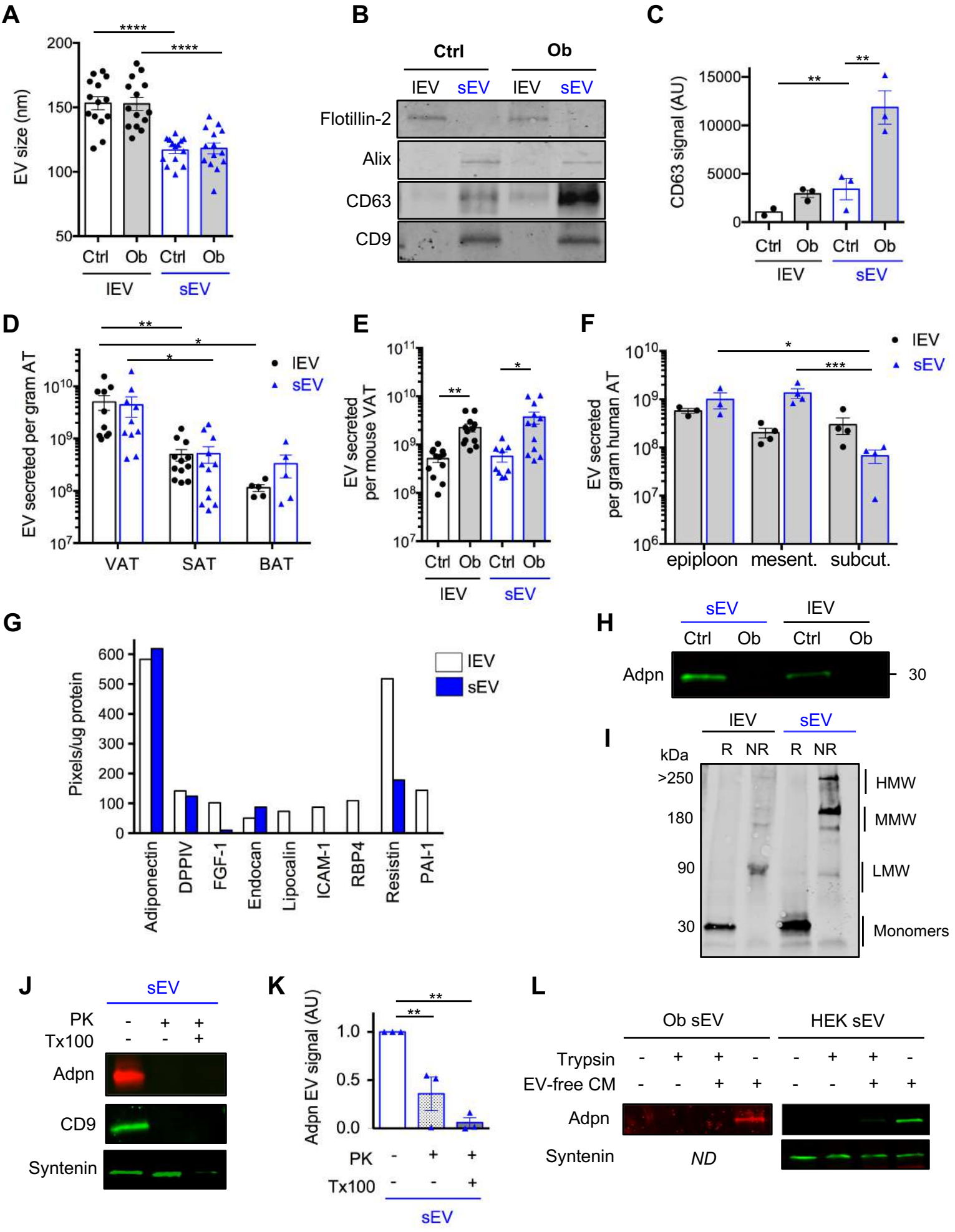
A
EV size (nm)
Ctrl
Ob
IEV
sEV
B
Ctrl
Ob
IEV
sEV
Flotillin-2
Alix
CD63
CD9
C
CD63 signal (AU)
D
EV secreted per gram AT
VAT
SAT
BAT
E
EV secreted per mouse VAT
F
EV secreted per gram human AT
epiploon
mesent.
subcut.
G
Pixels/ug protein
Adiponectin
DPPIV
FGF-1
Endocan
Lipocalin
ICAM-1
RBP4
Resistin
PAI-1
H
Adpn
30
I
kDa
R
NR
>250
180
90
30
HMW
MMW
LMW
Monomers
J
PK
Tx100
Adpn
CD9
Syntenin
K
Adpn EV signal (AU)
L
Ob sEV
HEK sEV
Trypsin
EV-free CM
Adpn
Syntenin
ND

Figure 2.

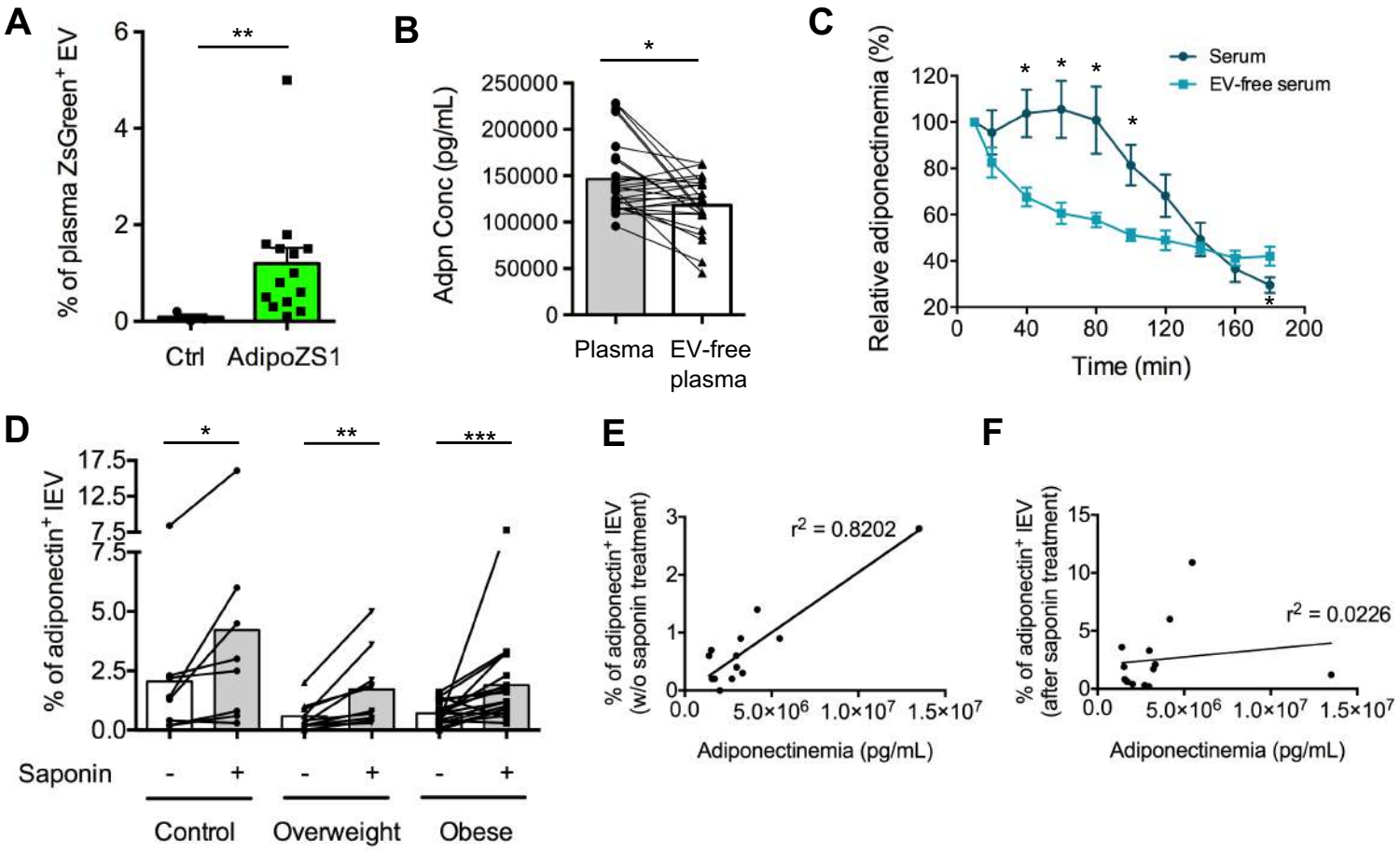
A
% of plasma ZsGreen+ EV
Ctrl
AdipoZS1
B
Adpn Conc (pg/mL)
Plasma
EV-free plasma
C
Relative adiponectinemia (%)
Serum
EV-free serum
Time (min)
D
% of adiponectin+ IEV
Saponin
Control
Overweight
Obese
E
% of adiponectin+ IEV (w/o saponin treatment)
r2 = 0.8202
Adiponectinemia (pg/mL)
F
% of adiponectin+ IEV (after saponin treatment)
r2 = 0.0226
Adiponectinemia (pg/mL)

Figure 3.

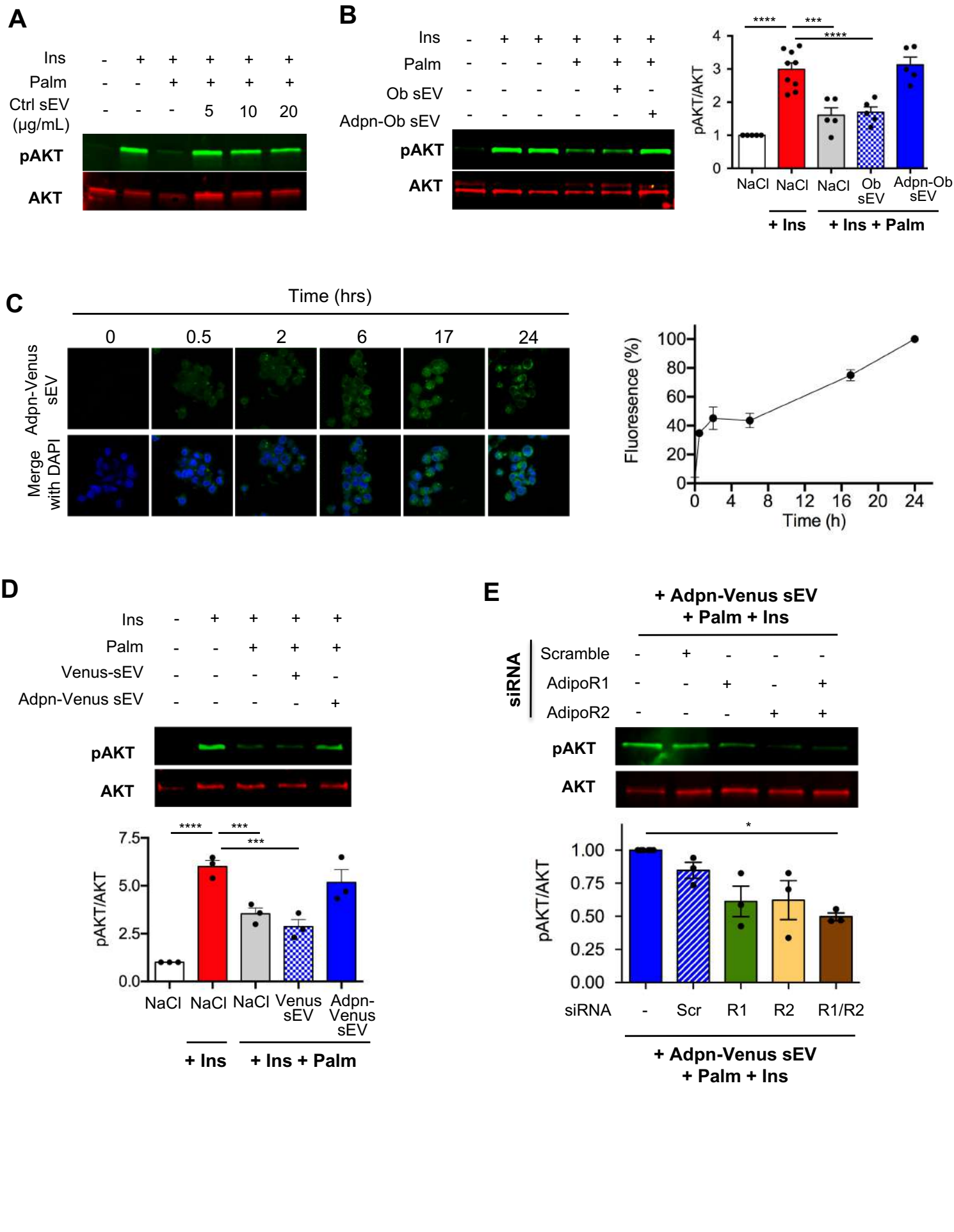
A
Ins
Palm
Ctrl sEV (µg/mL)
pAKT
AKT
B
Ins
Palm
Ob sEV
Adpn-Ob sEV
pAKT
AKT
pAKT/AKT
NaCl
Ob sEV
Adpn-Ob sEV
+ Ins
+ Ins + Palm
C
Time (hrs)
Adpn-Venus sEV
Merge with DAPI
Fluoresence (%)
Time (h)
D
Venus-sEV
Adpn-Venus sEV
Venus sEV
E
+ Adpn-Venus sEV
+ Palm + Ins
siRNA
Scramble
AdipoR1
AdipoR2
Scr
R1
R2
R1/R2

Figure 4.

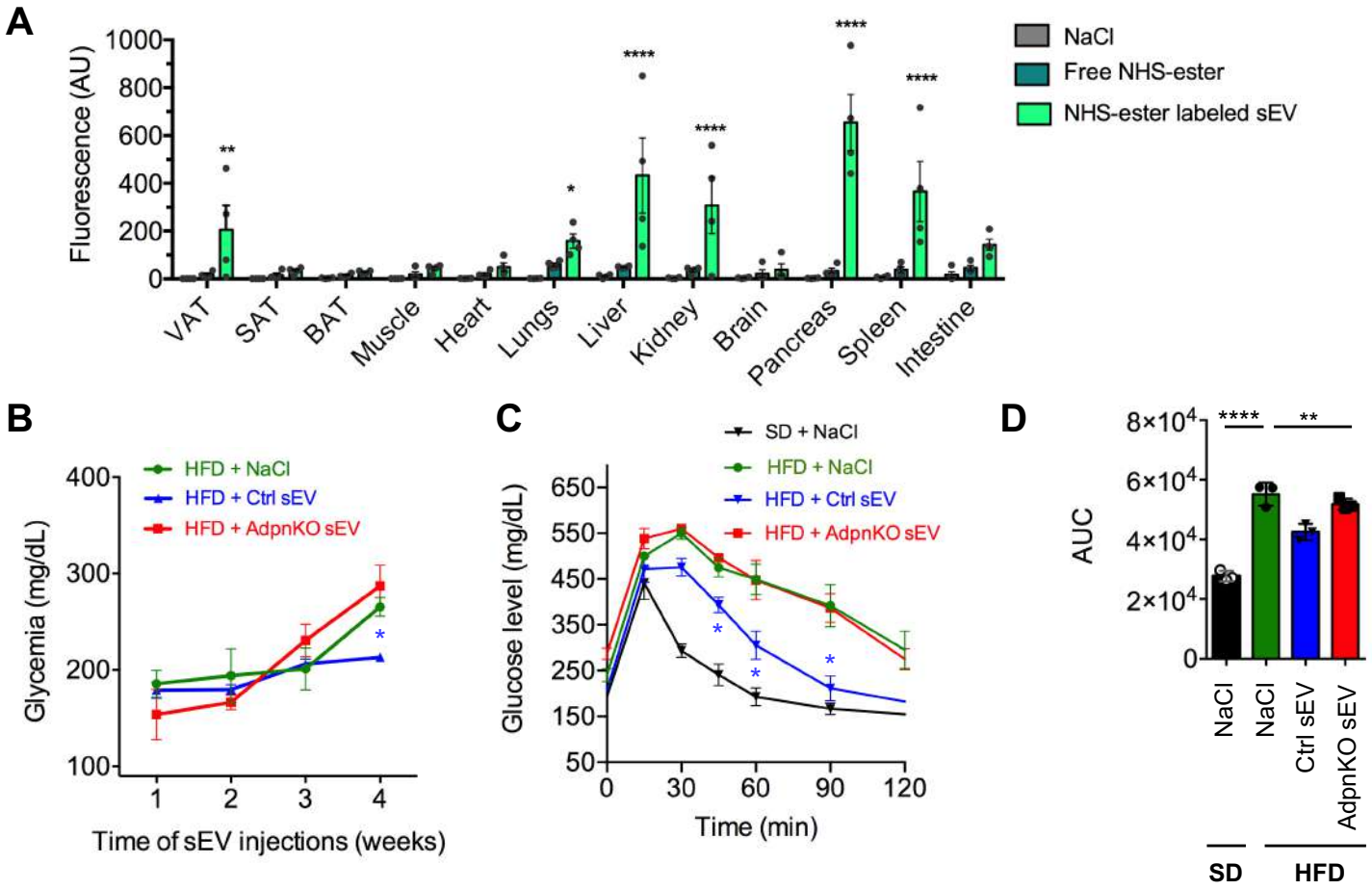
A
Fluorescence (AU)
NaCl
Free NHS-ester
NHS-ester labeled sEV
VAT
SAT
BAT
Muscle
Heart
Lungs
Liver
Kidney
Brain
Pancreas
Spleen
Intestine
B
Glycemia (mg/dL)
HFD + NaCl
HFD + Ctrl sEV
HFD + AdpnKO sEV
Time of sEV injections (weeks)
C
Glucose level (mg/dL)
SD + NaCl
HFD + NaCl
HFD + Ctrl sEV
HFD + AdpnKO sEV
Time (min)
D
AUC
NaCl
NaCl
Ctrl sEV
AdpnKO sEV
SD
HFD

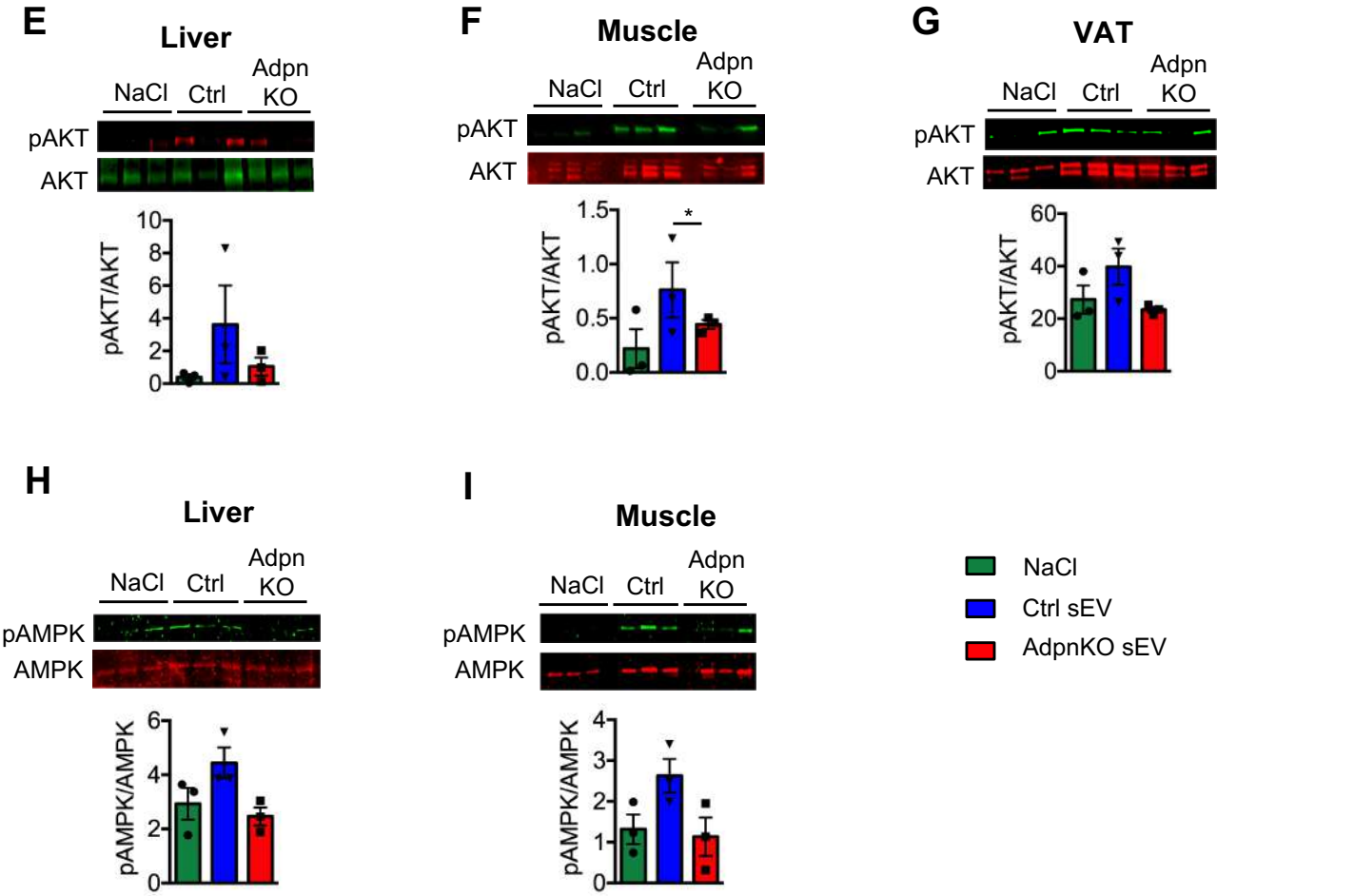
E
Liver
NaCl
Ctrl
Adpn KO
pAKT
AKT
pAKT/AKT
F
Muscle
G
VAT

H
Liver
pAMPK
AMPK
pAMPK/AMPK
I
Muscle
NaCl
Ctrl sEV
AdpnKO sEV

Figure S1

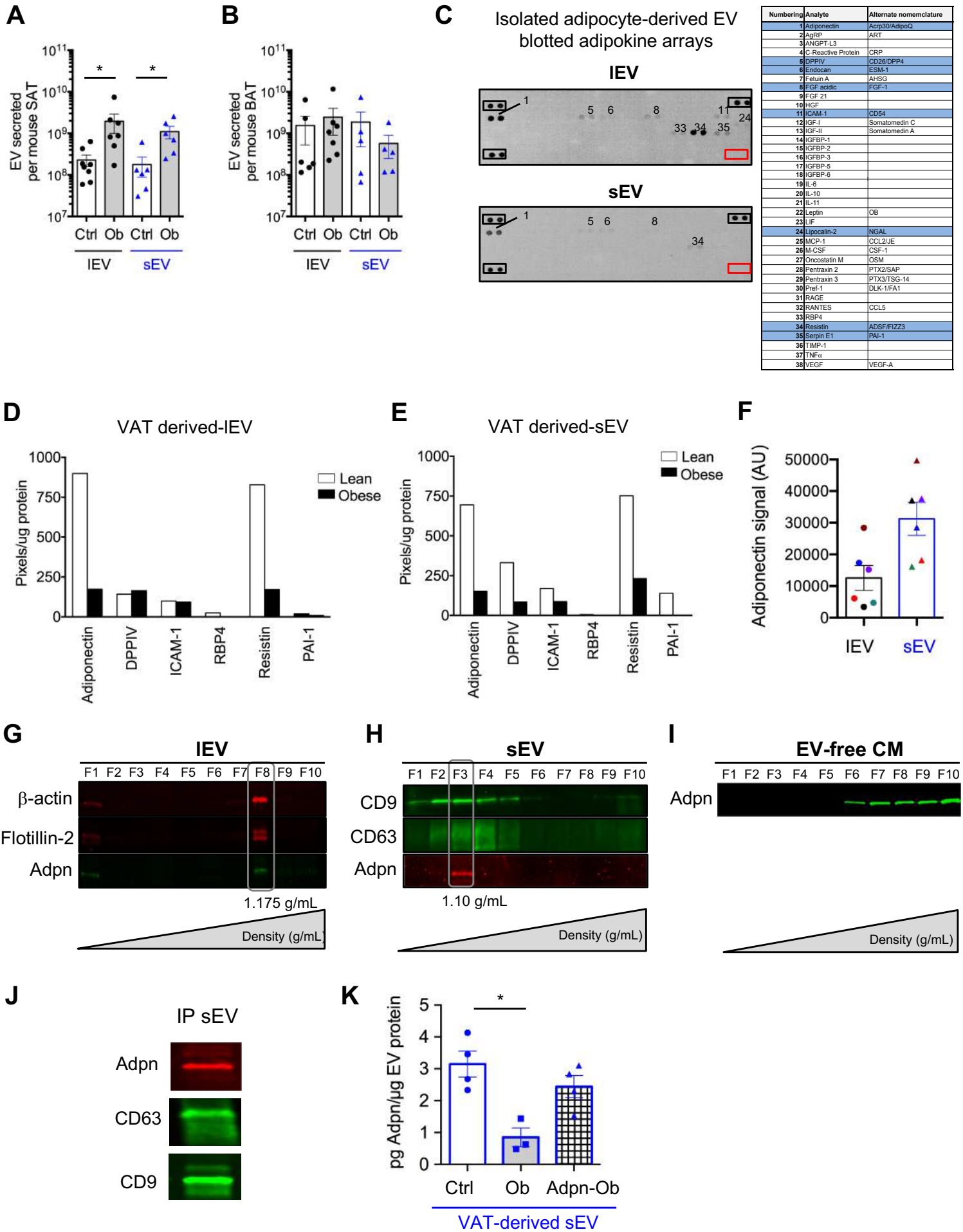

Numbering	Analyte	Alternate nomemclature
1	Adiponectin	Acrp30/AdipoQ
2	AgRP	ART
3	ANGPT-L3	
4	C-Reactive Protein	CRP
5	DPPIV	CD26/DPP4
6	Endocan	ESM-1
7	Fetuin A	AHSG
8	FGF acidic	FGF-1
9	FGF 21	
10	HGF	
11	ICAM-1	CD54
12	IGF-I	Somatomedin C
13	IGF-II	Somatomedin A
14	IGFBP-1	
15	IGFBP-2	
16	IGFBP-3	
17	IGFBP-5	
18	IGFBP-6	
19	IL-6	
20	IL-10	
21	IL-11	
22	Leptin	OB
23	LIF	
24	Lipocalin-2	NGAL
25	MCP-1	CCL2/JE
26	M-CSF	CSF-1
27	Oncostatin M	OSM
28	Pentraxin 2	PTX2/SAP
29	Pentraxin 3	PTX3/TSG-14
30	Pref-1	DLK-1/FA1
31	RAGE	
32	RANTES	CCL5
33	RBP4	
34	Resistin	ADSF/FIZZ3
35	Serpin E1	PAI-1
36	TIMP-1	
37	TNFα	
38	VEGF	VEGF-A

Figure S2

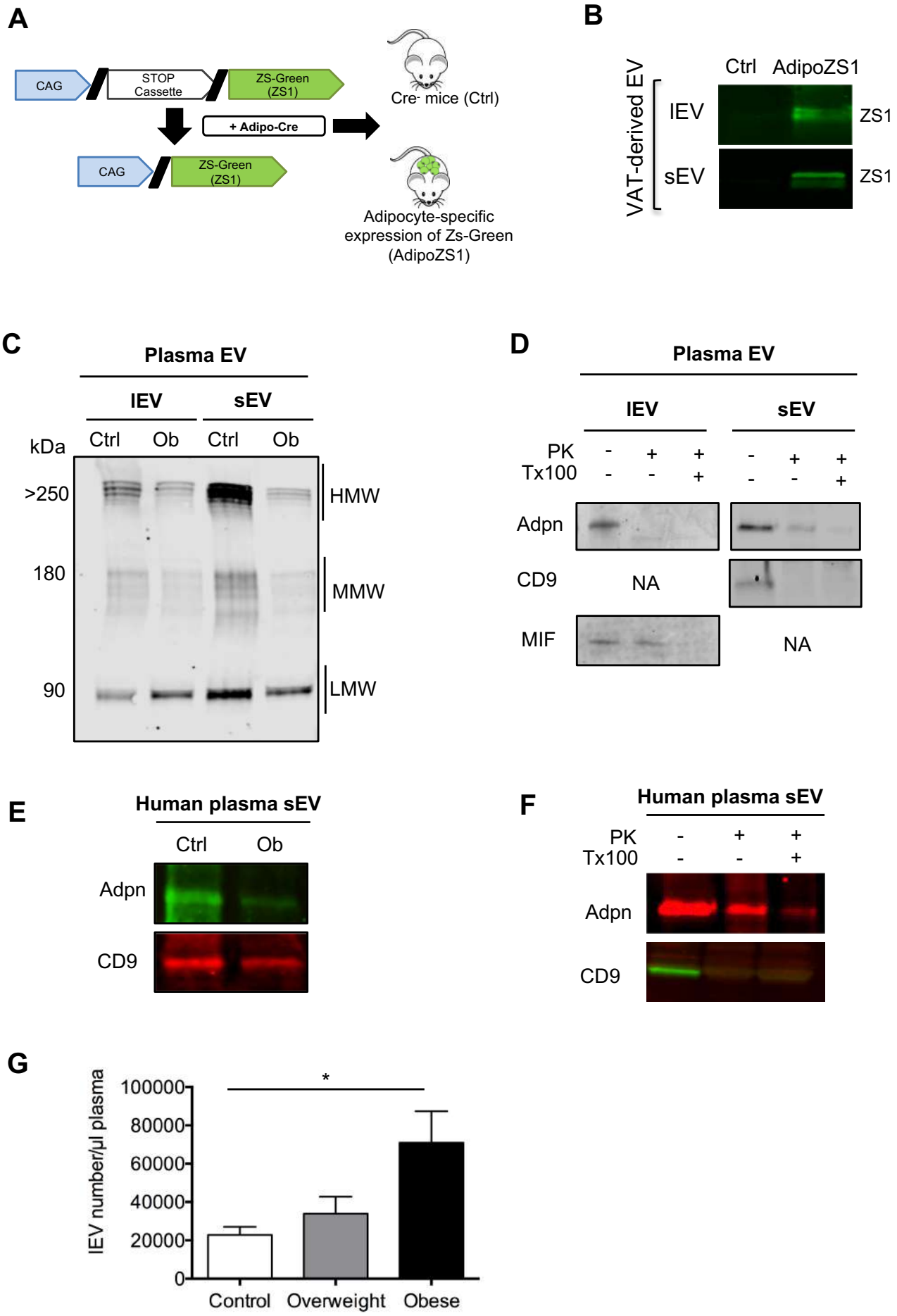
A
CAG
STOP Cassette
ZS-Green (ZS1)
+ Adipo-Cre
CAG
ZS-Green (ZS1)
Cre- mice (Ctrl)
Adipocyte-specific expression of Zs-Green (AdipoZS1)
B
Ctrl
AdipoZS1
VAT-derived EV
IEV
sEV
ZS1
ZS1
C
Plasma EV
IEV
sEV
kDa
Ctrl
Ob
Ctrl
Ob
>250
180
90
HMW
MMW
LMW
D
Plasma EV
IEV
sEV
PK
Tx100
Adpn
CD9
NA
MIF
NA
E
Human plasma sEV
Ctrl
Ob
Adpn
CD9
F
Human plasma sEV
PK
Tx100
Adpn
CD9
G
IEV number/µl plasma
100000
80000
60000
40000
20000
0
*
Control
Overweight
Obese

Figure S3

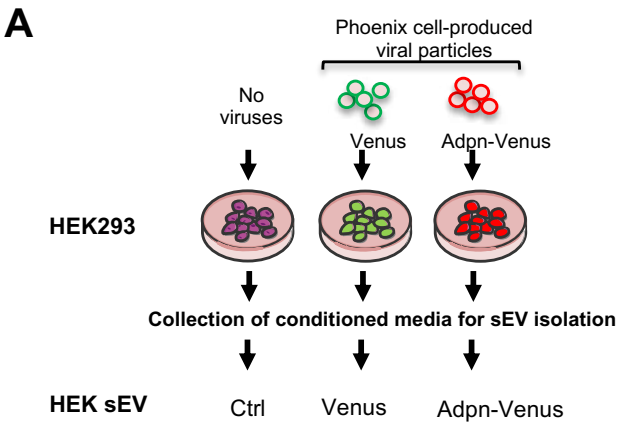
A
Phoenix cell-produced viral particles
No viruses
Venus
Adpn-Venus
HEK293
Collection of conditioned media for sEV isolation
HEK sEV
Ctrl
Venus
Adpn-Venus

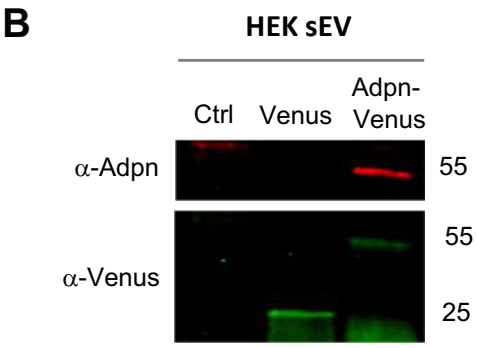
B
HEK sEV
Ctrl
Venus
Adpn-Venus
α-Adpn
α-Venus
55
55
25

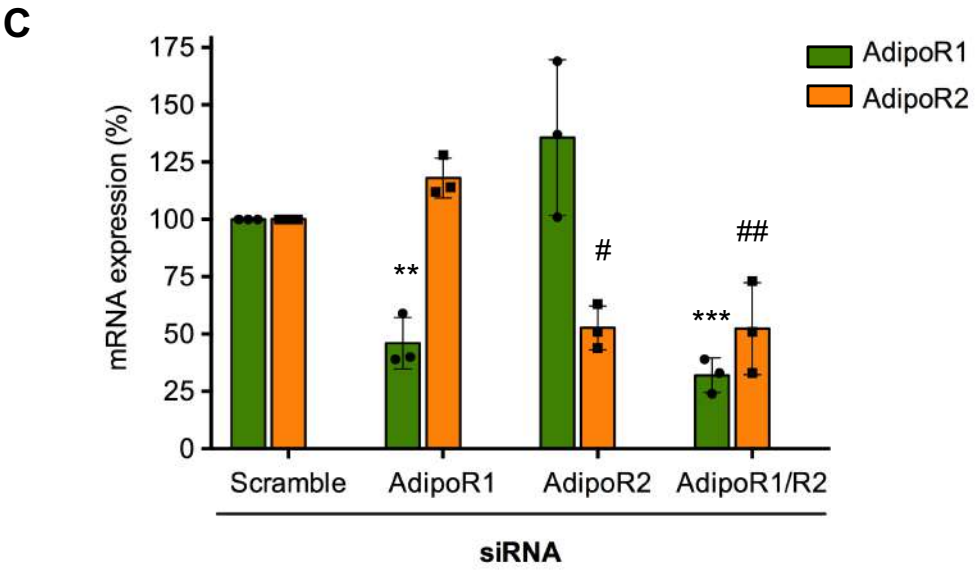
C
AdipoR1
AdipoR2
mRNA expression (%)
175
150
125
100
75
50
25
0
**
#
##
***
Scramble
AdipoR1
AdipoR2
AdipoR1/R2
siRNA

Figure S4

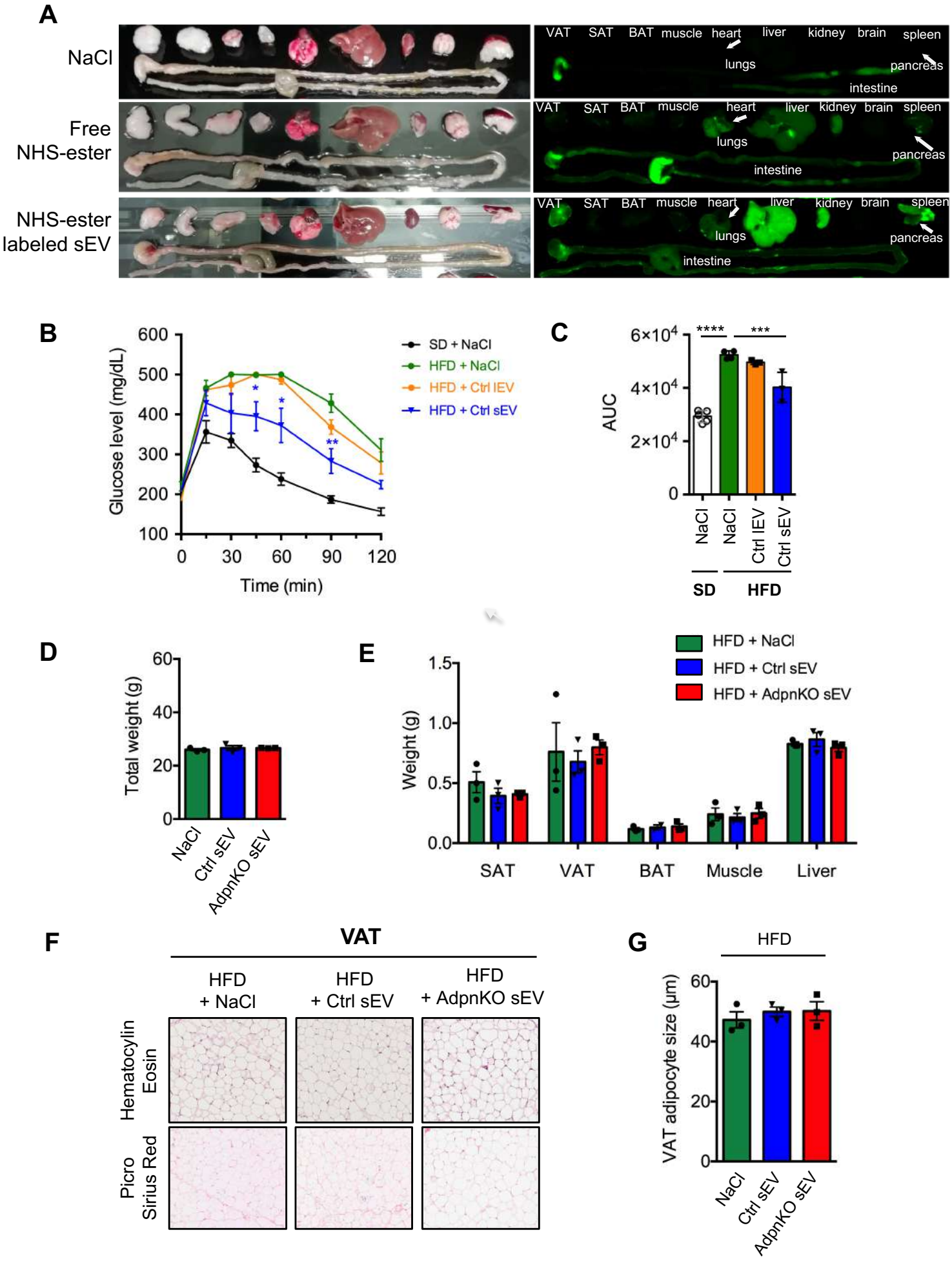
A
NaCl
Free NHS-ester
NHS-ester labeled sEV
VAT SAT BAT muscle heart liver kidney brain spleen
lungs
pancreas
intestine
B
Glucose level (mg/dL)
Time (min)
SD + NaCl
HFD + NaCl
HFD + Ctrl IEV
HFD + Ctrl sEV
C
AUC
NaCl
NaCl
Ctrl IEV
Ctrl sEV
SD
HFD
D
Total weight (g)
NaCl
Ctrl sEV
AdpnKO sEV
E
Weight (g)
HFD + NaCl
HFD + Ctrl sEV
HFD + AdpnKO sEV
SAT
VAT
BAT
Muscle
Liver
F
VAT
HFD + NaCl
HFD + Ctrl sEV
HFD + AdpnKO sEV
Hematocylin Eosin
Picro Sirius Red
G
HFD
VAT adipocyte size (μm)
NaCl
Ctrl sEV
AdpnKO sEV

	Control	Overweight (27<BMI<30)	Obese (BMI>30)
Number (Female/Male)	8 (4/4)	10 (3/7)	17 (8/9)
Mean age (Years)	54.9 ± 8.5	51.3 ± 13.7	50.9 ± 12.3
BMI (kg/m^2)	24.9 ± 1.4	28.6 ± 1.2***§	35.9 ± 6.0####
Waist circumference (cm)	89.7 ± 3.7	94.0 ± 9.8§§	115.5 ± 12.9####
Fasting glucose (mmol/L)	5.1 ± 0.4	5.6 ± 0.8	6.0 ± 0.9#
HbA1c (% of total Hb)	5.5 ± 0.2	5.8 ± 0.2	5.9 ± 0.7
Triglycerides (g/L)	0.9 ± 0.3	2 ± 0.9	1.8 ± 0.5###
HDL-Chol (g/L)	0.6 ± 0.2	0.5 ± 0.06§§§	0.4 ± 0.05#
LDL-Chol (g/L)	1.1 ± 0.4	1.8 ± 0.6	1.3 ± 0.3
Systolic blood pressure (mmHg)	123 ± 11	145 ± 16*	131 ± 16
Diastolic blood pressure (mmHg)	67 ± 23	85 ± 9.7	76 ± 9
Adiponectinemia (µg/mL)	3.2 ± 1.1	2.7 ± 1.4	2.2 ± 0.7

Table S1 : Clinical parameters of the patients included in the study

REAGENT or RESOURCE	SOURCE	IDENTIFIER
Antibodies		
Adiponectin (murine)	Thermofisher Scientific	#PA1-054
Adiponectin (human)	Abeomics	#10-7597
AKT pan (40D4)	Cell signaling	Cat #2920
Phospho-AKT (pAKT, Ser 473)	Cell signaling	Cat #4060S
AMPK	Cell signaling	Cat #2532
pAMPK (Thr172)	Cell signaling	Cat #2535
Alix	BD Biosciences	Cat #611620
murine CD9	BD Pharmingen	Cat #553758
human CD9	Santa Cruz	Cat #SC-13118
Murine CD63	MBL	Cat #D263-3
Flotillin-2	BD Pharmingen	Cat #610383
MIF (human)	R&D Systems	Cat #mab289
Syntenin-1	Abcam	Cat #ab19903
Zs-Green	Clontech	Cat #632598
Anti-adiponectin FITC coupled antibody	Assay-Pro	Cat #10361-05041
IRDye® 800CW and 680RD secondary antibody (anti-mouse and anti-rabbit)	LI-COR Biosciences	Cat #926-32211, #926-32210, #926-68071, #926-68070
siRNA sequences		
ON-TARGETplus Non-targeting Pool, 5 nmol	Horizon Discoveries	Cat #J-007800-10-0005
ON-TARGETplus Human ADIPOR1 (51094) siRNA individual, 5 nmol	Horizon Discoveries	Cat #J-007800-10-0005
ON-TARGETplus Human ADIPOR2 (79602) siRNA individual, 5 nmol	Horizon Discoveries	Cat # D-001810-10-05
Chemicals, Peptides, and Recombinant Proteins		
Bovine Serum Albumin (BSA) FFA free	Sigma	Cat #A7030
Collagenase A	Roche	Cat #10103586001
Dako Target Retrieval Solution	Agilent	Cat #S1699
Dako pen	Agilent	Cat #S2002
DMEM 4.5g/L Glucose	Gibco	Cat #41966-029
DMEM 1g/L Glucose	Gibco	Cat #31885-023
Elisa mouse Adiponectin/Acrp30	R&DSystems	Cat #DY1119 and #DY008
Exosome Isolation kit Pan, mouse	Miltenyi Biotec	Cat #120-041-065
Foetal Calf Serum (FCS)	Eurobio	Cat #CVFSVF00-01
Insulin 100UI/mL	Lilly	Cat #HI0210
Zeocin	Thermofisher Scientific	Cat #R25001
Palmitate	Sigma	Cat #P-0500
Proteinase K	Sigma Aldrich	Cat #P2308
PMSF	Santa Cruz	Cat #SC24948
ECBM	PromoCell	Cat #C22210
Fetal Bovine Serum	GIBCO BRL	Cat #10270-106, Lot 42G2078K
Fluoromount-G	Invitrogen	Cat #00-4958-02
Glutaraldehyde 25% solution	Electron Microscopy Sciences	Cat #16220
IRDye® 800CW NHS Ester	LICOR	Cat #92970021
Mini-Protean TGX gels	BioRad	Cat #4568083, #4568086,
Mowiol	Calbiochem	Cat #475904
Optiprep™ Density gradient medium	Sigma Aldrich	Cat #D1556
Odyssey blocking buffer (TBS)	LI-COR Biosciences	Cat #927-50010
Paraformaldehyde 32%	Electron Microscopy Sciences	Cat #15714
Running Buffer	Interchim	Cat #91495E
4X Laemmli Sample Buffer	Bio-Rad	Cat #161-0747
Triton X100	Sigma	Cat #T8787

Trans-Blot Turbo Transfer reagents	BioRad	Cat #10026938, #1704158, #1704271
Trypsin 0,05%	Corning	Cat #25-051-CI
RNAiMax Lipofectamine	Invitrogen	Cat #12323563
High-Fat Diet (HFD) 61% of the energy from fat (D12492 Premix AIN)	Safe Diet	Cat# SAFE® 233 HF
Commercial Assays and specific devices		
DC-Protein Assay	BioRad	Cat #5000111
Mouse Adipokine Array kit	R&D Systems	Cat #ARY013
Mouse adiponectin/Acrp30 DuoSet ELISA	R&D Systems	Cat #DY1119
Human magnetic Luminex set for adiponectin	Bio-Rad	Cat #171A7002M
Clinicells 25cm^3	GEDTECH	Cat #00108
Experimental Models		
Ob/Ob mice	Charles River	B6.Cg-Lep^{ob}/J, Stock N° 000632, JAX^{TM} mice strain
RCL-ZsGreen	The Jackson Laboratory	B6.Cg-Gt(ROSA)26Sor$^{tm6(CAG-ZsGreen1)Hze/J}$, Stock N°007906, JAX^{TM} mice strain
Adipoq- Cre-ERT2	The Jackson Laboratory	C57BL/6-Tg(Adipoq-cre/ERT2)1Soff/J, Stock N°025124, JAX^{TM} mice strain
Adiponectin KO mice (Adpn KO)	The Jackson Laboratory	B6;129-Adipoq^{tm1Chan}/J, Stock N° 008195
HEK 293	ATCC	Cat #CRL-1573
HepG2 cells	ATCC	Cat #HB-8065
Venus-Adiponectin lentiviral plasmid	Kind gift from Weiping Han	Laboratory of Metabolic Medicine, Singapore Bioimaging Consortium
Phoenix-AMPHO Cells	ATCC	Cat #CRL-3213
Software and Algorithms		
Image Studio software	LI-COR Biosciences	Bioscienceshttps://www.licor.com/bio/products/software/image_studio/
Image J	Downloaded from https://imagej.nih.gov/ij/	https://imagej.nih.gov/ij/
Nanosight NTA software (version 3.1)	Malvern Panalytical	https://www.malvernpanalytical.com/en/support/product-support/software/NanoSight-NTA-software-update-v3-10-l2
Bioplex manager software (version 4.1.1)	Bio Rad	http://www.bio-rad.com/fr-fr/product/bio-plex-manager-software-standard-edition?ID=5846e84e-03a7-4599-a8ae-7ba5dd2c7684
GraphPad Prism	GraphPad	https://www.graphpad.com/scientific-software/prism/

International Journal of
Molecular Sciences

MDPI

Review

Adipocyte-Derived Extracellular Vesicles: State of the Art

Sophie Rome [1,2,*], Alexia Blandin [3,4] and Soazig Le Lay [3,4,*]

1 CarMeN Laboratory, INSERM/1060- INRAE/1397, University of Lyon, Lyon-Sud Faculty of Medicine, 69310 Pierre Benite, France
2 Institute of Functional Genomic of Lyon (IGFL), ENS, CNRS UMR 5242, University of Lyon, 69364 Lyon, France
3 Université de Nantes, CNRS, INSERM, L'Institut du Thorax, F-44000 Nantes, France; alexia.blandin@inserm.fr
4 Univ Angers, SFR ICAT, F-49000 Angers, France
* Correspondence: sophie.rome@univ-lyon1.fr (S.R.); soazig.lelay@inserm.fr (S.L.L.)

Abstract: White adipose tissue (WAT) is involved in long-term energy storage and represents 10–15% of total body weight in healthy humans. WAT secretes many peptides (adipokines), hormones and steroids involved in its homeostatic role, especially in carbohydrate–lipid metabolism regulation. Recently, adipocyte-derived extracellular vesicles (AdEVs) have been highlighted as important actors of intercellular communication that participate in metabolic responses to control energy flux and immune response. In this review, we focus on the role of AdEVs in the cross-talks between the different cellular types composing WAT with regard to their contribution to WAT homeostasis and metabolic complications development. We also discuss the AdEV cargoes (proteins, lipids, RNAs) which may explain AdEV's biological effects and demonstrate that, in terms of proteins, AdEV has a very specific signature. Finally, we list and suggest potential therapeutic strategies to modulate AdEV release and composition in order to reduce their deleterious effects during the development of metabolic complications associated with obesity.

Keywords: adipocytes; extracellular vesicles; exosomes; obesity; diabetes; therapy

Citation: Rome, S.; Blandin, A.; Le Lay, S. Adipocyte-Derived Extracellular Vesicles: State of the Art. *Int. J. Mol. Sci.* **2021**, *22*, 1788. https://doi.org/10.3390/ijms22041788

Academic Editor: María Pardo Pérez
Received: 15 January 2021
Accepted: 8 February 2021
Published: 11 February 2021

1. Introduction

White adipose tissue (WAT) distributes in discrete anatomical depots identified as subcutaneous adipose tissue (SAT) or visceral adipose tissue (VAT). The expansion of both depots contributes to obesity. Nonetheless, the development of metabolic complications is preferentially associated with VAT expansion [1]. WAT represents overall 10–15% of total body weight in a healthy human and constitutes the main energy supply in the body, being mobilized according to the body's needs (for review [2]). WAT also has endocrine functions and secretes many peptides, hormones and steroids that participate in its homeostatic role, especially in carbohydrate–lipid metabolism regulation. Communication with other key metabolic tissues is moreover achieved through dense vascularization and innervation, all organized in a metabolically active connective tissue [2,3]. High plasticity of WAT to adapt and expand in response to energy surplus involved increased adipocyte size (hypertrophia) and/or recruitment and proliferation of precursor cells (hyperplasia) in combination with vascular and extracellular matrix remodeling.

At the cellular level, the storage of energy under the form of lipids, namely triacylglycerols, is ensured by adipocytes in a huge lipid droplet filling the cytoplasm. Fat cells are then highly expandable, with a size that can reach up to 150 µm in obese patients [4]. The rapid expansion of WAT in response to nutrient overload is signed by a profound remodeling of fat, involving all cellular components of this organ. Many cellular stresses associated with excessive fat mass development (local hypoxia, inflammation and oxidative or endoplasmic reticulum stresses) have indeed been associated with an increased macrophage infiltration within WAT, representing up to 40% of the total cell content in case of massive obesity [5]. This participates in the chronic inflammation state associated with

obesity, which, in addition to impacting WAT remodeling, also promotes the development of insulin resistance, a major metabolic dysfunction associated with obesity [2,3,6].

In this context, adipocyte-derived extracellular vesicles (AdEVs) have recently been highlighted as important actors of intercellular communication that participate in metabolic responses to control energy flux and immune response. In this review, we will focus on the role of AdEV in the cross-talks between the different cellular types composing WAT with regard to their contribution to WAT homeostasis and metabolic complications development. We will also discuss the AdEV cargoes (RNA, lipids, proteins) that participate in AdEV's biological effects on recipient cells. Finally, we will describe potential therapeutic strategies to modulate AdEV release and composition in order to reduce their deleterious effects during the development of metabolic complications associated with obesity.

2. Generalities on Extracellular Vesicles

Extracellular vesicles (EVs) have long been viewed as conveyors of cellular waste used by the cell to get rid of harmful or unnecessary molecules [7]. EVs designate nanovesicles derived from cells or organelle membranes that are secreted into the extracellular medium and circulate in all body fluids (blood, lymph, urine, milk, saliva, tears, etc.) [8,9]. EVs are now recognized as vectors of biological material (proteins, lipids and nucleic acids) and are able to target and transfer their content into various recipient cells inside the tissues (Figure 1). Different EV uptake mechanisms by the target cell have been described including membrane fusion, ligand binding interaction or EV endocytosis, as reviewed in [8]. These membranous vesicles are heterogeneous in size and have given rise to numerous names (exosomes, microvesicles, microparticles, prostasomes, oncosomes, neurospheres, apoptotic bodies, etc.). The growing interest in EVs and the recent advances in the characterization of their biogenesis pathways have led the scientific community to propose a nomenclature that essentially distinguishes two subtypes of EV based on their sizes: large and small EVs [10].

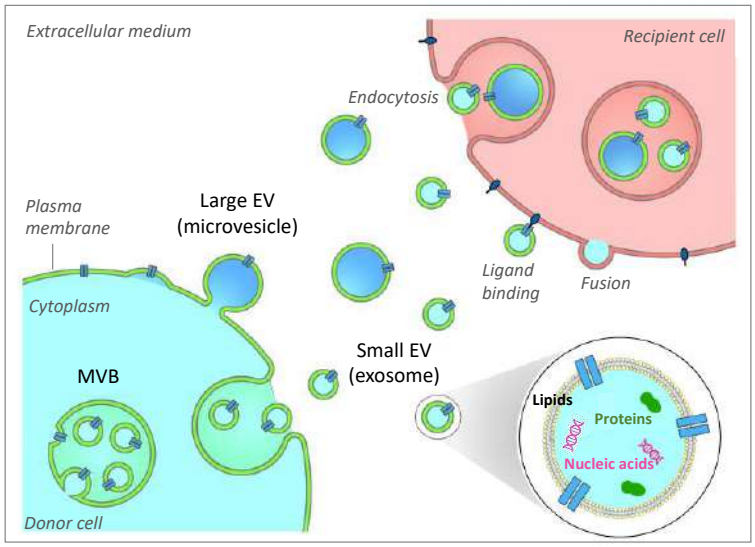

Figure 1. Extracellular vesicle biogenesis, secretion and interaction with recipient cells. Two subclasses of extracellular vesicles (EV) are released from mammalian cells and are mainly distinguished based on their sizes. Large EVs (lEV) can bud from the plasma membrane. They are also referred to as microvesicles. Small EVs are derived from the formation of intraluminal vesicles (ILVs) within the lumen of the multivesicular body (MVB). MVB can fuse with the plasma membrane to release ILVs, which are thus called exosomes. EVs participate in intercellular communication through EV-based exchanges of proteins, lipids and genetic material between cells. The fate of EVs in recipient cells includes membrane fusion, ligand binding or endocytosis mechanisms.

Large EVs (lEV), whose sizes vary between 250 nm to 500 nm in diameter and are mainly referred to as microvesicles, are secreted following the budding of the plasma membrane. This process is dependent on calcium influx, which induces modification of the asymmetric phospholipid distribution of plasma membranes and phosphatidylserine outer leaflet exposure through specific regulation of enzyme activities (flippase, floppase and scramblase) and favors the reorganization of cytoskeleton through calpain activation [11]. First considered as platelet wastes, they aroused particularly strong interest as diagnostic tools in pro-thrombotic diseases [12]. Small EV (sEV, 40–100nm), referred to as exosomes, are derived from intraluminal vesicles formed during the maturation of multivesicular bodies (MVB) in the endolysosomal pathway. They are secreted into the extracellular medium after fusion of MVB with the plasma membrane. Detailed mechanisms governing the biogenesis, secretion, targeting and fate of EVs have been reviewed elsewhere [8]. Several studies have demonstrated the ability of sEVs to regulate the immune and anti-tumor response, in particular due to their ability to transfer major histocompatibility complex (MHC) molecules between immune cells [13]. Despite different modes of biogenesis, lEV and sEV share many common characteristics such as their similar appearance, an overlapping size and common cargos, which makes it difficult to ascertain the respective origin and role of each EV subtype after purification. Whereas most studies refer to a mix of EVs, differential ultracentrifugation (dUC) is usually used to get rid of cell debris and to separate lEVs (10,000–20,000$\times$ *g* pellet) from sEVs (>100,000$\times$ *g* pellet). Regardless of the EVs' subclasses, numerous recent data point out that EVs convey biological messages and are critical actors of intercellular communication [14], being involved in tissue development and homeostasis in physiological and pathological conditions.

3. Adipocytes Are Important EV Providers

EV release has been recently identified as an essential part of the WAT secretome participating in autocrine, paracrine and endocrine communication [15]. We have investigated the ability of 3T3-L1 adipocytes to secrete EVs and demonstrated that adipocytes release two subtypes of EVs (lEV and sEV) [16]. The lEV fraction includes a heterogeneous population of vesicles, with a well-delimited double membrane, differing greatly in size, shape and electron density, whereas the sEV fraction corresponds to a pool of smaller spherical vesicles of similar sizes, with cup-shaped morphologies usually observed for exosomes. Quantification of AdEV revealed the ability of adipocytes to secrete important quantities of large and small EVs, from either in vitro adipocytes models (3T3-L1 or 3T3F442A) or mice primary adipocytes [16–18]. When compared to melanoma cells, which are known to secrete many extracellular vesicles, mature adipocytes appear as important EV providers as they release more sEV than cancer cells [18], whereas AdEVs' isolation rate can be significantly enhanced using size exclusion chomatography (SEC) by comparison to classical dUC technique [19]. However, the presence of the lipid droplet marker perilipin-1 and the high lipid content in SEC-isolated AdEV preparations suggest that a bias may reside in the co-isolation of lipid droplets and lipoproteins with AdEV.

3.1. Adipose-Derived EV: A Complex Network of Metabolic Signals Inside WAT

Studying EV production during the course of 3T3-L1 differentiation reveals that proliferative adipocytes secrete more EV than quiescent mature adipocytes [17]. Indeed, lipid-filling during the course of adipocyte differentiation is associated with enhanced EV secretion [18]. Accordingly, when large and small adipocytes are size-separated from the same fat pad, large adipocytes exhibit higher efficacy in releasing sEV harboring glycosylphosphatidylinositol (GPI)-anchored protein, CD73 compared to small adipocytes [20]. Besides adipocyte's intrinsic ability to secrete AdEV, the pathophysiological environment also influences AdEV secretion. Based on in vitro experiments, it was found that saturated fatty acids [16,21,22], pro-inflammatory cytokines [16] and hypoxia [23] significantly enhanced adipocyte-derived EV secretion and modulated EV content. Of interest, the mentioned stimuli are all related to the pathophysiological state of obesity and are in

agreement with experimental data showing that the number of sEVs shed by adipocytes from obese mice is higher than that from lean animals [18]. Interestingly, increased sEV secretion in obese conditions is not observed for other cell types found in WAT (referred to as "stromal vascular fraction" or SVF) [18] although the presence of SVF markers detected in WAT-derived EVs affects the ability of SVF to produce EV [24].

Active EV trafficking exists between different WAT cell types such as, for example, endothelial and adipocytes. For instance, endothelial EV-based transfer of caveolin into adipocytes has been demonstrated and shown to be sufficiently efficient to restore caveolin-1 protein levels in adipocytes depleted for caveolin-1 [24]. EV-based cross-talks have been documented between all cell types composing WAT (Figure 2). For instance, such AdEV traffic occurs between small and large adipocytes and participates in the different stages of fat development [20,23,25]. Another important EV-based dialogue is the one occurring between adipose stem cells and the immune or endothelial cells, which contribute to impact WAT properties by modulating inflammatory markers or by regulating vascularization of the tissue [24,26–28]. Finally, the most documented WAT EV-based communication in the literature is the one between adipocytes and immune cells, which regulates their respective phenotypes [19,29–31].

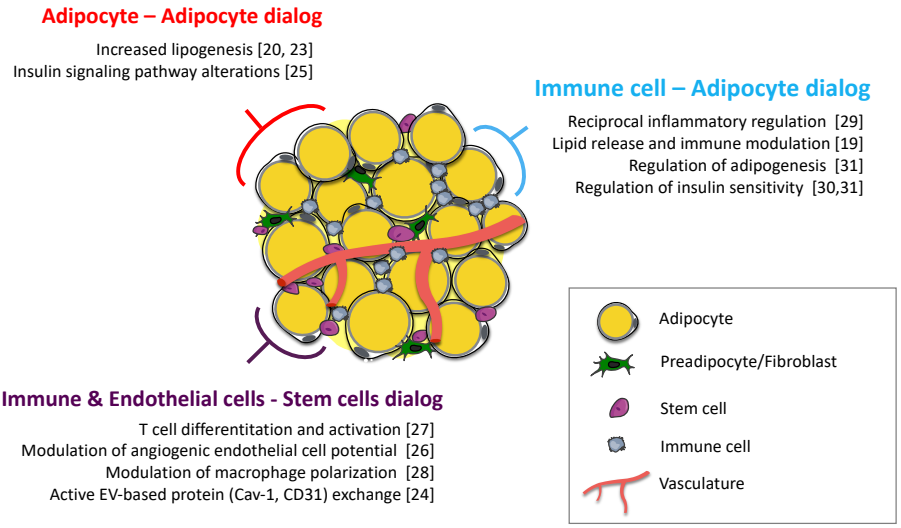

Figure 2. Cellular EV-based cross-talks between adipose tissue modulate fat metabolism by autocrine action. EV-based dialog within white adipose tissue (WAT) has been evidenced between the different fat cell types as illustrated between adipocytes themselves, or between stem cells/immune cells and endothelial cells and between immune cells and adipocytes. All these exchanges result in modulating cell recipients' metabolic responses and participate in maintaining fat homeostasis. The references of the publications cited as examples are given in brackets.

3.2. Contribution of Adipocyte-Derived EV to the Circulating Pool of EV in Biofluids

Evidence for the presence of AdEV in the blood is still scarce and difficult to evaluate in the absence of adipocyte-derived specific markers, but highly expressed adipocyte proteins such as aP2/FABP4, perilipin-1, adiponectin or PPAR have been identified in circulating EV [17]. Nonetheless, their use as specific adipocyte markers is limited by the fact that their expressions vary according to adipocyte differentiation and/or hypertrophy, and that most of these proteins are also expressed by WAT-derived macrophages. Using a fat-specific knockout of the miRNA-processing enzyme Dicer (ADicerKO), it was shown that fat was a major contributor to circulating exosomal miRNA [32]. Conversely, tracing plasma EV in mice expressing a fluorescent protein specifically in adipocytes revealed that AdEVs were indeed detected but represented a minority of circulating EV [19]. Further investigations will thus be needed in order to evaluate the exact contribution of AdEV in

the circulating pool of EV with regard to the well-known predominance of platelet-derived EV and to a lesser extent to endothelium and PBMC-derived EVs [33].

3.3. Adipose-Derived EV Regulate Glucose Homeostasis and Inflammation

Obesity, and particularly adipocyte hypertrophy, is an important contributor to type 2 diabetes (T2D), with insulin resistance being the main hallmark [34]. Different studies have investigated the metabolic effects of obese WAT-derived EV on insulin signaling. Blood injections of sEV derived from obese WAT into lean mice altered insulin sensitivity and induced insulin resistance compared to injections of sEVs isolated from lean fat depots, illustrating the potential of WAT-derived EVs to act as metabolic perturbators [35]. One particular mechanism linking obese adipose sEV and insulin resistance relies on the ability of obese AdEVs to chemoattract monocytes, therefore contributing to WAT inflammation [36,37]. Accordingly, sEVs released from macrophages from obese WAT also caused systemic insulin resistance when administered into lean mice, suggesting an important contribution of macrophages-derived sEV in addition to AdEV in metabolic diseases [30]. Finally, EV-induced adipose remodeling might also result from inter-organ EV trafficking as recently illustrated by hepatocyte-derived EV targeting adipocytes to regulate adipogenesis and lipogenesis [38].

Besides the role attributed to AdEV in WAT homeostasis, some studies have highlighted the endocrine effects of AdEV on distant cells from other tissues. EVs from brown adipose tissue (BAT) have been shown to regulate gene expression in the liver, although no evidence for specific organotropism was demonstrated [32]. Proatherogenic properties of obese adipose-derived sEV, specifically when isolated from visceral depots vs. subcutaneous WAT, have been reported to be exerted by regulating macrophage foam cell formation and polarization [39]. Finally, the role of AdEV in tumor-WAT communication has also been demonstrated [18,40]. Metabolic changes could be horizontally induced in melanoma cells by AdEV, which resulted in the increase in tumor aggressiveness, tumor cell migration and lung metastases, which were reinforced in the context of obesity [18].

Taken together, these studies position adipose-derived EVs as a novel means of intercellular communication within WAT and likely between WAT and other distant organs. Of note, most of these studies have focused on the sEV and have neglected the lEV subpopulation. In addition, the risk of contamination of AdEV with lipoproteins contaminants and/or macromolecular protein complex is not considered or discussed. Further studies using standardized and robust EV isolation protocols are thus needed to delineate the molecular mechanisms underlying EV paracrine and endocrine effects.

4. Adipose-Derived EV Content Explains Their Biological Functions

Different biological functions of AdEVs have been identified, and specific AdEV components (proteins, lipids or acid nucleics) have been assigned to these effects.

4.1. Protein Content of Adipocyte-Derived Extracellular Vesicles

The formation of EVs implies that membranes can bud away from the cytoplasm during the formation of large EVs or during the formation of the intraluminal vesicles inside late endosomes to generate sEV/sexosomes (Figure 1). During the budding process, membrane-associated proteins are incorporated into EVs and their nature is highly dependent on EV intracellular origins. EV-enclosed proteins can be those involved in the budding itself, like ESCRT machinery component for exosome/sEV formation (Endosomal Sorting Complexes Required for Transport [8]), or small GTPases (ARF62,18 and ARF119), Rab proteins and Rho (Rac1 and RhoA) for large vesicle formation [41]. Regarding proteins released into sEV, accumulating evidence suggests that post-translational modifications are necessary for their incorporation into sEV during MVB biogenesis [42]. In addition, since MVB are signaling platforms for many signaling pathways, scaffold proteins are also often retrieved into sEVs [43].

Therefore, when comparing 3T3-L1 adipocyte-derived EV proteomes, we highlighted specific protein subsets carried by lEV or sEV reflecting their respective mode of biogenesis [16]. Large EVs were enriched in plasma membrane proteins (including flotillin-1 and caveolin-1), organelle components and mitochondrial enzymes, whereas proteins from endosomal origin (including CD63 and CD9), from extracellular matrix or involved in cell adhesion were specifically retrieved in sEV. Of note, sEV proteins constitute an essential part of human WAT secretome [15]. As shown on Figure 3a, sEV proteins were specifically enriched in proteins for translation and RNA processing when compared with the subset of proteins released in a vesicle-free manner. Conversely, sEV proteins were depleted in proteins involved in immune response, which were enriched in the subset of vesicle-free proteins (Figure 3a). This analysis suggests that two pools of proteins with specific biological functions are released from adipocytes, and identifies sEV as a specific sorting pathway for proteins involved in RNA processing/translation. Surprisingly, 36% of the proteins found in human adipocyte-derived sEVs had conventional secretory signal peptides [15], suggesting either that these proteins are contaminants attached to AdEVs being precipitated during EV extraction, or that they are incorporated into MVBs during their intracellular trafficking export. In line with this second hypothesis, during lipolytic stimulation associated with lipid mobilization, FABP4, a lipid transporter usually exported under a free form in the plasma, is recruited into MVB and released into AdEV [44].

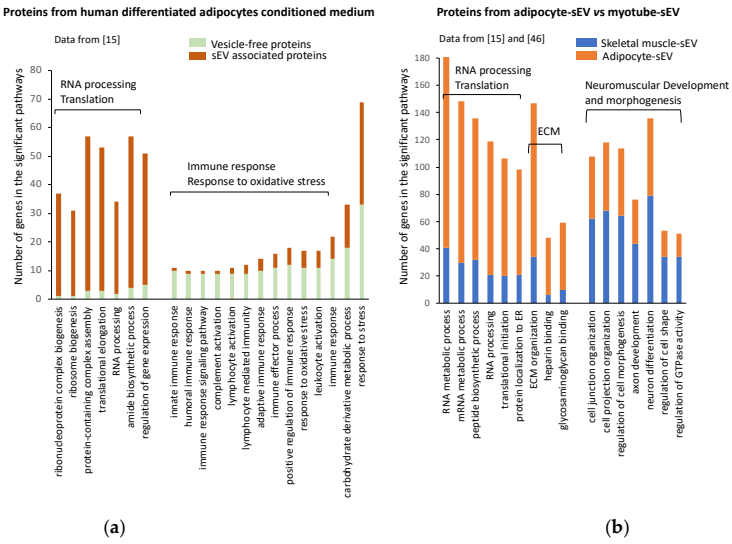

Figure 3. Adipocytes export a specific subpopulation of proteins into adipocyte-derived extracellular vesicles (AdEVs). (**a**) Significant GO biological functions enriched in proteins released in the conditioned medium from human differentiated adipocytes, either packed inside small extracellular vesicles or being released under a vesicle-free form. Proteomic data are from [15]. (**b**) Significant GO biological functions enriched in small EV (sEV) protein subsets released from human adipocytes vs. those released from human myotubes. Proteomic data are from [15] and [45]. Only functions containing more than 50 genes are presented. ECM, extracellular matrix; ER, endoplasmic reticulum. For (**a**) and (**b**), the significantly enriched pathways were retrieved using PANTHER version 11 [46].

In human blood, different adipocyte-enriched proteins or adipokines are still detected in circulating EVs even after post-depletion of the major population of circulating plasma-derived EV (including platelet, monocyte, endothelial cell and erythrocyte-derived EVs) [17]. These proteins, including adiponectin, FABP4, perilipin and PPARγ, could therefore use an adipocyte-EV secretory pathway to be exported in blood. Nonetheless, previous data demonstrated that adiponectin is mainly distributed at the exosomal surface, whereas adiponectin is not usually membrane-associated [47]. This raises the question of the proportion of co-precipitated or EV-adsorbed soluble material when evaluating adipocyte protein marker content in circulating EV. In addition, sequential depletion of

lEV then sEV from blood patients has a limited impact on most circulating adipokine concentrations, demonstrating that the EV secretory pathway remains negligible for most of these proteins [33]. An exception is the Macrophage Migration Inhibitory Factor (MIF), whose lEV transport accounts for half of its circulating concentration, a secretory pathway that, moreover, is conserved over different MIF-producing cells [33]. Large EV-associated MIF triggers rapid ERK1/2 activation in macrophages, and these functional lEV-MIF effects specifically rely on a non-canonical MIF tautomerase activity. Altogether, these results highlight that a specific adipokine sorting pathway does exist, besides their default encapsulation in EV, which would need to be reconsidered when studying metabolic effects of adipocyte secreted products.

Cellular origin is also likely to influence EV protein content. To illustrate the relative contribution of EV origin with regard to their EV protein content, we performed functional enrichment analyses of two different EV sets of proteins, respectively derived from subcutaneous human primary adipocytes [15] and human skeletal muscle cells (SkM) [45]. Figure 3b shows that human AdEVs vs. SkMEVs display different protein signatures. SkMEVs appeared to be enriched in proteins involved in neuromuscular development and cell differentiation, whereas AdEVs were significantly enriched in proteins involved in RNA processing and translation and in proteins from the extracellular matrix (ECM). Interestingly, proteomic analysis of murine 3T3-L1 adipocyte-derived sEV also demonstrated a significant number of ECM proteins in AdEV [16], as illustrated for AdEV-associated MMP-3, which can even be transferred into lung cancer cells [40]. Such sEV protein composition could reflect the important production and organization of ECM associated with WAT development [48,49].

AdEV release is also closely linked with the adipocyte developmental stages since sEV production from 3T3-L1 cells was greater for the pre-adipocyte stage than for mature adipocytes [50]. A plausible explanation is the saturation of the ubiquitin–proteasome or autophagy–lysosomal pathways due to high protein turnover associated to with proliferation, which favors the release of cellular toxic components by EV from preadipocytes [51]. In addition, AdEV composition varies during 3T3-L1 adipocyte differentiation [50]. Bioinformatics analyses of the proteomic signatures of pre- vs. differentiated adipocyte sEVs by using the same procedure described in Figure 3 indicate that pre-adipocyte-derived sEV are significantly enriched in proteins for angiogenesis (p-value: 3.77×10^{-10}) and positive regulation of cell motility (p-value: 6.04×10^{-10}). Conversely, differentiated 3T3-L1 adipocyte-sEV are enriched in proteins for RNA catabolic process (p-value: 1.38×10^{-5}), cell cycle phase (p-value: 6.09×10^{-4}), mitotic cell cycle phase (p-value: 6.09×10^{-4}), post-translational protein modification (p-value: 9.30×10^{-5}) and immune response-activating signal transduction (p-value: 6.09×10^{-4}).

AdEV production is also dependent on environmental signals, especially those associated with the development of obesity, as illustrated by an increase in AdEV release following lipid/glucose, hypoxic or inflammatory stimuli [16,22,23,37]. Metabolic alterations, such as insulin-resistance and lipid hypertrophy (induced by oleate or palmitate treatment) applied to murine cell-cultured adipocytes C3H10T1/2, moreover impacts the AdEV protein content [22]. Lipid hypertrophied AdEVs are characterized by ceruloplasmin, mimecan and perilipin 1 adipokines, and those from the insulin-resistant adipocytes by the striking presence of the transforming growth factor-beta-induced protein ig-h3 (TFGBI). AdEV cargo differential contents are likely to modulate metabolic responses of recipient cells. For instance, "hypoxic" AdEVs affect lipogenic activity in neighboring pre-adipocytes and adipocytes [23] and alter the insulin-stimulated signaling pathway [25]. AdEVs derived from hypertrophic adipocytes, following oleic acid or palmitate treatments, recapitulated differentiation/hypertrophy and induced insulin resistance in recipient adipocytes or promoted macrophage inflammation by stimulating IL-6 and TNFalpha expressions [22]. Finally, "inflammatory" AdEVs, produced from adipocytes treated with TNFalpha and co-exposed or not to hypoxia, induce VCAM-1 production in vascular endothelial cells, resulting in enhanced leukocyte attachment [37].

Proteomic studies performed on AdEV from WAT explants of lean or obese/diabetic rodents (genetic obesity or high-fat induced) confirmed alterations of AdEV protein content within the course of obesity [22,35,52,53]. Following a comparison of these three proteomic analyses, we found that AdEVs from high-fat-diet-induced obese animals (obese AdEVs) generally display higher content of proteins compared with AdEV from control rodents (Figure 4). Focusing on the proteins commonly found in obese AdEVs vs. control AdEV, a subset of 65 proteins could be identified (see the list in Table 1). Functional enrichment analysis indicated that the 65 proteins are involved in lipid catabolic processes and oxydo-reduction, cell migration and motility and were located in caveolae and extracellular matrix.

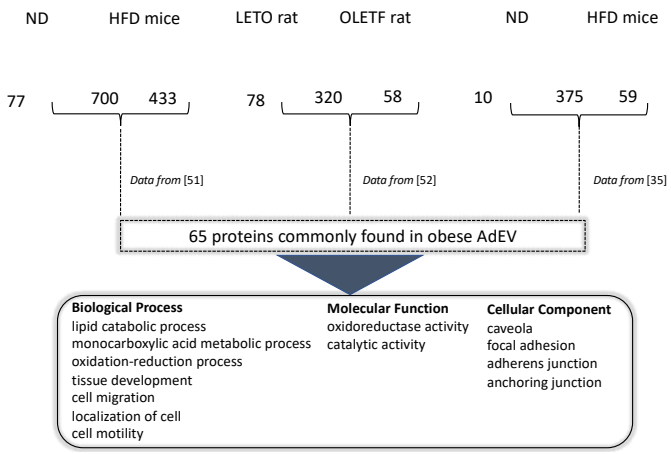

Figure 4. Significant enrichment analyses were performed on the 65 proteins commonly found in AdEVs released from obese mice adipose tissue based on proteomic data from [35,52,53] vs. the rest of the genome (PANTHER version 11). Only significant functions in each pathway are shown. The list of 65 proteins is available in Table 1.

Table 1. Common proteins from obese adipocyte-derived extracellular vesicles (see Figure 4). Data sets are from [35,52,53].

Gene Symbols	Protein Accession Numbers	Gene Names
Acadl	P51174	acyl-Coenzyme A dehydrogenase, long-chain
Acads	Q07417	acyl-Coenzyme A dehydrogenase, short chain
Aco2	Q99KI0	aconitase 2, mitochondrial
Acsl1	P41216	acyl-CoA synthetase long-chain family member 1
Adipoq	Q60994	adiponectin, C1Q and collagen domain containing
Agpat2	Q8K3K7	1-acylglycerol-3-phosphate O-acyltransferase 2 (lysophosphatidic acid acyltransferase, beta)
Aifm2	Q8BUE4	apoptosis-inducing factor, mitochondrion-associated 2
Aldh2	P47738	aldehyde dehydrogenase 2, mitochondrial
Aldh3a2	P47740	aldehyde dehydrogenase family 3, subfamily A2
Anxa1	P10107	annexin A1
Anxa6	P14824	annexin A6
Aoc3	O70423	amine oxidase, copper containing 3
Atp2a2	O55143	ATPase, Ca++ transporting, cardiac muscle, slow twitch 2
Atp5a1	Q03265	ATP synthase, H+ transporting, mitochondrial F1 complex, alpha subunit, isoform 1
Atp5b	P56480	ATP synthase, H+ transporting mitochondrial F1 complex, beta subunit
Cat	P24270	catalase
Cav1	P49817	caveolin, caveolae protein 1
Cav2	Q9WVC3	caveolin 2
Cct3	P80318	chaperonin subunit 3 (gamma)
Cd36	Q08857	CD36 antigen

Table 1. *Cont.*

Gene Symbols	Protein Accession Numbers	Gene Names
Cd47	Q61735	CD47 antigen (Rh-related antigen, integrin-associated signal transducer)
Cd9	P40240	CD9 antigen
Cltc	Q68FD5	clathrin, heavy polypeptide (Hc)
Col6a1	Q04857	collagen, type VI, alpha 1
Decr1	Q9CQ62	2,4-dienoyl CoA reductase 1, mitochondrial
Dlat	Q8BMF4	dihydrolipoamide S-acetyltransferase (E2 component of pyruvate dehydrogenase complex)
Eef1a1	P10126	eukaryotic translation elongation factor 1 alpha 1
Ehd2	Q8BH64	EH-domain containing 2
Etfa	Q99LC5	electron transferring flavoprotein, alpha polypeptide
Fasn	P19096	fatty acid synthase
Gnaq	P21279	guanine nucleotide binding protein, alpha q polypeptide
Gpd1	P13707	glycerol-3-phosphate dehydrogenase 1 (soluble)
Gpi	P06745	glucose phosphate isomerase 1
Hadh	Q61425	hydroxyacyl-Coenzyme A dehydrogenase
Hadhb	Q99JY0	hydroxyacyl-Coenzyme A dehydrogenase/3-ketoacyl- Coenzyme A thiolase/enoyl-Coenzyme A hydratase (trifunctional protein), beta subunit
Hsd17b12	O70503	hydroxysteroid (17-beta) dehydrogenase 12
Hsd17b4	P51660	hydroxysteroid (17-beta) dehydrogenase 4
Itgb1	P09055	integrin beta 1 (fibronectin receptor beta)
Kpnb1	P70168	karyopherin (importin) beta 1
Lamb2	Q61292	laminin, beta 2
Lamc1	P02468	laminin, gamma 1
Ldha	P06151	lactate dehydrogenase A
Lipe	P54310	lipase, hormone sensitive
Lpcat3	Q91V01	membrane bound O-acyltransferase domain containing 5
Lpl	P11152	lipoprotein lipase; similar to Lipoprotein lipase precursor (LPL)
Lrp1	Q91ZX7	low density lipoprotein receptor-related protein 1
Mcam	Q8R2Y2	melanoma cell adhesion molecule
Mdh2	P08249	malate dehydrogenase 2, NAD (mitochondrial)
Ogdh	Q60597	oxoglutarate dehydrogenase (lipoamide)
Pc	Q05920	pyruvate carboxylase
Pdhb	Q9D051	pyruvate dehydrogenase (lipoamide) beta
Pdia3	P27773	protein disulfide isomerase associated 3
Phb	P67778	prohibitin
Prkar2b	P31324	protein kinase, cAMP dependent regulatory, type II beta
Rab18	P35293	RAB18, member RAS oncogene family
Rab8b	P61028	RAB8B, member RAS oncogene family
Rras	P10833	Harvey rat sarcoma oncogene, subgroup R
Sdha	Q8K2B3	succinate dehydrogenase complex, subunit A, flavoprotein (Fp)
Sfxn1	Q99JR1	sideroflexin 1
Sts	P50427	steroid sulfatase
Tmed10	Q9D1D4	transmembrane emp24-like trafficking protein 10 (yeast)
Tubb3	Q9ERD7	tubulin, beta 3

Alternatively, a recent proteomic analysis was performed on human morbid obese visceral (VAT) and subcutaneous (SAT) WAT shed EVs from donors submitted to bariatric surgery [54]. Functional analysis of all the proteins identified in obese VAT and SAT vesicles showed the presence of proteins related to transport, catalytic, GTPase, structural molecule, protease and chaperone activity and a particular enrichment of extracellular matrix (ECM) constituents in SAT EVs. Importantly, the vast majority of proteins identified in previous proteomic reports from EVs derived from cultured adipocytes [15–18,22] were retrieved in human WAT EVs [54]. Other proteins, including leptin, have not been previously described in AdEV from in vitro adipocyte differentiated cultured models, which are also known to be low producers of this adipokine. The functional classification shows that obese VAT

vesicles display a specific enrichment of proteins implicated in WAT inflammation and insulin resistance, related to a specific increase in protein implicated in the immune system process, in comparison to SAT EVs [54]. Since obese VAT is recognized to be more inflamed than SAT due to important macrophage and immune cell infiltration, EVs derived from WAT-resident immune cell populations are likely to impact WAT-EV dynamic secretion and protein content. Finally, the authors revealed a particular enrichment of human obese WAT EVs in TGFBI and mimecan, two proteins that they also found associated with plasma EVs from obese patients [54]. Interestingly, plasma EV-associated TGFBI was significantly elevated in obese patients with a history of T2D compared to non-diabetic patients, and mimecan-EVs were higher in obese plasma compared to those in healthy lean individuals and may therefore represent candidate biomarkers to monitor T2D status in obese patients or to track obesity, respectively. However, one must be conscious that these two proteins are not exclusively secreted by WAT, and other cell types than adipocytes are likely to participate to increase their plasma TGFBI-EV or mimecan-EV levels.

Of interest, AdEV proteins could be transferred into various recipient cells and are likely to participate in cancer development [52], inflammation and insulin resistance development [35]. Indeed, AdEV stimulated mitochondrial metabolism and remodeling in tumor cells by providing both enzymes and substrates [52]. Alternatively, obese AdEVs were found to contain higher levels of the RBP4 protein compared to lean WAT-derived AdEV, involved in M1 macrophage polarization and insulin resistance in a TLR4/TRIF-dependent pathway [35]. Whether AdEV's deleterious metabolic effects operate via AdEV protein delivery into recipient cells or also involve AdEV indirect mechanisms, as illustrated by their TLR4-dependent immuno-modulatory effects [35], will definitely need further investigations.

4.2. RNA in Adipocyte-Derived Extracellular Vesicles

RNAs have been consistently found in EVs. Until now, the mechanisms favoring their export into EVs is unclear and unexplored in the case of AdEVs. Generally speaking, like for the majority of RNA-associated with EV, AdEV-RNA concentrations mirror cellular intracellular concentrations, suggesting a passive mechanism [55]. Nonetheless, for some small RNAs, different mechanisms underpin this EV-associated RNA sorting, which are not mutually exclusive, including (i) specific RNA sequences with affinity for raft-like region of MVB (review in [56]); (ii) binding to specific RNA-binding proteins that selectively shuttle miRNA into EV (review in [57]); (iii) the presence of specific acid nucleic extension, which might stabilize some miRNAs and favor their export [58]. The majority of sEV mRNA is fragmented, which may participate in their stability, localization and mRNA translational repression in recipient cells [59].

Only two studies have performed large-scale analyses of AdEV RNA content. Microarray profiling identified 7000 mRNA in 3T3-L1 adipocytes among the 9000 expressed in the cell [55]. This high number of AdEV mRNA is quite surprising given the fact that the authors indicated that the majority of RNA in AdEV were less than 200 nucleotides in length and contained little or no 28S and 18S ribosomal RNA compared to the parental adipocytes. Adipocyte-specific transcripts were identified coding for adiponectin, leptin, resistin, PPARgamma, FABP4, C/EBPs [55]. RAW264.7 macrophages incubated with AdEV expressed these adipocytes-specific transcripts, suggesting that mRNA can be transported into macrophages through the AdEV route [55]. These data corroborated the study of Müller et al. showing that AdEV from large adipocytes transfer transcripts coding for fatty acid esterification (glycerol-3-phosphate acyltransferase-3, diacylglycerol acyltransferase-2), lipid droplet biogenesis (FSP27, caveolin-1) and adipokines (leptin, adiponectin) into small adipocytes and that such RNA horizontal transfer correlates with the induction of lipid storage in the recipient cells [60]. By using RNA sequencing, 1083 mRNAs and 105 lncRNA were moreover identified in AdEV from bovine adipocytes out of the 12,082 mRNAs and 8589 lncRNA expressed in donor adipocytes, therefore confirming the presence of long RNA species in AdEV. Respectively, 498 mRNA and 68 lncRNA were found differentially

expressed between adipocytes and AdEV [61]. The 500 highly concentrated mRNA in AdEV coded for proteins involved in translation, protein folding and collagen fibril organization, or ribosome and cytoskeleton proteins. Interestingly, like for the protein content of AdEV, the extracellular matrix was among the enriched functions. Among the 105 lncRNAs, 3 lncRNAs (BGIR9913_49345, BGIR9913_54344 and URS0000B2F7C9) were detected in sEV irrespective of cellular origin suggesting a conserved mechanism for their upload into sEV. Until now, the functionality of AdEV mRNA, i.e., their translation into proteins in the recipient cells, has not been demonstrated. However, a previous study has shown that after incubation of human mast cells with mouse EV mRNA, new mouse proteins were found in human recipient cells, demonstrating that transferred mRNA could be translated into proteins in other cells [14]. In addition to mRNA and lncRNAs, it was found that AdEV also contained circular RNA [62]. Circular RNA functions as a sponge for miRNAs expressed in the recipient cells. They can also regulate RNA-binding proteins and can sometimes be translated into proteins. Circular RNAs contained in AdEV promoted hepatocellular carcinoma growth and reduced DNA damage by suppressing miR-34a, resulting in the activation of the USP7/Cyclin A2 signaling pathway [62]. AdEVs from adipocytes overexpressing circ_0075932 were enriched in circ_0075932 and induced inflammation and apoptosis in dermal keratinocytes. It was demonstrated that circ_0075932 binds the RNA-binding protein PUM2, a positive regulator of the AuroraA kinase, resulting in the activation the NF-κB pathway.

AdEVs also contain small RNA species. Out of the 378 miRNAs expressed in bovine adipocytes, 48 were sorted into AdEVs [61] and 140 were also found in 3T3-L1-released AdEVs [55]. Different pieces of evidence from in vitro data highlight AdEV-miRNA horizontal transfer into various recipient cells. For instance, hypertrophic adipocytes released AdEVs enriched in miR-802-5p, which contributed to insulin resistance in cardiac myocytes through its action on HSP60 [63]. miR-27a contained in AdEV derived from high-fat-diet-fed C57BL/6J mice induced insulin resistance in C2C12 skeletal muscle cells by repressing PPARγ and its downstream genes [64]. In addition to muscle cells, AdEVs were also implicated in the cross-talk between adipocytes and the liver. Thomou et al. found that miR-99b in AdEV reduced Fgf21 mRNA levels in the liver and demonstrated that FGF21 modulation only occurred through AdEV delivery of miR-99b and not in response to direct incubation with miR-99b [32]. This result has suggested, for the first time, a specific role of packed miRNAs vs. vesicle-free miRNAs in blood. AdEVs were also implicated in hepatic cancer development, as the transport of miRNA 23a/b into hepatic cancer cells via AdEV resulted in cancer cell growth and migration and development of chemoresistance through targeting of the von Hippel-Lindau/hypoxia-inducible factor axis [65]. Within WAT, it was demonstrated that AdEV could participate in macrophage polarization. Zhang et al. showed that miR-155 could be delivered into bone-marrow-derived macrophages by AdEV, which resulted in the targeting of SOCS1 and the modulation of M1 macrophage polarization via JAK/STAT signaling [66]. Interestingly, the conditioned medium of macrophages pre-stimulated with miR-155-bearing AdEV regulated insulin signaling and glucose uptake in adipocytes. Additionally, AdEV-released miR-34a could be transported into macrophages, resulting in the inhibition of M2 polarization through inhibition of the expression of Krüppel-like factor 4 [67]. Together, these data illustrate the complex interplay between adipocytes and macrophages, which can partly be explained by the exchange of vesicle-packed miRNA.

4.3. Lipids in AdEV

Although EVs are membrane-derived vesicles, one often-neglected component is their lipid content that EVs also transfer into recipient cells. EVs display specific lipid enrichment. Their membrane high protein/lipid ratio and the lipid asymetric distribution confer a high membrane rigidity in comparison with parent cells, which explains their stability in biofluids [68]. Interestingly, it was demonstrated that EV protein and lipid enrichment mechanisms are not linked. Indeed, some cell types differing in protein and

lipid composition secrete EV enriched in the same subgroup of proteins but not the same species of lipids. Conversely, EV lipid content might reflect the lipid composition of their parental cells, whereas the EV proteins differed [69]. These data strongly suggest that combining lipid and proteomic profiles from EVs could help better define specific AdEV biomarkers.

Several studies on cancer cells have shown that sEVs are strongly enriched in cholesterol, sphingomyelin (SM), glycosphingolipids and phosphatidylserine (PS) (mol% of total lipids) and depleted in phosphatidylcholine (PC) (see review in [70]). Interestingly, compared to these cancer-derived EV, AdEVs have a different lipid distribution and enrichment from the parental cells. Indeed, in both sEVs and lEVs released from 3T3-L1 adipocytes, PC represents by far the main phospholipids, whereas LysoPC, PS, phosphatidylinositol (PI) and phosphatidylethanolamine (PE) are proportionally minor phospholipids [16,50]. In addition, sEV and lEV lipid compositions relate to their mode of biogenesis [69]. For instance, whereas 3T3-L1-derived sEV and lEV display similar phospholipid profiles, sEVs have a specific cholesterol enrichment known to be a trait of exosomes acquired during their biogenesis, whereas a high amount of externalized PS is retrieved in lEV in line with the pro-coagulant potential of this lEV subclass [16].

Lipidomic analyses from AdEV are scarce, and the role of AdEV lipids in their biological functions in recipient cells needs urgently to be determined. During the development of obesity, important membrane remodeling occurs which is also illustrated by plasma membrane lipids reorganization. Of note, adipocyte plasma membrane lipids, such as cholesterol or sphingomyelin concentrations, are closely linked with the development of obesity-associated metabolic complications including insulin resistance [71,72]. Therefore, as a consequence, AdEV lipid composition might also be affected and could modulate some biological functions into the recipient cells. In line with this hypothesis, AdEV released from pre-differentiated or post-differentiated 3T3-L1 adipocytes displayed a different phospholipid composition closely resembling the phospholipid composition of the parental adipocytes, especially for PE and PS, confirming that modifications of adipocyte lipid composition could be reflected in AdEV [50]. Interestingly, Clement et al. demonstrated that AdEV free fatty acids could be taken up by melanoma cells stimulating fatty acid oxidation and melanoma migration [52]. Although this study did not indicate whether the lipid composition of AdEV also participated in melanoma aggressiveness, it demonstrated for the first time that AdEV could spread lipids in other tissues/cell types. Such AdEV lipid sorting has even been proposed as a second pathway of lipid release from adipocytes that is independent of the canonical lipolysis and that feeds local macrophages with AdEV lipids [19]. The authors estimated that WAT from lean mice may release ~1% of its lipid content per day via AdEVs ex vivo, a rate that is more than doubled in obese animals. Nonetheless, this percentage could be overestimated by a co-isolation of adipocytes with contaminant lipid droplets. The lipid class particularly enriched in sEVs is ceramides, which are also deleterious lipids interfering with insulin sensitivity in insulin-sensitive tissues [73]. AdEVs derived from WAT explants presented a specific signature in ceramides and displayed high levels of sphinganine, sphingosine-1 phosphate (S1P) and all sphingomyelin species, which are likely to alter a wide range of signaling pathways within WAT [24].

In the context of obesity, AdEVs released from adipocyte explants from high-fat-diet obese mice are strongly enriched in palmitic and stearic acids by comparison to AdEVs from standard diet mice, suggesting that the quality of the diet also has an impact on AdEV lipid composition [35]. For instance, a diet specifically enriched in palmitate triggered the release of EVs highly enriched in palmitate from skeletal muscle and changed their biological properties and perturbed skeletal muscle homeostasis [74].

5. Therapeutic Strategies to Decrease Ad EV Deleterious Effects

As AdEVs appear as important metabolic mediators in obesity-associated pathologies, designing EV-based strategies to counteract deleterious AdEV effects, particularly in the

pathophysiological context of obesity, might be envisaged. However, such approaches would imply specifically targetting AdEVs.

5.1. Targeting AdEV Extracellular Vesicle Biogenesis and Release

In order to counteract AdEVs' biological effects, one strategy to be envisaged might consist in modulating AdEV formation. Many drugs targeting either sEV formation or budding of the plasma membrane have been tested with promising results, mainly in the treatment of cancers (for a review, see [75]). Very interestingly, it seems that some of the tested inhibitors are known to regulate proteins involved in the development of insulinresistance in adipocytes and thus their use to restore insulin-sensitivity might also be a therapeutic strategy to reduce EV release from WAT. For instance, calpeptin, a cystein proteinase inhibitor, can be used to target calpains involved in lEV production. It has been shown that calpain inhibition attenuated WAT inflammation and suppressed macrophages migration to adipose tissue in vitro [76]. In addition, as calpain inhibition restores autophagy [77], it could favor the targeting of MVB to the autolysosome pathway for ILV degradation, resulting in a decrease in sEV sorting [78]. Another interesting drug is the anti-hypertensive Y27632 compound that targets RhoA-Rho kinase ROCK1/2 proteins involved in lEV formation [79,80]. Over-activation of the ROCK pathway has been implicated in the development of adipocyte hypertrophy, in the increase in inflammatory cytokine production and in the development of obesity-induced insulin resistance [81]. As partial deletion of ROCK1 or ROCK2 has been found to attenuate high-fat-diet obesity-induced insulin resistance [81,82], the use of Y27632 in patients suffering from obesity could be a strategy to decrease AdEV release and reduce cardiovascular diseases associated with obesity [83].

Besides modulating EV proteins involved in MVB biogenesis and lEV budding, the regulation of specific intracellular lipid concentrations could be also envisaged for EV production. Indeed, an alternative ESCRT-independent pathway for EV biogenesis has been described involving the generation of ceramides. Ceramides are cone-shaped lipids that can both induce inward budding of MVB to generate ILVs and the release of sEV, and plasma membrane budding to generate lEVs (Figure 1), as they preferentially accumulate in the inner membranes creating lipid-raft domains. The increased concentration of ceramides in tissues is associated with the consumption of high-saturated fatty acids diets and/or are induced by inflammatory cytokines. In this context, it might be interesting to test whether the drug GW4869, which can decrease the generation of sEV from cells through its action on the membrane neutral sphingomyelinase (nSMase) [84], could restore insulin-sensitivity in obese patients. In line with this suggestion, GW4869 has been shown to regulate inflammatory responses driven by TNFalpha from monocytes/macrophages [85]. In addition, inhibition of 3T3-L1 AdEV biogenesis and release following treatment with GW4869 could inhibit lipolysis and WAT browning, illustrating that such a strategy may be also useful for treating cancer-associated cachexia, a disorder characterized by unintended weight loss due to both skeletal muscle wasting and fat loss [86].

In addition to their involvement in EV release, lipids participate in the biological functions of EVs [74]. Therefore, modulation of AdEV lipid composition might beneficially modulate AdEV functions. In line with this suggestion, it was demonstrated that pharmacological inhibition of sphingosine kinase 1 (S1P1) in hepatocytes resulted in a significant reduction in S1P1-EV cargoes. Deleted-S1P1 EV decreased the migration responses of macrophages and consequently ameliorated non-alcoholic steatohepatitis [87]. Interestingly, pharmacological inhibition of sphingosine kinases 1 was shown to reverse obesity-inflammation in skeletal muscles of obese mice [88] and to reduce pancreatic lesions in spontaneously diabetic rats [89], therefore legitimating the use of such approaches to modulate both EV lipid composition and obesity-related disorders.

It has to be mentioned, however, that MVB trafficking and sEV/lEV release are parts of a complex intracellular trafficking and signaling networks, in close relationship with other cellular organelles to maintain cellular homeostasis and to release toxic components

from the cells. Therefore, the full abortion of AdEV release cannot be envisaged as it would induce apoptosis. In addition, the question of targeting specifically adipose ceramide production in vivo fully remains speculative considering that adipocytes may not be the primary source of ceramides in WAT, which can rather be produced by other SVF cells.

5.2. Modulation of AdEV Lipid Composition by the Diet

An alternative strategy to modulate AdEV lipid content is to modulate the intracellular lipid composition of the donor cells. Previous studies found a palmitate enrichment in AdEV, as well as other deleterious lipids, when AdEVs were isolated from mice fed with high-saturated-fat diets [35]. A supplementation in omega-3 polyunsaturated fatty acids at the expense of omega-6 ones has beneficial effects on WAT and increases the production of omega-3 metabolites, thereby exerting positive metabolic effects (for review, see [90]). Therefore, a diet enriched in polyunsaturated fats and low trans fat would impact adipocyte lipid content, and consequently AdEV lipid composition, enhancing their beneficial properties. In line with this suggestion, it has been demonstrated that dietary protein restriction modifies the protein composition of circulating EVs, demonstrating that diet can directly impact EV composition [91].

It is well admitted that insulin-resistance associated with obesity increases the risk of cholesterol synthesis and release by the liver and its accumulation in WAT, leading to adipocyte hypertrophy. It was recently demonstrated that cholesterol from the diet can participate in this alteration [92]. For instance, cholesterol from MVB membrane could influence the fate of EV: on the one hand, lowering intracellular cholesterol level redirects MVB to lysosome degradation [93], and on the other hand, high cholesterol level is associated with an increase in EV biogenesis, release and uptake. These data illustrate that hypertrophic AdEV might disseminate cholesterol among WAT during the consumption of high-cholesterol diet and/or during the development of metabolic syndrome [94]. They also suggest that part of the action of the statins used to lower blood cholesterol level by regulating its synthesis in the liver might rely on both the reduction of blood liver-derived EV and on the decrease of AdEV production.

Indirect diet-effects to restore WAT function may also be envisaged and could possibly contribute to modulating AdEV content in a healthy manner. For instance, the gut microbiota is now recognized as a key component in the development of obesity and related metabolic complications. Evidence from animal studies and human clinical trials has suggested beneficial effects from prebiotic and various probiotic strains on physical, biochemical and metabolic parameters related to obesity [95]. Therefore, prebiotic or probiotic supplementations might participate in the improvement of WAT homeostasis by promoting AdEV beneficial contents and favorable metabolic effects. Alternatively, supplementation with EV from external sources might also contribute to restoring obesity-related WAT function and thereby modulate AdEV biological functions. For instance, we demonstrated that nanovesicles from orange juice could reverse high-fat-diet-induced gut modifications (e.g., length of villi and immune response) in diet-induced obese mice [96]. Additional investigations will be required to envisage diet and/or supplements as a strategy to modulate AdEV content in order to counteract their deleterious biological effects.

5.3. Use of Extracellular Vesicles from Healthy Subjects

Recent data have provided proofs of concept that EVs from healthy/young subjects might be used in the management of metabolic complications associated with obesity such as insulin-resistance or in the management of aging-associated metabolic disorders. Indeed, injections of WAT macrophage-derived EVs isolated from lean mice improved glucose tolerance and insulin sensitivity in diet-induced obese mice [30]. Similarly, injection of young (3-month-old) mice blood EVs into aged (18-month-old) mice reversed the expression of aging-derived biomarkers [97]. Other studies have evidenced that EV isolated from adipose-derived stem cells from healthy patients displayed cardiac regenerative properties [98], or could improve insulin sensitivity, reduced obesity, and alleviated hepatic

steatosis in diet-induced obese mice by reducing inflammation [28]. Finally, some studies have suggested that many of the "exerkines" are contained within circulating EVs and might participate in the beneficial effects of exercise on obesity and type 2 diabetes (for review, [99]). Together, these studies suggest that the use of EVs derived from "healthy" WAT might be a potential strategy in addition to a modification of lifestyle and the use of drugs to normalize glycemia, and this would deserve to be investigated.

5.4. Use of Antibodies against AdEV

In the context of cancer, it has been demonstrated that blood injections of antibodies against CD63 and/or CD9, two tetraspanins expressed at the surface of all EVs, could significantly reduce the development of metastasis without any effects on tumor growth in mice [100]. As these two antibodies were not specific to the tumor-derived EVs, the authors explained this result by a general decrease in EV flux between organs, including the tumor, and demonstrated that these antibodies stimulated the uptake of EVs by patrolling macrophages. It was also demonstrated that the use sof a fragment of CD9-antibody could prevent the transfer of tumor-derived EV cargoes in recipient cells in vitro [101]. We previously demonstrated that obese patients have higher levels of circulating EVs in comparison to healthy patients [100], suggesting increased deleterious cross-talk between metabolic organs, including WAT. Therefore, the strategy to use antibodies against EV to reduce the EV flux in obese patients could be a complementary strategy during weight loss.

6. Conclusions

In this review, we provide evidence that extracellular vesicles released from adipocytes (AdEVs) participate in the homeostasis of adipose tissue by exchanging lipids, proteins and RNA between the different cells that compose the fat tissue. AdEV composition is closely connected to the composition of the secretory cells, and the pathophysiological context of obesity impacts EV content. AdEVs thereby participate in the instigation of inflammation and insulin resistance of adipose tissue and are also involved in the spread of cancer cells. Nonetheless, numerous questions remain unanswered. They will need to be resolved in the future prior to envisaging therapeutic avenues to counteract the deleterious effect of AdEV during the development of obesity.

Author Contributions: S.L.L. and S.R. wrote and edited the manuscript, A.B. edited the manuscript. All authors have read and agreed to the published version of the manuscript.

Funding: S.L.L. is supported by Société Francophone du Diabète, INSERM, Université d'Angers. S.R. is supported by the French National Research Agency (ANR-PRCE 2020-2023-ZENITH).

Institutional Review Board Statement: Not applicable.

Informed Consent Statement: Not applicable.

Data Availability Statement: No new data were created or analyzed in this study. Data sharing is not applicable to this article.

Acknowledgments: We thank Laurence Nieto who shared with us the proteomic data used in the Figure 4 and Table 1.

Conflicts of Interest: The authors declare no conflict of interest.

References

1. Despreés, J.-P.; Lemieux, I.; Bergeron, J.; Pibarot, P.; Mathieu, P.; LaRose, E.; Rodeés-Cabau, J.; Bertrand, O.F.; Poirier, P. Abdominal obesity and the metabolic syndrome: Contribution to global cardiometabolic risk. *Arter. Thromb. Vasc. Biol.* **2008**, *28*, 1039–1049. [CrossRef]
2. Kahn, C.R.; Wang, G.; Lee, K.Y. Altered adipose tissue and adipocyte function in the pathogenesis of metabolic syndrome. *J. Clin. Investig.* **2019**, *129*, 3990–4000. [CrossRef]
3. Crewe, C.; An, Y.A.; Scherer, P.E. The ominous triad of adipose tissue dysfunction: Inflammation, fibrosis, and impaired angiogenesis. *J. Clin. Investig.* **2017**, *127*, 74–82. [CrossRef]
4. Le Lay, S.; Dugail, I. Connecting lipid droplet biology and the metabolic syndrome. *Prog. Lipid Res.* **2009**, *48*, 191–195. [CrossRef]

5. Weisberg, S.P.; McCann, D.; Desai, M.; Rosenbaum, M.; Leibel, R.L.; Ferrante, A.W., Jr. Obesity is associated with macrophage ac-cumulation in adipose tissue. *J. Clin. Investig.* **2003**, *112*, 1796–1808. [CrossRef]
6. Hotamisligil, G.S. Inflammation and metabolic disorders. *Nature* **2006**, *444*, 860–867. [CrossRef]
7. Vidal, M. Exosomes: Revisiting their role as "garbage bags". *Traffic* **2019**, *20*, 815–828. [CrossRef] [PubMed]
8. Van Niel, G.; D'Angelo, G.; Raposo, G. Shedding light on the cell biology of extracellular vesicles. *Nat. Rev. Mol. Cell Biol.* **2018**, *19*, 213–228. [CrossRef] [PubMed]
9. Słomka, A.; Urban, S.K.; Lukacs-Kornek, V.; Żekanowska, E.; Kornek, M. Large extracellular vesicles: Have we found the holy grail of inflammation? *Front. Immunol.* **2018**, *9*, 2723. [CrossRef] [PubMed]
10. Théry, C.; Witwer, K.W.; Aikawa, E.; Alcaraz, M.J.; Anderson, J.D.; Andriantsitohaina, R.; Antoniou, A.; Arab, T.; Archer, F.; Atkin-Smith, G.K.; et al. Minimal information for studies of extracellular vesicles 2018 (MISEV2018): A position statement of the international society for extracellular vesicles and update of the MISEV2014 guidelines. *J. Extracell. Vesicles* **2018**, *7*, 1535750. [CrossRef]
11. Freyssinet, J.-M.; Toti-Orfanoudakis, F. Formation of procoagulant microparticles and properties. *Thromb. Res.* **2010**, *125*, S46–S48. [CrossRef] [PubMed]
12. Boulanger, C.M.; Loyer, X.; Rautou, P.-E.; Amabile, N. Extracellular vesicles in coronary artery disease. *Nat. Rev. Cardiol.* **2017**, *14*, 259–272. [CrossRef]
13. Théry, C.; Ostrowski, M.; Segura, E. Membrane vesicles as conveyors of immune responses. *Nat. Rev. Immunol.* **2009**, *9*, 581–593. [CrossRef] [PubMed]
14. Valadi, H.; Ekström, K.; Bossios, A.; Sjöstrand, M.; Lee, J.J.; Lötvall, J.O. Exosome-mediated transfer of mRNAs and microRNAs is a novel mechanism of genetic exchange between cells. *Nat. Cell Biol.* **2007**, *9*, 654–659. [CrossRef] [PubMed]
15. Hartwig, S.; De Filippo, E.; Göddeke, S.; Knebel, B.; Kotzka, J.; Al-Hasani, H.; Roden, M.; Lehr, S.; Sell, H. Exosomal proteins constitute an essential part of the human adipose tissue secretome. *Biochim. Biophys. Acta (BBA) Proteins Proteom.* **2019**, *1867*, 140172. [CrossRef]
16. Durcin, M.; Fleury, A.; Taillebois, E.; Hilairet, G.; Krupova, Z.; Henry, C.; Truchet, S.; Trötzmüller, M.; Köfeler, H.; Mabilleau, G.; et al. Characterisation of adipocyte-derived extracellular vesicle subtypes identifies distinct protein and lipid signatures for large and small extracellular vesicles. *J. Extracell. Vesicles* **2017**, *6*, 1305677. [CrossRef]
17. Connolly, K.D.; Wadey, R.M.; Mathew, D.; Johnson, E.; Rees, D.A.; James, P.E. Evidence for adipocyte-derived extracellular vesicles in the human circulation. *Endocrinology* **2018**, *159*, 3259–3267. [CrossRef]
18. Lazar, I.; Clement, E.; Dauvillier, S.; Milhas, D.; Ducoux-Petit, M.; Legonidec, S.; Moro, C.; Soldan, V.; Dalle, S.; Balor, S.; et al. Adipocyte exosomes promote melanoma aggressiveness through fatty acid oxidation: A novel mechanism linking obesity and cancer. *Cancer Res.* **2016**, *76*, 4051–4057. [CrossRef]
19. Flaherty, S.E., III; Grijalva, A.; Xu, X.; Ables, E.; Nomani, A.; Ferrante, A. A lipase-independent pathway of lipid release and immune modulation by adipocytes. *Science* **2019**, *363*, 989–993. [CrossRef]
20. Müller, G.A.; Schneider, M.; Biemer-Daub, G.; Wied, S. Upregulation of lipid synthesis in small rat adipocytes by microvesicle-associated CD73 from large adipocytes. *Obesity* **2011**, *19*, 1531–1544. [CrossRef]
21. Müller, G.; Jung, C.; Straub, J.; Wied, S.; Kramer, W. Induced release of membrane vesicles from rat adipocytes containing glycosylphosphatidylinositol-anchored microdomain and lipid droplet signalling proteins. *Cell. Signal.* **2009**, *21*, 324–338. [CrossRef]
22. Camino, T.; Lago-Baameiro, N.; Bravo, S.B.; Martis-Sueiro, A.; Couto, I.; Santos, F.; Baltar, J.; Casanueva, F.; Pardo, M. Vesicles shed by pathological murine adipocytes spread pathology: Characterization and functional role of insulin resistant/hypertrophied adiposomes. *Int. J. Mol. Sci.* **2020**, *21*, 2252. [CrossRef]
23. Sano, S.; Izumi, Y.; Yamaguchi, T.; Yamazaki, T.; Tanaka, M.; Shiota, M.; Osada-Oka, M.; Nakamura, Y.; Wei, M.; Wanibuchi, H.; et al. Lipid synthesis is promoted by hypoxic adipocyte-derived exosomes in 3T3-L1 cells. *Biochem. Biophys. Res. Commun.* **2014**, *445*, 327–333. [CrossRef] [PubMed]
24. Crewe, C.; Joffin, N.; Rutkowski, J.M.; Kim, M.; Zhang, F.; Towler, D.A.; Gordillo, R.; Scherer, P.E. An endothelial-to-adipocyte extracellular vesicle axis governed by metabolic state. *Cell* **2018**, *175*, 695–708.e13. [CrossRef]
25. Mleczko, J.; Ortega, F.J.; Falcón-Pérez, J.M.; Wabitsch, M.; Fernández-Real, J.M.; Mora, S. Extracellular vesicles from hypoxic adipocytes and obese subjects reduce insulin-stimulated glucose uptake. *Mol. Nutr. Food Res.* **2018**, *62*. [CrossRef]
26. Togliatto, G.; Dentelli, P.; Gili, M.; Gallo, S.A.; Deregibus, C.; Biglieri, E.G.; Iavello, A.; Santini, E.; Rossi, C.; Solini, A.; et al. Obesity reduces the pro-angiogenic potential of adipose tissue stem cell-derived extracellular vesicles (EVs) by impairing miR-126 content: Impact on clinical applications. *Int. J. Obes.* **2016**, *40*, 102–111. [CrossRef]
27. Eblázquez, R.; Sanchez-Margallo, F.M.; La Rosa, O.E.; Edalemans, W.; Ãlvarez, V.; Etarazona, R.; Macías-García, B.; Eblázquez, R.; Sanchez-Margallo, F.M.; La Rosa, O.E.; et al. Immunomodulatory potential of human adipose mesenchymal stem cells derived exosomes on in vitro stimulated T cells. *Front. Immunol.* **2014**, *5*, 556. [CrossRef]
28. Zhao, H.; Shang, Q.; Pan, Z.; Bai, Y.; Lining, Z.; Zhang, H.; Zhang, Q.; Guo, C.; Zhang, L.; Wang, Q. Exosomes from adipose-derived stem cells attenuate adipose inflammation and obesity through polarizing M2 macrophages and beiging in white adipose tissue. *Diabetes* **2018**, *67*, 235–247. [CrossRef] [PubMed]

29. Kranendonk, M.E.; Visseren, F.L.J.; Van Balkom, B.W.; Hoen, E.N.N.; Van Herwaarden, J.A.; De Jager, W.; Schipper, H.S.; Brenkman, A.B.; Verhaar, M.; Wauben, M.H.; et al. Human adipocyte extracellular vesicles in reciprocal signaling between adipocytes and macrophages. *Obesity* **2014**, *22*, 1296–1308. [CrossRef]
30. Ying, W.; Riopel, M.; Bandyopadhyay, G.; Dong, Y.; Birmingham, A.; Seo, J.B.; Ofrecio, J.M.; Wollam, J.; Hernandez-Carretero, A.; Fu, W.; et al. Adipose tissue macrophage-derived exosomal miRNAs can modulate in vivo and in vitro insulin sensitivity. *Cell* **2017**, *171*, 372–384.e12. [CrossRef] [PubMed]
31. De Silva, N.; Samblas, M.; Martínez, J.A.; Milagro, F.I. Effects of exosomes from LPS-activated macrophages on adipocyte gene expression, differentiation, and insulin-dependent glucose uptake. *J. Physiol. Biochem.* **2018**, *74*, 559–568. [CrossRef]
32. Thomou, T.; Mori, M.A.; Dreyfuss, J.M.; Konishi, M.; Sakaguchi, M.; Wolfrum, C.; Rao, T.N.; Winnay, J.N.; Garcia-Martin, R.; Grinspoon, S.K.; et al. Adipose-derived circulating miRNAs regulate gene expression in other tissues. *Nature* **2017**, *542*, 450–455. [CrossRef] [PubMed]
33. Amosse, J.; Durcin, M.; Malloci, M.; Vergori, L.; Fleury, A.; Gagnadoux, F.; Dubois, S.; Simard, G.; Boursier, J.; Hue, O.; et al. Phenotyping of circulating extracellular vesicles (EVs) in obesity identifies large EVs as functional conveyors of Macrophage Migration Inhibitory Factor. *Mol. Metab.* **2018**, *18*, 134–142. [CrossRef] [PubMed]
34. Acosta, J.R.; Douagi, I.; Andersson, D.P.; Bäckdahl, J.; Rydén, M.; Arner, P.; Laurencikiene, J. Increased fat cell size: A major phenotype of subcutaneous white adipose tissue in non-obese individuals with type 2 diabetes. *Diabetologia* **2016**, *59*, 560–570. [CrossRef]
35. Deng, Z.-B.; Poliakov, A.; Hardy, R.W.; Clements, R.; Liu, C.; Liu, Y.; Wang, J.; Xiang, X.; Zhang, S.; Zhuang, X.; et al. Adipose tissue exosome-like vesicles mediate activation of macrophage-induced insulin resistance. *Diabetes* **2009**, *58*, 2498–2505. [CrossRef] [PubMed]
36. Eguchi, A.; Mulya, A.; Lazic, M.; Radhakrishnan, D.; Berk, M.P.; Povero, D.; Gornicka, A.; Feldstein, A.E. Microparticles release by adipocytes act as "find-me" signals to promote macrophage migration. *PLoS ONE* **2015**, *10*, e0123110. [CrossRef] [PubMed]
37. Wadey, R.M.; Connolly, K.D.; Mathew, D.; Walters, G.; Rees, D.A.; James, P.E. Inflammatory adipocyte-derived extracellular vesicles promote leukocyte attachment to vascular endothelial cells. *Atherosclerosis* **2019**, *283*, 19–27. [CrossRef] [PubMed]
38. Zhao, Y.; Zhao, M.-F.; Jiang, S.; Wu, J.; Liu, J.; Yuan, X.-W.; Shen, D.; Zhang, J.-Z.; Zhou, N.; He, J.; et al. Liver governs adipose remodelling via extracellular vesicles in response to lipid overload. *Nat. Commun.* **2020**, *11*, 719. [CrossRef]
39. Xie, Z.; Wang, X.; Liu, X.; Du, H.; Sun, C.; Shao, X.; Tian, J.; Gu, X.; Wang, H.; Tian, J.; et al. Adipose-derived exosomes exert proatherogenic effects by regulating macrophage foam cell formation and polarization. *J. Am. Heart Assoc.* **2018**, *7*, e007442. [CrossRef] [PubMed]
40. Wang, J.; Wu, Y.; Guo, J.; Fei, X.; Yu, L.; Ma, S. Adipocyte-derived exosomes promote lung cancer metastasis by increasing MMP9 activity via transferring MMP3 to lung cancer cells. *Oncotarget* **2017**, *8*, 81880–81891. [CrossRef]
41. Tricarico, C.; Clancy, J.; D'Souza-Schorey, C. Biology and biogenesis of shed microvesicles. *Small GTPases* **2017**, *8*, 220–232. [CrossRef] [PubMed]
42. Carnino, J.M.; Ni, K.; Jin, Y. Post-translational modification regulates formation and cargo-loading of extracellular vesicles. *Front. Immunol.* **2020**, *11*, 948. [CrossRef]
43. Pálfy, M.; Reményi, A.; Korcsmáros, T. Endosomal crosstalk: Meeting points for signaling pathways. *Trends Cell Biol.* **2012**, *22*, 447–456. [CrossRef]
44. Ertunc, M.E.; Sikkeland, J.; Fenaroli, F.; Griffiths, G.; Daniels, M.P.; Cao, H.; Saatcioglu, F.; Hotamisligil, G.S. Secretion of fatty acid binding protein aP2 from adipocytes through a nonclassical pathway in response to adipocyte lipase activity. *J. Lipid Res.* **2015**, *56*, 423–434. [CrossRef] [PubMed]
45. Le Bihan, M.-C.; Bigot, A.; Jensen, S.S.; Dennis, J.L.; Rogowska-Wrzesinska, A.; Lainé, J.; Gache, V.; Furling, D.; Jensen, O.N.; Voit, T.; et al. In-depth analysis of the secretome identifies three major independent secretory pathways in differentiating human myoblasts. *J. Proteom.* **2012**, *77*, 344–356. [CrossRef] [PubMed]
46. Mi, H.; Huang, X.; Muruganujan, A.; Tang, H.; Mills, C.; Kang, D.; Thomas, P.D. PANTHER version 11: Expanded annotation data from Gene Ontology and Reactome pathways, and data analysis tool enhancements. *Nucleic Acids Res.* **2017**, *45*, D183–D189. [CrossRef]
47. Phoonsawat, W.; Aoki-Yoshida, A.; Tsuruta, T.; Sonoyama, K. Adiponectin is partially associated with exosomes in mouse serum. *Biochem. Biophys. Res. Commun.* **2014**, *448*, 261–266. [CrossRef]
48. Henegar, C.; Tordjman, J.; Achard, V.; Lacasa, D.; Cremer, I.; Guerre-Millo, M.; Poitou, C.; Basdevant, A.; Stich, V.; Viguerie, N.; et al. Adipose tissue transcriptomic signature highlights the pathological relevance of extracellular matrix in human obesity. *Genome Biol.* **2008**, *9*, R14. [CrossRef]
49. Ruiz-Ojeda, F.J.; Méndez-Gutiérrez, A.; Aguilera, C.M.; Plaza-Díaz, J. Extracellular matrix remodeling of adipose tissue in obesity and metabolic diseases. *Int. J. Mol. Sci.* **2019**, *20*, 4888. [CrossRef]
50. Connolly, K.D.; Guschina, I.A.; Yeung, V.; Clayton, A.; Draman, M.S.; Von Ruhland, C.; Ludgate, M.; James, P.E.; Rees, D.A. Characterisation of adipocyte-derived extracellular vesicles released pre- and post-adipogenesis. *J. Extracell. Vesicles* **2015**, *4*, 29159. [CrossRef]
51. Desdín-Micó, G.; Mittelbrunn, M. Role of exosomes in the protection of cellular homeostasis. *Cell Adhes. Migr.* **2017**, *11*, 127–134. [CrossRef]

52. Clement, E.; Lazar, I.; Attané, C.; Carrié, L.; Dauvillier, S.; Ducoux-Petit, M.; Esteve, D.; Menneteau, T.; Moutahir, M.; Le Gonidec, S.; et al. Adipocyte extracellular vesicles carry enzymes and fatty acids that stimulate mitochondrial metabolism and remodeling in tumor cells. *EMBO J.* **2020**, *39*, e102525. [CrossRef]
53. Lee, J.-E.; Moon, P.-G.; Lee, I.-K.; Baek, M.-C. Proteomic analysis of extracellular vesicles released by adipocytes of Otsuka Long-Evans Tokushima Fatty (OLETF) rats. *Protein J.* **2015**, *34*, 220–235. [CrossRef] [PubMed]
54. Tamara, C.; Nerea, L.-B.; Belén, B.S.; Alberto, M.-V.; Aurelio, S.; Iván, C.; Javier, B.; Felipe, C.F.; María, P. Human obese white adipose tissue sheds depot-specific extracellular vesicles and reveals candidate biomarkers for monitoring obesity and its comorbidities. *Transl. Res.* **2021**. [CrossRef] [PubMed]
55. Ogawa, R.; Tanaka, C.; Sato, M.; Nagasaki, H.; Sugimura, K.; Okumura, K.; Nakagawa, Y.; Aoki, N. Adipocyte-derived microvesicles contain RNA that is transported into macrophages and might be secreted into blood circulation. *Biochem. Biophys. Res. Commun.* **2010**, *398*, 723–729. [CrossRef] [PubMed]
56. Janas, T.; Janas, M.M.; Sapoń, K.; Janas, T. Mechanisms of RNA loading into exosomes. *FEBS Lett.* **2015**, *589*, 1391–1398. [CrossRef] [PubMed]
57. Groot, M.; Lee, H. Sorting mechanisms for MicroRNAs into extracellular vesicles and their associated diseases. *Cells* **2020**, *9*, 1044. [CrossRef] [PubMed]
58. Koppers-Lalic, D.; Hackenberg, M.; Bijnsdorp, I.V.; Van Eijndhoven, M.A.; Sadek, P.; Sie, D.; Zini, N.; Middeldorp, J.M.; Ylstra, B.; De Menezes, R.X.; et al. Nontemplated nucleotide additions distinguish the small rna composition in cells from exosomes. *Cell Rep.* **2014**, *8*, 1649–1658. [CrossRef]
59. Batagov, A.O.; Kurochkin, I.V. Exosomes secreted by human cells transport largely mRNA fragments that are enriched in the 3′-untranslated regions. *Biol. Direct* **2013**, *8*, 12. [CrossRef]
60. Müller, G.; Schneider, M.; Biemer-Daub, G.; Wied, S. Microvesicles released from rat adipocytes and harboring glycosyl-phosphatidylinositol-anchored proteins transfer RNA stimulating lipid synthesis. *Cell. Signal.* **2011**, *23*, 1207–1223. [CrossRef]
61. Yue, B.; Yang, H.; Wu, J.; Wang, J.; Ru, W.; Cheng, J.; Huang, Y.; Lei, C.; Lan, X.; Chen, H. Characterization and transcriptome analysis of exosomal and nonexosomal RNAs in bovine adipocytes. *Int. J. Mol. Sci.* **2020**, *21*, 9313. [CrossRef]
62. Zhang, H.; Deng, T.; Ge, S.; Liu, Y.; Bai, M.; Zhu, K.; Fan, Q.; Li, J.; Ning, T.; Tian, F.; et al. Exosome circRNA secreted from adipocytes promotes the growth of hepatocellular carcinoma by targeting deubiquitination-related USP7. *Oncogene* **2019**, *38*, 2844–2859. [CrossRef] [PubMed]
63. Wen, Z.; Li, J.; Fu, Y.; Zheng, Y.; Ma, M.; Wang, C. Hypertrophic adipocyte–derived exosomal miR-802-5p contributes to insulin resistance in cardiac myocytes through targeting HSP60. *Obesity* **2020**, *28*, 1932–1940. [CrossRef] [PubMed]
64. Yu, Y.; Du, H.; Wei, S.; Feng, L.; Li, J.; Yao, F.; Zhang, M.; Hatch, G.M.; Chen, L. Adipocyte-derived exosomal MiR-27a induces insulin resistance in skeletal muscle through repression of PPARγ. *Theranostics* **2018**, *8*, 2171–2188. [CrossRef]
65. Liu, Y.; Tan, J.; Ou, S.; Chen, J.; Chen, L. Adipose-derived exosomes deliver miR-23a/b to regulate tumor growth in hepatocellular cancer by targeting the VHL/HIF axis. *J. Physiol. Biochem.* **2019**, *75*, 391–401. [CrossRef] [PubMed]
66. Zhang, Y.; Mei, H.; Chang, X.; Chen, F.; Zhu, Y.; Han, X. Adipocyte-derived microvesicles from obese mice induce M1 macrophage phenotype through secreted miR-155. *J. Mol. Cell Biol.* **2016**, *8*, 505–517. [CrossRef] [PubMed]
67. Pan, Y.; Hui, X.; Hoo, R.L.C.; Ye, D.; Chan, C.Y.C.; Feng, T.; Wang, Y.; Lam, K.S.L.; Xu, A. Adipocyte-secreted exosomal microRNA-34a inhibits M2 macrophage polarization to promote obesity-induced adipose inflammation. *J. Clin. Investig.* **2019**, *129*, 834–849. [CrossRef]
68. Record, M.; Silvente-Poirot, S.; Poirot, M.; Wakelam, M.J.O. Extracellular vesicles: Lipids as key components of their biogenesis and functions. *J. Lipid Res.* **2018**, *59*, 1316–1324. [CrossRef] [PubMed]
69. Haraszti, R.A.; Didiot, M.-C.; Sapp, E.; Leszyk, J.; Shaffer, S.A.; Rockwell, H.E.; Gao, F.; Narain, N.R.; DiFiglia, M.; Kiebish, M.A.; et al. High-resolution proteomic and lipidomic analysis of exosomes and microvesicles from different cell sources. *J. Extracell. Vesicles* **2016**, *5*, 32570. [CrossRef]
70. Skotland, T.; Sandvig, K.; Llorente, A. Lipids in exosomes: Current knowledge and the way forward. *Prog. Lipid Res.* **2017**, *66*, 30–41. [CrossRef]
71. Le Lay, S.; Krief, S.; Farnier, C.; Lefrère, I.; Le Liepvre, X.; Bazin, R.; Ferré, P.; Dugail, I. Cholesterol, a cell size-dependent signal that regulates glucose metabolism and gene expression in adipocytes. *J. Biol. Chem.* **2001**, *276*, 16904–16910. [CrossRef]
72. Zeghari, N.; Vidal, H.; Younsi, M.; Ziegler, O.; Drouin, P.; Donner, M. Adipocyte membrane phospholipids and PPAR-γ expression in obese women: Relationship to hyperinsulinemia. *Am. J. Physiol. Metab.* **2000**, *279*, E736–E743. [CrossRef] [PubMed]
73. Sokolowska, E.; Blachnio-Zabielska, A. The role of ceramides in insulin resistance. *Front. Endocrinol.* **2019**, *10*, 577. [CrossRef]
74. Aswad, H.; Forterre, A.; Wiklander, O.P.B.; Vial, G.; Danty-Berger, E.; Jalabert, A.; Lamazière, A.; Meugnier, E.; Pesenti, S.; Ott, C.; et al. Exosomes participate in the alteration of muscle homeostasis during lipid-induced insulin resistance in mice. *Diabetologia* **2014**, *57*, 2155–2164. [CrossRef] [PubMed]
75. Catalano, M.; O'Driscoll, L. Inhibiting extracellular vesicles formation and release: A review of EV inhibitors. *J. Extracell. Vesicles* **2020**, *9*, 1703244. [CrossRef]
76. Muniappan, L.; Javidan, A.; Jiang, W.; Mohammadmoradi, S.; Moorleghen, J.J.; Katz, W.S.; Balakrishnan, A.; Howatt, D.A.; Subramanian, V. Calpain inhibition attenuates adipose tissue inflammation and fibrosis in diet-induced obese mice. *Sci. Rep.* **2017**, *7*, 14398. [CrossRef] [PubMed]

77. Ong, S.-B.; Lee, W.H.; Shao, N.-Y.; Ismail, N.I.; Katwadi, K.; Lim, M.-M.; Kwek, X.-Y.; Michel, N.A.; Li, J.; Newson, J.; et al. Calpain inhibition restores autophagy and prevents mitochondrial fragmentation in a human iPSC model of diabetic endotheliopathy. *Stem Cell Rep.* **2019**, *12*, 597–610. [CrossRef]
78. Xu, J.; Camfield, R.; Gorski, S.M. The interplay between exosomes and autophagy—Partners in crime. *J. Cell Sci.* **2018**, *131*, jcs215210. [CrossRef] [PubMed]
79. Dai, H.; Zhang, S.; Du, X.; Zhang, W.; Jing, R.; Wang, X.; Pan, L. RhoA inhibitor suppresses the production of microvesicles and rescues high ventilation induced lung injury. *Int. Immunopharmacol.* **2019**, *72*, 74–81. [CrossRef]
80. Wang, G.H.; Ma, K.L.; Zhang, Y.; Hu, Z.B.; Liu, L.; Lu, J.; Chen, P.P.; Lu, C.C.; Ruan, X.Z.; Liu, B.C. Caspase 3/ROCK1 pathway mediates high glucose-induced platelet microparticles shedding. *Biochem. Biophys. Res. Commun.* **2019**, *509*, 596–602. [CrossRef]
81. Soliman, H.; Varela, J.N.; Nyamandi, V.; Garcia-Patino, M.; Lin, G.; Bankar, G.R.; Jia, Z.; MacLeod, K.M. Attenuation of obesity-induced insulin resistance in mice with heterozygous deletion of ROCK2. *Int. J. Obes.* **2016**, *40*, 1435–1443. [CrossRef]
82. Lee, S.; Huang, H.; Choi, K.; Lee, D.H.; Shi, J.; Liu, T.; Chun, K.H.; Seo, J.-A.; Lima, I.S.; Zabolotny, J.M.; et al. ROCK1 isoform-specific deletion reveals a role for diet-induced insulin resistance. *Am. J. Physiol. Metab.* **2014**, *306*, E332–E343. [CrossRef]
83. Soliman, H.; Nyamandi, V.; Garcia-Patino, M.; Varela, J.N.; Bankar, G.; Lin, G.; Jia, Z.; MacLeod, K.M. Partial deletion of ROCK2 protects mice from high-fat diet-induced cardiac insulin resistance and contractile dysfunction. *Am. J. Physiol. Circ. Physiol.* **2015**, *309*, H70–H81. [CrossRef]
84. Menck, K.; Sönmezer, C.; Worst, T.S.; Schulz, M.; Dihazi, G.H.; Streit, F.; Erdmann, G.; Kling, S.; Boutros, M.; Binder, C.; et al. Neutral sphingomyelinases control extracellular vesicles budding from the plasma membrane. *J. Extracell. Vesicles* **2017**, *6*, 1378056. [CrossRef] [PubMed]
85. Al-Rashed, F.; Ahmad, Z.; Thomas, R.; Melhem, M.; Snider, A.J.; Obeid, L.M.; Al-Mulla, F.; Hannun, Y.A.; Ahmad, R. Neutral sphingomyelinase 2 regulates inflammatory responses in monocytes/macrophages induced by TNF-α. *Sci. Rep.* **2020**, *10*, 16802. [CrossRef] [PubMed]
86. Hu, W.; Ru, Z.; Xiao, W.; Xiong, Z.; Wang, C.; Yuan, C.; Zhang, X.; Yang, H. Adipose tissue browning in cancer-associated cachexia can be attenuated by inhibition of exosome generation. *Biochem. Biophys. Res. Commun.* **2018**, *506*, 122–129. [CrossRef]
87. Mauer, A.S.; Hirsova, P.; Maiers, J.L.; Shah, V.H.; Malhi, H. Inhibition of sphingosine 1-phosphate signaling ameliorates murine nonalcoholic steatohepatitis. *Am. J. Physiol. Liver Physiol.* **2017**, *312*, G300–G313. [CrossRef] [PubMed]
88. Rivas, D.A.; Rice, N.P.; Ezzyat, Y.; McDonald, D.J.; Cooper, B.E.; Fielding, R.A. Sphingosine-1-phosphate analog FTY720 reverses obesity but not age-induced anabolic resistance to muscle contraction. *Am. J. Physiol. Physiol.* **2019**, *317*, C502–C512. [CrossRef]
89. Kobayashi, K.; Sasase, T.; Ishii, Y.; Katsuda, Y.; Miyajima, K.; Yamada, T.; Ohta, T. The sphingosine-1-phosphate receptor modulator, FTY720, prevents the incidence of diabetes in Spontaneously Diabetic Torii rats. *Clin. Exp. Pharmacol. Physiol.* **2020**. [CrossRef]
90. Simopoulos, A.P.; DiNicolantonio, J.J. The importance of a balanced ω-6 to ω-3 ratio in the prevention and management of obesity. *Open Heart* **2016**, *3*, e000385. [CrossRef]
91. Eitan, E.; Tosti, V.; Suire, C.N.; Cava, E.; Berkowitz, S.T.; Bertozzi, B.; Raefsky, S.M.; Veronese, N.; Spangler, R.; Spelta, F.; et al. In a randomized trial in prostate cancer patients, dietary protein restriction modifies markers of leptin and insulin signaling in plasma extracellular vesicles. *Aging Cell* **2017**, *16*, 1430–1433. [CrossRef] [PubMed]
92. Chung, S.; Cuffe, H.; Marshall, S.M.; McDaniel, A.L.; Ha, J.-H.; Kavanagh, K.; Hong, C.; Tontonoz, P.; Temel, R.E.; Parks, J.S. Dietary cholesterol promotes adipocyte hypertrophy and adipose tissue inflammation in visceral, but not in subcutaneous, fat in monkeys. *Arter. Thromb. Vasc. Biol.* **2014**, *34*, 1880–1887. [CrossRef] [PubMed]
93. Möbius, W.; Ohno-Iwashita, Y.; Van Donselaar, E.G.; Oorschot, V.M.J.; Shimada, Y.; Fujimoto, T.; Heijnen, H.F.G.; Geuze, H.J.; Slot, J.W. Immunoelectron microscopic localization of cholesterol using biotinylated and non-cytolytic perfringolysin O. *J. Histochem. Cytochem.* **2002**, *50*, 43–55. [CrossRef]
94. Pfrieger, F.W.; Vitale, N. Thematic review series: Exosomes and microvesicles: Lipids as key components of their biogenesis and functions, cholesterol and the journey of extracellular vesicles. *J. Lipid Res.* **2018**, *59*, 2255–2261. [CrossRef] [PubMed]
95. Cerdó, T.; García-Santos, J.A.; Bermúdez, M.G.; Campoy, C. The role of probiotics and prebiotics in the prevention and treatment of obesity. *Nutrients* **2019**, *11*, 635. [CrossRef] [PubMed]
96. Berger, E.; Colosetti, P.; Jalabert, A.; Meugnier, E.; Wiklander, O.P.; Jouhet, J.; Errazurig-Cerda, E.; Chanon, S.; Gupta, D.; Rautureau, G.J.; et al. Use of nanovesicles from orange juice to reverse diet-induced gut modifications in diet-induced obese mice. *Mol. Ther. Methods Clin. Dev.* **2020**, *18*, 880–892. [CrossRef]
97. Lee, B.-R.; Kim, J.-H.; Choi, E.-S.; Cho, J.H.; Kim, E. Effect of young exosomes injected in aged mice. *Int. J. Nanomed.* **2018**, *13*, 5335–5345. [CrossRef]
98. Fleury, A.; Martinez, M.C.; Le Lay, S. Extracellular vesicles as therapeutic tools in cardiovascular diseases. *Front. Immunol.* **2014**, *5*. [CrossRef]
99. Safdar, A.; Saleem, A.; Tarnopolsky, M.A. The potential of endurance exercise-derived exosomes to treat metabolic diseases. *Nat. Rev. Endocrinol.* **2016**, *12*, 504–517. [CrossRef] [PubMed]
100. Nishida-Aoki, N.; Tominaga, N.; Takeshita, F.; Sonoda, H.; Yoshioka, Y.; Ochiya, T. Disruption of circulating extracellular vesicles as a novel therapeutic strategy against cancer metastasis. *Mol. Ther.* **2017**, *25*, 181–191. [CrossRef] [PubMed]
101. Santos, M.F.; Rappa, G.; Karbanová, J.; Vanier, C.; Morimoto, C.; Corbeil, D.; Lorico, A. Anti-human CD 9 antibody Fab fragment impairs the internalization of extracellular vesicles and the nuclear transfer of their cargo proteins. *J. Cell. Mol. Med.* **2019**, *23*, 4408–4421. [CrossRef] [PubMed]

Med Mal Metab 2020; 14: 250-257
en ligne sur / *on line on*
www.em-consulte.com/revue/mmm
www.sciencedirect.com

Exosomes, vésicules extracellulaires et dialogue inter-organes

Alexia Blandin, Soazig Le Lay

Disponible sur internet le :
30 mars 2020

Institut de biologie en santé–IRIS, UMR Inserm 1063 « Stress oxydant et pathologies métaboliques », Angers, France

Correspondance :
Soazig Le Lay, CHU d'Angers, Institut de biologie en santé–IRIS, Inserm U1063 « Stress Oxydant et Pathologies Métaboliques » (SOPAM), 4, rue Larrey, 49933 Angers cedex 09, France.
soazig.lelay@inserm.fr

Mots clés
Vésicules extracellulaires
Exosomes
Microvésicules
Métabolisme
Vecteurs biologiques
Communication inter-organes

Résumé

Les vésicules extracellulaires (VE), incluant les exosomes et les microvésicules, dérivent des membranes cellulaires et circulent dans l'organisme à la faveur des nombreux biofluides. Ces VE constituent de nouveaux vecteurs de la communication intercellulaire de par leur capacité à transférer du matériel biologique entre cellules/tissus. Les VE sont sécrétées par des cellules de différents tissus ou organes, tels que l'endothélium vasculaire, le tissu adipeux, le muscle, ou encore le foie. De nombreuses données expérimentales et cliniques ont mis en lumière le rôle de ces VE dans le développement des maladies métaboliques. Les VE apparaissent donc comme de nouveaux acteurs de la communication inter-organes, et représentent des biomarqueurs potentiels ainsi que des cibles intéressantes pour le développement d'approches thérapeutiques innovantes.

Keywords
Extracellular vesicles
Exosomes
Microvesicles
Metabolism
Biological vectors
Inter-organ communication

Summary

Exosomes, extracellular vesicles, and inter-organ communication

Extracellular vesicles (EVs), including exosomes and microvesicles, derive from cell membranes and circulate in body fluids. EVs are considered as new vectors of intercellular communication due to their ability to transfer biological material between cells/tissues. EVs are secreted by different cells from various tissues or organs such as vascular endothelium, adipose tissue, muscle or even liver. Numerous experimental and clinical data have highlighted their role in the development of metabolic diseases. EVs therefore appear as new players in inter-organ communication and represent potential biomarkers as well as interesting targets for the development of innovative therapeutic approaches.

Médecine des maladies Métaboliques
tome 14 > n°3 > mai 2020
10.1016/j.mmm.2020.01.013

Introduction

Les vésicules extracellulaires (VE) sont un ensemble hétérogène de nanovésicules dérivées des membranes cellulaires, sécrétées dans le milieu extracellulaire, et circulant dans les fluides de l'organisme. La sécrétion de ces VE est un processus conservé au cours de l'évolution, mis en évidence de la bactérie à l'homme, en passant par les plantes. Longtemps considérées comme de simples débris cellulaires, l'avènement de nouveaux outils technologiques permettant la purification des VE, leur quantification et leur visualisation, combinée à une meilleure connaissance des mécanismes d'exocytose, a contribué à mieux les caractériser.

Biogenèse et composition des VE

La communauté scientifique internationale a récemment proposé une nomenclature distinguant les sous-types de VE selon leur taille [1] (*figure 1*). Les VE de petite taille (*small EVs*, en anglais) réfèrent principalement aux exosomes, dont le diamètre est généralement compris entre 30 et 150 nm. Les VE de grande taille qualifient principalement les vésicules bourgeonnant directement de la membrane plasmique à la suite d'un remodelage du cytosquelette, à l'image des microvésicules (50 nm à 1 µm) ou des corps apoptotiques dérivés de cellules en apoptose dont la taille peut alors atteindre plusieurs microns.

Les exosomes, ou VE de petite taille

Les exosomes dérivent des vésicules intraluminales formées lors de la maturation des endosomes, qui sont ensuite sécrétées dans le milieu extracellulaire par fusion de ces corps multivésiculaires (CMV) avec la membranaire plasmique (*figure 1*). La formation des exosomes nécessite une machinerie protéique complexe (revue *in* [2]). La ségrégation de protéines cargos et de lipides, notamment de céramides générés par la sphingomyélinase neutre de type II, engendre la formation de microdomaines au sein de la membrane endosomale, puis l'invagination et la fission de vésicules intraluminales séquestrant du cytosol. Cette première étape est dépendante des différents complexes protéiques de la machinerie ESCRT (pour *endosomal sorting complex required for transport*), ainsi que des protéines adaptatrices ou de trafic membranaire à l'image des tétraspanines (CD9, CD63, CD81) ou des protéines Tsg101 (pour *Tumor susceptibility 101*) ou Alix. La formation d'exosomes peut cependant s'opérer en l'absence d'une machinerie ESCRT fonctionnelle, démontrant l'existence d'une voie de biogenèse exosomale indépendante d'ESCRT. Les mécanismes favorisant la sécrétion des CMV au dépens de leur dégradation lysosomale sont encore mal compris. L'implication des protéines Rab GTPases (pour *RAS-related protein*) dans l'adressage des CMV à la surface cellulaire a cependant été mise en évidence, de concert avec les protéines du cytosquelette et du complexe SNARE (pour *Soluble N-éthylmaleimide-sensitive-factor attachment protein receptors*) qui participent activement à l'ancrage des CMV à la membrane plasmique.

Les microvésicules (MV), ou VE de grande taille

Le bourgeonnement de MV membranaires est consécutif à un réarrangement du cytosquelette lié à une élévation des concentrations calcique intracellulaires [3] (*figure 1*). L'activation de machineries enzymatiques dépendante des niveaux de Ca^{2+} intracytosoliques fait intervenir des translocases, flippases, floppases et la calpaïne, et conduit, in fine, à l'externalisation de phosphatidylsérine (PS) du feuillet interne vers le feuillet externe membranaire. Cette perte de l'asymétrie membranaire couplée à un remodelage du cytosquelette favorise la formation de bourgeons membranaires à partir desquels sont émises les MV. La formation de microdomaines lipidiques membranaires, ainsi que la voie de signalisation RhoGTPases et des kinases associées à Rho, sont également des déterminants importants pour la genèse des MV.

Composition des VE

Les VE transportent un contenu varié de métabolites, protéines solubles ou membranaires, lipides et acides nucléiques, le tout délimité par une bicouche lipidique. La nature et l'abondance des cargos transportés par les VE dépendent de leur origine cellulaire, de l'état physiopathologique, ou du stimulus ayant induit la sécrétion des VE. Des analyses protéomiques de VE isolées de différents types cellulaires révèlent, cependant, la présence de cargos spécifiquement associés aux sous-types de VE [4,5] (*figure 1*). Différentes protéines contrôlant la formation et la sécrétion des exosomes incluant les tétraspanines (CD9, CD63, ou CD81), de protéines de trafic (Tsg101, Alix. . .), de chaperonnes (HSP70, HSC70), ou encore du complexe majeur d'histocompatibilité de classe II (CMHII), sont ainsi utilisées comme marqueurs protéiques des exosomes. Des protéines membranaires et protéines du cytosquelette (actine, tubuline, actinine-4) ou molécules d'adhésion (intégrines) sont utilisées pour caractériser les MV, par analogie à leur origine membranaire.

Le contenu lipidique des VE de petite et grande taille se compose principalement de phospholipides, à l'image de la composition des membranes cellulaires [4]. Les VE sont également enrichies en cholestérol, caractéristique des microdomaines membranaires des cellules dont elles sont issues. Enfin, une forte majorité de MV présente la PS externalisée, reflet de leur processus de biogenèse.

Différents acides nucléiques (séquences d'ADN, ARN, ARN messager [ARNm], ARN non codants, ou micro-ARN [miARN]) sont également retrouvés dans les VE, et leur empaquetage dans les VE pourrait se faire par interaction de protéines à des séquences nucléiques spécifiques [6].

Isolement et caractérisation des VE

Les VE peuvent être isolées à partir de différents biofluides, allant du sang à des milieux de culture conditionnés, en utilisant

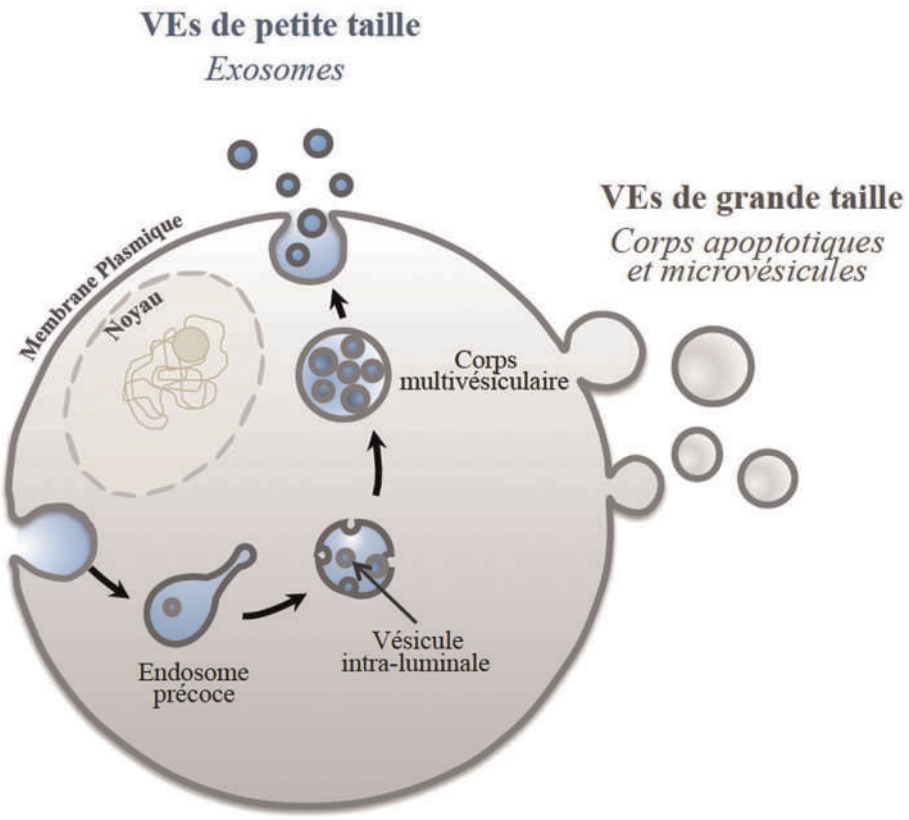

	VEs de petite taille	VEs de grande taille	
	Exosomes	Microvésicules	Corps apoptotiques
Origine	Endolysosomale	Membrane plasmique	
Taille	30-150nm	100-1000nm	>1000nm
Marqueurs protéiques	Tétraspanines (CD9, CD63, CD81) Protéines voies de biogenèse (Tsg101, Alix,..) Chaperonnes (HSP70, HSC70) CMH classe II	Protéines du cytosquelette (actine,tubuline, actinine-4) Molécules d'adhésion (intégrines…) Protéines de la membrane plasmique	
Cargos	Acides nucléiques (ADN, ARN, ARNm, ARN non-codant, micro-ARN) Lipides Protéines		

FIGURE 1

Représentation schématique de la biogenèse des sous-types de vésicules extracellulaires (VE) et de leurs caractéristiques respectives

Les VE de grande taille, comprenant les microvésicules et les corps apoptotiques, résultent d'un bourgeonnement de la membrane plasmique consécutif à un important remodelage membranaire

Les exosomes désignent les vésicules intraluminales formées lors de la maturation des corps multivésiculaires (CMV), et sécrétées dans le milieu extracellulaire après fusion des CMV avec la membrane plasmique

Bien que ces VE partagent des caractéristiques communes, leur origine subcellulaire, leur taille, et les cargos qu'elles transportent, diffèrent. Des marqueurs protéiques spécifiques sont ainsi utilisés pour les identifier

CMH : complexe majeur d'histocompatibilité

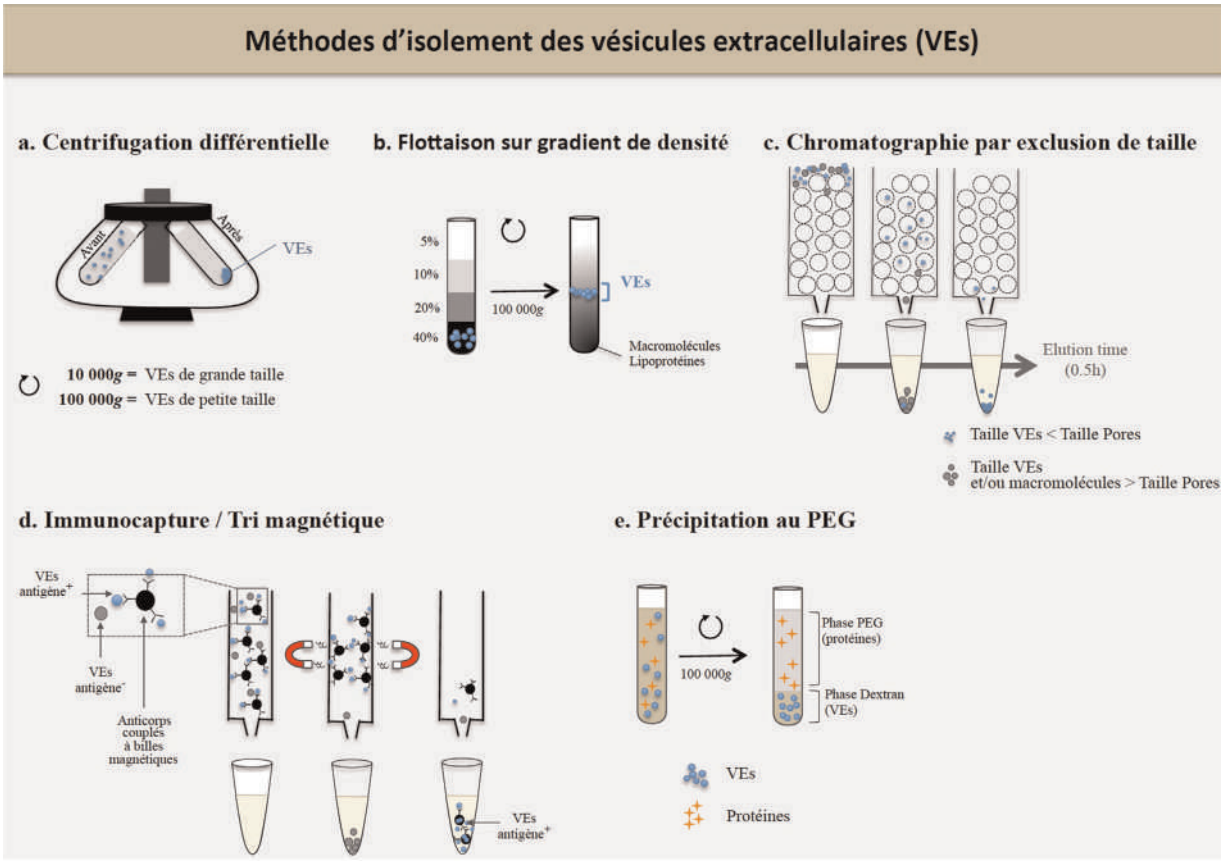

FIGURE 2

Représentation schématique des méthodes les plus couramment utilisées pour l'isolement des vésicules extracellulaires (VE)

La centrifugation différentielle (a) permet de culotter les VE de grande taille (à faible vitesse de centrifugation), puis celles de petite taille à forte vitesse (> 100 000 *g*). Des macromolécules et/ou lipoprotéines pouvant co-précipitées avec les VE, la flottaison des VE sur un gradient de densité (b) permet souvent d'optimiser leur purification et purifier plus avant les VE. La chromatographie par exclusion de taille (c) utilise une matrice poreuse (cercles en pointillés) où les VE plus petites que la taille du pore vont être retenues plus longtemps, permettant leur élution plus tardive que des VE de grande taille et/ou macromolécules. L'immunocapture, ou tri magnétique, illustré ici (d) permet la rétention des VE exprimant un antigène de surface (par exemple : CD9, CD63, ou CD81) à l'aide d'anticorps monoclonaux (dirigés contre cet antigène) couplés à des billes magnétiques retenues sur une colonne grâce à des aimants. En l'absence de champ magnétique, les VE positives pour cet antigène sont alors éluées. Les méthodes utilisant des solutions associant les polymères avec une solution de Dextran vont induire une séparation de phase, ou le dextran va induire la précipitation (à faible vitesse de centrifugation) des VE de par ses propriétés surfactantes, et le polyéthylène glycol (PEG) retenir les macromolécules et autres composants moléculaires

différentes techniques d'isolement [7] (*figure 2*). L'ultracentrifugation différentielle est la technique la plus communément employée pour séparer les VE de grande taille (par une centrifugation autour de 10 000 *g*) des VE de petite taille (ultracentrifugation à 100 000 *g*). La flottaison des VE ainsi isolées sur gradient de densité permet, en outre, de séparer les complexes macromoléculaires et/ou lipoprotéines coprécipitées avec les VE. La chromatographie par exclusion de taille est également utilisée, et permet la séparation des VE selon leur volume hydrodynamique. L'isolement de sous-populations de VE peut également être effectuée par immunocapture en utilisant des anticorps spécifiquement dirigés contre des antigènes portés par les VE, à l'image des tétraspanines. Enfin, la précipitation des VE par des mélanges de polymères (Dextran, polyéthylène glycol ou PEG. . .) permettant des séparations de phase à faible vitesse de centrifugation et la précipitation des VE est le principe de base de nombreux kits commerciaux (par exemple : ExoQuick TC^{TM}). Ces derniers présentent l'avantage d'être rapides et simples d'utilisation, mais conduisent bien souvent à la coprécipitation de complexes protéiques macromoléculaires, lipoprotéines, ou encore d'immunoglobulines.

Les caractéristiques et les propriétés biologiques des VE diffèrent selon la méthode employée pour les purifier. De surcroît, la contamination potentielle des préparations de VE par des macromolécules et/ou lipoprotéines nécessite d'être évaluée afin de caractériser au mieux les VE. Ainsi, la communauté scientifique internationale a édité des prérequis nécessaires à la qualification des VE et recommande de combiner plusieurs

techniques afin d'évaluer les critères morphologiques, biophysiques et biochimiques des vésicules [1]. La microscopie électronique reste la technique de référence permettant de visualiser directement les VE. De nouvelles technologies physicochimiques basées sur l'analyse du mouvement brownien des nanovésicules (*Nanoparticle Tracking Analysis* [NTA]), ou encore la mesure de leur résistivité lors de leur passage à travers un pore (*Tunable Resistive Pulse Sensing* [TRPS]), permettent ainsi d'estimer leur concentration et leur taille. Enfin, la détection de marqueurs protéiques spécifiques des sous-types de VE complète leur caractérisation [4,5].

Les VE : biomarqueurs potentiels des maladies métaboliques

Les VE représentent bien souvent le reflet de l'état physiopathologique de la cellule sécrétrice. Les VE sanguines ou urinaires, biofluides facilement accessibles et riches en VE, peuvent être ainsi utilisées pour évaluer l'état métabolique d'un patient.

La concentration de VE plasmatiques (de petite ou grande taille) est significativement augmentée chez des patients obèses par comparaison à des sujets sains [8]. L'augmentation des VE plasmatiques se retrouve également chez des patients hypertendus souffrant d'hyperlipémie, de pathologies athérothrombotiques, ou encore de diabète de type 2 (revue *in* [9]). La concentration circulante de VE plasmatiques corrèle bien souvent avec l'indice de masse corporelle, la pression artérielle, ou l'indice de résistance à l'insuline, suggérant leur implication dans le développement des maladies métaboliques [8,10]. La taille des MV étant compatible avec leur analyse par cytométrie en flux, il est possible de déterminer l'origine cellulaire des VE circulantes de grande taille sur la base de marqueurs de surface spécifiques. Les MV dérivées de plaquettes sont ainsi très largement majoritaires (50 à 90 % des MV circulantes) au regard des autres populations de MV circulantes mesurées d'origine monocytaire, lymphocytaire, érythrocytaire ou issues de cellules endothéliales [8]. L'augmentation de VE circulantes dans les maladies métaboliques se traduit principalement par une augmentation du taux de VE d'origine plaquettaire, endothéliale et érythrocytaire [8–10]. Plusieurs études ont ainsi documenté le potentiel des MV d'origine endothéliale comme marqueurs pronostic ou diagnostic des pathologies cardiovasculaires [11]. L'analyse du contenu des VE peut également servir de biomarqueur dans certaines pathologies métaboliques. En témoigne la présence d'aquaporines dans les VE urinaires considérées comme un biomarqueur prometteur pour le diagnostic de cancers rénaux ou, plus largement, des pathologies rénales [12]. L'association de certains microARNs ou ARNs longs aux VE pourrait également être utilisée [13].

En association avec d'autres facteurs de risque cardiométaboliques, l'analyse du taux et/ou contenu des VE circulantes pourrait contribuer à prédire et/ou diagnostiquer certaines maladies métaboliques. La procédure employée pour l'isolement des VE à partir des biofluides reste cependant un élément critique à considérer, afin de pouvoir procéder à des comparaisons interétudes et de s'affranchir d'un mode de conservation de ces VE qui pourrait altérer leur intégrité [14]. La prise de certains médicaments (par exemple : statines, antihypertenseurs, hypoglycémiants, etc.) est également à prendre en compte sachant qu'ils peuvent interférer avec la production de VE, et ainsi biaiser l'analyse et/ou l'interprétation des données.

Les VE : nouveaux médiateurs métaboliques de la communication inter-organes

Interactions avec les cellules cibles

Les VE peuvent être retrouvées dans les différents fluides de l'organisme (sang, lait, lymphe, sperme, ou encore urines) pour atteindre leurs organes cibles. La signature lipidique et/ou protéique unique des VE, liée à leur origine cellulaire et aux conditions de leur production, serait un facteur déterminant de leur adressage. Les VE utilisent des mécanismes variés pour interagir avec leurs cellules cibles et ainsi moduler leur signalisation cellulaire. L'endocytose des VE est ainsi un mécanisme d'internalisation largement décrit, qui peut impliquer différentes voies de manière concomitante (phagocytose, macropinocytose, endocytose par puits de clathrine, endocytose cavéolaire et/ou au niveau de radeaux lipidiques). L'interaction des VE avec un récepteur de surface, comme les intégrines par exemple, peut également initier une cascade de signalisation cellulaire. Enfin, la membrane des VE peut également fusionner avec la membrane cellulaire.

Une fois relargué dans le cytoplasme, le contenu biologique des VE (protéines, lipides, ou acides nucléiques) va pouvoir moduler différents processus cellulaires, comme la synthèse protéique (par exemple : miARN, ARNm...), la signalisation cellulaire (morphogènes, présentation d'antigènes...), ou être dégradé dans les lysosomes.

Outre leur rôle potentiel de marqueurs de l'état métabolique d'un patient, les VE sont des vecteurs de matériel biologique et peuvent agir comme des médiateurs métaboliques dans la communication intercellulaire. La réponse cellulaire induite par ces vésicules est liée principalement à leur qualité, influencée par leur origine cellulaire et leur composition. Des études précliniques ont ainsi révélé un certain nombre d'effets métaboliques de VE dérivées d'organes clés impliqués dans la genèse du syndrome métabolique (*figure 3*).

Effets vasculaires

L'injection à des souris de VE plasmatiques issues de patients présentant un syndrome métabolique se traduit par des altérations de la réactivité vasculaire, liée à une production accrue d'espèces réactives de l'oxygène (ERO) conduisant à une dysfonction vasculaire reflétant les altérations vasculaires

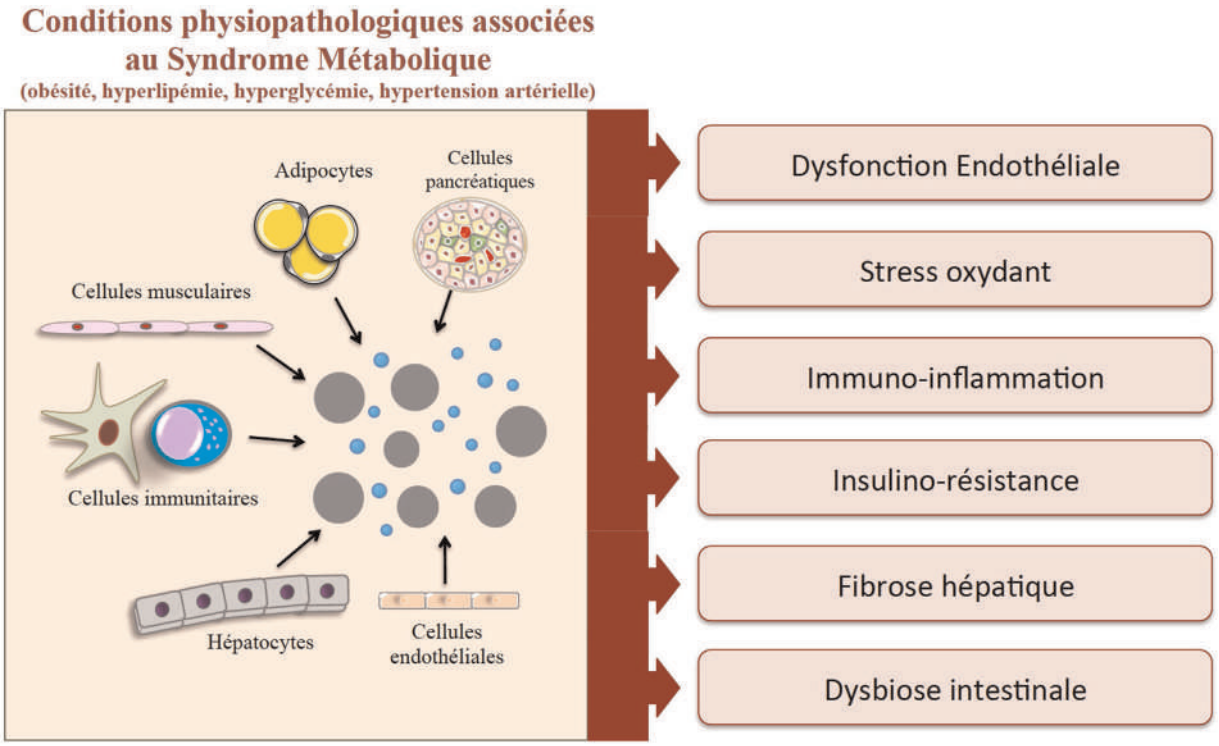

FIGURE 3

Effets métaboliques délétères des vésicules extracellulaires (VE) de différentes sources cellulaires participant au développement des complications métaboliques

De nombreux travaux mettent en évidence que les VE, isolées de cellules cultivées dans des conditions mimant la situation pathologique, sont capables de récapituler les dysfonctions métaboliques, illustrant leur rôle dans la communication inter-organes dans le contexte des maladies métaboliques

retrouvées chez les patients avec syndrome métabolique (revue *in* [9]).

Les VE dérivées de cellules endothéliales, après exposition à de fortes concentrations de glucose [15] ou d'angiotensine-II [16] induisent une réponse pro-inflammatoire, pro-coagulante et pro-oxydante. Elles favorisent, une fois injectées chez des rongeurs, le développement de plaques d'athérome, l'infiltration macrophagique et la production d'ERO. Parmi les nombreux mécanismes sous-jacents à ces effets délétères, différentes études pointent la modulation négative de facteurs pro-angiogéniques, incluant le facteur de croissance de l'endothélium vasculaire (*vascular endothelial growth factor* [VEGF]) ou encore des microARN (par exemple : miR-126), limitant les processus de réparation endothéliale qui opèrent en conditions physiologiques normales. Ces VE endothéliales contrôlent également l'inflammation en orientant le phénotype des cellules immunitaires vers un profil anti- ou pro-inflammatoire [17]. Ces échanges d'informations, véhiculées via les VE, au sein d'un tissu se font de manière multilatérale puisque les VE dérivées de cellules dendritiques, macrophages, ou de cellules spumeuses, contrôlent également la fonction endothéliale en amplifiant la réponse inflammatoire via l'activation de la voie NFkB (pour *nucleor factor-kappa B*), la production de signaux pro-inflammatoires et l'expression de molécules d'adhésion.

Les effets délétères des VE sont bien souvent observés lorsque les vésicules ont été produites à partir de cellules donneuses placées dans des conditions mimant la situation pathologique. À l'inverse, les VE dérivées de cellules souches mésenchymateuses possèdent des propriétés pro-angiogéniques et cardioprotectrices, qui suscitent un fort intérêt thérapeutique pour la médecine régénérative [18]. La présence du morphogène Sonic Hedgehog (Shh) dans les VE a été notamment reconnue comme un acteur majeur de la réponse pro-angiogénique (revue *in* [19].

Effets métaboliques et insulinosensibilité

Les adipocytes sont d'importants pourvoyeurs de VE dont la sécrétion est fortement induite par des stimuli pro-inflammatoires [4], à l'image de l'inflammation chronique de bas-grade décrite au cours de l'obésité. L'injection d'exosomes dérivés de tissu adipeux de souris obèses induit une insulinorésistance chez des souris saines [20]. Cette réponse métabolique est couplée à l'activation d'une réponse inflammatoire, via l'activation de

macrophages vers un profil pro-inflammatoire. Cette activation macrophagique résulterait du transfert de différents matériels biologiques des VE aux tissus cibles :

- des miARN qui altèrent la sensibilité à l'insuline et favorisent l'activation des voies de signalisation pro-inflammatoires et profibrotiques [21,22] ;
- des adipokines inflammatoires [23] ;
- ou encore, des lipides [24].

Les exosomes adipocytaires isolés de sujets obèses contribuent également à la réponse profibrotique hépatocytaire via le transfert de molécule profibrosante, telle que le TGF (*transforming growth factor*)-ß [25].

Les VE dérivées des hépatocytes ou de cellules musculaires, produites en réponse à un excès d'acides gras palmitate ou stéarate, contrôlent également la sensibilité à l'insuline et de la composante immuno-inflammatoire [26,27]. Dans un modèle murin d'insulinorésistance musculaire, suite à un gavage par de l'huile de palme, le muscle sécrète des exosomes enrichis en palmitate. Ces VE, incubées avec des cellules musculaires, sont capables de récapituler les effets lipotoxiques de cet acide gras saturé sur la sensibilité à l'insuline, la prolifération et la différenciation myoblastique. Ces exosomes se distribuent également dans d'autres tissus, comme le pancréas, où ils induisent une hyperprolifération des îlots pancréatiques, effet en partie lié au transfert de miARN exosomaux [27].

Les VE pourraient également moduler la fonction sécrétoire du pancréas. Les exosomes dérivés de cellules ß-pancréatiques portent en effet de nombreux auto-antigènes et chaperonnes immuno-inflammatoires qui pourraient participer à la réponse auto-immune conduisant à la dysfonction des cellules ß [28]. Plus généralement, les contenus des VE circulantes des patients diabétiques sont significativement altérés [29]. Cependant, dans le contexte du diabète de type 2, en raison de l'association avec d'autres composantes métaboliques, incluant l'obésité, l'hypertension artérielle, l'hyperglycémie, l'hypertriglycéridémie–toutes reconnues comme également associées à une augmentation des VE circulantes–, il est difficile de distinguer l'impact de chacune des composantes sur la sécrétion des VE.

Effets sur le microbiote intestinal

Les travaux de recherche de ces dernières années ont mis en évidence l'importance du microbiote intestinal, notamment des dysbioses associées bien souvent à une réduction de la diversité bactérienne, dans le développement des maladies métaboliques. Les VE produites par notre organisme pourraient, en plus de contrôler le métabolisme de nos propres organes, participer également à la mise en place et/ou le maintien de ces dysbioses intestinales. Ainsi, les miARN contenus dans les VE dérivées de cellules épithéliales intestinales peuvent être captés par les bactéries et moduler leur profil d'expression génique et la croissance bactérienne [30]. Cette communication est bilatérale, puisque des exosomes isolés du microbiote intestinal de souris obèses induisent une insulinorésistance lorsqu'ils sont transférés à des souris saines. Cependant, le transfert de matériel biologique entre hôte et microbiote ne se limite pas à des effets délétères. En effet, les VE dérivées d'*Akkermansia muciniphila*, une bactérie connue pour prévenir les altérations de la barrière intestinale ou l'insulinorésistance associées à l'obésité, récapitulent ces effets bénéfiques microbiens [31].

Conclusion

Les VE constituent de nouveaux outils biologiques importants dans la communication inter-organes. Leur utilisation en tant que biomarqueurs nécessitera néanmoins d'établir des protocoles robustes d'isolation des VE et de conservation afin de pouvoir les quantifier de manière facile et fiable. Mieux comprendre les mécanismes régissant leur rôle de bio-effecteurs métaboliques, à l'interface de nombreuses maladies métaboliques, permettra à terme de moduler au mieux leurs propriétés. Enfin, ces vecteurs biologiques d'origine naturelle en font également des outils prometteurs dans le cadre de thérapies acellulaires de réparation cellulaire.

Les VE apparaissent sans conteste comme des acteurs essentiels de la communication intercellulaire qui ouvriront, espérons dans un futur proche, de nouvelles opportunités biologiques et thérapeutiques.

Les points essentiels

- Les vésicules extracellulaires (VE) sont des nanovésicules dérivées des membranes cellulaires capables de transférer des informations biologiques entre cellules/organes.
- Leur contenu reflète bien souvent l'état métabolique de leur cellule d'origine.
- Les VE circulantes dans les biofluides sont des biomarqueurs prometteurs pour diagnostiquer/prédire les dysfonctions métaboliques.
- Les VE agissent comme des médiateurs métaboliques dans la communication inter-organes et pourraient ainsi participer au développement des maladies métaboliques.
- Ces vecteurs biologiques d'origine naturelle sont des outils cliniques prometteurs dans le cadre de futures thérapies acellulaires.

Remerciements : Les auteurs remercient le soutien de l'Inserm, CHU d'Angers et université d'Angers. Ce travail a été soutenu par la Société francophone du diabète (SFD).

Financement : Alexia Blandin est financée par une allocation doctorale Inserm/Région Pays de la Loire.

Déclaration de liens d'intérêts : les auteurs déclarent ne pas avoir de liens d'intérêts.

Références

[1] Théry C, Witwer KW, Aikawa E, et al. Minimal information for studies of extracellular vesicles 2018 (MISEV2018): a position statement of the International Society for extracellular vesicles and update of the MISEV2014 guidelines. J Extracell Vesicles 2018;7:1535750.

[2] van Niel G, D'Angelo G, Raposo G. Shedding light on the cell biology of extracellular vesicles. Nat Rev Mol Cell Biol 2018;19:213–28.

[3] Hugel B, Martinez MC, Kunzelmann C, Freyssinet JM. Membrane microparticles: two sides of the coin. Physiology (Bethesda) 2005;20:22–7.

[4] Durcin M, Fleury A, Taillebois E, et al. Characterisation of adipocyte-derived extracellular vesicle subtypes identifies distinct protein and lipid signatures for large and small extracellular vesicles. J Extracell Vesicles 2017;6:1305677.

[5] Kowal J, Arras G, Colombo M, et al. Proteomic comparison defines novel markers to characterize heterogeneous populations of extracellular vesicle subtypes. Proc Natl Acad Sci U S A 2016;113. E968-77.

[6] Villarroya-Beltri C, Gutiérrez-Vázquez C, Sánchez-Cabo F, et al. Sumoylated hnRNPA2B1 controls the sorting of miRNAs into exosomes through binding to specific motifs. Nat Commun 2013;4:2980.

[7] Konoshenko MY, Lekchnov EA, Vlassov AV, Laktionov PP. Isolation of extracellular vesicles: general methodologies and latest trends. Biomed Res Int 2018;2018:8545347.

[8] Amosse J, Durcin M, Malloci M, et al. Phenotyping of circulating extracellular vesicles (EVs) in obesity identifies large EVs as functional conveyors of Macrophage Migration Inhibitory Factor. Mol Metab 2018;18:134–42.

[9] Martinez MC, Andriantsitohaina R. Extracellular vesicles in metabolic syndrome. Circ Res 2017;120:1674–86.

[10] Li S, Wei J, Zhang C, et al. Cell-derived microparticles in patients with type 2 diabetes mellitus: a systematic review and meta-analysis. Cell Physiol Biochem 2016;39:2439–50.

[11] Boulanger CM, Loyer X, Rautou PE, Amabile N. Extracellular vesicles in coronary artery disease. Nat Rev Cardiol 2017;14:259–72.

[12] Oshikawa S, Sonoda H, Ikeda M. Aquaporins in urinary extracellular vesicles (exosomes). Int J Mol Sci 2016;17:E957.

[13] Pomatto MA, Gai C, Deregibus MC, et al. Noncoding RNAs carried by extracellular vesicles in endocrine diseases. Int J Endocrinol 2018;2018:4302096.

[14] Yuana Y, Böing AN, Grootemaat AE, et al. Handling and storage of human body fluids for analysis of extracellular vesicles. J Extracell Vesicles 2015;4:29260.

[15] Jansen F, Yang X, Franklin BS, et al. High glucose condition increases NADPH oxidase activity in endothelial microparticles that promote vascular inflammation. Cardiovasc Res 2013;98:94–106.

[16] Burger D, Turner M, Xiao F, et al. High glucose increases the formation and pro-oxidative activity of endothelial microparticles. Diabetologia 2017;60:1791–800.

[17] Hosseinkhani B, Kuypers S, van den Akker NM, et al. Extracellular vesicles work as a functional inflammatory mediator between vascular endothelial cells and immune cells. Front Immunol 2018;9:1789.

[18] Amosse J, Martinez MC, Le Lay S. Extracellular vesicles and cardiovascular disease therapy. Stem Cell Investig 2017;4:102.

[19] Soleti R, Martinez MC. Sonic Hedgehog on microparticles and neovascularization. Vitam Horm 2012;88:395–438.

[20] Deng ZB, Poliakov A, Hardy RW, et al. Adipose tissue exosome-like vesicles mediate activation of macrophage-induced insulin resistance. Diabetes 2009;58:2498–505.

[21] Thomou T, Mori MA, Dreyfuss JM, et al. Adipose-derived circulating miRNAs regulate gene expression in other tissues. Nature 2017;542:450–5 [Erratum in: Nature 2017;545:252].

[22] Ying W, Riopel M, Bandyopadhyay G, et al. Adipose tissue macrophage-derived exosomal miRNAs can modulate *in vivo* and *in vitro* insulin sensitivity. Cell 2017;171. 372-84.e12.

[23] Kranendonk ME, Visseren FL, van Balkom BW, et al. Human adipocyte extracellular vesicles in reciprocal signaling between adipocytes and macrophages. Obesity (Silver Spring) 2014;22:1296–308.

[24] Flaherty SE, 3rd, Grijalva A, Xu X, et al. A lipase-independent pathway of lipid release and immune modulation by adipocytes. Science 2019;363:989–93.

[25] Koeck ES, Iordanskaia T, Sevilla S, et al. Adipocyte exosomes induce transforming growth factor beta pathway dysregulation in hepatocytes: a novel paradigm for obesity-related liver disease. J Surg Res 2014;192:268–75.

[26] Hirsova P, Ibrahim SH, Verma VK, et al. Extracellular vesicles in liver pathobiology: small particles with big impact. Hepatology 2016;64:2219–33.

[27] Rome S, Forterre A, Mizgier ML, Bouzakri K. Skeletal muscle-released extracellular vesicles: state of the art. Front Physiol 2019;10:929.

[28] Cianciaruso C, Phelps EA, Pasquier M, et al. Primary human and rat ß-cells release the intracellular autoantigens GAD65, IA-2, and proinsulin in exosomes together with cytokine-induced enhancers of immunity. Diabetes 2017;66:460–73.

[29] Freeman DW, Noren Hooten N, Eitan E, et al. Altered extracellular vesicle concentration, cargo, and function in diabetes mellitus. Diabetes 2018;67:2377–88.

[30] Liu S, da Cunha AP, Rezende RM, et al. The host shapes the gut microbiota via fecal microRNA. Cell Host Microbe 2016;19:32–43.

[31] Chelakkot C, Choi Y, Kim DK, et al. *Akkermansia muciniphila*-derived extracellular vesicles influence gut permeability through the regulation of tight junctions. Exp Mol Med 2018;50:e450.

médecine/sciences 2021 ; 37 : 1125-32

Vésicules extracellulaires et maladies métaboliques

Des liaisons dangereuses

Alexia Blandin[1,2], Soazig Le Lay[1,2]

> Les vésicules extracellulaires (VE) correspondent à un ensemble hétérogène de nanovésicules membranaires sécrétées dans le milieu extracellulaire et circulant dans les différents fluides de l'organisme. Ces VE véhiculent du matériel biologique (protéines, lipides, acides nucléiques) qu'elles peuvent transférer à des cellules/tissus cibles, modulant ainsi leur réponse et/ou leur phénotype. Les dysfonctions caractérisant les maladies métaboliques liées à l'obésité sont associées à des modifications des concentrations circulantes de VE ainsi qu'à des altérations de leur contenu. L'intérêt grandissant porté aux VE comme nouveaux vecteurs de communication intercellulaire a conduit à s'interroger sur leur rôle dans le développement des complications métaboliques. Dans cette synthèse, nous résumerons la littérature portant sur les VE circulantes comme potentiels marqueurs des maladies métaboliques. Nous détaillerons ensuite le dialogue vésiculaire inter-organes responsable du développement des complications associées à l'obésité. Enfin, nous discuterons les futures pistes de recherche qui contribueront à mieux appréhender le lien entre VE et maladies métaboliques. <

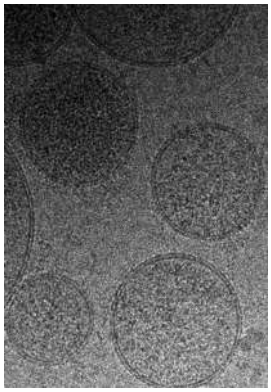

[1]Université de Nantes, CNRS, Inserm, Institut du thorax, F-44000 Nantes, France.
[2]Univ Angers, SFR Interactions cellulaires et applications thérapeutiques (ICAT), F-49000 Angers, France.
soazig.lelay@inserm.fr

La coexistence de plusieurs troubles physiologiques d'origine lipidique, glucidique ou vasculaire, associés à un excès de poids chez un même individu, définit le syndrome métabolique (SMet) [1]. L'association de ces facteurs de risque augmente considérablement le risque de maladies cardiométaboliques, à l'instar du diabète de type 2 (DT2), de maladies cardiovasculaires et hépatiques, de troubles respiratoires (apnées du sommeil) ou encore de cancers. L'obésité viscérale est considérée comme un des facteurs les plus délétères dans le développement des maladies métaboliques et est souvent associée à une inflammation chronique et générale dite de bas-grade. L'évaluation des différents critères métaboliques définissant le SMet (tour de taille, glycémie à jeun, triglycérides, lipoprotéines de haute densité [HDL]-cholestérol, pression artérielle), associée au dosage de cytokines/adipokines, est utilisée en pratique clinique pour définir le profil métabolique du patient, mais n'est pas informative sur les atteintes métaboliques respectives des différents organes. Dans ce contexte, les vésicules extracellulaires (VE), dont le contenu reflète l'état physiopathologique des cellules qui les sécrètent, apparaissent comme des biomarqueurs et/ou des médiateurs des complications métaboliques.

Les VE constituent un ensemble hétérogène de nanovésicules membranaires sécrétées dans le milieu extracellulaire et circulant dans les différents fluides de l'organisme (sang, urine, lymphe, etc.). Elles regroupent, d'une part, des vésicules de grande taille (gVE, 100 nm-1 µm), libérées par bourgeonnement de la membrane plasmique, et, d'autre part, des vésicules de petite taille (pVE, <100 nm) correspondant à la sécrétion par exocytose des vésicules intra-luminales des corps multivésiculaires [2]. Ces VE véhiculent du matériel biologique (protéines, lipides, acides nucléiques) qu'elles peuvent transférer à des cellules/tissus cibles. Dès les années 1990, la cytométrie en flux a permis de déterminer l'origine cellulaire des gVE circulantes et d'établir que les plaquettes sanguines étaient la source cellulaire principale de ces gVE circulantes à côté des gVE d'origine monocytaire, lymphocytaire, érythrocytaire ou endothéliale (les gVE plaquettaires représentant, selon les études, entre 50 et 90 % des gVE circulantes). Les concentrations circulantes de gVE totales, et de certaines sous-populations de gVE ont ainsi été largement étudiées dans les maladies

Vignette (© Guillaume van Niel, Aurélie di Cicco, Graça Raposo, Daniel Levy).

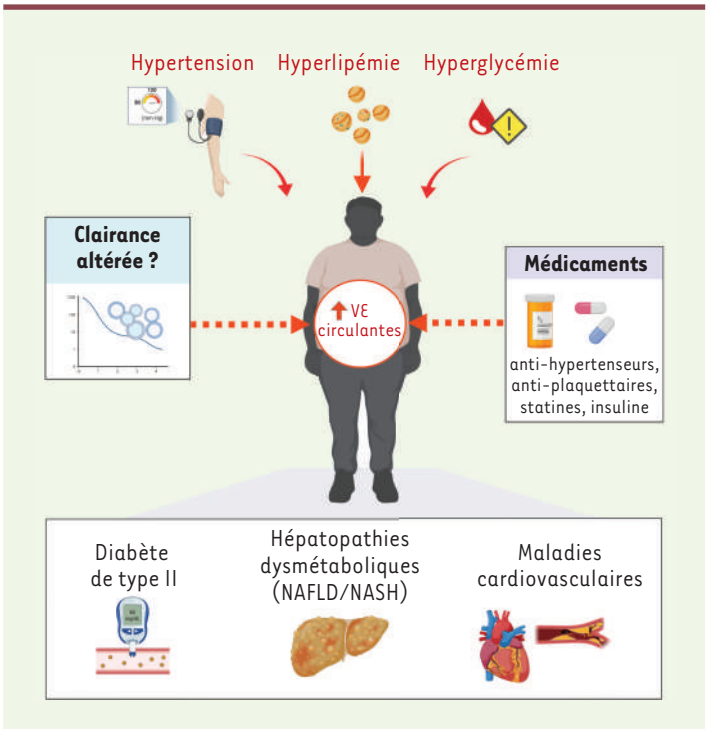

Figure 1. ***Les maladies métaboliques sont associées à une augmentation des concentrations de vésicules extracellulaires (VE) circulantes.*** Les facteurs de risque associés au développement des maladies métaboliques stimulent la sécrétion des VE, contribuant à augmenter leurs concentrations circulantes. La prise de médicaments ou encore une clairance altérée pourraient également participer à maintenir des concentrations plasmatiques élevées de VE.

cardiovasculaires [3]. L'intérêt porté à ces vésicules s'est élargi ces dernières années aux pVE dans le contexte des maladies métaboliques.

Les VE circulantes : des biomarqueurs des maladies métaboliques ?

Les VE constituent de potentiels biomarqueurs de l'état métabolique du patient, ce qui a conduit à les quantifier et à les caractériser dans des biofluides facilement accessibles, tels que le sang ou les urines, chez des patients à risque ou souffrant de maladies métaboliques.

Les maladies métaboliques sont associées à de fortes concentrations de VE circulantes

Les concentrations de pVE et de gVE plasmatiques sont significativement augmentées chez les patients souffrant de SMet [4, 5], et sont corrélées à l'indice de masse corporelle (IMC), soulignant l'importance de l'obésité [6] (*Figure 1*). Cette augmentation se retrouve également chez des patients hypertendus présentant une hyperlipémie ou souffrant de maladies athéro-thrombotiques [3], chez des patients diabétiques de type 2 (DT2) [7], et chez des patients souffrant d'hépatopathies dysmétaboliques [8]. La réduction des concentrations de VE plasmatiques observée lors d'une perte de poids, suite à une restriction alimentaire ou à une chirurgie bariatrique, suggère que les VE adipocytaires pourraient participer à cette élévation [9]. Cependant, l'absence de marqueurs spécifiques permettant l'identification des VE sécrétées par les adipocytes ne permet pas la quantification des VE adipocytaires circulantes. En revanche, l'élévation des VE plasmatiques observée dans les complications métaboliques associées à l'obésité s'accompagne généralement d'une élévation concomitante des VE d'origine plaquettaire, érythrocytaire, leucocytaire ou endothéliale [3, 6, 7].

Les niveaux accrus de VE plasmatiques peuvent résulter de l'activation ou de l'apoptose de différentes cellules vasculaires à la suite d'un stimulus pathologique, bien qu'une clairance altérée de ces VE causée par différents facteurs de risque cardiovasculaire ne puisse être exclue [3]. L'insulino-résistance (IR) et l'hyperglycémie associées induisent également la sécrétion de VE contribuant à maintenir de fortes concentrations de VE circulantes chez les patients diabétiques [10]. Enfin, les médicaments (anti-plaquettaires, anti-hypertenseurs, statines ou insuline) bien souvent prescrits aux patients présentant un risque cardiovasculaire élevé, influencent également les niveaux de VE circulantes et/ou leur contenu [3]. Il est difficile de distinguer l'effet direct de ces médicaments sur la sécrétion cellulaire des VE et leur bénéfice sur l'hypertension ou la dyslipidémie, paramètres métaboliques modulant également la composition et la concentration des VE.

Les vésicules extracellulaires circulantes : de nouveaux biomarqueurs des maladies métaboliques ?

Les VE sécrétées dans le milieu extracellulaire transportent des composants cellulaires provenant des cellules dont elles sont issues. Leur caractérisation peut ainsi avoir une valeur diagnostique et/ou pronostique pour certaines maladies métaboliques.

Plusieurs études ont ainsi démontré un fort taux circulant de gVE plaquettaires ou endothéliales chez des patients souffrant d'athérosclérose [11], tandis que des niveaux circulants élevés de gVE leucocytaires sont associés à des plaques athérosclérotiques instables [12]. Les gVE d'origine endothéliale améliorent le potentiel prédictif pour identifier les patients à risque de survenue d'évènements cardiovasculaires [13]. À ce jour, la caractérisation des pVE dans les maladies cardiovasculaires reste limitée, principalement en raison des difficultés à les quantifier par cytométrie en flux et à les séparer des lipoprotéines plasmatiques avec lesquelles elles partagent des caractéristiques physico-chimiques.

Le contenu vésiculaire peut également être informatif de l'évolution des maladies métaboliques. Ainsi, la

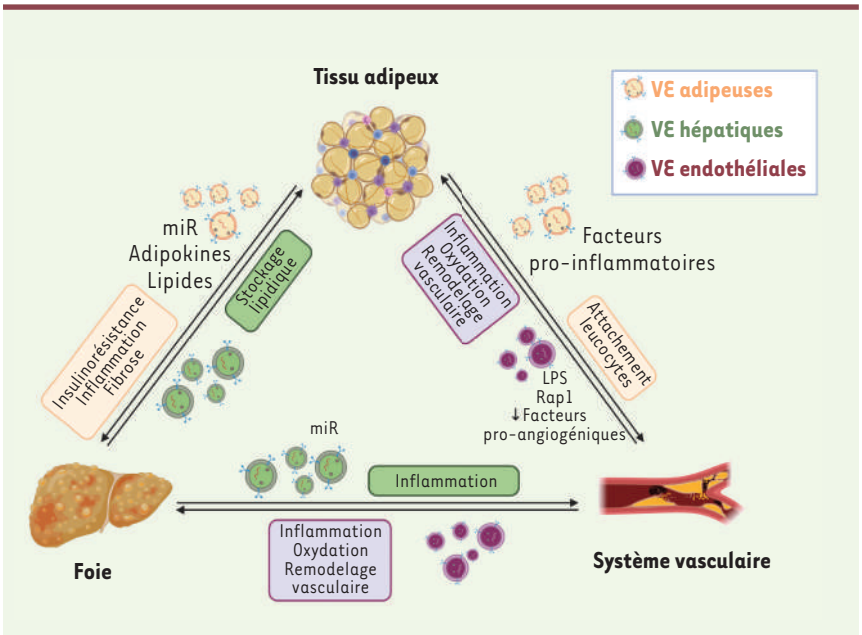

Figure 2. ***Le dialogue vésiculaire inter-organes contribue à la mise en place des dysfonctions métaboliques.*** Dans un contexte d'obésité et de fort risque cardiométabolique, différents organes participant au métabolisme sécrètent des VE. Les cargos qu'elles transportent, de natures protéique, nucléique ou lipidique, reflètent l'état physiopathologique de l'organisme. Leur transfert à des cellules/tissus cibles conduisent à des réponses délétères participant à la mise en place des dysfonctions métaboliques.

présence d'aquaporines, protéines des canaux hydriques, dans les pVE urinaires, constitue un biomarqueur prometteur pour le diagnostic de cancers rénaux ou, plus largement, de maladies rénales [14]. Le contenu des VE en matériel génétique, à l'image des nombreux petits ARN (micro-ARN ou miR) qu'elles transportent, est aussi modulé par les différents facteurs de risque métabolique. Ainsi, les pVE plasmatiques de patients obèses ou insulino-résistants sont enrichies en miR capables de réguler le contenu lipidique ou la signalisation insulinique des adipocytes [15]. Le criblage de certains miR vésiculaires, ou plus largement du contenu des VE, pourrait ainsi être utilisé à des fins diagnostiques. Plusieurs miR ou protéines, enrichis dans les VE urinaires ou sanguines de patients souffrant de maladies hépatiques, représentent ainsi des candidats potentiels [8]. Cette perspective représente un intérêt majeur pour les maladies hépatiques pour lesquelles l'utilisation des VE comme outil diagnostic renseignerait sur l'évolution de la maladie, remplaçant la biopsie de foie, plus invasive.

Les vésicules extracellulaires (VE), actrices du dialogue inter-organe dans les maladies métaboliques ?

Les VE et le diabète de type 2

L'obésité est généralement associée au développement d'une résistance à l'insuline, qui précède souvent l'apparition d'un diabète de type 2 (DT2). Cette résistance à l'hormone se traduit par une réduction de ses effets métaboliques, c'est-à-dire un défaut d'entrée de glucose et une moindre inhibition de la lipolyse dans les tissus insulino-dépendants, l'ensemble favorisant une hyperlipémie. Le tissu adipeux n'assumant plus son rôle de stockage, les lipides se déposent alors de manière ectopique dans le foie, le muscle squelettique, le cœur ou dans les vaisseaux, ce qui conduit à des phénomènes de lipotoxicité.

Les adipocytes sécrètent d'importantes quantités de gVE et de pVE qui présentent des signatures protéiques et lipidiques distinctes, présageant d'effets métaboliques variés [16]. Les stimulus environnementaux associés à l'obésité, comme l'afflux massif de lipides, l'hypoxie ou l'inflammation, stimulent la sécrétion de ces VE adipocytaires, conduisant à leur augmentation chez les sujets obèses [16, 17]. En outre, les VE sécrétées par la fraction stroma-vasculaire du tissu adipeux (composée de préadipocytes, de cellules endothéliales, de cellules immunitaires, etc..) participent également à l'important trafic vésiculaire existant au sein de ce tissu. Ce trafic dépendant des VE participe ainsi à l'homéostasie du tissu adipeux, à sa vascularisation, sa capacité de stockage lipidique ou à son inflammation [17].

L'injection de pVE dérivées d'explants de tissu adipeux de souris obèses est suffisante pour instaurer une insulinorésistance chez des souris saines, démontrant le potentiel de ces VE adipeuses à reproduire les effets délétères du sécrétome adipeux de souris obèses [18]. La résistance induite est couplée à l'activation de macrophages adipeux résidents et leur orientation vers un profil pro-inflammatoire (de type M1) [18]. Elle peut également être induite par l'injection de VE dérivées uniquement des macrophages de tissus adipeux obèses [19]. L'invalidation du gène codant le récepteur de l'immunité innée TLR4 (*Toll-like receptor 4*) suffit à contrer les effets délétères des pVE de tissus adipeux obèses, suggérant que l'insulinorésistance induite par ces pVE est fortement liée à une réponse inflammatoire dépendante de l'immunité innée.

Plusieurs composants véhiculés par les VE adipeuses pourraient être impliqués dans ces effets délétères (*Figure 2*). Le tissu adipeux constitue une source importante de miR véhiculés par les VE, parmi lesquels certains régulent l'expression de protéines clés de la signalisation insulinique et/ou l'activation de voies de signalisation pro-inflammatoires et pro-fibrotiques

dans des organes cibles, dont le foie [19]. Plusieurs adipokines, aux propriétés pro-inflammatoires, pro-fibrosantes ou régulant le métabolisme glucido-lipidique, sont également des cargos protéiques des VE adipeuses [6, 20]. Enfin, l'afflux massif de palmitate, fortement enrichi dans notre alimentation actuelle, stimule la sécrétion de VE adipocytaires, hépatocytaires ou musculaires [16, 17]. Ces VE se retrouvent enrichies en lipides lipotoxiques qui altèrent ainsi la sensibilité à l'insuline des cellules cibles [21].

L'ensemble de ces données soulignent l'importance des VE, notamment celles sécrétées par le tissu adipeux dans un contexte d'obésité, dans le développement du DT2, complication métabolique considérée comme initiatrice des autres dysfonctions métaboliques associées à l'obésité.

VE, maladies métaboliques et maladies cardiovasculaires

La dysfonction endothéliale est une altération vasculaire précoce qui favorise la survenue de maladies cardiovasculaires. Elle apparaît souvent suite à une résistance à l'insuline. La communication entre les cellules endothéliales et leur microenvironnement tissulaire contribue à la libération de signaux pour attirer les cellules immunitaires et les capter à partir de la circulation, ce qui favorise le développement de plaques athéromateuses. Les VE participent à cette communication intercellulaire (*Figure 2*).

L'injection de gVE ou de pVE plasmatiques isolées de patients souffrant de SMet (VE SMet) à des souris favorise la dysfonction endothéliale [4, 5]. Que ce soit avec des gVE ou des pVE, les altérations vasculaires observées se caractérisent par une baisse de la production de monoxyde d'azote (NO), puissant vasodilatateur, et une production accrue d'espèces réactives de l'oxygène (ERO) pro-inflammatoires. Les gVE SMet sont spécifiquement enrichies en Rap1 (*Ras-related protein 1*), une petite GTPase liée à différents facteurs de risque cardiovasculaire [22]. Ces gVE-Rap1$^+$ favorisent les processus d'inflammation et de remodelage vasculaire et s'accumulent dans les plaques athéromateuses [22]. Les pVE SMet sont, elles, enrichies en LPS (lipopolysaccharide), comparativement aux pVE plasmatiques de sujets sains [5]. La neutralisation du récepteur TLR4 réduit la production d'ERO induite par ces pVE-LPS$^+$, révélant ainsi un mécanisme différent de celui des gVE SMet dans la mise en place de la dysfonction endothéliale.

L'environnement physiopathologique contribue à favoriser la production de VE délétères en terme métabolique. Ainsi, l'hyperglycémie ou encore l'élévation de l'hormone hypertensive angiotensine-II favorisent la sécrétion de VE endothéliales aux propriétés pro-coagulantes, pro-inflammatoires et pro-oxydantes [23, 24]. L'injection de ces VE endothéliales à des rongeurs induit une altération de la réactivité vasculaire, le développement de plaques d'athérome, l'infiltration par des macrophages et la production d'ERO [24]. Différentes études mettent en évidence la modulation négative de facteurs pro-angiogéniques, comme le VEGF ou le miR-126, qui contribuent normalement à la réparation endothéliale dans des conditions physiologiques [23].

Ces échanges d'informations *via* les VE au sein du mur vasculaire se font de manière multilatérale, puisque les VE dérivées des cellules dendritiques, des macrophages ou des cellules spumeuses, modulent également la fonction endothéliale en amplifiant la réponse inflammatoire *via* l'activation de la voie NF-κB, la production de signaux pro-inflammatoires et l'expression de molécules d'adhérence [25]. Les VE produites par des adipocytes hypoxiés et inflammatoires favorisent, quant à elles, l'attachement des leucocytes aux cellules endothéliales vasculaires, suggérant leur participation dans le processus d'athérosclérose [26]. Enfin, des VE adipocytaires produites dans un environnement hyperglycémique et hyperlipémique, exacerbent les lésions d'ischémie/reperfusion du myocarde chez des souris diabétiques [27]. Ainsi, les VE adipocytaires (produites dans un contexte obésogène) pourraient constituer le lien moléculaire sous-tendant les effets délétères d'une hypertrophie des tissus adipeux périvasculaires et/ou péricardiques et le développement des maladies cardiovasculaires.

Les VE et hépatopathies dysmétaboliques

La stéatopathie non alcoolique (NAFLD) est considérée comme la manifestation hépatique du SMet et se caractérise par une accumulation anormale de graisse intrahépatique en l'absence de consommation excessive d'alcool. Cette stéatose isolée peut évoluer vers une forme plus agressive se caractérisant par une stéatose avec inflammation définissant la stéatohépatite non alcoolique (NASH), qui peut évoluer vers la cirrhose et ses complications (insuffisance hépatique, hépatocarcinome).

La sécrétion de VE hépatiques participe à la pathogenèse de ces hépatopathies dysmétaboliques en favorisant les processus inflammatoires, immunitaires, fibrotiques et angiogéniques [8] (*Figure 2*). Ainsi, l'enrichissement des pVE dérivées d'hépatocytes stéatosiques en facteurs pro-inflammatoires [28] ou en lipides lipotoxiques (céramides ou sphingosine-1-phosphate) [29] contribuent à la chémoattraction des macrophages vers le foie. La présence de certains miR, comme le miR192, contribue, en outre, à l'activation des macrophages [30]. L'accumulation de lipides dans le foie stimule la sécrétion de pVE hépatocytaires enrichies en vanine-1 (VNN1), une enzyme dotée d'une activité pro-fibrosante [31]. La VVN1 vésiculaire induit la migration des cellules endothéliales et la formation de tubes vasculaires, deux processus nécessaires à l'angiogenèse pathologique dans le foie, résultant de la NASH.

L'internalisation de VE dérivées d'hépatocytes stéatosiques par les cellules étoilées du foie (HSC) quiescentes conduit à leur activation - un processus critique dans le développement de la fibrose associée aux hépatopathies dysmétaboliques. Ce phénomène fait suite au transfert de miR-128-3p, conduisant à l'inhibition de l'expression de PPAR-γ (*peroxisome proliferator-acti-*

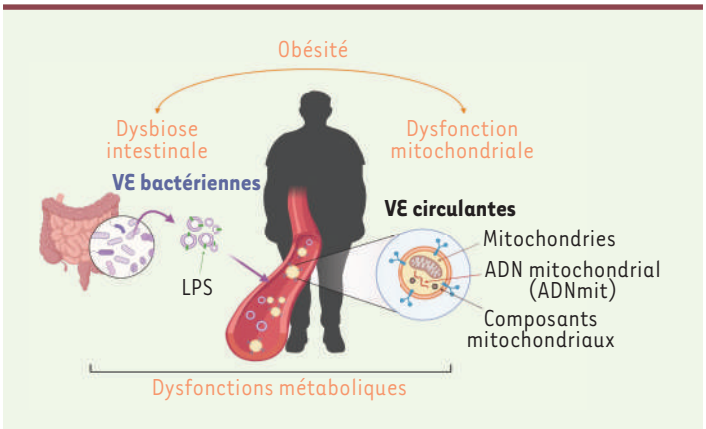

Figure 3. ***Le transport vésiculaire de mitochondries ou de composés bactériens participe à la mise en place des dysfonctions métaboliques.*** Les complications métaboliques de l'obésité sont associées à une altération du microbiote intestinal (ou dysbiose), conduisant à la production de VE bactériennes, reflet de cette dysbiose. La dysfonction mitochondriale, souvent associée aux maladies métaboliques, se traduit également par l'export cellulaire, *via* les VE, de mitochondries ou de constituants mitochondriaux. Le trafic de cet ensemble de VE à l'échelle de l'organisme participe au développement de dysfonctions métaboliques.

vated receptor γ) normalement chargé de maintenir les HSC dans un état quiescent [32]. D'autres miR, tels que le miR-122 et le miR-192, sont également impliqués dans les effets inflammatoires et fibrosants des pVE hépatocytaires produites dans des conditions lipotoxiques [8]. Des corrélations positives entre ces miR, les enzymes hépatiques et la gravité de la maladie hépatique suggèrent que la signature de ces miR vésiculaires pourrait être utilisée comme biomarqueur de l'atteinte hépatique.

Au-delà de leurs effets sur le foie, les VE hépatocytaires pourraient également participer à un dialogue inter-organes contribuant à favoriser les dysfonctions métaboliques. Ainsi, les pVE dérivées d'hépatocytes stéatosiques favorisent l'inflammation et atténuent l'athérosclérose de souris déficientes en ApoE (apolipoprotéine E), suggérant un couplage entre hépatopathies dysmétaboliques et maladies cardiovasculaires dépendant des pVE [33]. Les pVE dérivées d'hépatocytes primaires isolés de souris obèses favorisent le stockage lipidique adipocytaire [34]. Enfin, l'hypertrophie adipocytaire conduit à la libération de VE adipocytaires qui favorisent la fibrose et la résistance à l'insuline dans le foie [20].

Le dialogue vésiculaire dans un contexte d'obésité pourrait donc s'auto-amplifier, contribuant à entretenir les effets métaboliques délétères *via* les VE et à favoriser le développement de complications métaboliques.

Nouvelles pistes de recherche et perspectives

Les VE : des vecteurs de mitochondries

Les mitochondries sont des organites spécifiques des cellules eucaryotes assurant la respiration cellulaire et la production d'ATP ; elles jouent donc un rôle majeur dans le métabolisme énergétique. Leur particularité est de posséder leur propre génome sous la forme d'un ADN circulaire (ou ADN mitochondrial, ADNmit), transmis uniquement par la mère et distinct de l'ADN nucléaire. La détection de mitochondries fonctionnelles dans des gVE circulantes a formellement démontré la capacité des VE à transporter des organites entiers [35]. Bien que la taille des pVE soit difficilement compatible avec l'encapsulation de mitochondries entières, plusieurs travaux révèlent leur enrichissement en enzymes, lipides (cardiolipines) et ADN mitochondriaux [36, 37].

De récents travaux ont montré une forte augmentation d'ADNmit dans le plasma de patients, ou de souris, souffrant de la NASH [38]. La majorité de cet ADNmit est encapsulé dans des gVE d'origine hépatocytaire, et peut activer le récepteur TLR9, une voie de signalisation impliquée dans le contrôle du développement de la NASH. Le ciblage de l'activation de TLR9 *via* l'ADN mitochondrial vésiculaire pourrait donc constituer une perspective thérapeutique pour le traitement de cette maladie.

Le transfert de mitochondries *via* des gVE monocytaires pourrait également participer à la pathogenèse de l'athérosclérose (*Figure 3*). Le traitement de monocytes par du lipopolysaccharide (LPS) bactérien induit la sécrétion de gVE enrichies en mitochondries dysfonctionnelles, auxquelles sont associés du TNF-α ou de l'ARN mitochondrial oxydé, capables d'induire une réponse pro-inflammatoire dans les cellules endothéliales [39]. Une récente étude suggère que cette excrétion mitochondriale serait couplée à un processus d'autophagie [40]. Les auteurs de cette étude ont également montré que les gVE secrétées par les cardiomyocytes sont phagocytées par les macrophages, phénomène amplifié lors d'un stress cardiaque, révélant un nouveau processus par lequel les cellules immunitaires résidentes du cœur participent à l'homéostasie du tissu cardiaque.

Enfin, plusieurs études ont rapporté des effets protecteurs et immunorégulateurs faisant suite au transfert intercellulaire de mitochondries par les VE. Une étude récente a ainsi mis en évidence un transfert de mitochondries *via* les VE entre des adipocytes et des macrophages résidents du tissu adipeux [41]. Ce transfert participerait à l'homéostasie immunométabolique de ce tissu, mais serait altéré dans un contexte d'obésité. En outre, des adipocytes « stressés », comme c'est le cas à la suite d'un stress oxydant consécutif à une dysfonction mitochondriale, induit la sécrétion de pVE enrichies

en mitochondries dysfonctionnelles capables de diffuser dans la circulation et d'être captées par les cardiomyocytes [42]. Il en résulte l'activation d'une réponse compensatrice anti-oxydante par le cœur qui protège les cardiomyocytes du stress oxydant aigu, conformément à un paradigme de préconditionnement s'apparentant au concept « d'hormèse »[1]. Les mitochondries transférées par des VE dérivées de cellules souches mésenchymateuses (MSC) vont également contribuer à un remodelage tissulaire bénéfique. L'injection de telles VE dans des souris utilisées comme modèle murin de défaillance rénale aiguë atténue ainsi la dysfonction rénale et la réponse inflammatoire suite au transfert vésiculaire d'ADNmit et d'ARNm codant un facteur mitochondrial dans les tubules rénaux [43]. À noter que des VE dérivées de cellules souches pluripotentes différenciées en cardiomyocytes, injectées dans le cœur, sont également capables de transférer des cargos mitochondriaux favorisant la biogenèse mitochondriale et la récupération énergétique du cœur après infarctus du myocarde chez des souris [44].

Ces résultats ouvrent donc la voie à des thérapies innovantes fondées sur le transfert spécifique de composés mitochondriaux ou de mitochondries, dans le traitement de maladies présentant une dysfonction mitochondriale.

Les VE dérivées du microbiote intestinal : une piste bactérienne à explorer

Les maladies métaboliques associées à l'obésité sont reliées à des modifications du nombre et de la diversité bactérienne, un phénomène appelé dysbiose. L'avènement de la métagénomique a permis d'identifier des microbiotes obésogène et diabétogène spécifiques de différentes maladies métaboliques. L'altération de l'intégrité de la paroi intestinale, associée au SMet, favorise la translocation de molécules bactériennes, comme le LPS, hautement inflammatoires, ce qui conduit à une endotoxémie métabolique. L'observation concomitante de bactéries dans les fèces de patients et de VE bactériennes présentes dans leur sérum ou leurs urines, illustre la capacité de ces VE, qui dérivent du microbiote intestinal, à traverser la barrière intestinale alors altérée et à se distribuer dans différents fluides de l'organisme [45]. De surcroît, comparées à des pVE plasmatiques de sujets sains, les pVE SMet sont enrichies en LPS ; elles pourraient ainsi signer l'endotoxémie métabolique que l'on retrouve chez les patients souffrant de SMet [5].

Plusieurs études précliniques suggèrent le rôle de médiateurs métaboliques exercé par les VE bactériennes dans le développement des dysfonctions métaboliques (*Figure 3*). L'ingestion de VE bactériennes, isolées de fèces de souris sous régime gras, par des souris saines conduit à leur biodistribution dans plusieurs tissus métaboliques et au développement d'une insulinorésistance [46]. Des analyses métagénomiques de VE dérivées du microbiote de souris obèses, révèlent un enrichissement en VE dérivées de bactéries *Pseudomonas panacis* (phylum Proteobacteria) qui, à elles seules, peuvent induire une résistance à l'insuline lorsqu'elles sont administrées à des souris saines. De même, des VE dérivées de *Porphyromonas gingivalis*[2] transportent des protéases, parmi lesquelles des gingipaïnes, des enzymes associées aux parodontites, qui se retrouvent dans le foie des souris où elles modulent la sensibilité à l'insuline et contribuent au développement du DT2 [47]. Dans les cellules avec lesquelles elles interagissent, les VE bactériennes stimulent également plusieurs mécanismes moléculaires qui se traduisent par des réponses inflammatoires. Parmi ces mécanismes, on peut citer leur liaison au récepteur TLR4, exprimé par les cellules de l'immunité innée, qui déclenche une réponse immunitaire et la sécrétion de cytokines pro-inflammatoires [48].

Dans un contexte de dysbiose, il serait intéressant de promouvoir la production de VE dérivées de bactéries bénéfiques, comme *Akkermansia muciniphila* dont l'abondance est associée à un statut métabolique sain qui se traduit notamment par une meilleure sensibilité à l'insuline [49]. Les VE dérivées de cette bactérie sont à l'origine d'effets bénéfiques, supérieurs à ceux induits par la bactérie elle-même, sur la barrière intestinale, l'inflammation, la balance énergétique ou les paramètres métaboliques globaux [50].

Ces résultats ouvrent donc la voie à de nouvelles perspectives thérapeutiques consistant en un apport exogène de VE dérivées de bactéries bénéfiques.

Conclusion

L'ensemble des données de la littérature révèle les vésicules extracellulaires (VE) comme des actrices importantes de la communication inter-organes, participant au développement de dysfonctions métaboliques en régulant l'inflammation, le remodelage tissulaire, la sensibilité à l'insuline ou l'homéostasie énergétique. Selon leur origine cellulaire et l'environnement physiopathologique, les VE vont produire des réponses cellulaires variées dont les processus restent encore largement méconnus. Mieux caractériser les mécanismes régulant la sécrétion de ces VE, leur biodistribution et leur mode d'action sont autant de champs qui restent à explorer. Malgré l'intérêt certain que ces VE suscitent en tant que biomarqueurs diagnostiques ou vecteurs thérapeutiques, plusieurs limites techniques et métho-

[1] L'hormèse est un processus par lequel un organisme, à qui l'on administre de faibles doses d'agents générateurs de stress, se trouve renforcé et montre ensuite une plus grande résilience à des doses plus élevées de ces mêmes facteurs de stress.

[2] *Porphyromonas gingivalis* est une espèce de bactéries présentes dans la cavité buccale, responsable de gingivite.

dologiques restent néanmoins à dépasser avant d'envisager leur utilisation clinique. Ces nanovésicules ont donc su mobiliser la communauté scientifique, dont l'intérêt risque d'aller grandissant au vu des nombreuses propriétés métaboliques qu'on leur prête ainsi que des nombreux mécanismes sous-jacents à leur production et à leurs fonctions restant encore à décrypter. ◊

SUMMARY

Extracellular vesicles and metabolic diseases: Dangerous liaisons

Extracellular vesicles (EVs) correspond to a heterogeneous set of membrane nanovesicles secreted in the extracellular medium and circulating in the various fluids of the body. These EVs convey biological material (proteins, lipids, nucleic acids) that they can transfer to target cells/tissues thus modulating their response and/or phenotype. The metabolic dysfunctions characterizing metabolic diseases associated with obesity are associated with changes in circulating EV concentrations as well as alterations in their content. The growing interest in EVs as new vectors of intercellular communication has led to question about their role in the development of metabolic complications. In this review, we will discuss the literature on circulating EVs as potential markers of metabolic diseases and then detail inter-organ dialogue based on this EV trafficking underlying the development of related obesity. Finally, we will discuss future avenues of research that will help to better understand the link between EVs and metabolic diseases. ◊

REMERCIEMENTS

Les auteures remercient le soutien financier de l'Inserm, de la Société francophone du diabète, la fondation Genavie et la Région Pays de la Loire. Les figures ont été créées avec Biorender.com.

LIENS D'INTÉRÊT

Les auteures déclarent n'avoir aucun lien d'intérêt concernant les données publiées dans cet article.

RÉFÉRENCES

1. Alberti G, Zimmet P. The IDF consensus worldwide definition of the METABOLIC SYNDROME. *International Diabetes Federation* 2006.
2. van Niel G, D'Angelo G, Raposo G. Shedding light on the cell biology of extracellular vesicles. *Nat Rev Mol Cell Biol* 2018 ; 19 : 213-28.
3. Boulanger CM, Loyer X, Rautou PE, Amabile N. Extracellular vesicles in coronary artery disease. *Nat Rev Cardiol* 2017 ; 14 : 259-72.
4. Agouni A, Lagrue-Lak-Hal AH, Ducluzeau PH, *et al.* Endothelial dysfunction caused by circulating microparticles from patients with metabolic syndrome. *Am J Pathol* 2008 ; 173 : 1210-9.
5. Ali S, Malloci M, Safiedeen Z, *et al.* LPS-enriched small extracellular vesicles from metabolic syndrome patients trigger endothelial dysfunction by activation of TLR4. *Metabolism* 2021 : 154727.
6. Amosse J, Durcin M, Malloci M, *et al.* Phenotyping of circulating extracellular vesicles (EVs) in obesity identifies large EVs as functional conveyors of Macrophage Migration Inhibitory Factor. *Mol Metab* 2018 ; 18 : 134-42.
7. Li S, Wei J, Zhang C, *et al.* Cell-Derived Microparticles in Patients with Type 2 Diabetes Mellitus: a Systematic Review and Meta-Analysis. *Cell Physiol Biochem* 2016 ; 39 : 2439-50.
8. Srinivas AN, Suresh D, Santhekadur PK, *et al.* Extracellular Vesicles as Inflammatory Drivers in NAFLD. *Front Immunol* 2020 ; 11 : 627424.
9. Le Lay S, Rome S, Loyer X, Nieto L. Adipocyte-derived extracellular vesicles in health and diseases: Nano-packages with vast biological properties. *FASEB BioAdvances* 2021 ; 00 : 1-13.
10. Freeman DW, Noren Hooten N, Eitan E, *et al.* Altered Extracellular Vesicle Concentration, Cargo and Function in Diabetes Mellitus. *Diabetes* 2018 ; 67 : 2377-88.
11. Boulanger CM, Scoazec A, Ebrahimian T, *et al.* Circulating microparticles from patients with myocardial infarction cause endothelial dysfunction. *Circulation* 2001 ; 104 : 2649-52.
12. Sarlon-Bartoli G, Bennis Y, Lacroix R, *et al.* Plasmatic level of leukocyte-derived microparticles is associated with unstable plaque in asymptomatic patients with high-grade carotid stenosis. *J Am Coll Cardiol* 2013 ; 62 : 1436-41.
13. Sinning JM, Losch J, Walenta K, *et al.* Circulating CD31+/Annexin V+ microparticles correlate with cardiovascular outcomes. *Eur Heart J* 2011 ; 2011 ; 32 : 2034-41.
14. Oshikawa S, Sonoda H, Ikeda M. Aquaporins in Urinary Extracellular Vesicles (Exosomes). *Int J Mol Sci* 2016 ; 17.
15. Santamaria-Martos F, Benitez ID, Latorre J, *et al.* Comparative and functional analysis of plasma membrane-derived extracellular vesicles from obese vs. nonobese women. *Clin Nutr* 2020 ; 39 : 1067-76.
16. Durcin M, Fleury A, Taillebois E, *et al.* Characterisation of adipocyte-derived extracellular vesicle subtypes identifies distinct protein and lipid signatures for large and small extracellular vesicles. *J Extracell Vesicles* 2017 ; 6 : 1305677.
17. Rome S, Blandin A, Le Lay S. Adipocyte-Derived Extracellular Vesicles: State of the Art. *Int J Mol Sci* 2021 ; 22.
18. Deng ZB, Poliakov A, Hardy RW, *et al.* Adipose tissue exosome-like vesicles mediate activation of macrophage-induced insulin resistance. *Diabetes* 2009 ; 58 : 2498-505.
19. Ying W, Riopel M, Bandyopadhyay G, *et al.* Adipose Tissue Macrophage-Derived Exosomal miRNAs Can Modulate In Vivo and In Vitro Insulin Sensitivity. *Cell* 2017 ; 171 : 372-84 e12.
20. Kranendonk ME, Visseren FL, van Balkom BW, *et al.* Human adipocyte extracellular vesicles in reciprocal signaling between adipocytes and macrophages. *Obesity (Silver Spring)* 2014 ; 22 : 1296-308.
21. Aswad H, Forterre A, Wiklander OP, *et al.* Exosomes participate in the alteration of muscle homeostasis during lipid-induced insulin resistance in mice. *Diabetologia* 2014 ; 57 : 2155-64.
22. Perdomo L, Vidal-Gomez X, Soleti R, *et al.* Large Extracellular Vesicle-Associated Rap1 Accumulates in Atherosclerotic Plaques, Correlates With Vascular Risks and Is Involved in Atherosclerosis. *Circ Res* 2020 ; 127 : 747-60.
23. Jansen F, Yang X, Franklin BS, *et al.* High glucose condition increases NADPH oxidase activity in endothelial microparticles that promote vascular inflammation. *Cardiovasc Res* ; 98 : 94-106.
24. Burger D, Montezano AC, Nishigaki N, *et al.* Endothelial microparticle formation by angiotensin II is mediated via Ang II receptor type I/NADPH oxidase/ Rho kinase pathways targeted to lipid rafts. *Arterioscler Thromb Vasc Biol* 2011 ; 31 : 1898-907.
25. Hosseinkhani B, Kuypers S, van den Akker NMS, *et al.* Extracellular Vesicles Work as a Functional Inflammatory Mediator Between Vascular Endothelial Cells and Immune Cells. *Front Immunol* 2018 ; 9 : 1789.
26. Wadey RM, Connolly KD, Mathew D, *et al.* Inflammatory adipocyte-derived extracellular vesicles promote leukocyte attachment to vascular endothelial cells. *Atherosclerosis* 2019 ; 283 : 19-27.
27. Gan L, Xie D, Liu J, *et al.* Small Extracellular Microvesicles Mediated Pathological Communications Between Dysfunctional Adipocytes and Cardiomyocytes as a Novel Mechanism Exacerbating Ischemia/Reperfusion Injury in Diabetic Mice. *Circulation* 2020 ; 141 : 968-83.
28. Ibrahim SH, Hirsova P, Tomita K, *et al.* Mixed lineage kinase 3 mediates release of C-X-C motif ligand 10-bearing chemotactic extracellular vesicles from lipotoxic hepatocytes. *Hepatology* 2016 ; 63 : 731-44.
29. Kakazu E, Mauer AS, Yin M, Malhi H. Hepatocytes release ceramide-enriched pro-inflammatory extracellular vesicles in an IRE1alpha-dependent manner. *J Lipid Res* 2016 ; 57 : 233-45.
30. Liu XL, Pan Q, Cao HX, *et al.* Lipotoxic Hepatocyte-Derived Exosomal MicroRNA 192-5p Activates Macrophages Through Rictor/Akt/Forkhead Box Transcription Factor O1 Signaling in Nonalcoholic Fatty Liver Disease. *Hepatology* 2020 ; 72 : 454-69.
31. Povero D, Eguchi A, Niesman IR, *et al.* Lipid-induced toxicity stimulates hepatocytes to release angiogenic microparticles that require Vanin-1 for uptake by endothelial cells. *Sci Signal* 2013 ; 6 : ra88.
32. Povero D, Panera N, Eguchi A, *et al.* Lipid-induced hepatocyte-derived extracellular vesicles regulate hepatic stellate cell via microRNAs targeting PPAR-gamma. *Cell Mol Gastroenterol Hepatol* 2015 ; 1 : 646-63 e4.

RÉFÉRENCES

33. Jiang F, Chen Q, Wang W, *et al.* Hepatocyte-derived extracellular vesicles promote endothelial inflammation and atherogenesis via microRNA-1. *J Hepatol* 2020 ; 72 : 156-66.
34. Zhao Y, Zhao MF, Jiang S, *et al.* Liver governs adipose remodelling via extracellular vesicles in response to lipid overload. *Nat Commun* 2020 ; 11 : 719.
35. Al Amir Dache Z, Otandault A, Tanos R, *et al.* Blood contains circulating cell-free respiratory competent mitochondria. *FASEB J* 2020 ; 34 : 3616-30.
36. Haraszti RA, Didiot MC, Sapp E, *et al.* High-resolution proteomic and lipidomic analysis of exosomes and microvesicles from different cell sources. *J Extracell Vesicles* 2016 ; 5 : 32570.
37. D'Acunzo P, Perez-Gonzalez R, Kim Y, *et al.* Mitovesicles are a novel population of extracellular vesicles of mitochondrial origin altered in Down syndrome. *Sci Adv* 2021 ; 7.
38. Garcia-Martinez I, Santoro N, Chen Y, *et al.* Hepatocyte mitochondrial DNA drives nonalcoholic steatohepatitis by activation of TLR9. *J Clin Invest* 2016 ; 126 : 859-64.
39. Puhm F, Afonyushkin T, Resch U, *et al.* Mitochondria Are a Subset of Extracellular Vesicles Released by Activated Monocytes and Induce Type I IFN and TNF Responses in Endothelial Cells. *Circ Res* 2019 ; 125 : 43-52.
40. Nicolas-Avila JA, Lechuga-Vieco AV, Esteban-Martinez L, *et al.* A Network of Macrophages Supports Mitochondrial Homeostasis in the Heart. *Cell* 2020 ; 183 : 94-109 e23.
41. Brestoff JR, Wilen CB, Moley JR, *et al.* Intercellular Mitochondria Transfer to Macrophages Regulates White Adipose Tissue Homeostasis and Is Impaired in Obesity. *Cell Metab* 2021 ; 33 : 270-82 e8.
42. Crewe C, Funcke JB, Li S, *et al.* Extracellular vesicle-based interorgan transport of mitochondria from energetically stressed adipocytes. *Cell Metab* 2021 ; 17 : S1550-4131(21)00365-X.
43. Zhao M, Liu S, Wang C, *et al.* Mesenchymal Stem Cell-Derived Extracellular Vesicles Attenuate Mitochondrial Damage and Inflammation by Stabilizing Mitochondrial DNA. *ACS Nano* 2021 ; 15 : 1519-38.
44. Ikeda G, Santoso MR, Tada Y, *et al.* Mitochondria-Rich Extracellular Vesicles From Autologous Stem Cell-Derived Cardiomyocytes Restore Energetics of Ischemic Myocardium. *J Am Coll Cardiol* 2021 ; 77 : 1073-88.
45. Nah G, Park SC, Kim K, *et al.* Type-2 Diabetics Reduces Spatial Variation of Microbiome Based on Extracellur Vesicles from Gut Microbes across Human Body. *Sci Rep* 2019 ; 9 : 20136.
46. Choi Y, Kwon Y, Kim DK, *et al.* Gut microbe-derived extracellular vesicles induce insulin resistance, thereby impairing glucose metabolism in skeletal muscle. *Sci Rep* 2015 ; 5 : 15878.
47. Seyama M, Yoshida K, Yoshida K, *et al.* Outer membrane vesicles of Porphyromonas gingivalis attenuate insulin sensitivity by delivering gingipains to the liver. *Biochim Biophys Acta Mol Basis Dis* 2020 ; 1866 : 165731.
48. Gilmore WJ, Johnston EL, Zavan L, *et al.* Immunomodulatory roles and novel applications of bacterial membrane vesicles. *Mol Immunol* 2021 ; 134 : 72-85.
49. Dao MC, Everard A, Aron-Wisnewsky J, *et al.* Akkermansia muciniphila and improved metabolic health during a dietary intervention in obesity: relationship with gut microbiome richness and ecology. *Gut* 2016 ; 65 : 426-36.
50. Ashrafian F, Shahriary A, Behrouzi A, *et al.* Akkermansia muciniphila-Derived Extracellular Vesicles as a Mucosal Delivery Vector for Amelioration of Obesity in Mice. *Front Microbiol* 2019 ; 10 : 2155.

TIRÉS À PART
S. Le Lay

Alexia BLANDIN

0674458513

10 Rue du Poitou 85600 La Guyonnière, France

linkedin.com/in/alexia-blandin-3b7853101/

alexiablandin0@gmail.com

FORMATION

2018-2021 Université d'Angers_France
Directrice de thèse : Soazig LE LAY

- **DOCTORAT EN BIOLOGIE**
  "Etude des vésicules extracellulaires adipeuses dans un contexte d'obésité : Caractérisation de leur contenu en lipides et en adiponectine"

2018 Université de Nantes_France
Encadrant : Cédric LE MAY

- **STAGE (6 mois)**
  "Régulation post-transcriptionnelle de PCSK9 dans l'intestin"

2016-2018 Université de Nantes_France

- **MASTER DE SCIENCE EN BIOLOGIE**
  Spécialité " Biologie Biotechnologie et Recherche Thérapeutique"

2014-2016 University of Nantes_France

- **LICENCE DE SCIENCE EN BIOLOGIE-BIOCHIMIE**
  Spécialité "Biologie cellulaire et physiologie animale"

EXPERIENCE PROFESSIONNELLE

COMPETENCES TECHNIQUES

Analyse des vésicules extracellulaires
- Développement and standardisation de la production de vésicules extracellulaires (VE)
- Centrifugation différentielle
- Nanoparticle Tracking Analysis (NTA), Videodrop
- Microscopie Electronique à Transmission (TEM)
- Gradient de densité au Iodixanol
- Cytométrie en flux
- Tests enzymatiques sur les VE (Proteinase K, Trypsin)
- Immunocapture

Biochimie
- Western Blot
- ELISA
- Immunohistochimie (Cellules; Tissus)
- PCR

COMPETENCE MANAGERIALES

- Encadrement d'étudiants en licence et en master
- Vulgarisation scientifique ('Déclics', Nuit Européenne des Chercheurs)
- Participation au programme de création d'entreprise 'Les Entrep'

Culture cellulaire
- Lignées cellulaires stables (HepG2, 3T3-L1, HEK 293)
- Explants de tissu adipeux murins et humains
- Adipocytes primaires
- Production lentivirale et infection des cellules
- Transfection de plasmides et siRNA

Expérimentation Animale
- Diplôme d'expérimentation animale
- Ethique et intégrité scientifique
- Exploration fonctionnelle in vivo *(T*raitement avec les VE)

COMMUNICATION SCIENTIFIQUE

5 Communications orales ➔ Société internationale des vésicules extracellulaires (ISEV), Association française d'étude et de recherche sur l'obésité (AFERO)…

2 Posters ➔ Société française des vésicules extracellulaires (FSEV), Société Francophone du Diabète (SFD)

3 Revues
- Sophie Rome, **Alexia Blandin** and Soazig Le Lay *Adipocyte-Derived Extracellular Vesicles: State of the Art.* Int. J. Mol. Sci. **2021**, 22(4)
- **Alexia Blandin**, Soazig Le Lay *Exosomes, vésicules extracellulaires et dialogue inter-organes* Med Mal Metab **2020**; 14: 250-257
- **Alexia Blandin**, Soazig Le Lay *Vésicules extracellulaires et maladies métaboliques : des liaisons dangereuses* Médecine/Sciences

2 Manuscripts
- *Lipidomic analysis of adipose-derived extracellular vesicles reveals their potential as lipid mediators of obesity-associated metabolic complications :* **En révision à Cell Reports** *(Biorxiv: https://biorxiv.org/cgi/content/short/2021.12.10.472057v1 + Sneak Peek : https://papers.ssrn.com/sol3/papers.cfm?abstract_id=3924604)*
- *Extracellular vesicles are stable carriers of adiponectin with insulin-sensitive properties :* **En soumission à Cell Reports**

1 demande de brevet déposée le 6/12/2021 numéro EP 21 306 717.6. Co-inventeurs : Ciloa & S.Le Lay/A.Blandin (Inserm)

Compétences Informatiques

Microsoft Office
Image J
GraphPad Prism
Odyssey LiCor
MetaboAnalyst

Qualités

Curieuse
Facilité d'adaptation
Organisée
Motivée
Sociable

Langues

Français : ●●●●●
Anglais : ●●●○○

Loisirs

Randonnée, Cuisine, Course, Musique, Voyages

Références

Soazig LE LAY (CR INSERM)
soazig.lelay@inserm.fr

Marie LHOMME
m.lhomme@ican-institute.org